UNIVERSITY OF Southampton
School of Engineering Sciences

PhD THESIS

Carbon Nanotube Surfaces for Low Force Contact Application

by

Pg. Hj. Md. Esa Al-Islam bin Pg. Hj. Md. Yunus

20th April 2009

DECLARATION OF AUTHORSHIP

I, Pg Hj Md Esa Al-Islam bin Pg Hj Md Yunus, declare that the thesis entitled

Carbon Nanotube Surfaces for Low Force Contact Application

and the work presented in the thesis is both my own, and have been generated by me as the result of my own original research. I confirm that:

- this work was done wholly or mainly while in candidature for a research degree at this University;
- where any part of this thesis has previously been submitted for a degree or any other qualification at this University or any other institution, this has been clearly stated;
- where I have consulted the published work of others, this is always clearly attributed;
- where I have quoted from the work of others, the source is always given. With the exception of such quotations, this thesis is entirely my own work;
- I have acknowledged all main sources of help;
- where the thesis is based on work done by myself jointly with others, I have made clear exactly what was done by others and what I have contributed myself;
- a part of this work is in Press for IEEE Transactions on Components and Packaging Technologies: Yunus, E.M., McBride, J.W., and Spearing, S.M., 2009, "*The Relationship between Contact resistance and Contact Force on Au Coated Carbon Nanotube Surfaces Under Low Force Conditions"* (Appendix 10).
- a part of this work is submitted for publication in The European Physical Journal AP section: Yunus, E.M., McBride, J.W., and Spearing, S.M., 2009, *"Improving the Contact Resistance at Low Force using Gold Coated Carbon Nanotube Surfaces"* (Appendix 10).

Signed: ……..

Date: 20th April 2009

ABSTRACT

This thesis focuses on developing a testing method to estimate the mechanical and electrical characteristics of CNT-based contact surfaces. In particular the use of gold thin films deposited on a CNT forest has potential to offer a very effective contact surface. Two different pieces of experimental apparatus were used in this research to determine the mechanical and electrical properties of gold/multi-walled carbon nanotube (Au/MWCNT) composites: 1) a modified nano-indentation; and 2) a PZT actuator test rig.

These apparatuses were used to mimic force-displacement and contact behaviour of the MEMS relay's contact at a maximum load of 1 mN with dry-circuit and hot-switched conditions. The surfaces were compared with reference Au-Au and Au-MWCNT contact pairs studied under the same experimental conditions. In the modified nano-indentation experiment, tests of up to 10 cycles were performed. The results showed that the Au-MWCNT pair electrical contact resistance improved when the Au-Au/MWCNT pair was used. Additionally the Au-Au/MWCNT pair electrical contact resistance (R_c) was comparable with the Au-Au contact pair. When the Au-Au/MWCNT composite surface is in contact with the Au hemispherical probe it provides a compliant surface. It conforms to the shape of the Au hemispherical probe.

For a higher number of cycles, a PZT actuator was used to support Au/MWCNT planar coated surfaces. This surface makes electrical contact with a gold coated hemispherical probe to mimic the actuation of a MEMS relay's contact at higher actuation frequencies. This apparatus allows the performance of the contact materials to be investigated over large numbers of switching cycles. Different current loads were used in this experiment, 1mA, 10mA, 20mA and 50mA at 4V supply. The R_c of these surfaces was investigated as a function of the applied force under repeated cycles. Under current loads of 1mA and 10mA the Au/MWCNT composite surface provides a stable contact resistance of up to more than a million cycles and no degradation was observed on the surface. Compared with Au-Au contact pair, degradation occurred after 220 cycles. The Au-Au contact pair shows delamination of the Au surface on the probe. The possible reason is the softening or melting of the Au surface. Furthermore, under higher current loads of 20mA to 50mA, degradation had occurred after 50 million cycles (at 20mA) and degradation had occurred at around 45 to 150 cycles for 50mA to 30mA respectively. This is because of the softening or melting of the Au and Au fatigue after a large number of cycles.

This study is the first step to show the potential of CNT surfaces as an interface in low force electrical contact applications. With this research, current trends in materials used on contacts and fabrication methods can be explored and even modified or adopted. The use of CNT's and their composites for contacts can be tested using the available apparatus to look at their performance and reliability in terms of mechanical and electrical properties. This is useful for MEMS contacts that form part of MEMS relay devices.

Acknowledgement

Thank you to God, the most kind, the most merciful, who knew how events would unfold before I did.

A huge heartfelt thank you to my irreplaceable supervisors: Professor John McBride and Professor Mark Spearing, for their constant support and guidance, and who brought a thin idea to a fat conclusion. Without you, this thesis would be illiterate.

Also deserve my gratitude, Dr. David Smith of the School of Physics and Astronomy, for providing the facilities for developing the MWCNT deposition, and to Mr. Tim Hartley for his dedication in designing and fabricating the PZT actuator test apparatus. Mr. Zondy Webber of the School of Physics and Astronomy has not only become a friend, but one who deserves my huge thanks for giving me training on the evaporator, sputter and SEM. A thank note also goes to Mr. Deyi Zheng, my office mate, who has help me a lot with the Lab View programming. Dr. Rosemary Boltryk, who does the copy editing, always deserve my thanks for catching the errors that inevitably crop up in my draft.

I am immeasurably grateful to my parents, Pg. Hj. Md. Yunus bin Pg Hj Besar and Dyg. Hjh Shafiah bte Dato Setia DiRaja Hj Md Yusof, my brother Pg Md Adam Nor-Islam, and my sisters, Dk. Hjh. Rina Yusnita Iman, Dk. Hjh. Wina Amal Khatijah, for your helping hands, encouragement and support, and to my late father in law, Allahyarham Hj Salleh bin Hj Mukibat (Al-Fatihah), who always taught me to never give-up, and my mother in law, Hjh Tiapnah bte Hj Metussin, for your prayers. To my brother Waleed and sister Anjum, thank you for looking after my welfare since my Higher National Diploma in Mechanical Engineering (1989) until now. I just could not imagine how our friendship and brotherhood keeps on growing. Many thanks.

My special thanks go to my beloved wife, my forever best friend, and PhD companion, Hjh Noor Maya. It has been a whirlwind since the beginning, and can't imagine experiencing any of it with anyone else. My beloved children: Hazim Wadhihan, Danial Zaki and Nur Sabrina – while I love them dearly, I am proud of each and every one of them for being tremendously wonderful and patient.

TABLE OF CONTENTS

LIST OF FIGURES & TABLES

Chapter 1

Chapter 2

Chapter 3

Chapter 4

Chapter 5

Tables

Nomenclature

Au	- Gold
AuNi5	- Gold Nickel Alloy
A	- Cross-sectional area
a	- Mean a-spot radius
α	- Cluster radius or Holm radius
α_c	- Critical vertical deformation
α	- Asperity vertical deformation
A_c	- Area of contact
Ag	- Silver
Cu	- Copper
C	- Capacitance
CNT	- Carbon nanotubes
d	– Gap between the bonded samples
d	– Thickness
dB	- Decibel
DLC	- Diamond-Like Carbon
ε_R	- Dielectric permittivity constant for epoxy resin
ε_o	- Permittivity of free space
F or F_c	- Force applied
Fe	- Iron
H	- Hardness of the softer material or Meyer hardness
I	– Current
K	- Knudsen number
K_Y	- Yield coefficient
L	- Uniform length
l_e	- Elastic mean path
L_0	- Lorenz constant
MWCNT	- Multi-walled carbon nanotubes
NH_3	- Ammonia
n	- Number of contact spots in cluster
η	- Empirical coefficient of order unity for clean interface
Ni	- Nickel
Pd	– Palladium
Pt	- Platinum
R_s	- Spreading resistance
r	- Contact radius
ρ_s	- Resistivity of the substrate material
ρ_f	- Film resistivity
ρ	- Resistivity
ρ_1 *and* ρ_2	- Resistivity
Rh	- Rhodium
R_f	- Film resistance
R_t	- Total resistance
R_a	- Average roughness value
R_b	- Bulk resistance
R_{cons}	- Constriction resistance
R_c	- Contact resistance
R'_c	- Wexler Resistance for elastic-plastic material deformation
R_c *(ballistic)*	- Contact resistance equation based on ballistic electron transport and elastic-plastic material deformation
R_c *(diffusive)*	- Contact resistance equation based on diffusive electron transport and elastic-plastic material deformation
r_{eff}	- Effective contact area radius
Ru	– Ruthenium
Rh	– Rhodium
SiO_2	– Silicon Dioxide
Sb	– Antimony

SiC	- Silicon Carbide
SWCNT	- Single-walled carbon nanotubes
Γ(K)	- Gamma function
Ti	- Titanium
TiN	– Titanium Nitride
T	- Thickness of the cantilever
T_m	- Maximum temperature in a contact spot
T_0	-Bulk temperature (far from the contact spot)
V	- Potential drop
v	- Poisson's ratio
Vs	- Softening Voltage
Vm	- Melting Voltage
W	- Width of the cantilever
CVD	- Chemical Vapour Deposited
DFM	– Direct Force Measurement
ECS	- Electrical contact resistance
IFM	– Interfacial Force Microscope
MEMS	- Microelectromechanical systems
MPECVD	– Microwave PECVD
NEMS	– Nanoelectromechanical Systems
PECVD	- Plasma Enhance CVD
SEM	- Scanning Electron Microscopy

CHAPTER 1: INTRODUCTION

1.1 Introduction

This research concerns the use of a new material; multi-walled carbon nanotubes (MWCNTs) and Au/MWCNT composites and testing it in low force contacts for MEMS relay applications. In this study, a new experimental method was developed using a modified nano-indentation apparatus and a PZT actuator test rig. This chapter provides background on various types of MEMS relay, the motivations for using MEMS relays, a brief explanation of the research background and finally, an overview of the aims and objectives of the research.

1.2 Types of MEMS relays

MEMS is the acronym for Micro-Electro-Mechanical Systems, devices which generally range in size from a micrometer to a millimeter and combine mechanical and electrical function. A MEMS relay is a miniaturized electrical switch that opens and closes under the control of another electrical circuit. It transfers power in a transmission line when it acts as a closed circuit (ON-state). A MEMS relay has two basic designs: (1) a contact situated at the tip of a micro-cantilever as shown in Figure 1.1. The cantilever actuates thus making the open and closed circuit; and (2) a micro-bridge structure as shown in Figure 1.2(a). The micro-bridge will bend when an actuating force provided by the driving electrode is applied thus giving the ON-state. As shown in Figure 1.2(b) the MEMS relay's nickel/gold contact bar (micro-bump) which is situated in the middle is in contact with the gold contact line [1].

The most common actuation mechanism for MEMS relays is electrostatic followed by thermal, magnetic and piezoelectric force [1]. For example in electrostatic the actuation mechanism can be capacitive or ohmic. In capacitive actuation, the cantilever is commonly made from a dielectric layer such as silicon dioxide or silicon nitride, which is partially covered with a conductive layer for the contact and the actuation electrode. In ohmic actuation, the cantilever can be made entirely from a conductive material, which is layered with a dielectric material such as silicon dioxide [2,3].

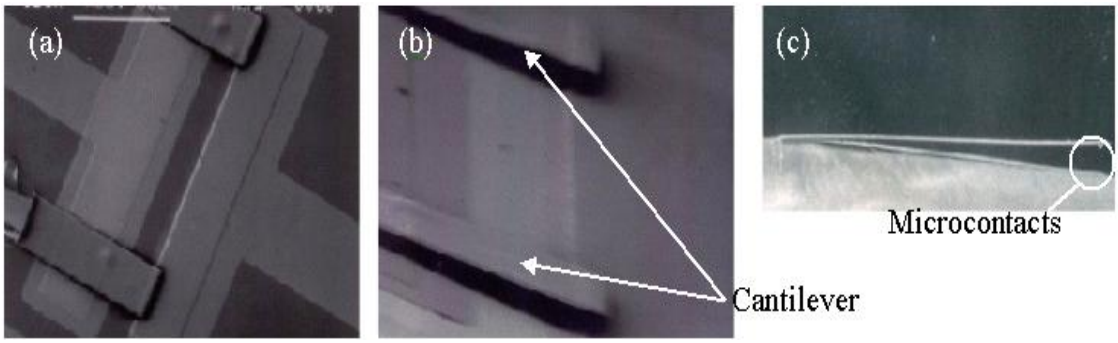

Figure 1.1: SEM image of MEMS relay cantilever type (a) top view (b) angled view and (c) side view [4].

(a)

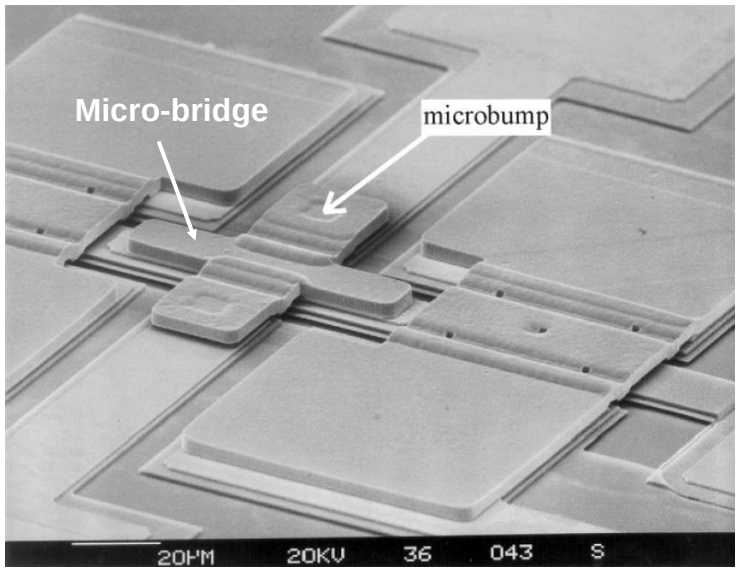

(b)

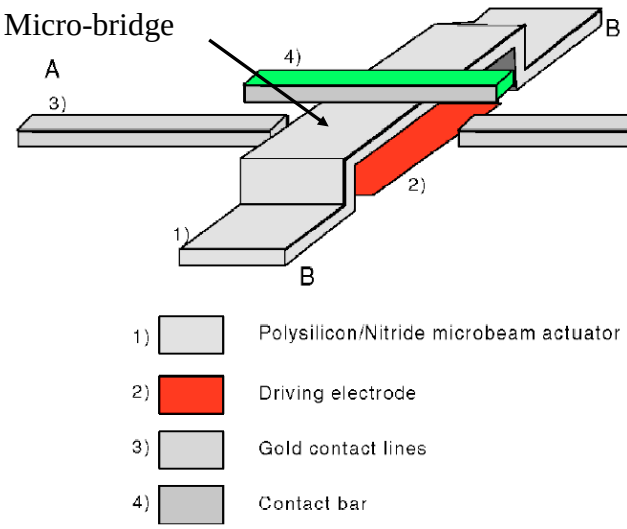

Figure 1.2: (a) SEM image of micro-bridge, (b) schematic diagram of micro-bridge MEMS relay [5].

Generally in the electrostatic actuation an electrical current is applied. As shown in Figure 1.3 the MEMS relay relies on a dc voltage, such that when applying a

sufficiently high dc bias it pulls the cantilever down and the contacts close. The signal line is now shorted between input and output. The MEMS relay is in the ON-state but when the dc bias is removed and there is no actuation force acting on it, the cantilever will move back to its original position due to the spring effect.

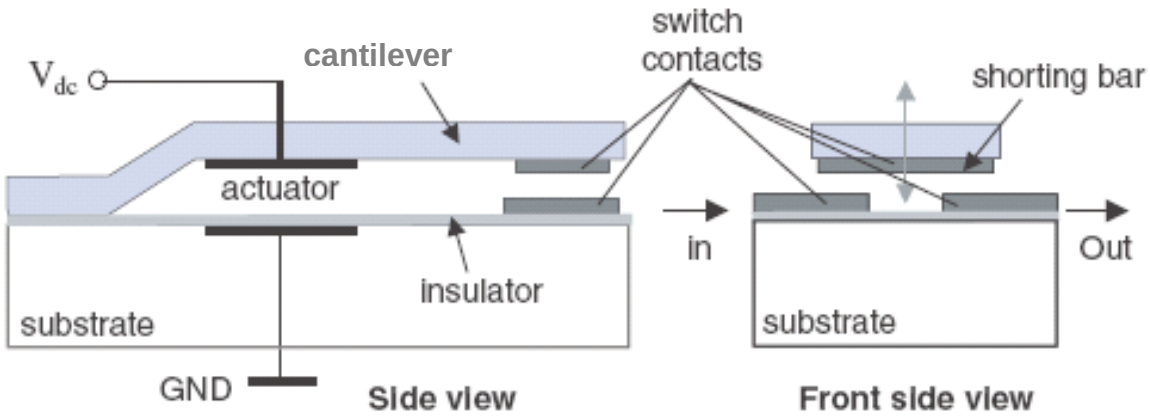

Figure 1.3: Schematic view of an electrostatically actuated MEMS relay [6].

A thermally actuated MEMS relay relies on thermal expansion through Joule heating. In Figure 1.4 (a) when voltage is applied, the Ni film at the top of the beam heats up and as a result expands. This results in the deflection and actuation forces acting on the cantilever or micro-bridge beam thus closing the circuit as shown in Figure 1.4(c). When the applied voltage is removed, it deflects back to its original position, the OFF-state, due to silicon stiffness and cooling of the Ni film.

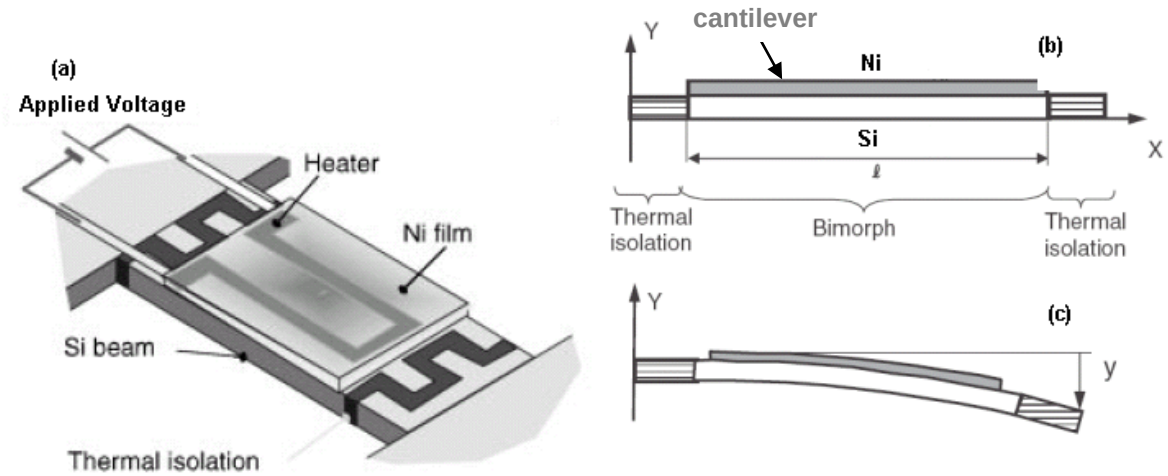

Figure 1.4: (a) Structure of Ni/Si bimorph MEMS relay and (b) side-view in the unloaded state and (c) in the loaded state [7].

In a magnetic MEMS relay, Figure 1.5 shows the cantilever can be deflected up or down by switching on and off the electromagnetic coil thus actuating the cantilever. This actuation consists of a magnetic core and a magnetically deformable cantilever beam, Figure 1.5(a). When current is present around the core it generates the magnetic field as shown in Figure 1.5(b). The magnetic field gives rise to a magnetic force that attracts the cantilever beam from its initial position. Figure 1.5(b) shows the deformation of the cantilever at any given time instant, thus giving the ON-state of the MEMS relay. When the electromagnetic coil is turned off the cantilever returns to its initial position, due its stiffness, constituting the OFF-state.

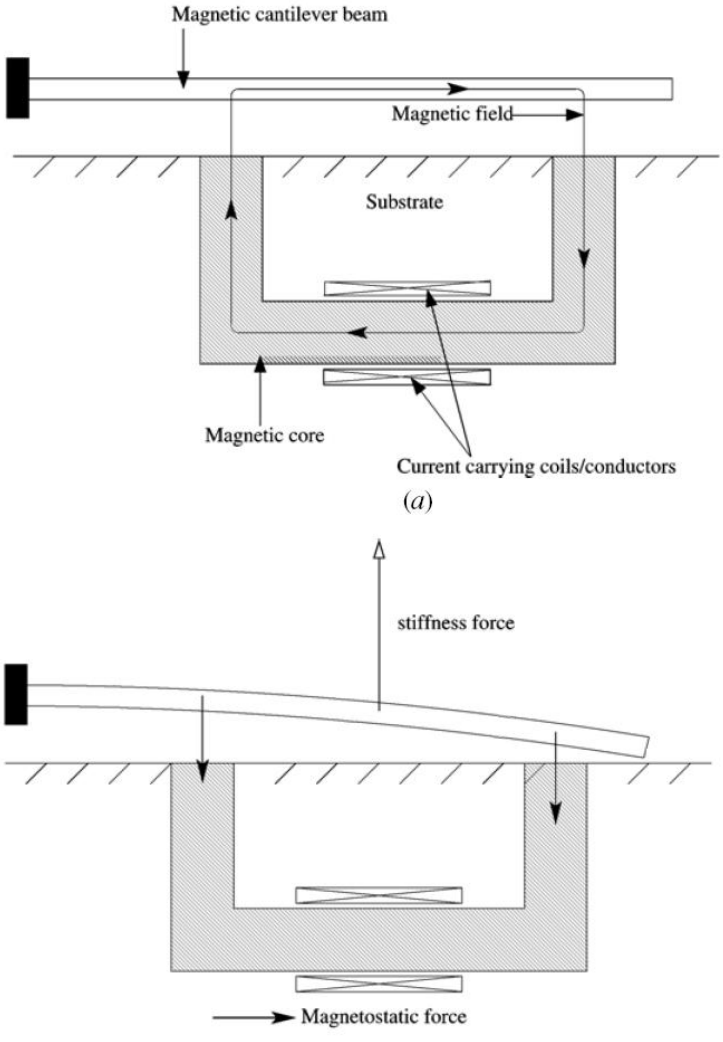

Figure 1.5: (a) Schematic diagram of magnetic actuated MEMS relay (b) deformed shape in magnetic field [8].

Finally, MEMS relays can be actuated using a piezoelectric (PZT) layer such as Zinc oxide or lead-zirconate-titanate materials. The piezoelectric actuation of MEMS relays is typically based on a bimaterial cantilever, where a differential contraction due to the piezoelectric effect causes the structure to bend. These layers produce a displacement via electrical actuation as in a piezoelectric bimaterial (electric field(s) cause one layer to extend and the other layer to contract). When a voltage is applied to the PZT layer it produces a mechanical force, thus bending the cantilever producing the ON-state.

Overall there are two microstructure designs for MEMS relays; the cantilever and the micro-bridge, and there are 4 types of actuation methods generally in use; electrostatic, thermal, magnetic and piezoelectric. The most common is the cantilever type using electrostatic actuation because it is simple and easily fabricated.

1.3 MEMS relays versus other relays

Electromechanical relays (EMR) have been used for decades. An EMR is an electrical switch that opens and closes under the control of another electrical circuit, the switch is operated by an electromagnet to open or close one or many sets of contacts. Generally two properties are observed in relay devices insertion loss and isolation. Insertion loss is a measure of power dissipation at the output port relative to the power at the input port of a device in the ON-state and isolation is the measure of power isolation between a contact pair in the OFF-state. EMRs' have a low insertion loss (typically 0.1dB) in the ON-state and high isolation (typically 80dB) when they are in the OFF-state. Both are expressed as dB or power ratio, this scale is most conveniently used because of the very wide range of the power amplitude between the input and output [9]. Furthermore EMR have good power handling capabilities, however, they are large in size and need higher power to switch and can only achieve a slow switching rate (1-40ms) as shown in Table 1. Due to the need for higher power to switch, a faster switching rate and miniaturization these relays are unsuited for the applications and are relatively bulky. If designing a circuit, this will

present a dilemma. Even with the smallest relay such as reed relays (reed relay is one or more reed switches sealed in a long, narrow glass tube, controlled by an electromagnet. The contacts are of magnetic material and the electromagnet acts directly on them without requiring an armature to move them) as shown in Figure 1.6, they are relatively heavy, expensive, take up critical circuit board space, and add unnecessary volume to a design, which puts limitations on the overall systems [10].

Characteristic	MEMS Relay	GaAs FET	PIN diode	EMR
Size	Small	Very small	Small	Large
Resistance	0.5Ω	1-5Ω	1-5Ω	0.5Ω
Switching power	2W	0.5W	5W	35W
Switching rate	0.5-20µs	10-100ns	10-100ns	1-40ms
Insertion loss	0.25dB	0.5dB	0.5dB	0.1dB
Isolation	40dB	30dB	30dB	80dB
Power consumption	Very low	Low	Low	High

Table 1: Comparison of MEMS relay and other relays [11].

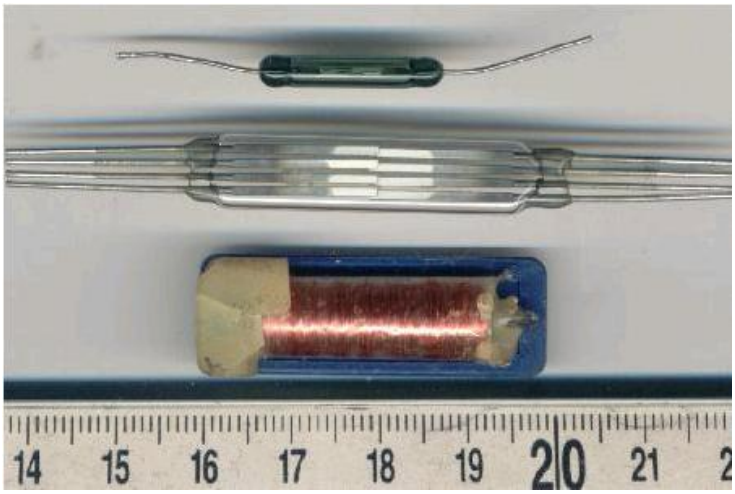

Figure 1.6: Example of reed relay in different sizes (scale in cm) [10].

Solid-state relay technologies (PIN diode- and FET-based) as shown in Table 1 are utilized for their high switching rate (10-100ns), commercial availability, low cost, and reliability. In spite of these advantages, two major areas of concern with solid-state relays exist: (1) the fundamental insertion loss is higher than for MEMS relays; and (2) the isolation during the OFF-state is lower t han for MEMS relays [12].

Even though MEMS relays are slower in terms of switching rate and have lower power handling capabilities, by utilizing an electromechanical architecture on a micro-scale, high frequency MEMS relays (typical range from 10kHz to hundreds of GHz) [13] combine the advantages of traditional electromechanical switches (low insertion loss and high isolation) with those of solid-state relays (low power consumption, low mass, long lifetime), together with the potential for high reliability and long operational lifetimes. These factors make MEMS relays a promising solution to existing low-power high frequency technology limitations. Furthermore as stated by Coutu et al. (2006) MEMS relays are ideally suited for high frequencies MEMS relay application because of their small geometries, exceptional high frequency performance, and low power consumption [14].

1.4 Research background

The MEMS electronics industry is interested in the reliable performance of MEMS relay contacts. There are many potential applications for MEMS relays, including radio frequency (RF) switches for communications, automobile, military, aerospace and instrumentation [9]. A large investment has occurred in the past decade in this area of research. This has resulted in a transition from a research curiosity towards a multi-billion dollar commercial enterprise [15]. This shows how important relay contacts are to MEMS devices.

A survey of MEMS relays reveals that they can resonate dynamically in the range of 100Hz to 100kHz, with power handling between 0.01W to 10W as shown in Figure 1.7, where power handling is the power that the MEMS relay can handle or withstand during the ON-STATE for a period of time without incurring damage. When compared with EMR, MEMS relays have lower power handling and when compared with solid-state relays they have a lower switching frequency. Switching frequency is defined as the number of actuations to which a cantilever can respond in a given time period, usually expressed as Hertz. EMR power handling exceeds 10W and the switching frequency of a solid-state relay reaches more than 100MHz. It would be

desirable to develop a MEMS relay that could exceed 100kHz switching frequency without mechanical and electrical failure.

MEMS relays are advantageous due to their small size and they have a significantly better performance in-terms of low insertion loss and high isolation at high frequencies over existing traditional technologies instrumentation (EMR and solid state relays), making them desirable to the electronic industry.

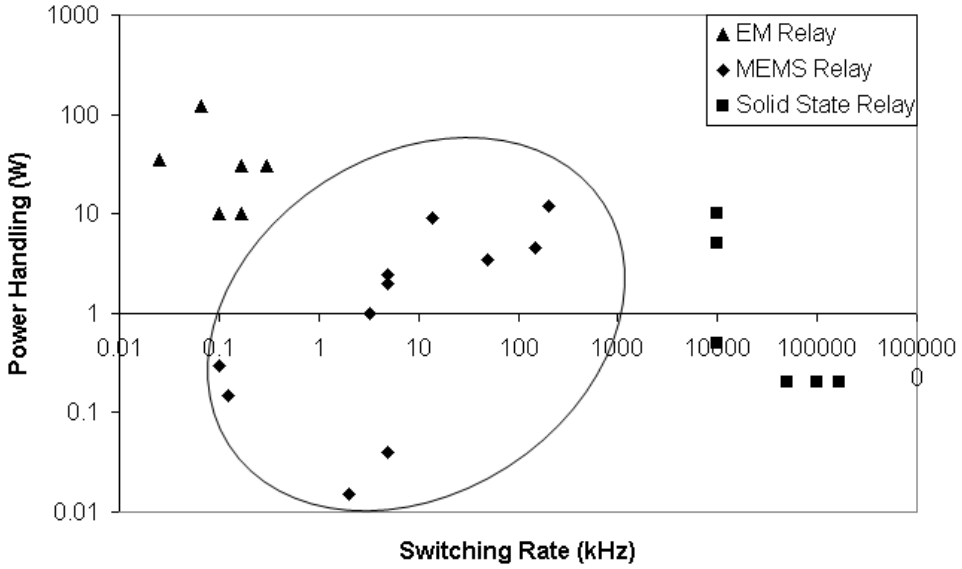

Figure 1.7: Performance of power handling vs. switching rate with different types of relays [16-25].

Increasing power handling and switching frequency would be attractive for MEMS electronics applications. This is because such a device can potentially transfer power faster and more efficiently through its transmission line without incurring any power loss, damage and failure to its contact. This places tremendous stress on the micro-structure. It is important that the contact is continuously conductive but if it wears and degradation occurs this will affect the overall performance of the MEMS devices. Currently, there are MEMS devices but these are unreliable due to degradation of the contact material surfaces [26].

Generally failure occurs during hot-switching (this is when the voltage supply exceed the melting voltage, for example Au's melting voltage is 0.43V) of a MEMS relay's contact and this is commonly caused by the erosion and wear of the contact surfaces. This often results in the exposure of electrical contact

constituents, which result in the build-up of more reactive elements on the contact surfaces. Degradation can be due to contamination of the contact coming from native or foreign origins. Melting, adhesion and micro-welding of the contacts can cause failure of the device. These degradation phenomena will increase the contact resistance (R_c) eventually causing failure of the whole MEMS relay. Therefore, improvement of the performance and reliability of the contact will materialise if the degradation and failure of the contact with different materials is understood.

This research aims to investigate and improve the mechanical and electrical properties of MEMS relay contact surfaces under low force applications. The performance and reliability of a MEMS relay that operates dynamically depends on its contact resistance, conductivity and resistance to deterioration. Experiments on electrical contacts and contacts using different types of material have been conducted. This is to improve the mechanical and electrical properties thus prolonging the overall lifetime of the device. The materials that are widely under investigation are thin metal films, silicon carbide and conductive diamond films. These materials were introduced to identify which material is most suitable and reliable. Currently, the most commonly used contact material is gold (Au) and its alloys in the form of thin films.

Silicon carbide and diamond film coatings have been investigated, however their electrical performance is greatly inferior to Au and its alloys. Au has a low resistivity and it resists surface oxidation and the formation of sulfide layers. However, Au wears readily and has adhesion problems due to Au's relatively low hardness (0.2-2GPa). Therefore, alternative materials need to be identified. A new material form; carbon nanotubes (CNTs) and their composites, are emerging for MEMS electronic devices. CNTs have mechanical and electrical properties comparable with diamond and gold respectively. This makes them attractive for investigation.

This research concerns with the fabrication, performs testing and compares the results of a MEMS relay contact coated with Au, MWCNT and Au/MWCNT composite materials. Both Au and MWCNTs specimens were fabricated by

coating contact surfaces using a sputter and chemical vapour deposition (CVD) apparatus respectively. The experiments were conducted using a modified nano-indentation apparatus and a PZT actuator test rig with a coated flat substrate attached at the tip. This coated planar surface makes a contact with the Au hemispherical probe. Dry-circuit and MEMS current load conditions were used in the experiment.

A MEMS relay is usually operated in a hermetically sealed package, to prevent the contamination of the contact that leads to the device's failure. This method is not totally effective for extended life applications. If leaks occur, the contact is easily degraded by reaction with an adsorbed contaminant, causing oxidation that over time leads to the build-up of oxide layers on the contact surfaces. This is why most experiments performed by other researchers have been conducted in controlled environments using environmental chambers. These experiments use an inert gaseous environment. This is to isolate the contact from premature degradation due to contamination and reduces the formation of an insulating surface layer. In some cases, an actual MEMS relay might encounter sudden exposure to contamination. Thus mimicking the situation by using the environmental chamber to sudden exposure of oxygen, vacuum, organic vapours and silicon vapour is also performed.

In this research the experiment uses controlled temperature and ambient air to mimic the actual life cycle of a non-hermetic MEMS relay. This is because it would be more economical to produce a non-hermetic MEMS relay than a hermetic MEMS relay. Thus the MEMS industry would be able to manufacture the MEMS relay devices commercially and economically in the future. New findings towards the capabilities of the novel materials, CNTs and their composites is revealed. Moreover, through these experiments, the important understanding of the degradation phenomena will help us to design contacts that are less susceptible to the failure mechanisms and consequently have much longer field lifetimes. In addition, understanding the failure mode of the contact would be beneficial to developers and users of the MEMS devices thus enabling the micro/nano industry to move ahead.

1.5 Aim and objectives

The research focuses on fabricating and testing commonly used materials and a new composite material for contact electrodes in MEMS relay devices. The research will be relevant to future electronic devices applications. The overall aim of the study is *to investigate and improve the performance and reliability of contacts in MEMS relays at low force using new materials; MWCNTs and a Au/MWCNT composite*.

The subsidiary objectives of the study focus on the fabrication and testing of commonly used materials and the new composite material that can be utilised on a MEMS relay's contacts. Specifically, the objectives of the research are:

1. To explore MWCNT and MWCNT/metal composites as promising materials for contacts, including developing fabrication methods,
2. To perform tests using a modified nano-indentation apparatus to test the contact performance under quasi-static actuation,
3. To perform tests using a designed and fabricated PZT test rig for testing relays at higher number of cycles under higher frequency,
4. To investigate Au/MWCNT composite surfaces under low force contact conditions with dry-circuit and hot-switched conditions, and
5. To understand failure mechanisms of Au/MWCNT composite contact surfaces, in terms of their mechanical and electrical behaviour.

Overall, this is a novel approach to producing a contact at low force, by using Au/MWCNT composite. Where the Au is supported on a forest of vertically aligned carbon nanotubes, reduces the scale of plastic deformation without compromising the contact resistance. Au is used because of its low resistivity and resistance to oxidation. MWCNT is used because of its unique mechanical and electrical properties. If the experiment is successful and CNT/metal composite is proven to be the best material it will improve MEMS relays' performance and reliability. This is important for MEMS relay devices if they are to survive the competition, especially with the current and traditional relays. Up to date, as stated by McKillop (2007), commercial MEMS relays are currently

available from only two companies [27]. This includes the MEMS relays fabricated by Tera Victa but these relays have a 100 million cycle lifetime at hot-switched condition [28]. Furthermore, as stated by Bouchaud (2007) MEMS relays entered the commercialisation phase in 2003 but reliability is still a major hurdle [29]. The possible degradation would be with their contact materials.

In this research the new material will be used on a new application; (low force contact typically with a maximum load of 1mN) because it has the promising properties for a relay, good mechanical and electrical properties as compared to the existing material used on contacts. This would materialize if the above experiment and fabrication of a test rig for MEMS relays is a success. This would be the first step in testing and observing their real life performance and reliability. This would be the validation phase of the performance and reliability of the potential material.

1.6 Scope of the thesis

This thesis consists of the following chapters:

Chapter 2: Literature Review

This chapter discusses published information on MEMS relays and contact area. It presents a summary of contact theory, reviews the current experiments on electrical contacts and reviews the properties and fabrication methods for carbon nanotubes. This discussion aims to identify gaps in the literature and to put this research work into perspective.

Chapter 3: Research Methodology

This section explains the fabrication methods for Au, MWCNT and Au/MWCNT composite samples and the experimental setup. It also explains how the data from the experiment are collected for this research.

Chapter 4: Results & Discussion

In this section the results and discussion are presented. It shows the results of contact resistance against number of cycles of the Au-Au, Au-MWCNT and Au-Au/MWCNT contact pair during dry-circuit and hot switching condition. It explains the characteristic behaviour of the samples. The experiment was validated using Scanning Electron Microscope (SEM) images, a TaiCaan Technology XYRIS 4000L laser scanner and X-ray spectroscopy to observe any changes on the surface of the contact.

Chapter 5: Conclusion

This chapter summaries and concludes the main findings. Overall, it is concluded that Au/MWCNT composite shows very good potential to be used in low force contact for MEMS relays application. This chapter presents the future work that needs to be undertaken if Au/MWCNT composites are to be developed in viable materials for MEMS relays.

CHAPTER 2: LITERATURE REVIEW

2.1 Introduction

This chapter introduces a study of previous work on electrical contacts. The theory of a classical electrical contact is explored and this theory will be used to estimate contact resistance (R_c) and the electrical or power loss for MEMS relays. More recent work of electrical contact theory for low force contacts is also presented and compared with the classical contact theory. Furthermore, reviews of experimental trends are presented and with these trends, the results from the experiments can be compared. The current materials in use for MEMS relay contacts such as thin metal films, silicon carbide and diamond is presented. The materials' advantages and disadvantages when used in MEMS relay applications are identified. Finally, the proposed new materials, carbon nanotubes (CNTs) and its composites are presented.

2.2 Electrical Contact Theory

A contact with low electrical contact resistance (typically < 10Ω) when closed is desired for MEMS relays and it should provide no path for conduction when opened (typically > 100MΩ) [30]. Holm presented a wide study of electrical contacts in terms of mechanical and electrical properties [31]. In the study of electrical contacts one of the most important quantities is the contact resistance. Contact resistance consists of bulk resistance, constriction resistance and film resistance. Bulk resistance, R_b, is defined by its uniform length, L, cross-sectional area, A and resistivity, ρ , as shown in Figure 2.1.

$$R_b = \rho \frac{L}{A} \qquad \text{[Equation 2.2.1]}$$

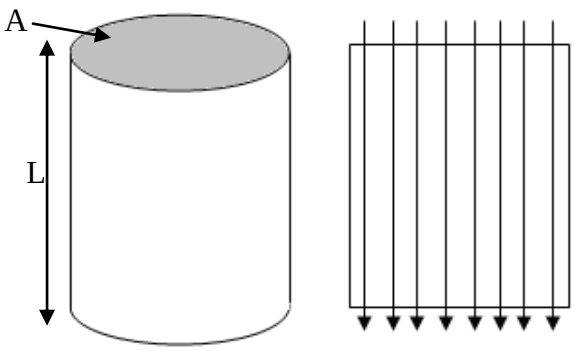

Figure 2.1: Unbroken solid conductor.

In an electrical contact the contact resistance is between the two surfaces brought together. Constriction resistance is defined as the resistance arising from the constriction of current flow through the two surfaces as shown schematically in Figure 2.2 (a) and (b).

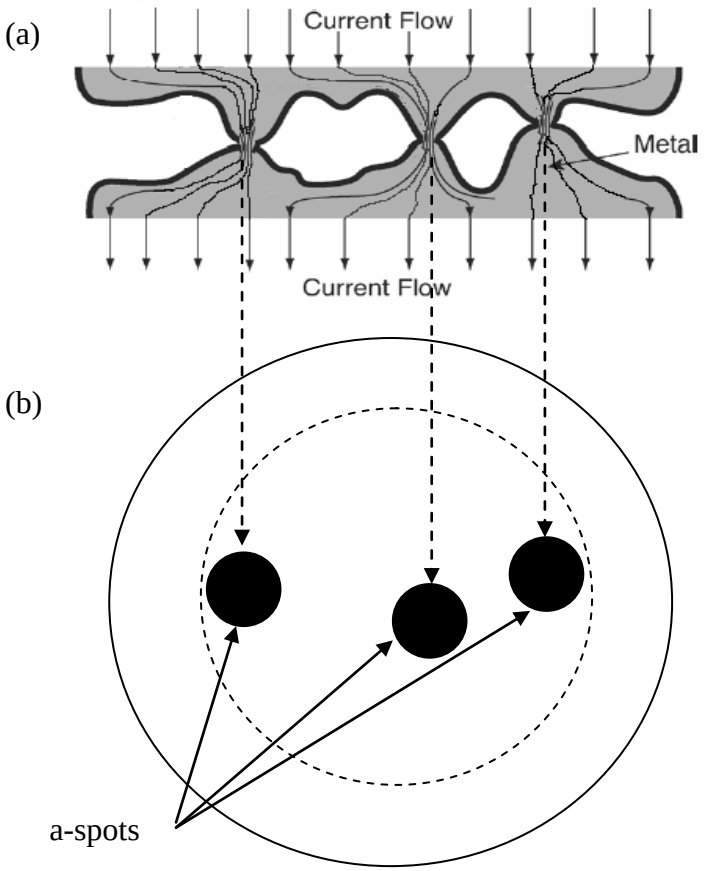

Figure 2.2: (a) Constriction resistance due to asperities of two-member conductor (b) top view: a-spots.

This occurs because the two surfaces in contact are rough (having asperities) on the micro-scale, and, therefore, not all of the apparent areas of the surfaces

are in contact. To make the contact resistance calculation simple the contact spots or a-spots are summed and assumed to be circular as shown in Figure 2.2 (b), free of surface films, small compared to the width of the bulk conductor and consisting of a monometallic (same material) contact. This gives:

$$\text{constriction resistance, } R_{cons} = \frac{\rho}{2r} \qquad \text{[Equation 2.2.2]}$$

where r is total contact radius.

This expression is widely used in electrical contact problems relating to the design of electrical contacts. For example when using the equation 2.2.2 for pure gold (resistivity $2.24 \times 10^{-8}\Omega m$) and silver (resistivity $1.58 \times 10^{-8}\Omega m$) to obtain a comparatively low contact resistance of 1 mΩ; the contact radius will only be ~11μm and ~8μm respectively. It is obvious that the contact radius is much smaller than that of the apparent conductor area. It is also apparent that the contact resistance will increase due to the constriction (i.e. if the contact radius decreases) and redirection of the current path through the contact. Furthermore, in some instances the contacts consist of two different materials, with resistivity of ρ_1 and ρ_2 as shown in Figure 2.3.

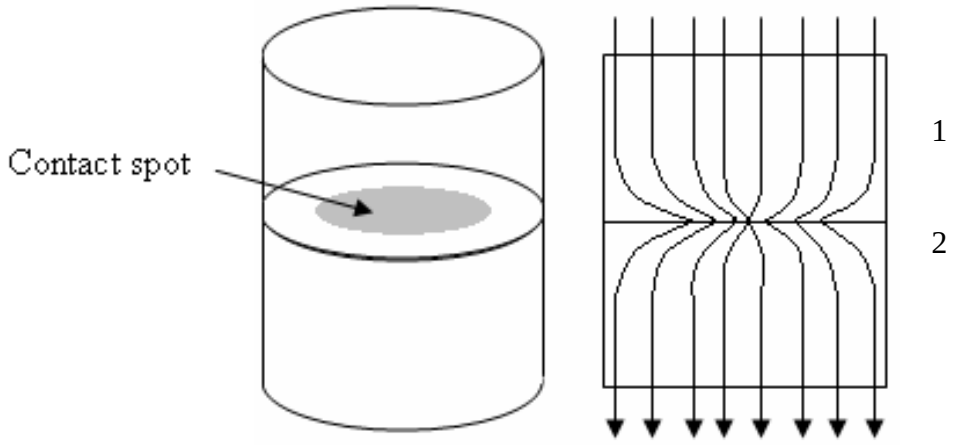

Figure 2.3: Two different materials contact.

The constriction resistance associated with each half of the contact is then $R_1 = \frac{\rho_1}{4r}$ and $R_2 = \frac{\rho_2}{4r}$.

The total constriction resistance is considered in series and then becomes:

$$R_{cons} = R_1 + R_2$$

$$= \frac{\rho_1}{4r} + \frac{\rho_2}{4r}$$

Therefore, $R_{cons} = \frac{(\rho_1 + \rho_2)}{4r}$ (Equation 2.2.3)

These models assume that there is only one contact spot but in reality due to asperities and the contact mechanics of the metal surfaces the contact is expected to comprise many contact spots. From Greenwood (1966), who assumed that a contact occurs between clusters of circular contact spots, the contact resistance can be given as follows [32]:

$$R_c = \rho\left(\frac{1}{2nr} + \frac{1}{2\alpha}\right)$$ (Equation 2.2.4)

Where *n* is the number of contact spots in a cluster and *α* is the radius of the cluster spot (contact spot) sometimes defined as the Holm radius. If we assume that the number of contact spots is numerous, the equation reduces to:

$$R_c \approx \frac{\rho}{2\alpha}$$ (Equation 2.2.5)

The above formula has been derived without considering any force acting on the surfaces. The equation 2.2.5 can now be used to derive a formula for the contact resistance dependence on contact force. Assuming it deforms plastically, $F = A_c H$, where F is the force applied, A_c is the area of contact and H is hardness of the softer material. Now considering that the area of contact is circular, this gives $A_c = \eta \pi \alpha^2$, where η is an empirical coefficient of order unity, for a clean interface, η=1 (no surface contamination or film). Then substituting the above equations into equation 2.2.5 gives the following formula [31]:

$$R_c = \left(\frac{\rho^2 \eta \pi H}{4F} \right)^{\frac{1}{2}} \qquad \text{(Equation 2.2.6)}$$

The above formula assumes a plastically deforming contact surface and this is acceptable, as Greenwood has shown that asperity deformation is generally plastic in most practical applications. Equations 2.2.2, 2.2.3, 2.2.5 and 2.2.6 can be used to calculate the contact resistance if the surface is clean. A further consideration is the formation of thin films on the contact surfaces. The film-metal interface can be defined as a nearly equipotential surface, thus the current density in the film is approximately uniform across the contact spot or a-spot, thus the constriction resistance is given as $R_{cons} = \frac{\rho_s}{4a}$,

where the ρ_s is the resistivity of the substrate material. The current passes through the resistive film of area πa^2, thickness *d* and resistivity ρ_f. Then the film resistance is $R_f = \frac{\rho_f d}{\pi a^2}$. The total resistance $R_t = R_{cons} + R_f$, thus the expression becomes [31]:

$$R_t = \frac{\rho_s}{4a} + \frac{\rho_f d}{\pi a^2} \qquad \text{(Equation 2.2.7)}$$

Equations 2.2.2 to 2.2.7 represent the simple electrical contact theory for solid-solid interfaces. These equations show the fundamental properties that affect the electrical contact such as surface hardness, surface film, contact force and the deformation mechanism. These formulas have been used to give an approximation which is useful for designing electrical contacts, but this classical theory is expected to provide errors when compared to the experiments conducted in this research. These errors could be due to: (1) the film thickness; (2) the formation of thin film or contaminants on the surface of contact being ignored; (3) the classical model assuming a large solid conduction body rather than a thin film; (4) the complexity of the contact surfaces; and (5) a diffusion dominated conduction model rather than ballistic transport conduction. Ballistic transport conduction occurs when an electron injected at one end of a

conductive medium should come out the end without losing energy. It is also indicated that a conductor will be a ballistic conductor if the mean free path is larger than the length of the conductor [33]. The mean free path is the average length that the electron can travel freely before interacting with an atom or subatomic particle and deviating from its original path, possibly losing some kinetic energy. The electron travels over the free mean path, typically for metals in ~50nm. In the present experiments the contacts are formed at very low force (ranging from tens of μN to a few mN) and with thin film surfaces thus the Holm's model will need to be modified.

2.3 Modification of the Holm model for low force contacts

Consideration is firstly given to the breakdown of the classical Holm conduction model. This follows a study by Coutu et al. (2006), where the influence of elastic-plastic material deformation and the associated contact resistance under the low force conditions typical of MEMS relays, where conduction is likely to be dominated by ballistic and diffusive electron transport; were considered [14]. Using the formula from Coutu et al. (2006) [14];

$$R'_c = R_c(ballistic) + \Gamma(K) R_c(diffusive) \qquad \text{(Equation 2.2.8)}$$

Where $R_c(ballistic)$ is the contact resistance based on ballistic electron transport and elastic-plastic material deformation, $R_c(diffusive)$ is the contact resistance based on diffusive electron transport and elastic-plastic material deformation and $\Gamma(K)$ is the Gamma function. This formulation is an updated micro-contact resistance model for low force contact developed using Chang's [34] improvement to the Chang, Etsion, and Bogy (CEB) model [35] and the Gamma function in Wexler interpolation [36], where;

$$R_c(ballistic) = \frac{4\rho K}{3\pi}\sqrt{\frac{H\pi\left[1.062 + 0.354\left(\frac{2}{3}K_Y - 3\left(\frac{\alpha_c}{\alpha}\right)\right)\right]}{F}} \qquad \text{(Equation 2.2.9)}$$

and

$$R_c(diffusive) = \frac{\rho}{2}\sqrt{\frac{H\pi\left[1.062+0.354\left(\frac{2}{3}K_Y - 3\left(\frac{\alpha_c}{\alpha}\right)\right)\right]}{F}} \qquad \text{(Equation 2.2.10)}$$

where, ρ is the resistivity of the sputtered Au on the micro-contact, H is the hardness of sputtered Au, F is the applied load (range from 10μN to 1mN), K is the Knudsen number, K_Y is the yield coefficient which is the function of Poisson's ratio, v, α_c is the asperity critical vertical deformation, that is when the top part of the asperity starts to deform plastically, and α is the asperity vertical elastic deformation.

To calculate the Knudsen number [14,37];

$$K = \frac{l_e}{r_{eff}} \qquad \text{(Equation 2.2.11)}$$

The Knudsen number, K, is a dimensionless number describing the 'flow' of the electron particles and is defined as the ratio of the molecular mean free path length to a representative physical length scale; the length scale example would be the radius of the contact surface. l_e is elastic mean path (for most metals ~50nm [14,37]) and r_{eff} is effective contact area radius. In a single effective asperity model, the individual contact spots are close enough together that their interactions are not independent. In this circumstance Coutu et al. (2006) [14] assumes that the effective contact area is defined as the sum and not the parallel combination of the individual contact areas.

To understand the implication of the modified contact resistance model consider the 1mN contact force with the values of H and ρ used in equation 2.2.6, assume $\eta=1$, this leads to a predicted contact area of 0.58μm^2 based on $A=F/H$. This generates a predicted constriction resistance of 26mΩ as shown in Figure 2.5. The corresponding contact radius is 430nm, based on a single circular contact. The corresponding relationship with force is shown in Figure 2.5. To determine the adjustment to the predicted resistance based on the

application of equation's 2.2.8, 2.2.9 and 2.2.10. If we assume the same area of contact then using equation 2.2.11, $K= 0.000116$. Thus for the selected area the contribution to the resistance of the ballistic transmission model is negligible. To determine the contribution to the resistance resulting from the modified diffusive model the yield coefficient can be calculated using [14];

$$K_Y = 1.1282 + 1.158v \qquad \text{(Equation 2.2.12)}$$

where v is Poisson's ratio for Au (0.42), thus, K_Y is 1.61456.

When the asperities are considered having elastic-plastic deformation, the α (asperity vertical deformation) and α_c (critical vertical deformation) are assumed equal [34,35]. To estimate the $\Gamma(K)$ Gamma function we can use the graph as shown in Fig. 2.4 [36,38,39].

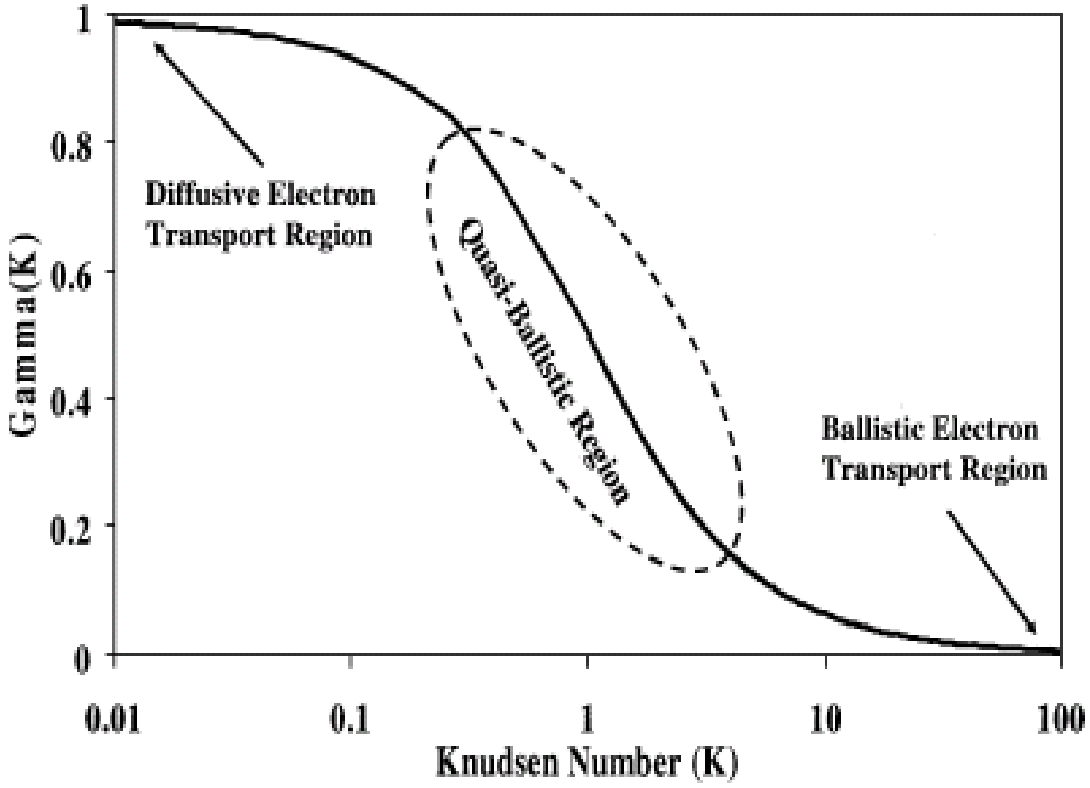

Figure 2.4: Graph of Gamma against Knudsen Number for gamma function plotted by Mikrajuddin et al. [36].

Since K (Knudsen number) is 0.000116, from the graph the Gamma function is ~1. By substituting equations 2.2.9 and 2.2.10 and the above data into equation 2.2.8 a new analytical model is plotted as shown in Figure 2.5.

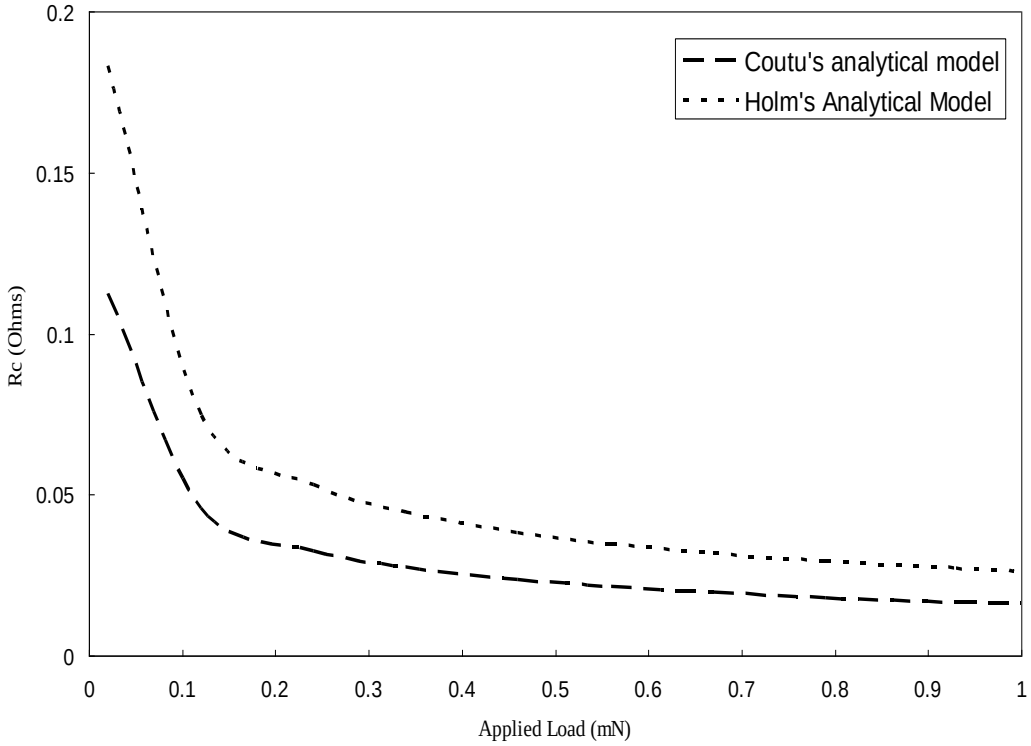

Figure 2.5: Calculated model of contact resistance as a function of applied load.

The Coutu's analytical model (equation 2.2.8) gives a contact resistance slightly lower than Holm's contact resistance model in (equation 2.2.6). In this model: (1) the new micro-contact resistance considers elastic-plastic material deformation; (2) it uses a single effective contact area rather than multiple a-spots; (3) conduction during the micro-relay's closure is considered to be a mixture of ballistic and diffusive electron transport; and (4) the contact load discontinuity, which exists at the transition from ideal elastic to ideal elastic-plastic behavior, is accounted for.

Au is a logical choice as a contact material for MEMS relay contacts because it: (1) has a low propensity to form alien surface films; and (2) is corrosion resistant [14]. However, Au has the tendency to have a thin layer of carbon on its surface that is residue from the cleaning process and/or is adsorbed due to

exposure to air [40]. For example, it has been reported that there are 2-4nm thick of adsorbed hydrocarbons on freshly cleaned Au [41,42] and this will increase the contact resistance. Therefore, surface films and contaminants should not be ignored when designing a new contact resistance analytical model.

In addition, the use of a single effective contact area rather than multiple a-spots [14] will need to be reconsidered. Even though at low contact force, multiple a-spots will be formed during contact because of the asperities on the surface. The asperities will have different heights and radii [43] thus adding complication. Coutu et al. (2006) and Timsit (2006) also noted that the single effective asperity model did not accurately represent the actual contact area for these electrical contacts' surfaces [14,39].

A new technique to investigate the contact surfaces as shown by McBride (2006) [43] and measuring the contact resistance in-situ could be considered. This used a new system to measure the loaded surface profile, based on a non-contact 3D laser profiler. A test contact is mounted on a force sensor on an adjustable screw support such that it can move into contact with the fixed transparent surface. The laser performs the scan through this transparent flat slide supported in a fixed position above the base. This system allows the measurement of contact area and deformation in terms of the contact force and plane displacement while the surfaces are actually in contact.

2.4 Voltage-temperature relation

Another consideration when designing an electrical contact is the influence of temperature during the contact. Under such conditions significant Joule heat is produced within the constriction, the crowding of the current lines within the a-spot generates enough heat to soften or melt the contact surfaces. For example, the theoretical voltage for softening and melting Au is V_s, 0.08V and V_m, 0.43V respectively [31].

In the theory of electrical contacts, the voltage-temperature (V-T) relation is expressed as below [31,44].

$$T_m = \left[T_0^2 + \frac{V^2}{4L_0} \right]^{1/2} \qquad \text{(Equation 2.2.13)}$$

Where T_m is the maximum temperature in a contact spot, T_0 is the bulk temperature (far from the contact spot), V is the voltage-drop across the contact and L_0 is the Lorenz constant.

The voltage drop, V, is calculated by;

$$V = IR_c \qquad \text{(Equation 2.2.14)}$$

where I is the current passing through the contact spot and R_c is the contact resistance of the surface in contact. Equation (2.2.5) or (2.2.6) can be substituted into equation (2.2.14) and then into equation (2.2.13), but these equations are no longer valid due to the unique features of electrical conduction in thin film and low force contacts. Even with the modified electrical contact, equation (2.2.8) [14] is established but this equation still gives error. This is due to no consideration of the formation of thin films or contaminants, the use of a single effective contact rather than multiple a-spot and the surface roughness.

The above consideration needs to be addressed when formulating the equation that calculates contact resistance. If we use the above equation to calculate the maximum temperature it will be invalid. The formation of contaminants is unavoidable because in this research the contact material is exposed to air and its surroundings such as water vapour or dust. Furthermore the use of a single effective contact and surface roughness needs to be reconsidered because in the micro-scale the surface contact is not smooth. They have asperities and due to this there will be multiple a-spots and the effective contact radius needs to be the sum of the multiple a-spots.

2.5 Contact materials

2.5.1 Commonly used materials

This section reviews materials which have been studied for use in MEMS relay contacts including thin metal films, silicon carbide (SiC), diamond and CNTs. Silicon has been in use by the electronic integrated circuit industry for decades. It is unquestionably the choice of material for MEMS devices because of its availability for fabrication. However, silicon has poor mechanical and tribological properties, including a low wear resistance, poor brittle fracture strength, and a tendency to adhere to surfaces in contact [45]. Furthermore there are demands in harsher environment applications for the MEMS devices (for example, high temperature and pressure in the automotive and aerospace industry). Thus other materials have been explored and tested. This is to find alternatives to conventional silicon technology to allow even smaller and more reliable electronics to be fabricated [46].

There are several contact materials used including gold, platinum, silver, palladium, cadmium, tungsten and base metals (Ni, Fe, Ti and Sb) and their alloys [47,48,49]. Gold, silver and its alloys (with palladium or platinum) were mainly in use in the experiments by Coutu et al. (2004) to select a reliable material for contacts [50]. Recent research by Dickrell et al. (2005) also focuses on thin metal film such as Au, Pt, Ti, and TiN [51]. The most widely used thin metal films considered for contacts are gold and its alloys. This is due to gold's low resistivity ($2.24 \times 10^{-8}\Omega m$), high oxidation resistance and ease of integration with available device fabrication processes. However as stated by Coutu et al. (2004) [50], it is a very soft metal, has a relatively low melting point, and adsorbs a carbonaceous layer which makes gold contacts susceptible to degradation, erosion and wear. Thus, to minimize its erosion and wear, gold is usually hardened by alloying it with elements such as nickel, palladium, silver or platinum.

Additionally, repetitive contact at high contact current will lead to contact wear and failure. This is why the MEMS electronics industry is looking at other

materials that can withstand such conditions. Other materials that are of interest to the MEMS and electronics industry are silicon carbide and diamond. These materials have been used as structural materials for MEMS devices such as for micro-resonators (micro-mechanical oscillators). Both materials have considerable advantages, particularly their hardness, high Young's modulus, resistance to harsh chemical environments, mechanical stability at high temperature and very high thermal conductivity [52]. Given these properties there is a strong drive to make high performance MEMS relays with these materials.

Silicon carbide (SiC) is an alternative material for contacts in harsher environments, especially high temperature oxidizing environments. Efforts have been made to develop silicon carbide for MEMS devices and the extension of silicon-based MEMS technology to harsher environments [53]. Most, articles report on the issues of fabrication and improving SiC material quality for MEMS electronics applications. An attempt to improve its electrical resistivity has shown that silicon has a resistivity of 640Ωm but when SiC film is doped with NH_3 (ammonia) the resistivity drops to 1×10^{-4}Ωm [54].

The above literature demonstrates that a MEMS relay structure and its contact is usually made from metal microstructures such as gold, silver, or platinum and their alloys and silicon carbide. These MEMS relay devices contain interstructural insulation. It is often provided by silicon oxide or nitride with mechanical and thermal properties essentially differing from those of conductive materials in the same device [55], thus giving non-homogeneous material stacking which leads to temperature-dependent electrical and mechanical device characteristics. This will lead to the increase of cost in fabricating the different elements for a MEMS relay device. Therefore limiting the set of materials in use and their composition will promote high production rates and less complex fabrication processes, and this will cut costs.

Diamond-like carbon (DLC) can be used as a substitute for all of the above materials as an insulator or conductor. Figure 2.6 shows an example schematic of DLC with different band gap. As stated by Adamschik et al. (2002) they have

produced insulative to conductive DLC. For example as shown in Figure 2.6, the cantilever could be made from an insulator and the contacts are conductive DLC. It possesses superior material properties such as high thermal conductivity (thus excellent heat dissipation in the MEMS devices), high mechanical fracture strength and high Young's modulus. In addition it is chemically inert and has a high wear resistance. This makes DLC the material of choice for harsh environments. There have been experiments using DLC films for micro-systems but these are more concerned with the mechanical properties than the electrical and chemical properties [56,57,58]. DLC has high electrical resistivity. This material is more suited to mechanical elements and the use of it will offer greater potential for increasing MEMS devices' mechanical performance.

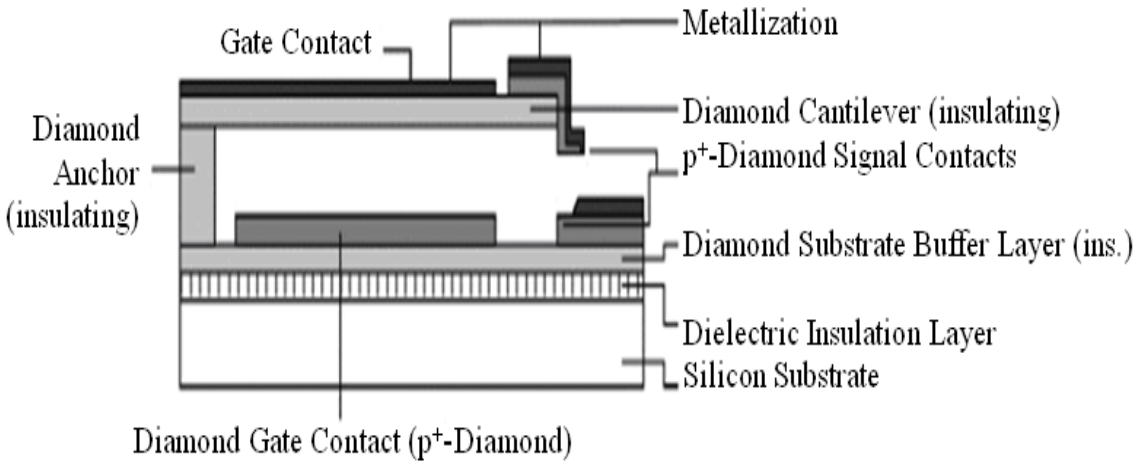

Figure 2.6: Schematic cross-section of doped diamond micro relay made from different band gap of doped DLC [59].

There has been research on the electrical capability of DLC and how to improve it. A pure DLC film has a resistivity of 1 x $10^{10}\Omega$m and attempts have been made to reduce the resistivity by doping it with metals such as gold (Au) nanoparticles. By introducing Au into DLC the resistivity reduces to 30Ωm [60]. It has also been revealed that doping DLC with boron makes the films more conductive with a resistivity of ~9 x $10^{-5}\Omega$m at 300K [61]. Another study of using boron-doped DLC films produced an even lower resistivity of 7.5 x $10^{-5}\Omega$m [55]. The introduction of ruthenium to DLC (Ru-Doped DLC) has been shown to increase its electrical conductivity thus reduce its resistivity to 1 x $10^{-5}\Omega$m [62].

Although diamond is ideal for MEMS relay devices in harsh environments, it still has a high resistivity and this will affect the electrical contact resistance if applied to contacts. Au-alloys such as Au-(6.3%)Pt with resistivity of 7.17 x 10^{-8} Ωm, [50] are still the best materials for utilization in MEMS relays, but due to their poor performance in handling mechanical wear and contamination, new materials need to be developed.

2.5.2 Carbon Nanotubes

Carbon nanotubes are a tubular form of carbon with a structure formed by rolling up the planar hexagonal net structure of graphite, with at least one end typically capped with a hemisphere structure. There are two forms of CNT: multi-walled carbon nanotubes (MWCNT) Figure 2.7(a) or single-walled carbon nanotubes (SWCNT) Figure 2.7(b) [63].

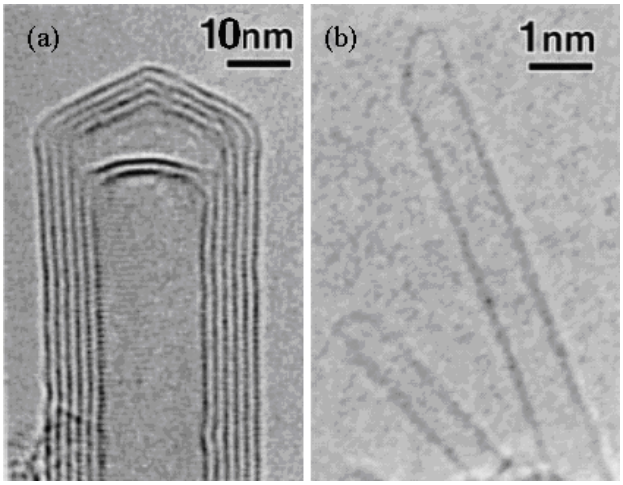

Figure 2.7: TEM image of (a) multi-walled and (b) single walled CNT [63].

The most common way to produce CNTs is by using chemical vapour deposition (CVD). The growth mechanism using CVD of CNT starts with the diffusion of a catalyst, usually of transition metal such as Fe, Co or Ni on a silicon, silicon dioxide or aluminium oxide substrate. When the growth temperature is reached (600-1200^{o}C) the catalyst will agglomerate to form nano size particles, Figure 2.8(a). Then a hydrocarbon gas such as methane, acetylene, or ethylene is introduced. The gas adsorbed on the catalytic particle surface releases carbon upon decomposition, which dissolves and diffuses into

the metal particle. At this temperature carbon precipitates in a crystalline tubular carbon solid form, thus forming CNTs.

The rationale for choosing the transition metals as a catalyst for CVD growth of carbon nanotubes lies in the phase diagrams for the metals and carbon. At high temperatures, carbon has finite solubility in these metals, which leads to the formation of metal-carbon solutions and therefore the nanotubes' growth mechanism. In Figure 2.8(b), the nanotubes appear to be vertically well aligned and it reveals that CNT can grow like vines and support each other due to van der Waals forces [64].

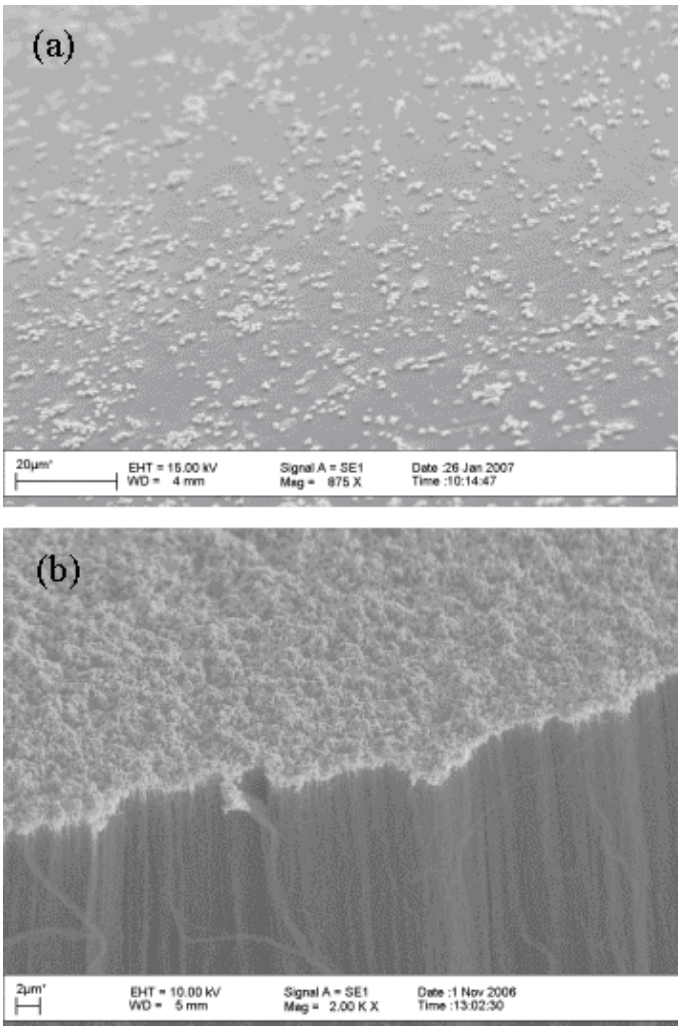

Figure 2.8: (a) Example of agglomerisation of Fe catalyst and (b) forest of CNT grown as part of the experimental review.

2.6 Experimental trends

This section presents several experimental methods to study electrical contacts. This is to compare the experimental trends identified in the present research and to validate the experimental set-up. All the experiments below use an environmental chamber, and an experimental set up in which applied load and contact resistance are measured.

Wang et al. (1992) used an experimental set up as illustrated in Figure 2.9 [65]. This consists of a spherical impactor of 2.4mm radius (to simulate the movable contact), a flat disc as the target (to simulate the stationary contact), which was coated with a gold thin film. The shaker when activated moves the impactor to and fro impacting the target with a load of 0.5N and a frequency 100Hz, which simulates the on and off switching events of a macro-contact. The shaker cannot provide a predictable and accurate force due to the impact mechanics which leads to complexity and much greater dynamic forces.

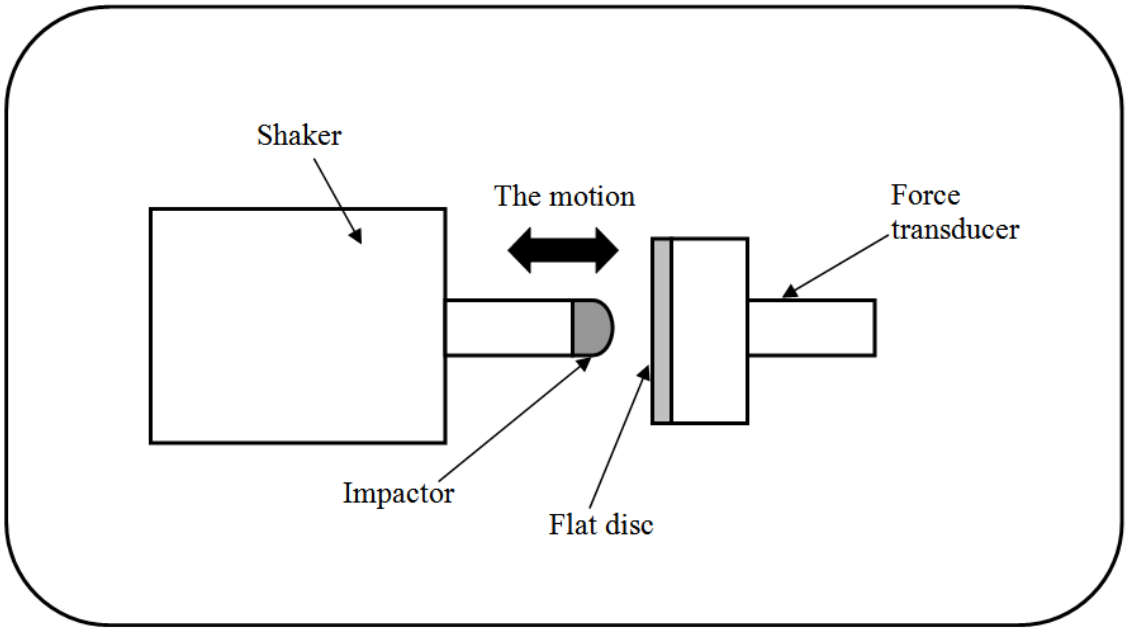

Figure 2.9: Schematic of the experimental setup of horizontal impactor.

The test was performed using electrical loads varying from 5 to 13.3V. A mixture of air and organic vapours are fed to the environmental chamber. This is to imitate the formation of carbon on the contact. The formation is because of

pyrolysis (decomposition of a chemical by extreme heat) of the organic vapour by the spark. As carbon builds up on the contact surface the contact resistance increases. The electrical contact resistance was measured using 2-wire measurement methods.

Schiele et al. (1997) fabricated an electrostatically actuated cantilever beam [66]. They fabricated three different types of micro relay: the cantilever type, a fixed-fixed beam and torsional springs. They varied the beam length to investigate the pull-in voltage necessary to pull down the beam, thus making the contact. It was found that the torsional springs were poor for the purpose due to their tendency to buckle. Gold electrodes were used on all the beam types. The electrical resistance was calculated using the contact pressure, actuation voltage and contact area.

Hyman et al. (1998) used a direct force measurement scheme as shown in Figure 2.10 [67]. The probe simulates the movable contact and the sample simulates the substrate on a MEMS relay. Gold contact coatings were used in this experiment and the test was performed in dry nitrogen. The forces were varied from 100 to 500μN and the contact resistance was measured using a 4-wire measurement method (with the DC current varied from 0.1 to 200mA). The geometry, surface damage, and material deposition were examined using Scanning Electron Microscopy (SEM). The conclusion to this experiment is that heat dissipation is the critical design criterion for maintaining a low contact resistance, a high power handling, and minimum surface adhesion wear. Thus, an effective heat sink design is essential for contacts in MEMS relays.

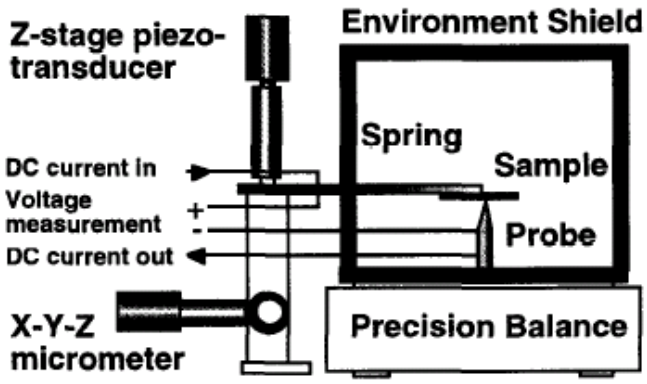

Figure 2.10: Direct force measurement experiment apparatus [67].

Schimkat (1998) used the experimental setup shown in Figure 2.11 [68]. The top contact is brought together with the bottom sample by a piezodrive. The force is measured using the force sensor attached to the bottom (load ranges from 0.1mN to 10mN) and the electrical resistance is measured using a 4-wire measurement method (using a maximum current of 4mA). Au, $AuNi_5$ and Rh (Rhodium) coatings were used in this experiment under a nitrogen atmosphere. It was concluded that pure Au is not suitable for the contact material because of its high adhesion force, while $AuNi_5$ and Rh are better suited as contact materials.

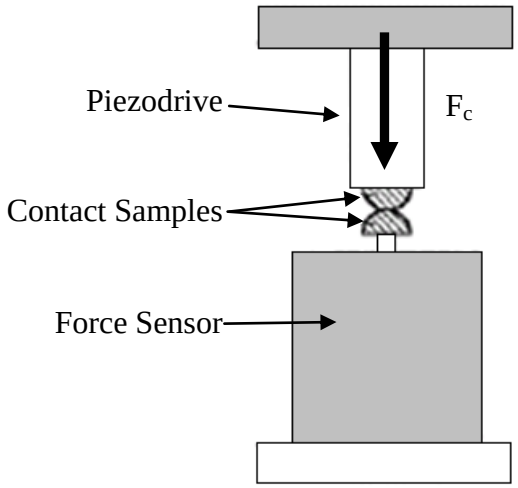

Figure 2.11: Experimental setup of force and distance controlled [68].

Tamai (2000) investigated the reaction of a gold alloy switching contact exposed to a silicone vapour environment [69]. This was to investigate the formation of SiO_2 and its effects on the contact. Low molecular weight silicone evaporates gradually from silicone compound under elevated temperatures. The silicone compounds such as silicone rubber and oil will contaminate the MEMS relay devices. SiO_2 is formed by chemical decomposition of the adsorbed silicone molecules. When SiO_2 is formed on the contact, failure occurs because it is an insulator. They developed a micro relay with a contact consisting of Ag(40wt%)-Pd(60wt%) doped with trace amounts of magnesium. A force was applied and the electrical contact resistance was also measured. This material shows improvement of the contact resistance in comparison with usual Ag-Pd contacts.

In another experiment, Tzeng et al. (2003) used an inch-worm with nanometer linear resolution to control the movement of the upper and lower electrode coated with CNT [70]. The contact resistance, R_c was measured between CNT coated electrodes in ambient air and in a vacuum. The author concluded that the contact resistance, R_c was found to be much lower in ambient air (~160Ω) than in a vacuum (>4kΩ). They claimed the reason was that the CNTs coated on the two electrodes attached to each other more easily during electrical current conduction in the ambient air than in vacuum during the contact. Thus, a much larger effective contact area between attached CNTs coated on the two electrodes resulted in a much lower electrical contact resistance.

Tringe et al. (2003) used a standard Interfacial Force Microscope (IFM) with a single asperity to study Au/Au electrical contacts as shown in Figure 2.12 [49]. In this experiment the probe made from an electrochemically sharpened gold coating was brought towards the sample and the attractive and repulsive forces were measured using the self-balancing force sensor in a dry nitrogen atmosphere. The electrical resistance was also measured using the 4-wire measurement methods. It was concluded that the contact resistance and adhesion were dominated by the adsorbed contamination layers such as hydrocarbons, and traces of sulphur and iodine. This can be broken down by increasing the applied force and voltage.

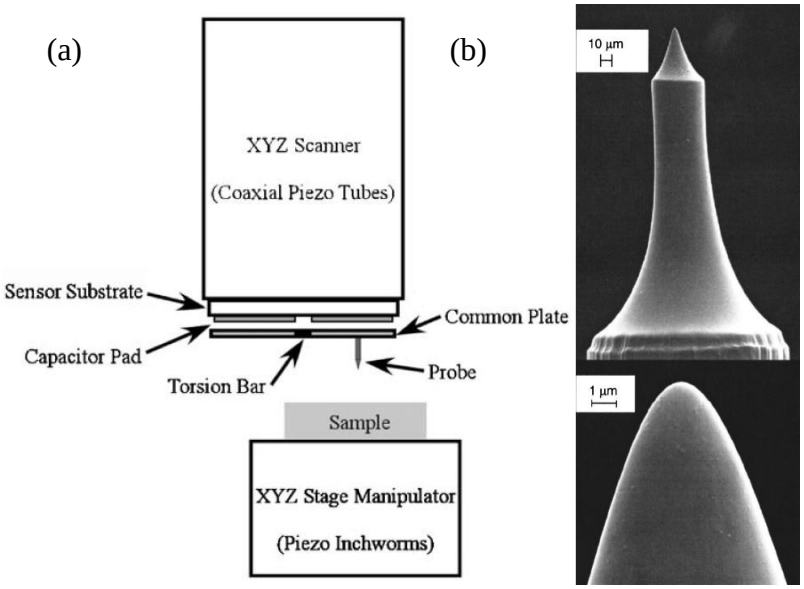

Figure 2.12: (a) Schematic example of IFM [71] (b) SEM images of probe tip [49].

Dickrell et al. (2003) performed an experiment using a modified nano-indentation apparatus as shown in Figure 2.13 [51]. The substrate (coated with Platinum) was brought towards the spherical sample (sputtered with gold). The apparatus measured the force applied (the maximum force applied was 100μN) and the displacement of the sphere electrode. It also measured the electrical contact resistance using a 4-wire measurement method. The open-circuit voltage was limited to 3.3V and the current source was set to 3mA. The experiment was enclosed in an environmental chamber filled with nitrogen. The experiment showed that the contact resistance increased after around 5 to 10 actuation cycles due to contamination formation. They claimed that this was caused by a current produced by the sphere and the substrate samples having a static charge which when brought closer together produced contact arcing or discharge, which decomposes the adsorbed surface contamination. This can be circumvented using an RC element in parallel with the contact. This provides an alternative discharge path for the stored electrical energy as the contact forms and then breaks.

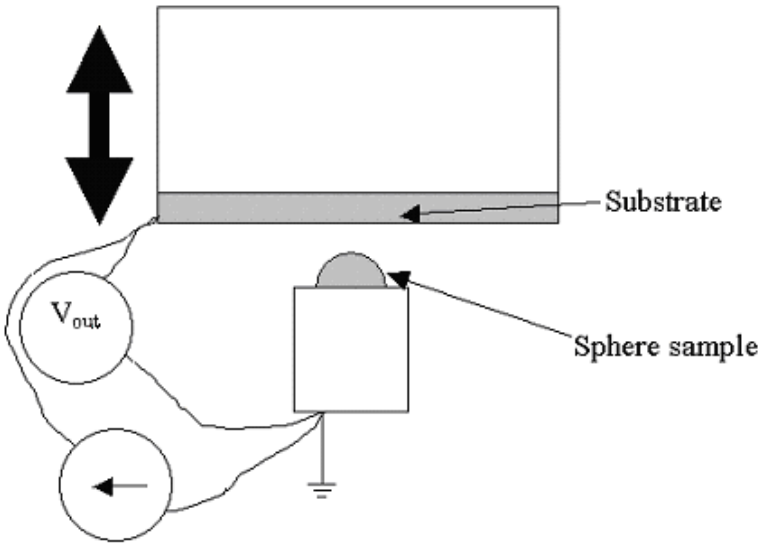

Figure 2.13: Schematic modified nano-indenter apparatus.

Yaglioglu et al. (2006) presented a method and experimental setup to characterize the contact resistance between two dense forests of tangled single-walled carbon nanotube (SWCNT) films [72]. They also demonstrated a method to characterize the contact resistance between metal surfaces and SWCNT films (with 1μm thickness). The SWCNT and gold-plated ball was

brought near to the SWCNT surface substrate, as shown in Figure 2.14. The test was performed with a CETR UMT microtribometer which allows simultaneous force/displacement (maximum load is ~150mN) and contact resistance measurements. Their results showed that the contact resistance (at maximum load, the contact resistance is ~2Ω) improved when the metal surfaces were brought to the SWCNT surfaces. This is because of the low resistivity of Au and the SWCNT conforming to the contact shape. The method is versatile and can be used to characterize SWCNT films of different properties and morphologies and can serve as a platform for future research.

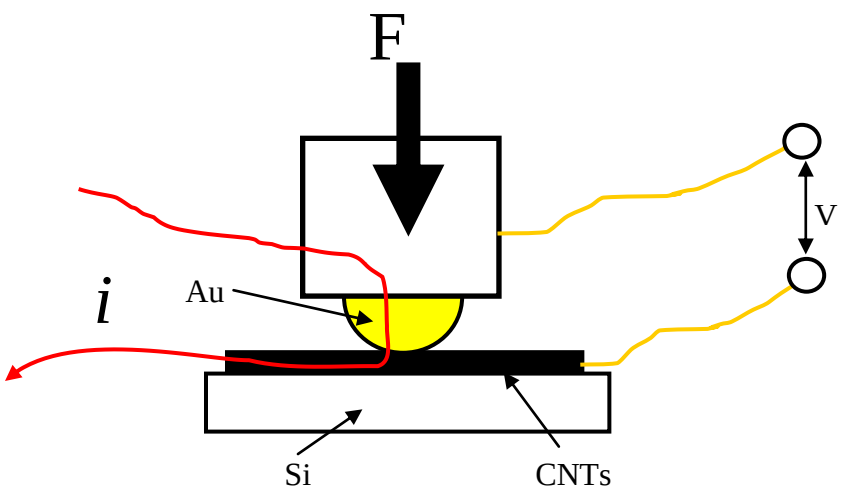

Figure 2.14: Schematic diagram of experimental set-up [72].

Bult et al. (2008) investigated Au sputter-coated (5μm thick) vertically aligned MWCNT (100μm long) using a modified nano-indenter [73]. The purpose of using a vertically aligned MWCNT (VAMWCNT) was because they have better penetration or infiltration than tangled CNTs when sputtering Au. The diamond indenter was replaced with an Au coated hemispherical probe (with 2mm diameter in size) and mated with the Au/MWCNT flat surface at a maximum load of ~25mN with 5V supplied voltage and 5mA supplied current (hot-switched). The author concluded that there was little degradation of the switch performance, either mechanically or electrical over 3000 cycles. The contact resistance measured was 0.4Ω throughout the 3000 cycles.

All of the above experiments replicate the actuation of the contacts with a certain applied force. This is to determine the contact mechanical and electrical

behaviour. The experiments were performed with dynamic forces of 100μN to 0.5N. It is important to have a high degree of controllability and accuracy when applying such low load (ranging from tens of μN to a few mN). For this reason the nano-indentation apparatus and PZT actuator (with high resolution force sensor) are used in the current work to determine the quasi-static and dynamically applied forces. Typically the maximum dynamic force used in MEMS relays is ~1mN. It is important to replicate the actuation at this dynamic force level to determine any mechanical failure.

These previous experimental studies were mostly performed on electrical contacts in hermetic environments. Hermetic means the MEMS devices are completely sealed and airtight so that no contamination occurs. The long-term viability of hermetic packages for MEMS relays is questionable because hermetic packaging requires several complex fabrication processes. As indicated by Rebeiz (2003), this makes the cost of packaging quite expensive (US$2 – US$50 per unit) compared with non-hermetic packaging which requires only about US$0.2 – US$0.5 per unit [74].

Previous tests included using an inert gas environment chamber such as nitrogen and under clean room conditions. This is to screen out any potential contaminant such as oxide layers forming on metal contacts, thus making the electrical contacts fail prematurely due to contamination rather than mechanical failure. Others used environmental chambers to replicate the sudden exposure to contaminants, such as oxide layers, water vapour, or other hydrocarbons that can degrade the electrical contact resistance causing the MEMS relay to fail. Furthermore as stated by Tzeng et al. (2003), the contact resistance, R_c of CNT-CNT pair was found to be much lower in ambient air than in a vacuum [70] and that is why in this study such condition was replicated.

Common materials used as contacts are Au and its alloys but these materials show poor mechanical and electrical properties. Carbon nanotubes have been tested and these have shown their potential to be used in contacts during experiments by Yaglioglu et al. (2006) and Bult et al. (2008) [72,73]. Furthermore to establish the reliability of the contact material, a large number of

cycles is needed (typically >>10^6 cycles). The experiments reported above were typically based on ten cycles to three thousand cycles. In this research the number of cycles is greater than 10^6 cycles. This is to determine CNT's potential as contact material.

2.7 CNT's properties

CNT's have unique electronic properties and they are one of the strongest material forms yet discovered in comparison with the mechanical and electrical properties of silicone, thin metal films, silicon carbide, diamond and doped diamond. CNTs have been tested to have a tensile strength of 63GPa [75], which compares favourably with high-carbon steel which has a tensile strength of approximately 1.2GPa.

An experiment using atomic force microscopy made a direct measurement of the elastic modulus and bending strength of individual structurally isolated multi-wall carbon nanotubes and indicated values of 1.26TPa and 14.2GPa [76] respectively. An experiment was also conducted on CNT using nano-indentation apparatus and it was determined that the bending modulus was 1.24TPa, axial modulus 1.23TPa, and wall modulus 5.61TPa [77]. Another report shows that a CNT has an elastic modulus greater than 1TPa [78] compared to diamond, which is 1.2TPa.

In addition one important parameter to improve the contact is its hardness. By improving the hardness of a material it will make a surface more resilient to wear. In an experiment performed by Kim et al. (2007) in which CNT/Cu metal nanocomposites were fabricated, the hardness of the nanocomposites was 1.1GPa, which is about 1.8 times higher than for Cu without CNT [79]. The hardness increases almost linearly with increasing CNT volume fraction up to 10% [79]. Besides the outstanding mechanical properties, CNT's also possess superior electrical properties such as their current carrying capacity which is higher than for copper wires [80]. With this there are attempts to measure the resistivity of CNTs. It is indicated that it is achievable to have ultra-low resistivity (50% lower than Cu) of CNTs at room temperature [81]. This is because CNTs

act as ballistic conductors. Hjortstam et al. (2004) estimated that a 4μm long high quality SWCNT with a diameter of 1.2nm has a resistivity of 0.88 x 10^{-8}Ωm [81]. The calculation is performed using the theory of ballistic conductors and it is assumed that the CNT is defect-free. This compares favourably with values of 1.67 x 10^{-8} and 1.59 x 10^{-8}Ωm at room temperature for Cu and Ag respectively. In addition, Hjortstam et al. (2004) illustrated that when CNTs are filled with metal to form a composite, its resistivity falls to 0.35 x 10^{-8}Ωm [81]. They claimed that the reduction of the resistivity was due to the metal composite.

For more than a decade the trend in research includes improving the mechanical and electrical properties of CNT by forming composites, doping or filling. In addition, development of simulation software using techniques such as Molecular Dynamics and Atomistic simulation methods is also common. These simulations were developed to simulate and investigate a NEMS (Nanoelectromechanical systems) electrostatic CNT cantilever's structural properties [82,83,84]. It is found that the low pull-in time of CNT cantilever implies that they can switch very quickly (typically in tens of picoseconds) and the switching frequencies can range from several tens to hundreds of GHZ. An investigation of how to fabricate a suspended CNT across metallic trenches was also reported and its structural properties were investigated as shown in Figure 2.15 [85,86]. These simulations were used to promote and understand its mechanical and electrical behaviour in NEMS application.

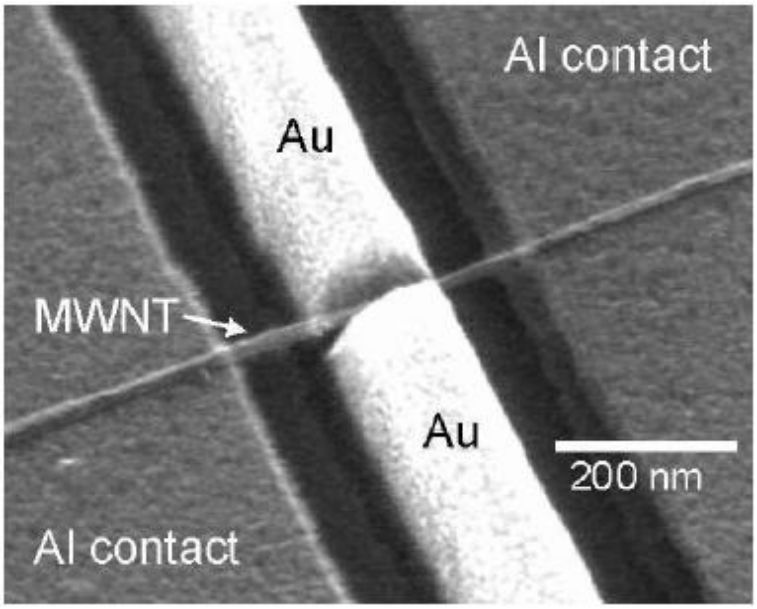

Figure 2.15: An example of suspended carbon nanotubes [87].

Since 1990 research on CNT has increased involving the simulation or the actual fabrication of the CNT wire on NEMS, but no experiments with low force contact, typically 1mN, using vertically aligned MWCNT or metal/MWCNT composite contacts have been conducted. All the above experiments have been conducted on either one single fibre or a tangled forest of CNTs to determine their mechanical properties. These mechanical properties will not be in agreement with this study which utilises a vertically aligned multiwalled carbon nanotubes (VAMWCNT) and their metal composites (in this case the use of Au/MWCNT composites).

A more recent experiment performed by Cao et al. (2005) reported that vertically aligned multiwalled carbon nanotubes (with thickness of 860μm to 1.2mm) exhibit compressible foamlike behaviour [88]. Cao et al. (2005) stated that after every cycle of compressive loading along the film-thickness direction (along nanotube axis), the nanotubes unfold the buckles and recover to their near original lengths, resulting in a strong cushioning (compliant) effect. For example, when compressing a thickness of 860μm VAMWCNT and unloading, it recovers back to the thickness of 720μm. Cao et al. (2005) also stated that VAMWCNT are exceptionally compliant with an elastic modulus of approximately 50MPa (as compared with Au, 77GPa). With this compliant characteristic it can reduce the wear and degradation during two electrodes in dynamic contact as stated by Bult et al. (2008) [73].

For this to materialize, the challenge is to fabricate or synthesise a dense forest of vertically aligned CNT and CNT metal composite on the contact so that it can be applied to MEMS relays and ultimately to see its behaviour, adaptability and reliability on MEMS relay contacts.

2.8 CNT's Fabrication Methods

In this section the fundamental techniques to grow CNT are reviewed. The fabrication or synthesis methods to produce carbon nanotubes include arc-discharge, laser ablation, and chemical vapour deposition. Iijima (1991) first

observed nanotubes synthesized by using electric-arc discharge methods as shown in Figure 2.16 [89]. Two high purity graphite rods were used as anode and cathode. Both rods are brought close together under a helium atmosphere and a voltage is applied until a steady arc is achieved. The anode was consumed and the gap between anode and cathode had to be kept constant by adjusting the position of the anode. Fibrous carbon nanotubes and other carbon particles were deposited on to the cathode.

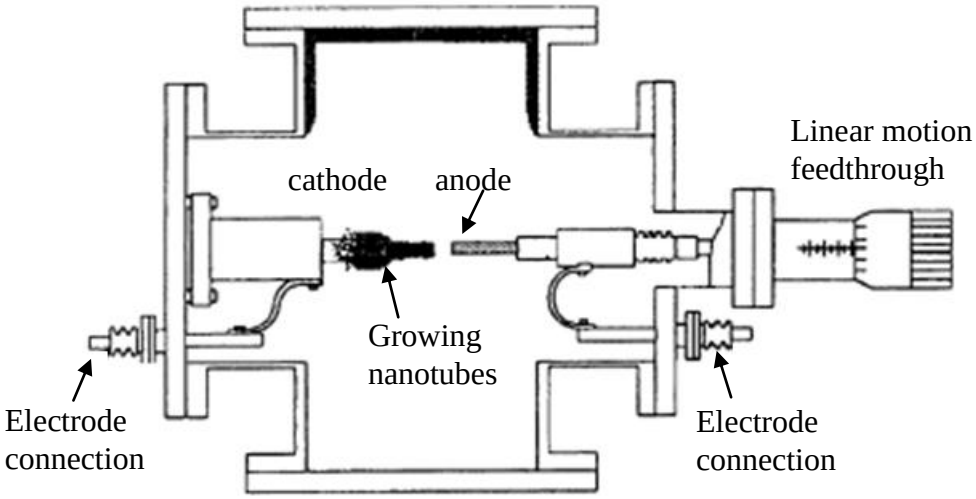

Figure 2.16: Schematic arc-discharge technique [90].

In the laser ablation technique shown in Figure 2.17, a laser was used to vaporize a graphite target held in a controlled atmosphere oven with Argon gas at a temperature of 1200ºC and pressure of 0.7bars. The condensed material was then deposited on a water-cooled target, which is the copper collector.

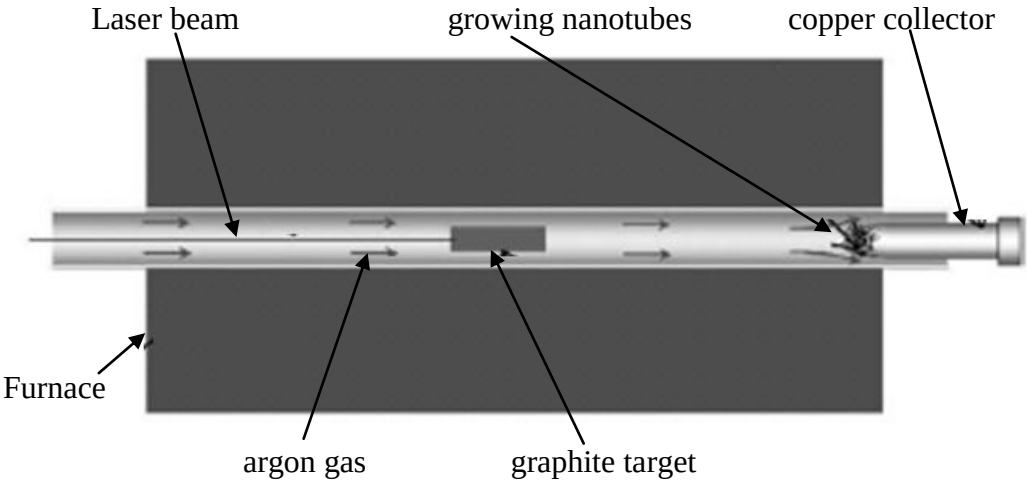

Figure 2.17: Schematic laser ablation process [91].

Chemical vapor deposition (CVD) is widely used in the semiconductor industry, as part of the semiconductor device fabrication process, to deposit various films such as polycrystalline and amorphous materials, SiO_2, silicon germanium, tungsten, silicon nitride, titanium nitride, and carbon nanotubes. Chemical vapour deposition (CVD) as shown in Figure 2.18 is achieved by using a commonly used carbon-containing gas such as carbon monoxide and low molecular weight hydrocarbons. The gas is heated up by an energy source such as plasma or a resistively heated coil to around 600 - 1200ºC [92]. The importance of the growth temperature can be seen in the experiment performed detailed in Appendix 1. The carbon diffuses towards the sample, which is heated and coated with a catalyst typically nickel, iron or cobalt, which grows the carbon nanotubes.

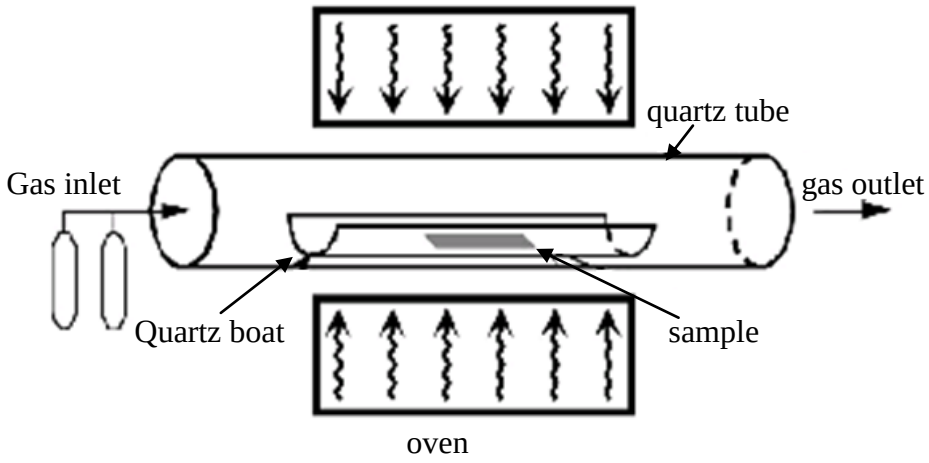

Figure 2.18: Schematic typical chemical vapour deposition (CVD) [93].

When comparing Arc-discharge and laser ablation with CVD, CVD has distinct advantages over the other two processes. This propels us towards the use of CVD for growing CNT in the present work. Arc-discharge and laser ablation have limits on the volume of material it can produce. Moreover, they need purification steps to separate CNTs and undesirable by-products such as other carbon particles. The CVD process produces pure CNT's in high quantities. Furthermore CVD has the ability to synthesize aligned forests of single walled carbon nanotubes (SWCNT) with controlled diameter, length, straightness and compactness as shown in Figure 2.19.

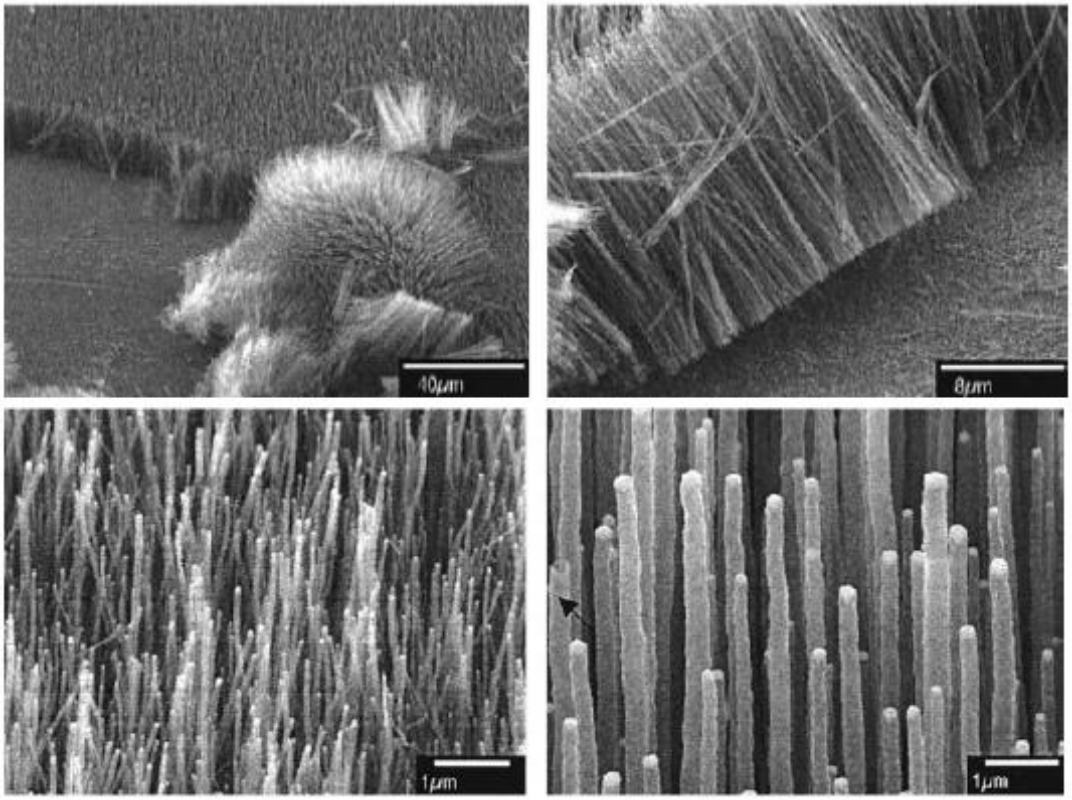

Figure 2.19: Micrograph showing straightness, different diameter and compactness of CNT produced by PECVD [94].

By adjusting the thickness of the catalyst it is possible to control the diameter of the CNTs. Controlling the growth time and temperature respectively can control the length and graphitization of CNT. By introducing carbon monoxide as the carbon source forests of SWCNT can be produced with high purity [95]. Aligned SWCNT can be produced by using Plasma Enhanced CVD (PECVD) where the plasma can be excited by a DC source or a Microwave source.

In an experiment conducted by Bower et al. (2000) to prove that PECVD grows aligned SWCNT, used PECVD for two minutes followed by 70 minutes with the plasma off [96]. The result is shown in Figure 2.20. The portion in which the plasma is on the SWCNT is aligned and portion where plasma is off shows a random and curled SWCNT. When a DC source is used the CNTs grow in the direction of the plasma and if microwave frequency is used the CNTs grows normal to the surface of the substrate as shown in Figure 2.21.

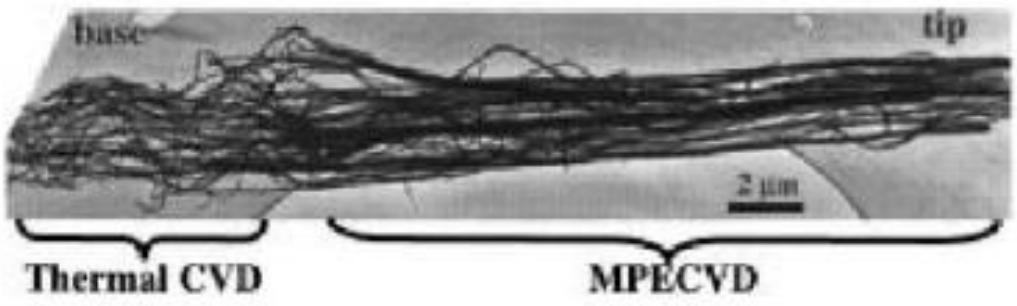

Figure 2.20: Micrograph showing the influence of microwave plasma enhanced chemical vapour deposition (MPECVD) on the SWCNT [96].

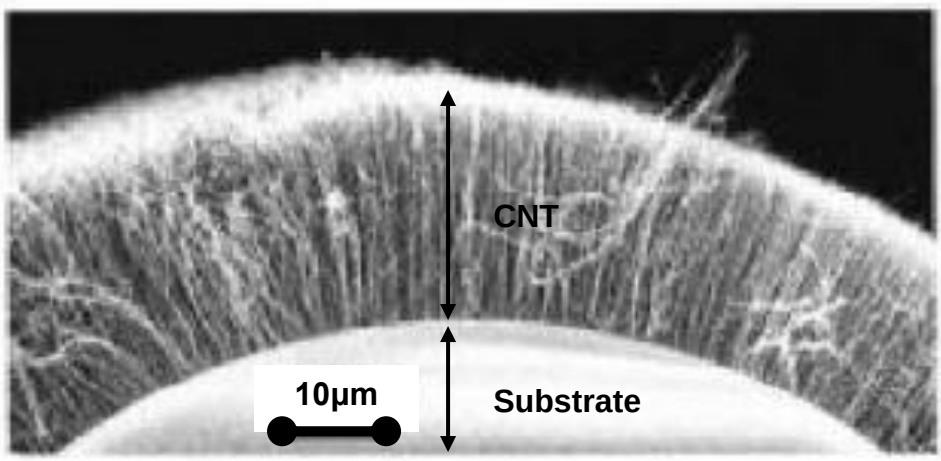

Figure 2.21: Micrograph showing SWCNT growth normal to the surface of a substrate using MPECVD [96].

It is obvious that CVD has the potential to grow a dense forest of CNT that is aligned, having required length, and diameter for the present research. The success of this approach will be shown later in chapter 4.

2.9 Analytical model

As stated by Yaglioglu et al. (2006) in the case of contacting CNT, the effective area calculation was not straightforward as the CNT film was made of tangled carbon nanotubes and the theory was difficult to apply directly [72]. No attempt was made to calculate the contact resistance of a thin film of CNTs, in particular for a dense forest of vertically aligned multi-walled carbon nanotubes surfaces. The following calculation was developed for a short forest of SWCNTs [81], with the purpose to show the potential of having SWCNTs instead of MWCNTs. In this study a dense forest of vertically aligned MWCNTs and in a future work, this

will be replaced with SWCNTs. This is because SWCNTs is claimed to have a lower resistivity [81] and a better performance (in term of their strength and resilience) than VAMWCNTs surfaces [88]. This would materialize if a plasma enhanced chemical vapour deposition (PECVD) were used. It would be interesting to compare the results here with the experiment performed on SWCNTs surfaces, but as for now the following calculations were produced.

Although silicon carbide and diamond are ideal MEMS relay materials because of their mechanical properties, unfortunately, they still have high resistivity. Resistivity is important in determining the contact resistance of a material both theoretically and practically. Currently, the best resistivity for NH_3 doped silicon carbide and ruthenium-doped DLC are $1.0 \times 10^{-4}\Omega m$ and $1.0 \times 10^{-5}\Omega m$ respectively. As indicated by Coutu et al. (2004), Au-alloys such as Au-(6.3%)Pt was still the best material that can be utilized on MEMS relays with resistivity of $7.17 \times 10^{-8}\Omega m$ [50].

To demonstrate the importance of resistivity, a simple model to approximate the contact resistance of silicon carbide, ruthenium-doped DLC and Au-(6.3%)Pt using equation (2.2.5), has been constructed. Even though this formula gives an error (around 3 orders of magnitude) in calculating the contact resistance compared with the experiment it can be used to compare and approximate the theoretical contact resistance model of different materials. Assuming the contact radius is 10μm and using the above resistivity values the calculated contact resistances are 5Ω, 0.5Ω and 3.6mΩ respectively. This shows that theoretically the contact resistance of the Au-(6.3%)Pt is much lower than the two materials, thus this is still preferred as a contact material.

By using a simple model to calculate the electrical or resistive loss due to power dissipation through the microstructure using the classical theory, it is possible to estimate the overall effect of different electrode materials on the MEMS relay. There are different types of MEMS relay design as described in chapter 1. Generally a MEMS relay with an anchored micro-cantilever and a contact at the tip is commonly in use. The cantilever can be fabricated using the same

material as the contact and the cantilever as shown in Figure 2.22 and will be isolated by an interlayer of dielectric material such as SiO_2.

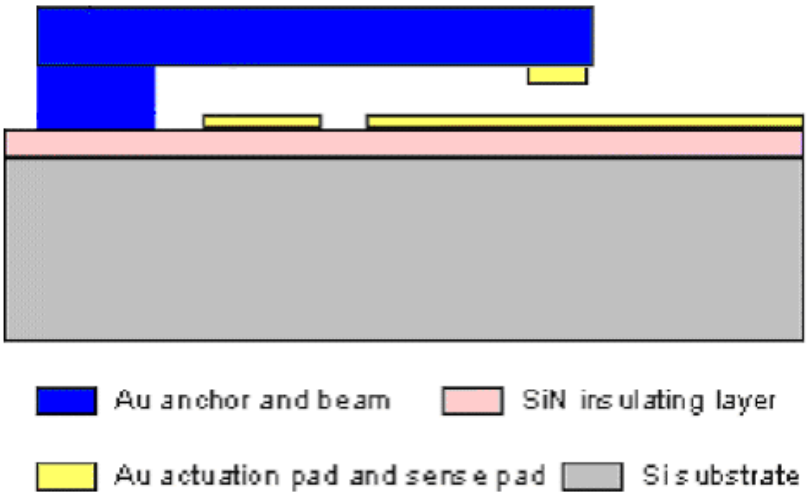

Figure 2.22: Au micro-relay cross-section [2].

To calculate the electrical or resistive loss of a typical MEMS relay microstructure a system using the material indicated in Table 2 is considered (refer to Appendix 2). It is assumed that the current, I is 1 mA and the contact radius, α is 10μm, the cross-sectional area of the cantilever, A is 2 x $10^{-10}m^2$ (having thickness 2μm and width 100μm) and the length of the cantilever is varied between 900μm to 1.5mm and resistivity of different materials (these materials are used in MEMS relay) is that shown in Table 2.

Material	Resistivity (Ωm)	Ref
Gold	$2.24x10^{-8}$	[52]
Silver	$1.58x10^{-8}$	[52]
Silicon	640	[52]
DLC	$100x10^{8}$	[52]
Au-(6.3%)Pt	$7.17x10^{-8}$	[50]
Au-(6.4%)Ag	$6.20x10^{-8}$	[50]
NH_3-doped SiC	$10x10^{-5}$	[54]
Au-doped DLC	30	[60]
Ruthenium-doped DLC	$1.0x10^{-5}$	[62]
Boron-doped DLC	$7.5x10^{-5}$	[55]

Table 2: Resistivity of materials.

Thus the following log-graph of Electrical loss (W) against the Length of Actuator (μm) is generated.

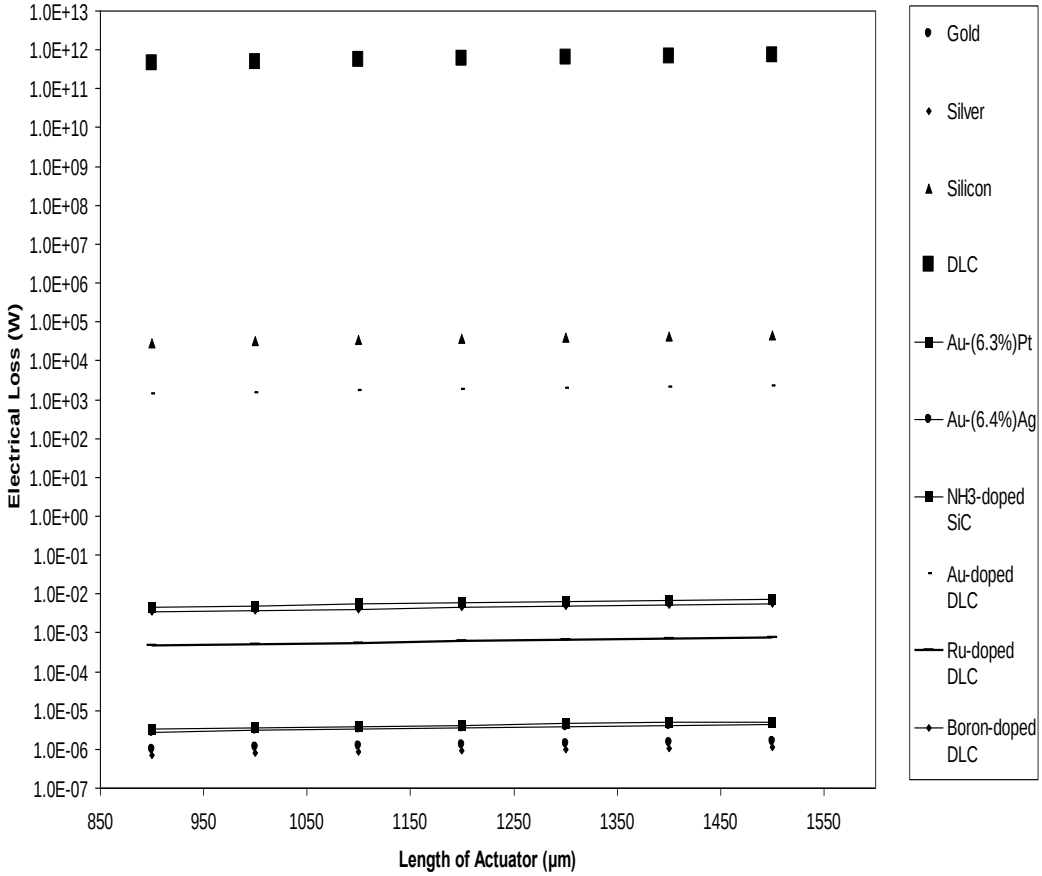

Figure 2.23: Log-graph of electrical loss against length of actuator.

Although silicon carbide and Ru-doped diamond have advantages over gold and its alloys in terms of its mechanical properties, it has a higher electrical loss than gold alloys as shown in Figure 2.23. Ruthenium-doped DLC and NH_3-doped SiC have three to four orders of magnitude greater loss respectively compared to Au-alloys. This is undesirable for MEMS relays because it can affect the overall performance of MEMS devices. Therefore alternative materials need to be investigated to increase its overall performance.

CNT is the material that can substitute other materials because of its excellent mechanical and electrical properties. Using a simple model to calculate the

contact resistance using equation 2.2.5 with the following materials and assuming the contact radius is again 10μm, the resistivity is as shown in Table 3.

Material	**Resistivity (Ωm)**	**Contact Resistance** (Ω)	**Ref**
Au-(6.3%)Pt	7.17×10^{-8}	0.0036	[50]
Boron-doped DLC	7.5×10^{-5}	3.75	[55]
Boron-doped CNT	7.4×10^{-7}	0.037	[97]
CNT	5.3×10^{-6}	0.27	[97]
CNT-Metal Composite	0.35×10^{-8}	0.0002	[81]

Table 3: Resistivity of CNT, Au-alloy and doped DLC.

In all the above calculations it is assumed that surface contact is smooth and there is no formation of a thin film or contaminants. It is observed from Table 3, that the contact resistance of the CNT-metal composite was much less than for the Au-alloy. Now it would be useful to use a simple model to calculate the resistive loss of the above material to determine its overall performance. Assuming the current I is 1mA and the contact radius varies from 1μm to 30μm, then by using the equation 2.2.17 (refer to Appendix 2) and substituting R into the contact resistance equation 2.2.5, the following graph is generated as shown on Figure 2.24. This graph shows that the resistive loss of a CNT coated contact is several orders of magnitude lower than Boron-doped diamond and approximately one order of magnitude lower than for Au-alloys. This is because of the resistivity of the CNT-metal composite is much lower than Au-alloys.

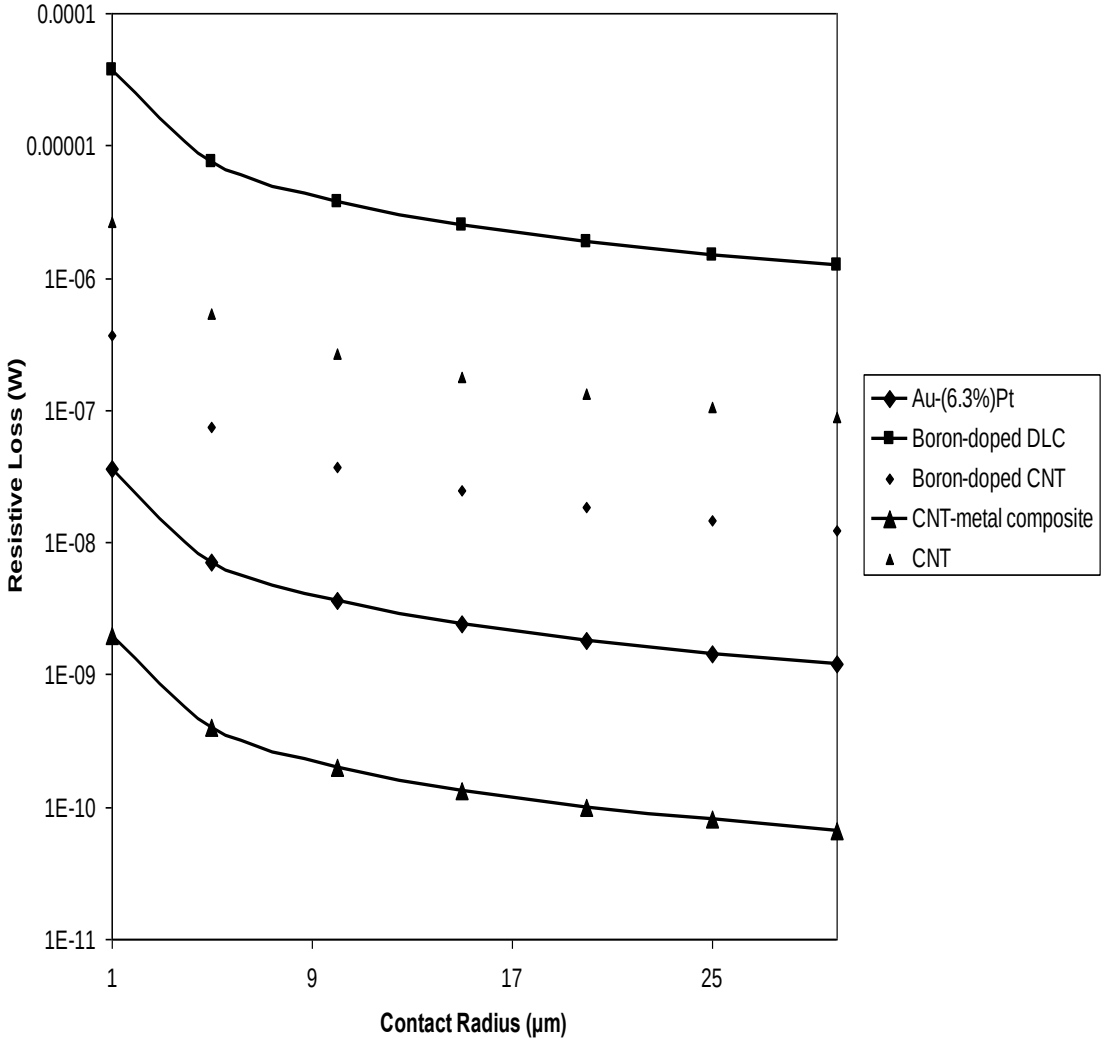

Figure 2.24: Graph of resistive loss against contact radius.

To obtain a realistic calculation of the resistive loss with current passing through it at 1mA, the applied force and plastic or elastic-plastic deformation needs to be considered for the contact surfaces as stated by Holm (2000) [44] and Coutu et al. (2006) [14].

It is assumed that the MEMS relay consists of a cantilever with the length 1mm and area $2x10^{-10}m^2$ (having thickness 2µm and width 100µm) and contact pad as shown in Figure 1 (see Appendix 2) of which is made from Au or Cu/CNT composites. By substituting Holm's or Coutu's analytical model into equation 2.2.18 the equation below is formed:

Resistive loss for plastic deformation (W) = $I^2(\rho L/A + R_c)$ (Equation 2.2.19)

Resistive loss for elastic-plastic deformation (W) = $I^2(\rho L/A + R'_c)$ (Equation 2.2.20)

where $R_c = \left(\frac{\rho^2 \eta \pi H}{4F} \right)^{\frac{1}{2}}$ for plastic deformation (From equation 2.2.6)

And from Coutu et al. (2006), modified contact resistance,

$R'_c = R_c\ (ballistic) + \Gamma(K)R_c\ (diffusive)$

(From equation 2.2.8)

By substituting the Au and CNT/Cu composites data (from Table 4) into equation 2.2.6 and finally into equation 2.2.19 the "Resistive loss for plastic deformation" is plotted as shown in Figure 2.25. Then again by substituting the Au and CNT/Cu composites data (from Table 4) into equations 2.2.9 and 2.2.10 and then into equation 2.2.8 and finally into equation 2.2.20 for "Resistive loss for elastic-plastic deformation" is plotted as shown in Figure 2.25. This graph "resistive loss (W) against applied load" has an applied force ranging from 10µm to 1mN.

Material	Hardness	Poisson's ratio	Resistivity
Au	1.7GPa [14]	0.42 [14]	2.24×10^{-8}
CNT/Cu composites	1.1GPa [79]	0.19 [98]	0.35×10^{-8} [81]

Table 4: Material properties for Au and Cu/SWCNT composites.

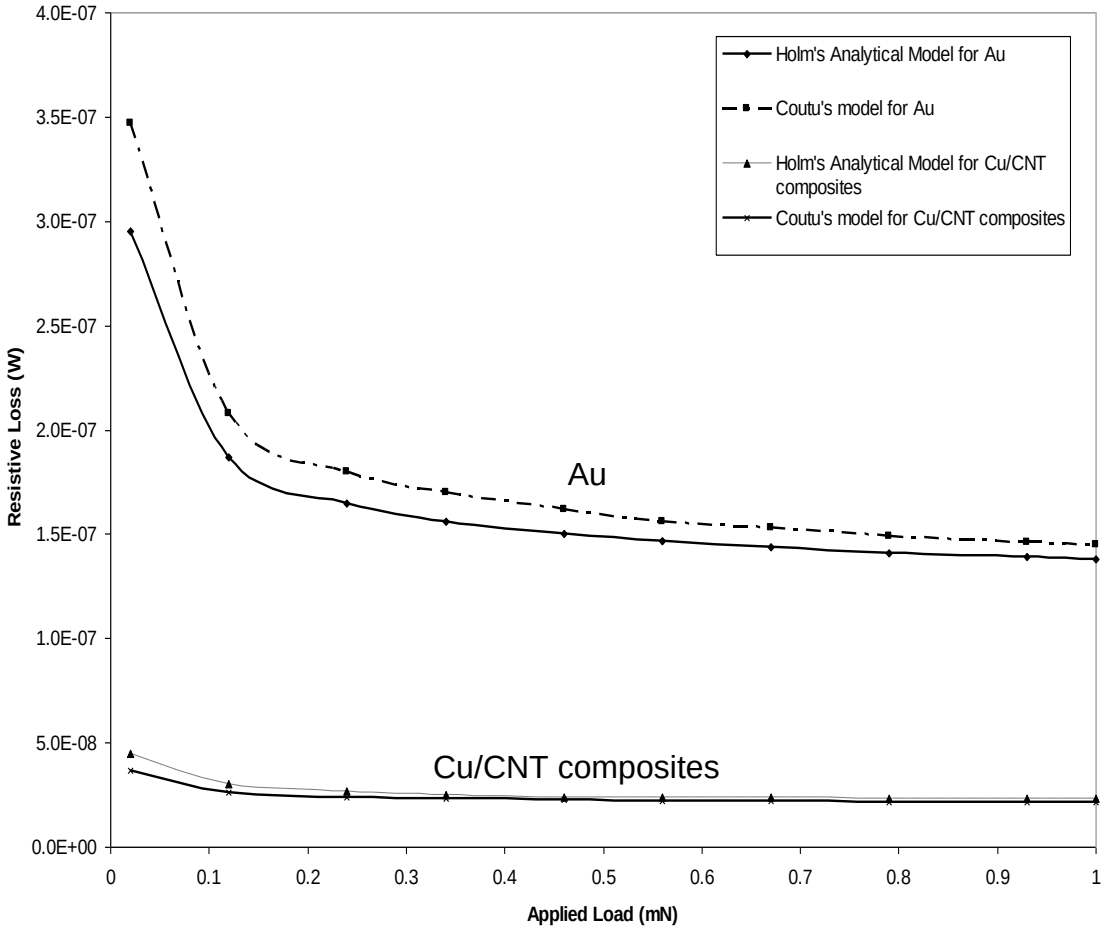

Figure 2.25: Graph of a calculated resistive loss against applied load for Au and CNT/metal composites.

The graph shows that the resistive loss for CNT/metal composite using Holm's or Coutu's analytical model is several orders less than the Au contact. From here it is indicative that theoretically the CNT has potential and shows that CNT can have lower contact resistance and resistive loss. This is attractive to the MEMS and electronics industries.

2.10 Summary

This chapter has presented an overview of solid-solid interface mechanics theory of electrical contacts. The factors that could affect the choice of formulas to estimate electrical contact resistance in plastic deformation were reported. The electrical contact theory was presented for homogenous bulk contacts and presented errors when compared with the experiments results. Furthermore, with the use of low force (ranging from tens of μN to a few mN) conditions the

analytical model needs to be modified. Coutu et al. (2006) has considered the contact mechanics and the associated contact resistance of Au and its alloys under the low force conditions typical of MEMS relays [14].

The author considered that the conduction process could be dominated by a mixture of ballistic and diffusive electron transport models. The new contact model was presented and compared with the classical electrical contact. The graph in Figure 2.5 shows that the new analytical model and the Holm's analytical model are similar in form, but predict a slightly higher contact resistance than the classical model. This is due to the following:
(1) the classical model assumes bulk solid-solid contacts rather than thin metal films;
(2) the classical analytical model only consider plastic deformation but the new analytical model considers the possibility of elastic-plastic deformation;
(3) the new analytical model uses a single effective a-spot rather than multiple a-spot;
(4) during the ON-state the conduction is considered to be a mixture of ballistic and diffusive electron transport; and
(5) the contact load discontinuity is accounted for in the new model.

In the objectives of this research a new experimental set-up is prepared, a new material and its fabrication is utilised. Therefore we need to look at experimental trends for electrical contacts. The most common material used in the experiment is Au and its alloys but due to poor mechanical properties failure occurs, thus alternative material need to be developed. More recent experiments show that CNTs offer good mechanical and electrical properties and that they have good potential to be used in MEMS relay contact applications.

Experiment performed by Yaglioglu et al. (2006) and Bult et al. (2008) show the potential for CNTs in such applications [72,73]. In Yaglioglu et al. (2006) they have used tangled SWCNT surfaces [72]. They mated two films of tangled SWCNT surfaces and the contact resistance was higher than with Au-plated ball-SWCNT contact pair at the maximum applied force of ~150mN. To reduce

the contact resistance further (which is desirable on a MEMS relay) the applied force has to be increased but this will go beyond the MEMS relay's applied force (typically ~1mN). An approach by Bult et al. (2008) was developed to decrease the contact resistance [73]. They used vertically aligned MWCNT (100µm thick) and infiltrated them by sputtering Au with a thickness of 5µm. It reduces the contact resistance but the size of the samples poses drawbacks in integrating it on to MEMS relays. Furthermore, they performed 3000 cycles and showed no degradation on the CNT surface but for reliability testing it needs to be greater than 10^6 cycles (preferably for MEMS relays $>10^{10}$-10^{11} cycles). This is in order to achieve a more realistic testing of contact materials. In this study a thinner Au/MWCNT composite, typical maximum applied force of MEMS relays and reliability testing greater than 10^6 cycles are used.

Furthermore, most of the experiments replicate the actuation of the contact in a controlled environment using an environmental chamber. This is to mimic the actuation of hermetic MEMS relays. Packaging hermetic MEMS relays is expensive therefore it would be economical to have non-hermetic MEMS relays. Furthermore, CNT tends to produce a low contact resistance in ambient air than in vacuum. Moreover, due to its controllability, the experimental set-up in this study is done using a modified nano-indentation apparatus and PZT actuator incorporating the sample and the experiment is done at constant temperature and normal atmospheric conditions.

CHAPTER 3: RESEARCH METHODOLOGY

3.1 Introduction

This chapter explains how gold is coated and the CNT surface is synthesized on the substrate. The deposition of a thin film and the growing of CNT on the contact can be achieved using sputterer and CVD apparatus. The Au-Au and Au-MWCNT and Au-Au/MWCNT composite contact pair samples are used as a reference for the performance of in terms of their mechanical performance and contact resistance. With these samples a testing method looking especially at the micro-tribology, micro-mechanical properties [99], chemical composition and electrical phenomena [100] is set up. The procedure uses a modified nano-indentation apparatus where the diamond nano-indenter tip is replaced with an Au hemispherical probe to replicate the real mechanics of MEMS relay's contact actuation. Due to the limitation of the modified nano-indentation apparatus to apply a sufficiently large number of cycles, a PZT actuator is used to support the sample planar or substrate coated surfaces. This test rig is used to mimic the actuation of a relay. This will help to understand better the performance and reliability of the contact materials.

3.2 Samples for modified nano-indentation apparatus

In the modified nano-indentation apparatus experiment, there are three specimen configurations:

1) "Sample 1" is a Au-Au contact pair,
2) "Sample 2" is a Au-MWCNT contact pair, and
3) "Sample 3" is a Au-Au/MWCNT contact pair.

The fabrication methods are explained as below:

The hemispherical probe and flat substrate material under study are Au to Au, Au to multi walled carbon nanotubes (MWCNT) and Au to Au/MWCNT composite contact pairs. If a flat to flat surface contact is used there will be an issue of the top and bottom electrode not making the full contact due to tilting of the surface, thus to avoid this hemispherical probe is used. The hemispherical

probe sample (2mm in diameter) represents the movable contact electrode of a MEMS relay and is sputtered with Au 500nm thick. Sputtering is selected as the chosen method of metal deposition instead of evaporation so as to ensure good deposition coverage [101]. Moreover sputtered gold is known to have a higher hardness which is expected to minimize surface damage of the metallic contacts [41].

The surfaces are mounted inside the chamber of the sputterer apparatus (Figure 3.1) under a reduced pressure of approximately ~1.9x10^{-2}mbar. Low pressure is necessary to reduce contamination. The deposition process involves thermally emitted electrons, which collide with inert gas atoms such as Argon gas, which accelerate towards and impact upon a negatively charged electrode that is a target (for example gold disc) for the coating material. The impacting ions dislodge atoms of the target material, which are in turn projected to and deposited on the hemispherical probe or substrate to form the thin layer.

The next deposition process is on the silicon substrate (~5mm by ~5mm), which is sputtered with 500nm thick gold contact layers. This thickness is chosen because it replicates typical MEMS relay contacts [9,42,51,102,103]. This sample is fabricated as a baseline with which to compare MWCNT and Au/MWCNT contact resistance.

Figure 3.1: Kurt J. Lesker sputterer, University of Southampton.

To produce a dense forest of MWCNT on the silicon wafer, thermal CVD is used. This apparatus is shown in Figure 3.2(a). To grow carbon nanotubes a catalyst is needed. Commonly used catalysts include nickel, iron or cobalt. In this experiment, Fe catalyst and the under-layer of Al_2O_3 are deposited onto a silicon substrate (5mm by 5mm) by sputtering. The Fe catalyst is used because of its ability to catalytically decompose gaseous carbon-containing molecules [104]. The thickness of Fe and Al_2O_3 is ~2nm and ~7.5nm respectively, and with thicker Fe catalyst layer (≥ 1nm) a rapid and thicker growth of MWCNT will occur [105]. The Al_2O_3 was sputtered first followed by Fe. Aluminium oxide is a good catalyst support for nanotube growth [106]. Al_2O_3 acts as a buffer layer [107], de-wets the catalyst to form discrete particles and strong dispersion effects [108]. Barrier layers (buffer layers) are the layers sandwiched between a catalyst and a substrate. This is to reduce undesired catalyst-substrate chemical reactions, atomic diffusion and oxidation of the catalyst which in turn support and influence the growth and purity of the CNTs, and as thick as ≥ 5nm Al_2O_3 is enough to act as buffer [109]. The wafer with the Fe catalyst and Al_2O_3 under-layer is loaded in the thermal CVD. The thermal reactor consists of a one-inch-diameter quartz tube enclosed in a high-temperature furnace and equipped with mass flow controllers to monitor the feed gases as shown schematically in Figure 3.2(b).

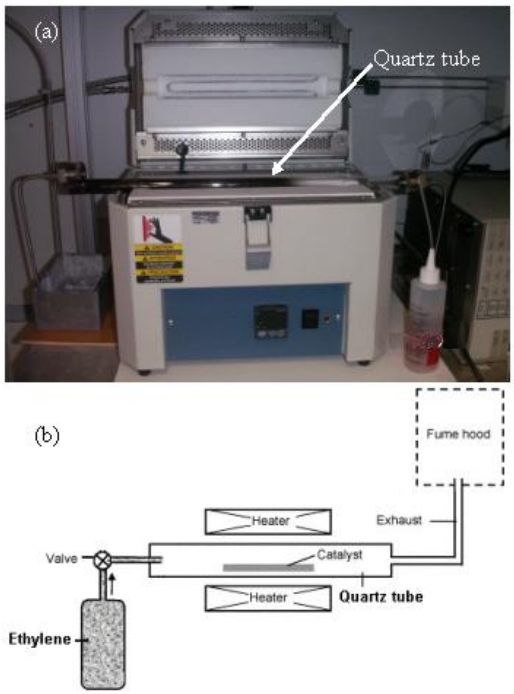

Figure 3.2: (a) Thermal CVD and (b) schematic diagram of thermal CVD.

The reactor is purged with argon and hydrogen while the furnace is heated to 875^{o}C (growth temperature). At this temperature a dense forest of vertically aligned MWCNT was achieved (this is shown in the experiment performed by Dr David Smith at different growth temperature, as shown in Appendix 1). After the furnace reaches the growth temperature, it is allowed an additional 5 minutes for the temperature to reach equilibrium and an annealing process occurs on the catalyst. The gas flow is then switched to ethylene for 3 minutes. The carbon will diffuse towards the substrate, which is heated and coated with the Fe catalyst, which grows carbon nanotubes. After the growth process is complete, argon flow is used to purge ethylene from the tube and prevent backflow of air into the tube. The furnace is cooled below 300^{o}C before exposing the MWCNT coated specimen to air to avoid damage to it at elevated temperatures. The last sample is the Au/MWCNT composite as shown in Figure 3.3, which is produced by sputtering Au directly on to MWCNT surfaces.

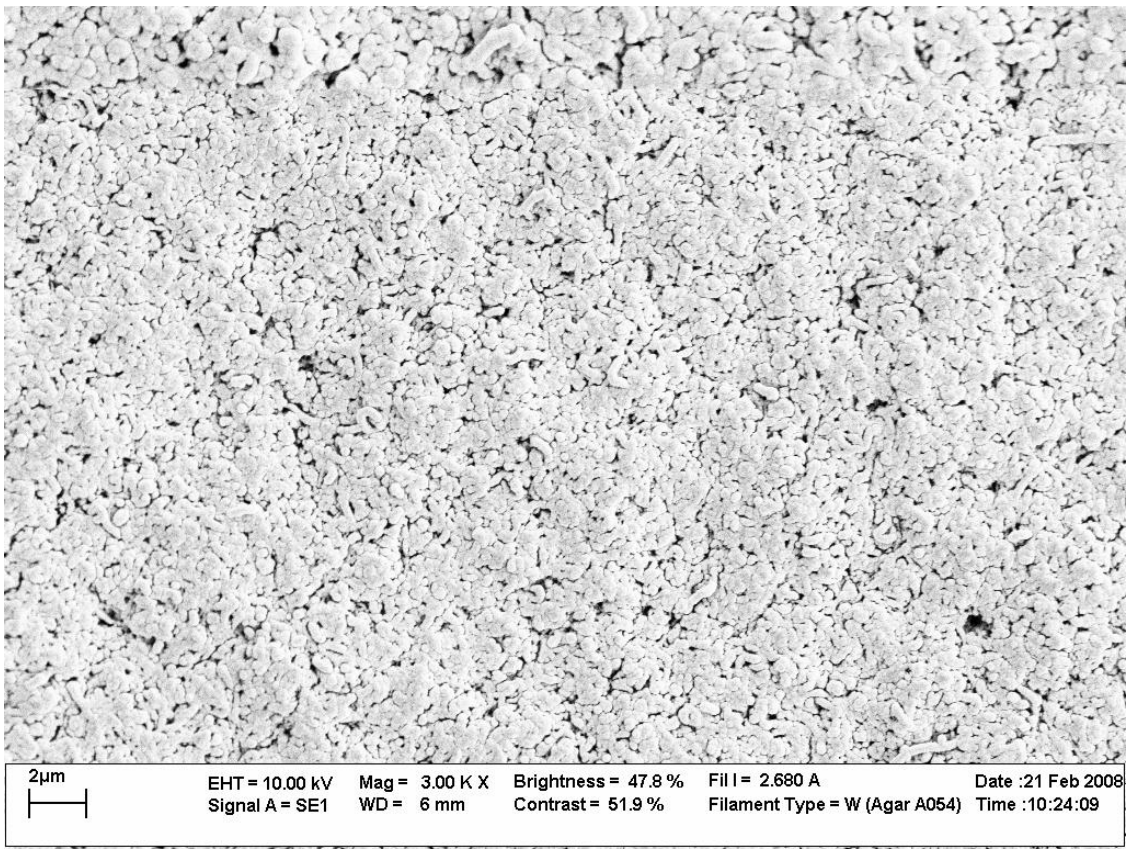

Figure 3.3: Top view of MWCNT composite sputtered with Au.

3.3 Samples for PZT actuator test rig

The PZT actuator test rig experiment uses the same samples as used in the modified nano-indentation apparatus (see section 3.2). The only difference is in the size of the silicon (Si) substrate used (~2mm by 7mm). This is so that the sample can be accommodated on the tip of the PZT actuator as shown in Figure 3.4.

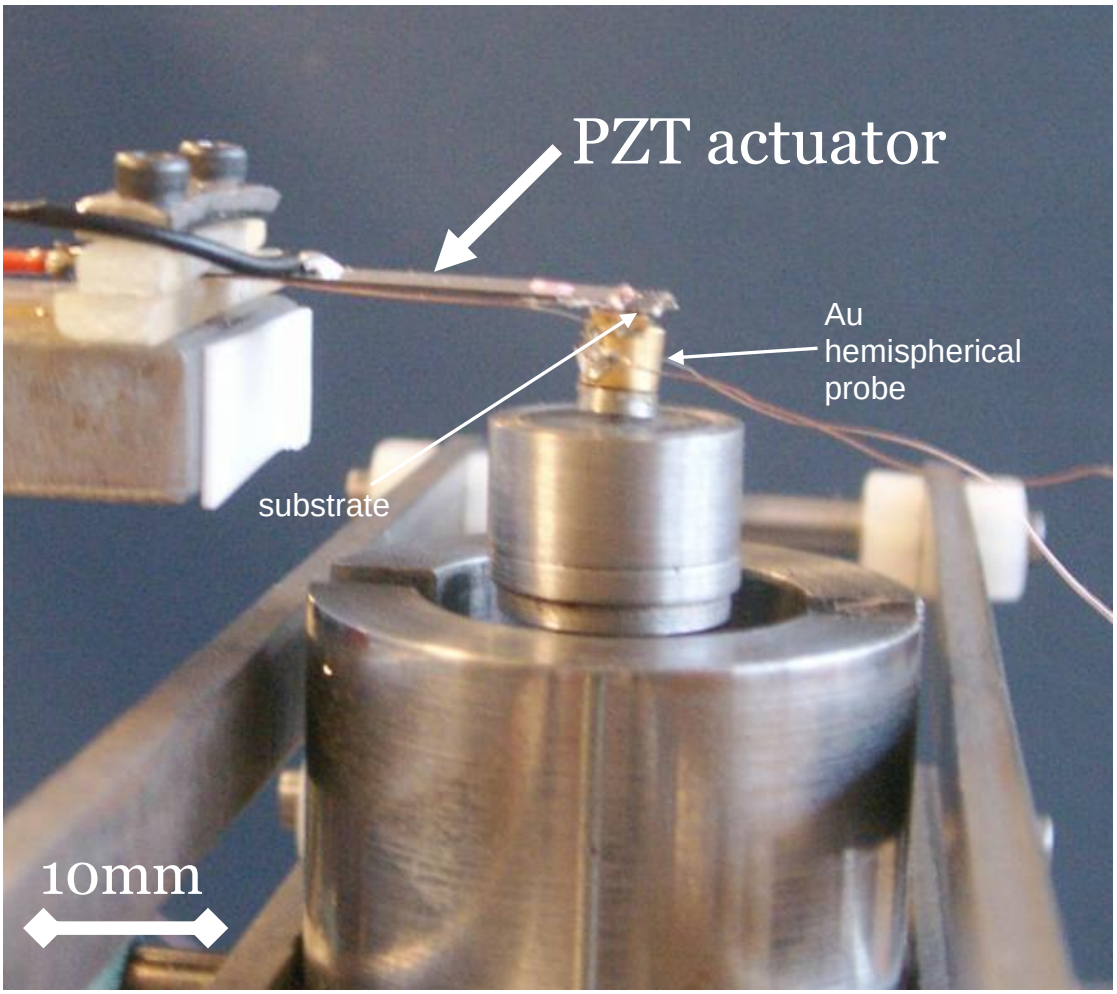

Figure 3.4: Side view of the PZT actuator with planar specimen attached.

3.4 Nano-indentation apparatus

3.4.1 Experiment 1: Modified nano-indentation apparatus

A modified nano-indenter apparatus is used in this experiment, by replacing the diamond indenter tip with a Au coated hemispherical probe as shown in Figure 3.5 (a) and (b) and a 4 wire measurement is attached onto the Au hemispherical probe and substrate as shown in Figure 3.6. The hemispherical probe is brought into contact with the coated substrate (Sample 1-3) at a controlled loading rate of 0.2mN/s until the maximum load of 1mN is reached.

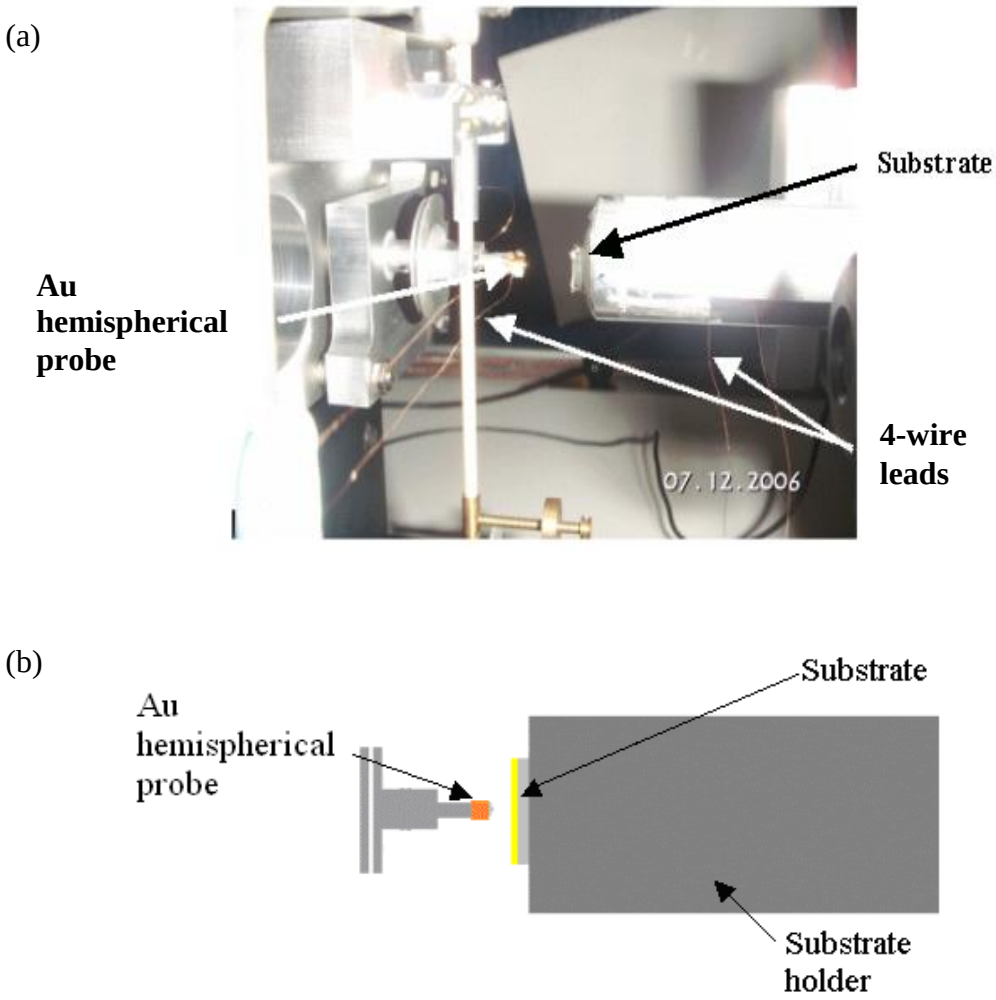

Figure 3.5: (a) Modified nano-indentation apparatus, (b) schematic arrangement of modified nano-indenter for Au hemispherical probe and coated substrate.

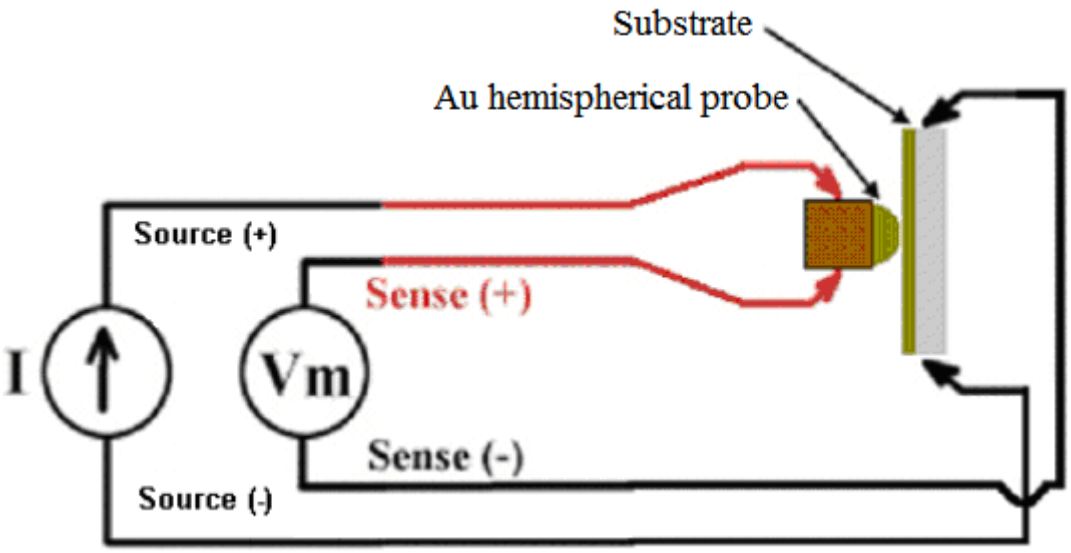

Figure 3.6: Schematic of contact zone with its electrode and contact resistance measurement.

Before going into detail about the experiment, a brief explanation of how the nano-indentation apparatus operates is given. The pendulum is the most important part of the nano-indentation apparatus as shown in Figure 3.7. When a current is passed through the coil it is attracted towards the permanent magnet, thus producing movement of the Au hemispherical probe towards the substrate. The displacement of the probe is measured by means of the capacitor plates. The capacitance changes between the two capacitor plates and this is measured by means of a capacitance bridge.

The substrate is brought towards the Au hemispherical probe by a DC motor that drives the micrometer stages in an XYZ configuration. The motor power supply is generated from the computer and the limit stop defines the maximum movement of the contact and the operating movement of the pendulum, when a load is applied. When the Au hemispherical probe and substrate are in contact the capacitance changes and this is translated to the force applied and displacement reading by the nano-indenter software system.

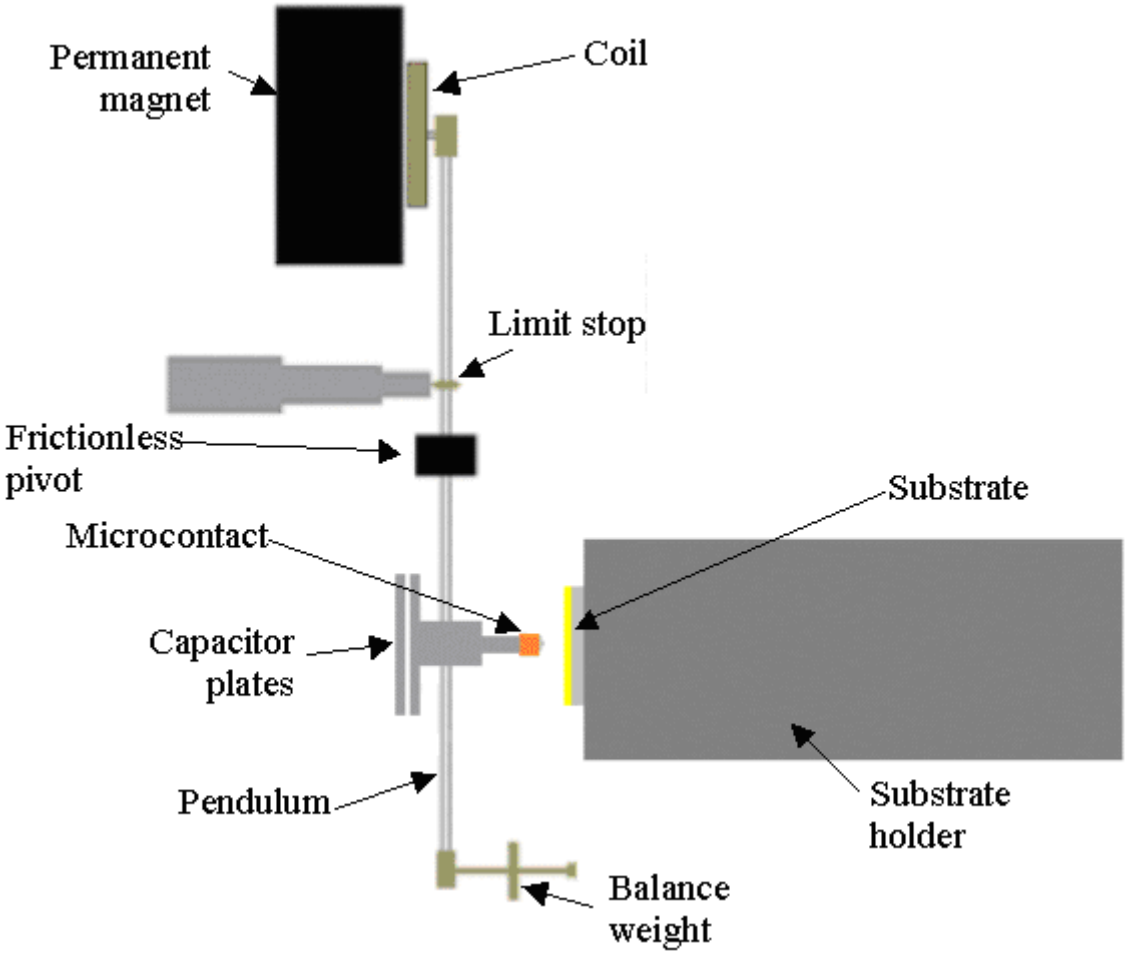

Figure 3.7: Schematic side view of nano-indentation apparatus [110].

Using this modified nano-indentation apparatus, the contact surfaces can be brought into contact at a maximum load of 1mN. This is to mimic a MEMS relay's contact action at low forces. The force used in this experiment is at the typical high end of the range commonly used in MEMS relay contacts [111,112,113]. In an actual MEMS relay, the force is achieved using MEMS actuators typically either by electrostatic, electromagnetic or piezoelectric actuation mechanisms. The force measurement is intrinsic to the apparatus and the contact resistance is measured using a 4-wire measurement method as shown in Figure 3.6. During contact, the targeted load is held for 10 seconds so that an average peak load contact resistance value can be determined. The electrode contacts are then unloaded at the same rate until they separate. Figure 3.8 shows an example of the contact resistance variation over one load cycle. Over the first 5 seconds as the contacts are loaded the contact resistance falls and then remains relatively stable during the holding time; during the

unloading period the contact surfaces remain together for 20 seconds, as a result of the Au on the two contact surfaces adhering. The procedure is repeated in order to detect any cyclic changes in the electrical contact resistances.

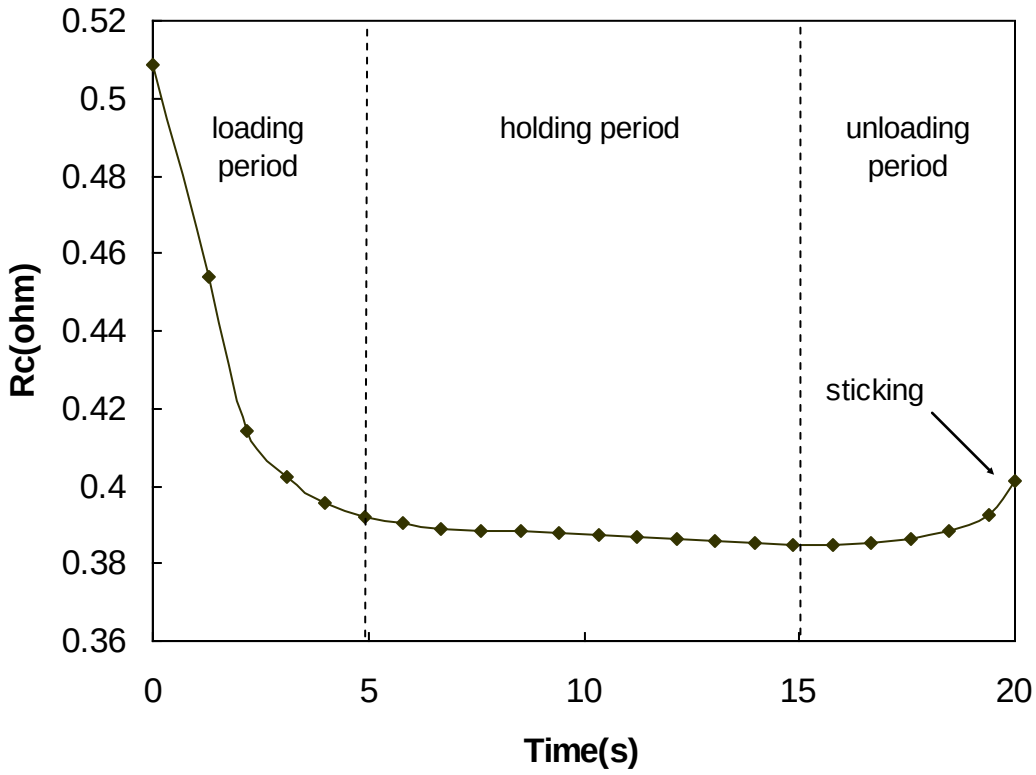

Figure 3.8: Example of one load cycle for Au-Au contact pair.

The DC current source across the contact is set at 1mA with a maximum supply voltage of 20mV using a Keithley 580 micro-ohmeter (Appendix A). The experimental apparatus is contained in a booth maintained at a constant temperature of ~31^{o}C to prevent thermal drift affecting the experiment due to expansion of the apparatus or the samples.

Figure 3.9 shows a graph of one load cycle versus displacement of Au-Au contact pair without the wires being attached. This data is extracted from the nano-indentation apparatus. The plot shows the load applied up to the maximum of 1mN loading (curve in region 1) and then unloading (curve in region 3) of the contact. Region 2 shows there is creep deformation that occurs over a period of time (in this experiment, the holding time is 10 seconds).

Region 4 is the permanent depth deformation retained after the contact pair separates.

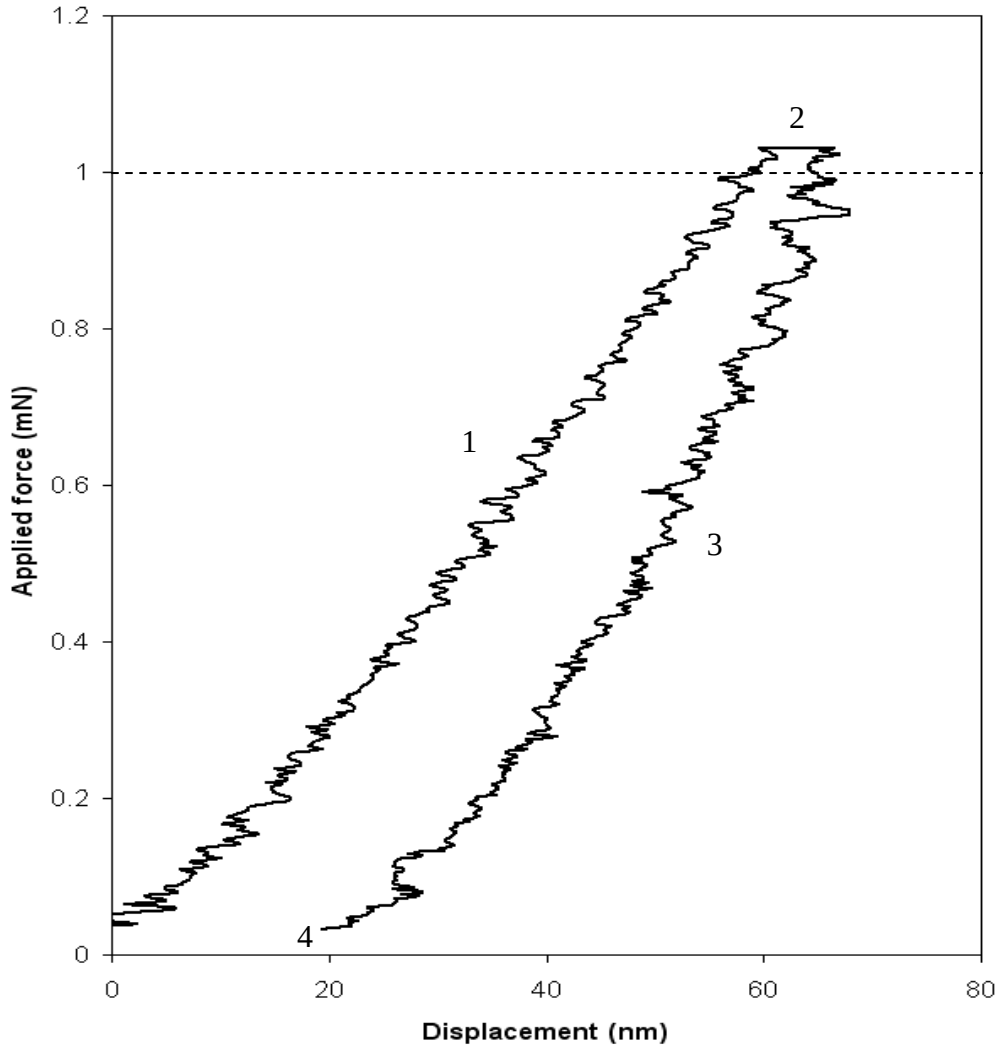

Figure 3.9: Graph of applied load against displacement for Au-Au contact pair.

Before the experiment can proceed a control measure is needed to make sure that the contact resistance measurement is between the two contact surfaces as shown in Figure 3.10 (a) and not the bulk resistance as shown in Figure 3.10 (b). By changing the width between the Sense (-ve) and Source (-ve) point on the substrate as shown in Figure 3.10 (c), the contact resistance was measured at two width positions of 5mm and 10mm apart.

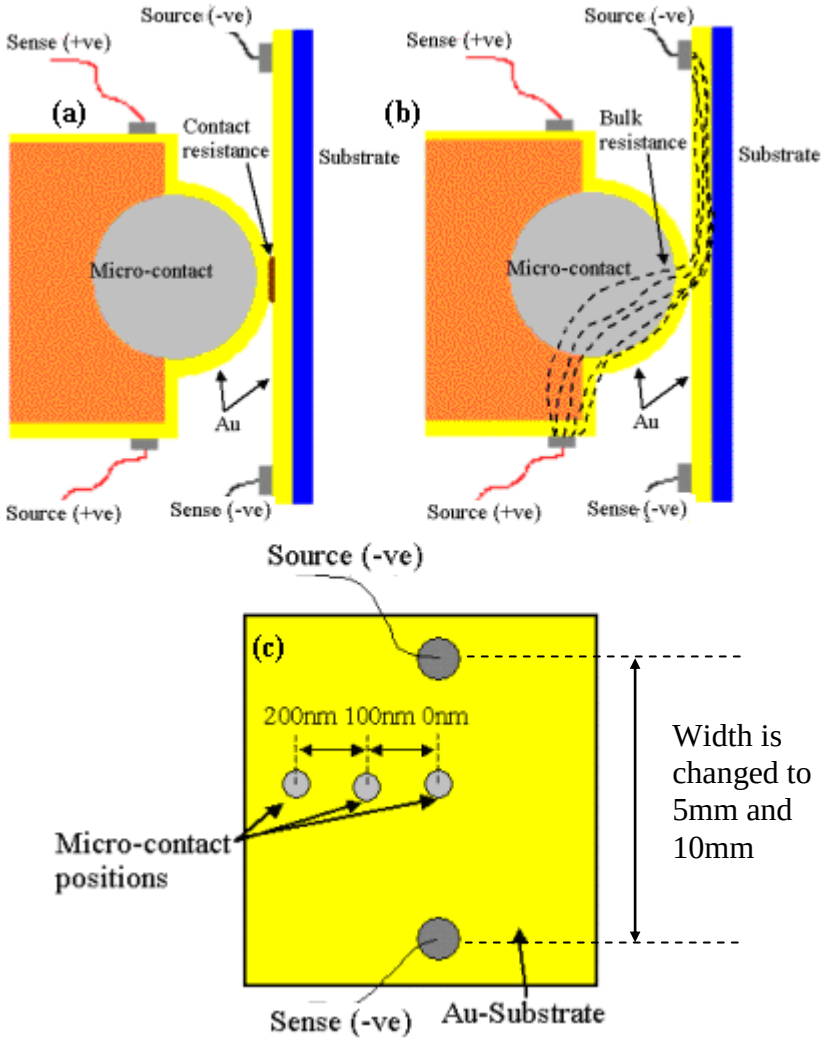

Figure 3.10: Side view of (a) contact resistance, and (b) bulk resistance and (c) top view-contact positions on the Au-substrate.

In addition the contact was moved across by 100nm and 200nm as shown on the schematic diagram in Figure 3.10 (c). Both tests gave the same resistance reading of ~0.38Ω. This shows that the 4-wire measurement method consistently measures the contact resistance and not the bulk resistance. In another control measure, the contact resistance across the Au contact with the substrate surface consisting of a coating of catalyst only (i.e. no MWCNT) is measured and no conduction is detected. This shows that the conduction mechanism is through the MWCNT and Au/MWCNT coatings and not the substrate.

3.4.2 Hemispherical Au contact tip

The design is detailed on Appendix 3 and 4. The ball bearing is recessed in the copper holder. Copper is used because it is readily available and is a good conductor. The copper holder is bonded with epoxy resin to a stainless steel tip as shown in Figure 3.11.

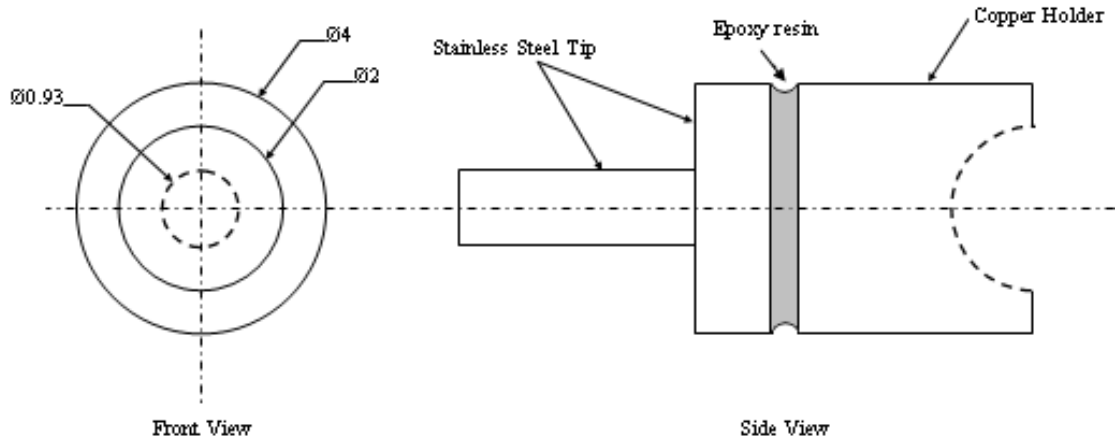

Figure 3.11: Copper holder bonded with epoxy resin.

The epoxy electrically isolates the copper holder and the ball from the main apparatus of the nano-indenter. To evaluate whether the epoxy resin can isolate the copper holder, the capacitance between the bonded samples can be calculated using the equation given [114]:

$$C = \frac{\varepsilon_R \varepsilon_o A}{d} \qquad \text{(Equation 2.2.21)}$$

Where;

ε_R - Dielectric permittivity constant for epoxy resin (constant value of 4).

ε_o - Permittivity of free space (constant value of 8.85 x 10^{-12}F/m).

A - Surface area (π x (2 x 10^{-3})^2) (m^2).

d – the gap between the bonded samples (approximately 10μm)

The capacitance is approximately 4.5 x 10^{-11}F. Measuring the potential drop using the micro-ohmmeter, which gives an overload resistance result, confirms

that isolation of the copper holder is achieved. The contact holder is then fitted onto the nano-indentation apparatus as shown in Figure 3.5.

3.4.3. The 4-Wire Measurement Methods

As shown in Figure 3.6, a 4-wire lead is connected to the contact and substrate. The micro-ohmmeter has four connections; two from the current source and the other two from the voltmeter called the “sense” lead. Generally, this measurement method is used because of its accuracy in measuring small contact resistance values.

To measure the contact resistance a 2-wire resistance measurement or 4-wire measurement technique can be used. In a 2-wire measurement only two leads are connected to the device under test. This set up has the advantage of using just two wires to connect to the sample but in 2-wire measurements the voltmeter is really measuring the voltage across the two samples and the test leads.

4-wire measurements can be attached to the contact and substrate as shown in Figure 3.6 and 3.7. It is best to connect them as near as possible to the contacting surfaces. It will give an accurate resistance measurement of the contacting surface without the resistance of the test leads. The contact resistance can be determined by using the current source, I and the potential drop, V and the formula to calculate contact resistance can be used as follows:

$$R_c = \frac{V}{I} \qquad \text{(Equation 2.2.22)}$$

The micro-ohmmeter converts the potential drop and current source to a contact resistance and this value can just be read off. The 4-wire testing is used because it can accurately measure contact resistances of less than 1Ω thus allowing measurement of resistance values lower than for 2-wire testing. This is important to the experiment because most MEMS relays have contact resistances less than 2Ω. Moreover as proved in the experiment shown in

Figure 3.10 (c), the contact resistance is measured between the contacting surfaces and not the bulk resistance.

3.5 PZT actuator test rig

3.5.1 Experiment 2: PZT actuator test rig (dry-circuit condition)

In order to determine the performance of the surfaces under repeated switching actions an apparatus has been designed (detailed drawing of test rig see Appendix 5), in which a PZT actuator is used to support the planar coated surfaces as shown in Figure 3.12 (a) and (b). This surface makes electrical contact with the hemispherical Au-coated probe to mimic the actuation of a MEMS relay contact. The apparatus has been designed to allow control of the gap and to allow the performance of the contact materials to be investigated ultimately over large numbers of switching cycles (>>10^6).

.

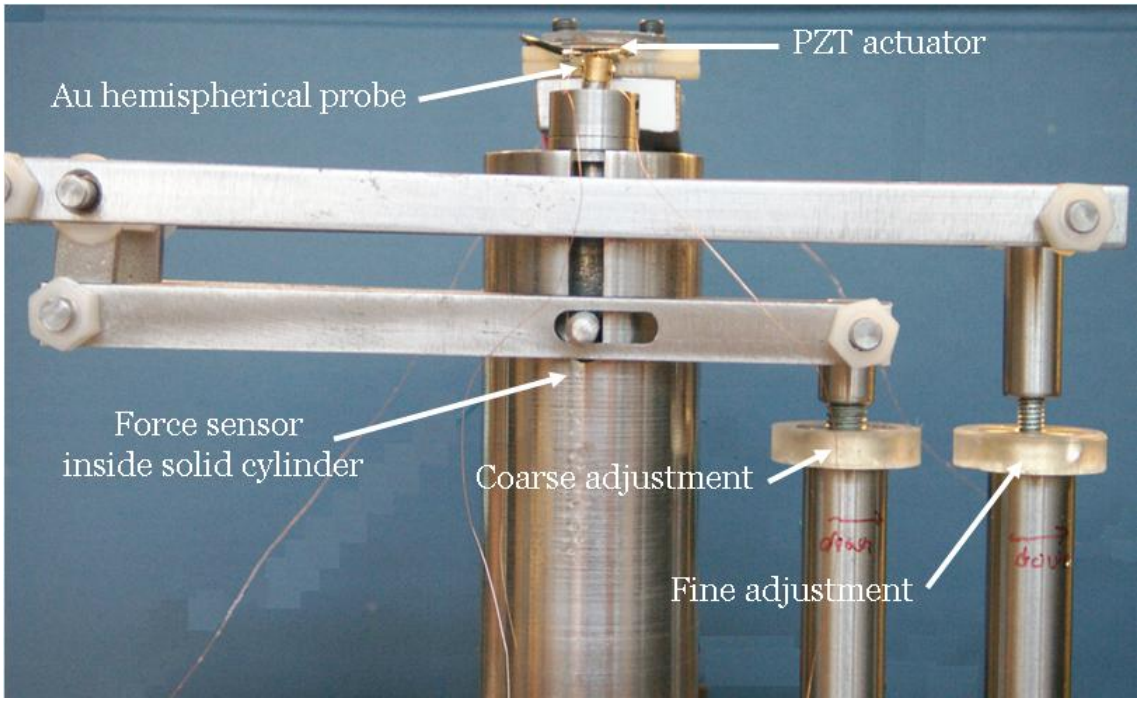

Figure 3.12: (a) Side view of the test rig with PZT actuator apparatus.

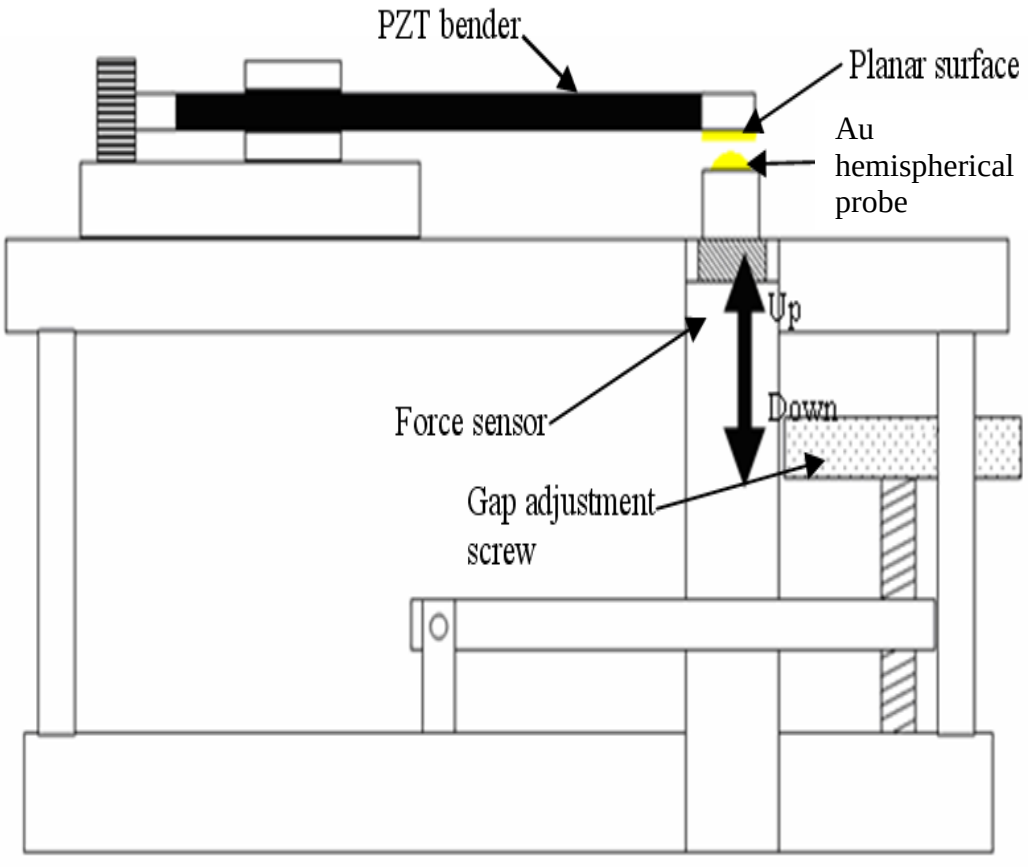

Figure 3.12: (b)Schematic side view of the test rig.

A signal generator with voltage amplification is used to actuate the PZT actuator as shown in Figure 3.13. The PZT actuator's layers consist of Nickel (1st layer), PZT material (Lead Zirconate Titanate) (2nd layer), Nickel (3rd layer) and Kovar (Nickel-Cobalt ferrous alloy, final layer). The resonance frequency of the PZT actuator is ~1693Hz (1st harmonic, see Appendix 6). In this experiment the PZT actuator is actuated at a low frequency of 0.2Hz to allow a quasi-static study of the contact surfaces. The dynamic force is measured using a piezoelectric force sensor (see Appendix B) [115,116,117,118] situated as shown in Figures 3.12 and 3.13. The force sensor is amplified using a charge amplifier and the dynamic force monitored.

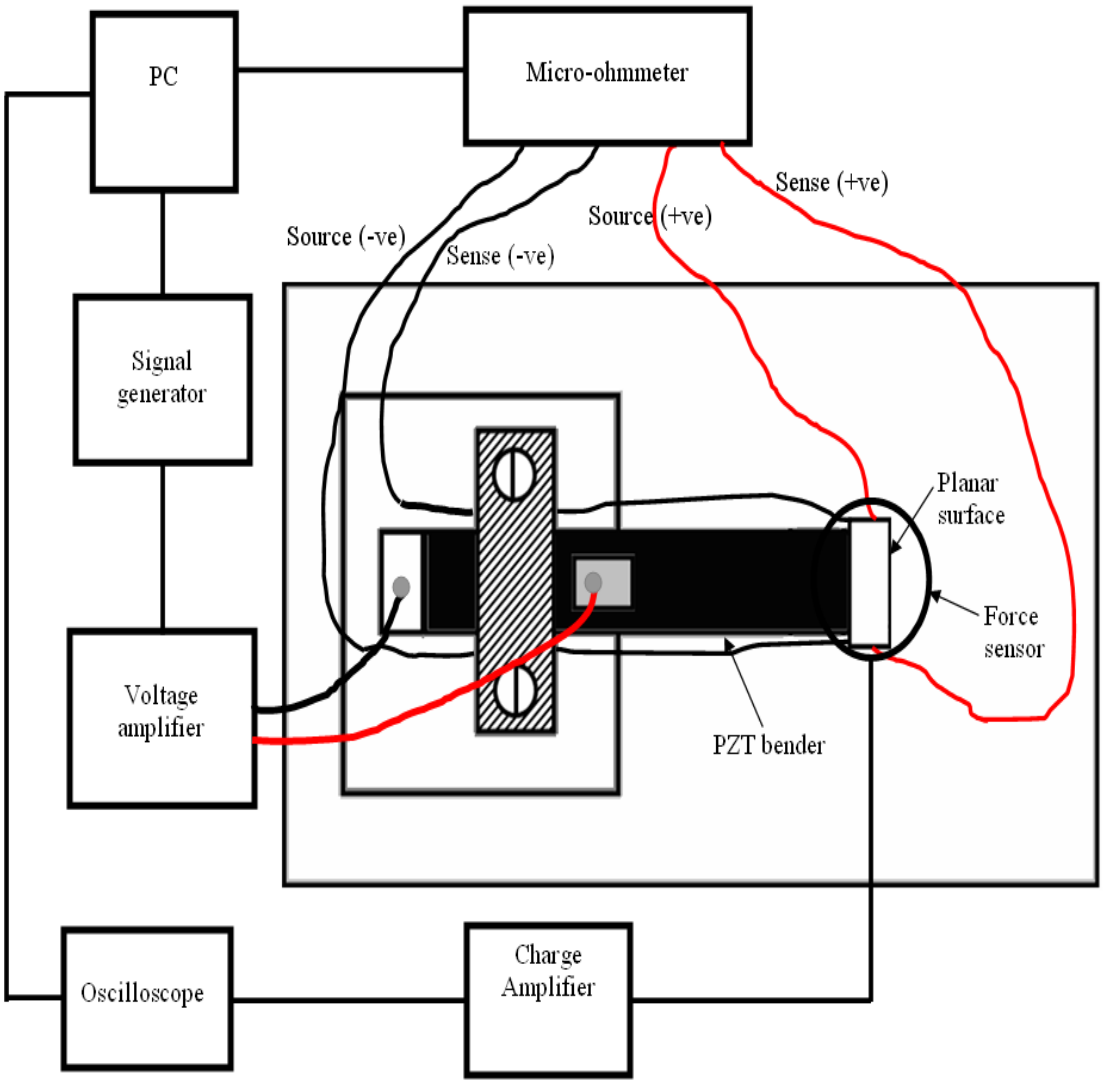

Figure 3.13: Schematic top view of the test system

There are several methods to control the applied force as follows: 1) by controlling the gap [119], achieved by turning the adjustment screw as shown in Figure 3.12; 2) by controlling the length of the actuator [117]; and 3) by controlling the amplitude of the supply voltage to the actuator. In the experiment presented here all other parameters are held constant, with the contact gap used to set the contact force at 1mN.

The contact resistance, R_c is measured using the 4 wire-measurement methods as shown in Figure 3.14 (refer to Appendix A). The DC current source across the planar coated surfaces and contact is set at 1mA using a Keithley 580 micro-ohmmeter. The number of cycles and contact resistance can be controlled and extracted by using the control and data acquisition system (Lab

View). The apparatus is enclosed and held in ambient air at room temperature. Before each contact resistance was measured the temperature is monitored. This is to ensure there was no large temperature difference that could effect the contact resistance measurement due to thermal drift (the measured temperature is ~20^{o}C).

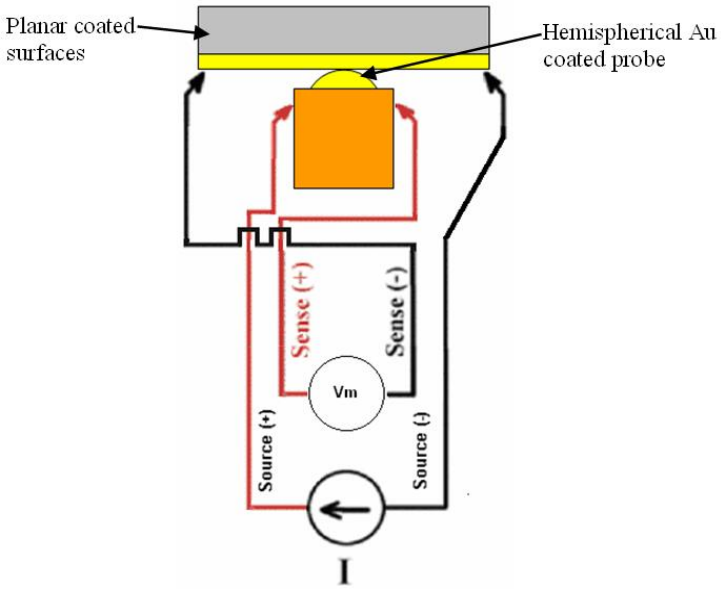

Figure 3.14: Schematic of contact zone with its electrode and R_c measurement.

In this experiment, the PZT actuator is actuated up to 1000 cycles at 0.2Hz under dry-circuit conditions with the contact resistance R_c measured simultaneously. The aim of this study is to determine the stability of the contact surfaces, prior to longer duration testing at higher frequencies.

In order to replicate the conditions of a MEMS relay, a dynamic applied force of 1mN was used. The coated planar surface and Au ball were brought into contact at 0.2Hz using an applied square wave form, and the gap adjusted so that a maximum load of 1 mN was reached. The targeted load was applied for ~3 seconds so that a representative average contact resistance value could be determined. Figure 3.15 (a) shows an example of the load history over a period of time. The measured load versus time for an Au-Au contact pair was found to have a noisy signal. This is partially due to the use of a low-pass filter of 10Hz on the charge amplifier. Since the frequency used to actuate the PZT actuator was 0.2Hz, any external signal or disturbance above this frequency was then

detected. Figure 3.15 (b) shows the variation in R_c over a period of time at a frequency of 0.2Hz. This procedure was repeated in order to detect any cyclic changes in the electrical contact resistance.

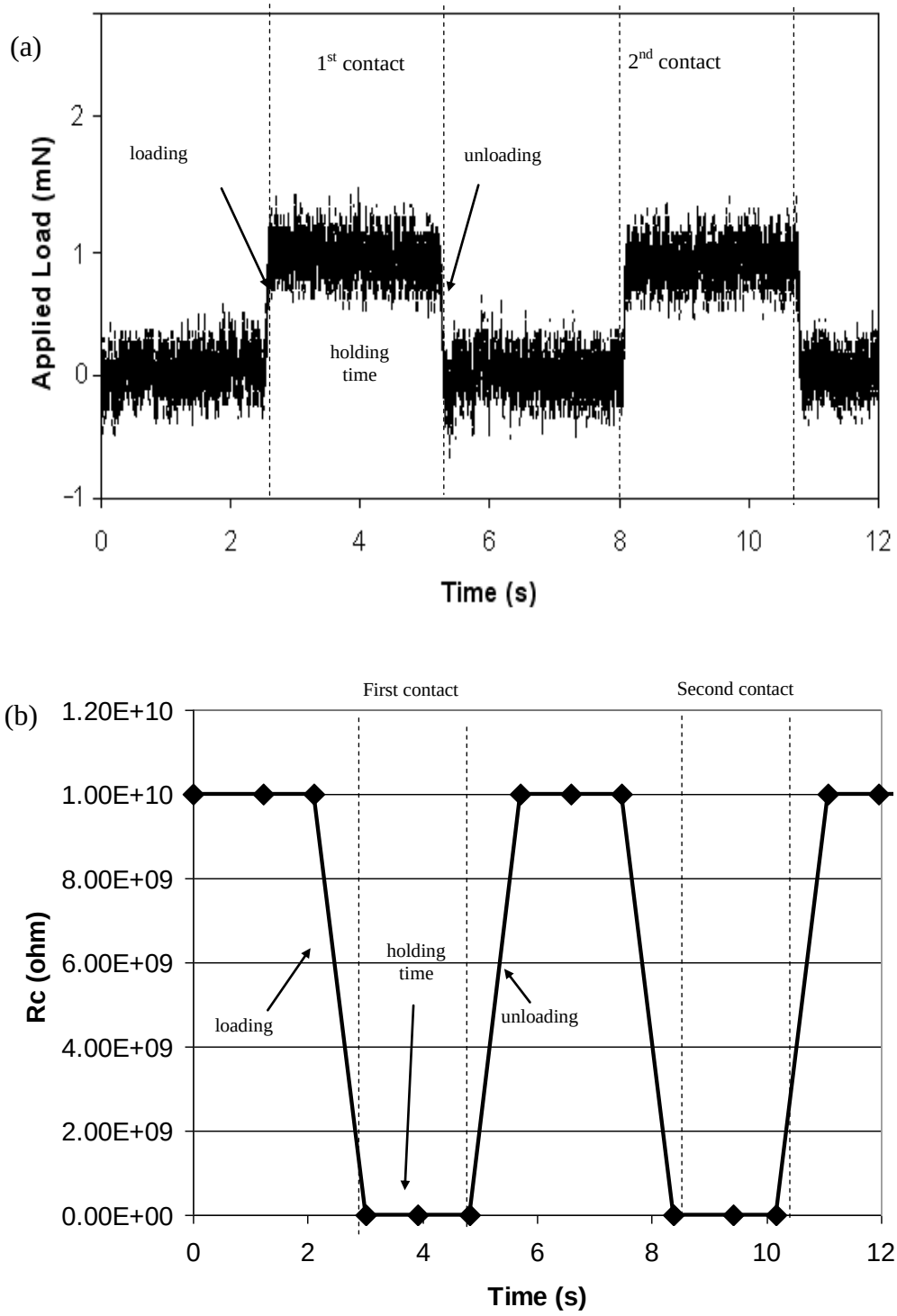

Figure 3.15: Example of (a) load cycles (0.2Hz) for an Au-Au contact pair at 1mN, (b) contact resistance during load cycling for Au-Au contact pair.

The same experimental setting is utilized but the PZT actuator is actuated at a higher frequency (10 Hz) to study the contact surfaces at a high number of cycles. 1mN and 3mN applied force with the same current and supply voltage were used. When the electrical contact resistance was measured, the frequency was reduced to quasi-static (0.2Hz) actuation. This was to allow the determination of an average contact resistance value using a 4-wire measurement. The electrical contact resistance was measured at 3000, 6000, 9000, 10000, 300000, 865000, and over one million cycles.

3.5.2 Experiment 3: PZT actuator test rig (hot-switched condition with 1mA and 10mA at 4V)

In this test, the same experimental setting as in chapter 3.5.1 was used, except that a hot-switching condition was used. The PZT actuator was first actuated at low frequency (0.2Hz) to allow a quasi-static study of the contact surfaces up to 1000 cycles at the applied force of 1mN. The hot-switching current used was 1mA and 10mA at a supply voltage of 4V. Typically, in most experiments the current used was between (for low current) 1-10μA and (for high current) 1-10mA. If the current was greater than 10mA there was a tendency for contact instability and degradation [40]. Figure 3.16 (a) and (b) show an example of the load history over a period of time. Figure 3.17 shows the circuit arrangement for the hot-switching experiment, where the substance is the cathode and the Au hemispherical probe the anode. After every 10^{th} cycle the current and supply load was switched off and the R_c was measured using the 4 wire measurement as shown in Figure 3.17.

To study the contact surfaces over a million or more cycles the PZT actuator was actuated at a higher frequency (10Hz as shown in Figure 3.16 (c), load history over a period of time) and the same applied load, current load and supply voltage was used during hot-switching. R_c is measured during quasi-static frequency (0.2Hz) actuation and using 4-wire measurement methods, after 3000, 6000, 9000, 10000, 300000, 865000, and over one million cycles. The hot-switching current and supply voltage for both experiments is typical of those used in MEMS relays thus the high current range (1mA-10mA) and

supply voltage range are represented [13,40,51,120].

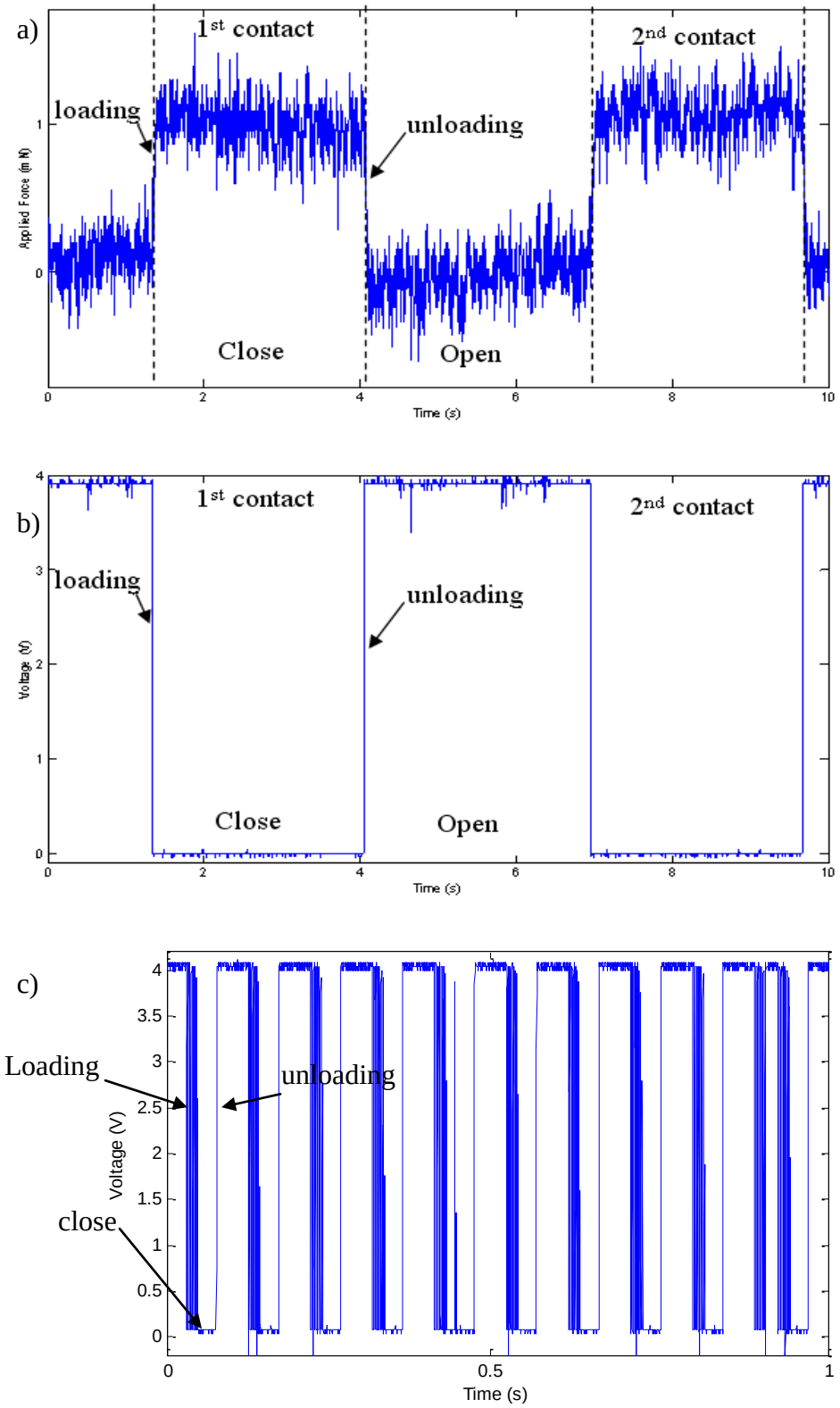

Figure 3.16: (a) Example of applied force against time at 1mN, 0.2Hz for Au-Au pair (b) example of voltage against time for 1mN applied force at 1mA/4V (0.2Hz) for Au-Au pair and (c) example of voltage against time for Au-Au/MWCNT contact pair at 10Hz.

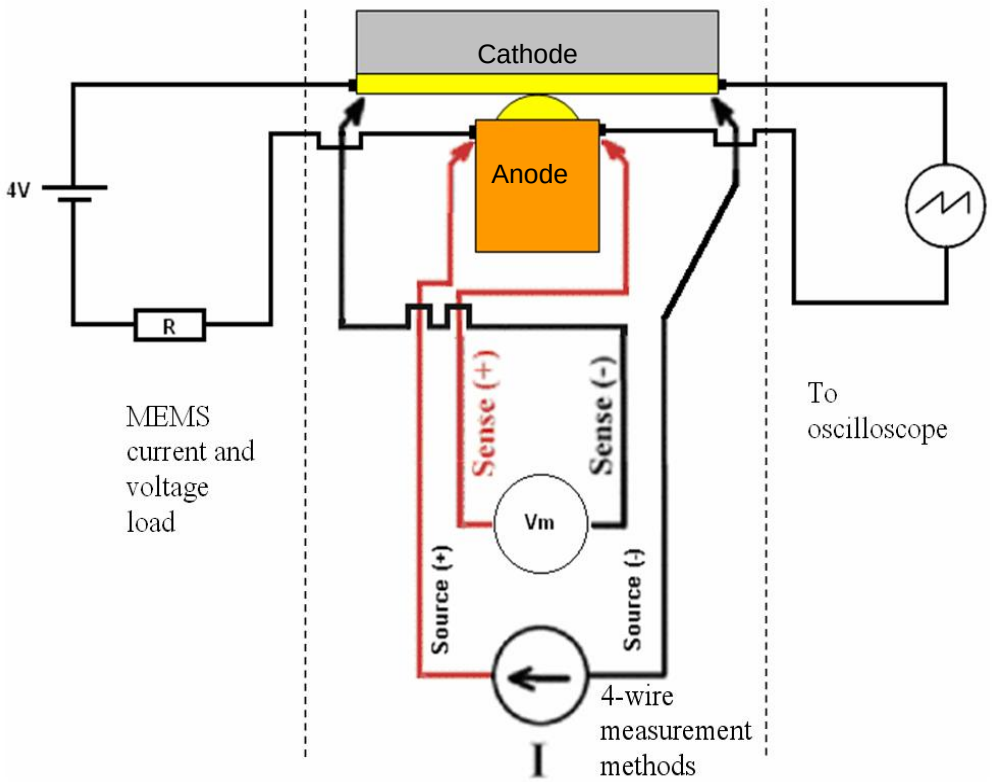

Figure 3.17: Schematic of the hot switching test configuration with its electrode, current and supply load, 4 wire measurement and oscilloscope.

3.5.3 Experiment 4: PZT actuator test rig (hot-switched condition with 20mA-50mA at 4V)

The same experimental set-up as in chapter 3.5.2 was used, but with a higher current load (20mA-50mA). For currents 30mA-50mA the PZT actuator was actuated at 0.2Hz. After every 10 cycles the current and supply voltage was switched off and the contact resistance, R_c was measured. For current of 20mA the sample was actuated at 0.2Hz, 10Hz and 20Hz. At 0.2Hz every 10 cycles the R_c was measured. After 1000 cycles the frequency was changed to 10Hz and R_c was measured after 10000, 100000 and one million cycles. After one million cycles the frequency was changed to 20Hz (see Figure 3.18 for load history over period of time) and every 2 million cycles R_c was monitored.

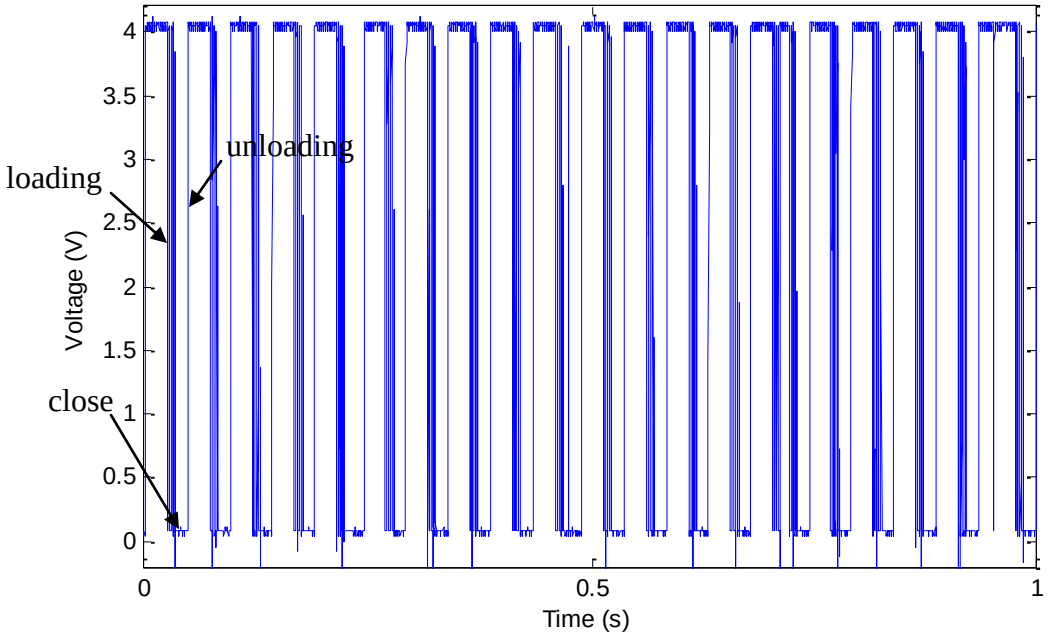

Figure 3.18: Example of voltage against time for Au-Au/MWCNT contact pair at 20Hz.

The test rig apparatus is enclosed and held at ambient air and room temperature. The average temperature is measured every time the contact resistance is measured. This is to make sure that the contact resistance measured at the same average temperature, because slight change to temperature can affect the it due to expansion of the samples. The average temperature measured was ~20^{o}C.

The aim of this study was to determine the stability, reliability and durability of the contact surfaces, prior to longer duration testing under variable MEMS current load conditions. The performance of the Au-Au/MWCNT surfaces was compared to a reference Au-Au contact pair under the same experimental conditions in order to assess their mechanical and electrical stability and reliability. SEM images, TaiCaan Technology XYRIS 4000L laser scanner and X-ray spectroscopy were used to confirm any changes on the contact surface samples such as degradation and wear.

3.6 Summary

In this study the materials Au, multi-walled carbon nanotubes (CNT) and Au/MWCNT composites were fabricated and tested. Gold was used because of its capability to resist oxidation and its outstanding low contact resistance compared with other materials considered for use in MEMS relays. However, due to its poor mechanical properties alternative materials need to be discovered. CNTs have potential if grown properly on the contact's electrodes. At this stage multi-walled carbon nanotubes were grown on the Si substrate.

Gold, MWCNT and Au/MWCNT composite contacts were tested using a modified nano-indentation apparatus. The testing was performed so as to observe its mechanical and electrical properties in a controlled temperature enclosure. The use of nano-indentation apparatus to test the contact surfaces at low applied force (1mN) was desirable because of its controllability and accuracy. The contact resistance was measured using a 4-wire measurement apparatus. In this experiment, the Au-Au/MWCNT composite contact pair combination was compared with Au-Au and Au-MWCNT contact pairs as a benchmark for the composite material. Only ten cycles were achieved in these tests due to the frequency limitations of the modified nano-indentation apparatus.

Therefore, a PZT actuator was used to apply a higher number of cycles at higher frequencies. The same samples as used in the modified nano-indentator test were used. Tests were conducted up to 2 million cycles or more. Two test types were conducted: dry-circuit condition and hot-switching (current load of 1mA - 50mA at 4V). The actuation frequency was between 0.2Hz to 20Hz. Contact resistance was measured using the 4-wire measurement methods and all the measurements were performed during low frequency actuation (0.2Hz). The test approach appears to be a very promising route towards obtaining in situ measurements of contact resistance on representative surfaces.

This experimental method is applicable to MEMS relay contacts and will serve as a platform for future research and investigations of Au/MWCNT-Au/MWCNT

and Au/SWCNT-Au/SWCNT contact pairs with different packing densities and lengths of CNT and thickness of the Au coatings on the carbon nanotubes. Future work will conduct testing at higher frequencies and realistic numbers of cycles for MEMS switch applications.

CHAPTER 4: RESULTS AND DISCUSSION

4.1 Introduction

In this chapter the results from the experiment using the modified nano-indentation apparatus and the new test rig are presented and discussed. The Au-Au/MWCNT contact pair surfaces were compared with a baseline reference Au-Au and Au-MWCNT contact pair studied under the same experimental conditions and the results linked to established contact theory.

The surfaces of the samples were analysed using a Scanning Electron Microscope (SEM), a non-contact 3D laser profiler (TaiCaan, Xyris 4000CL) and X-ray (EDX) spectroscopy, to observe any degradation on the contact surfaces. An SEM is used to observe any deterioration on the contact surface after contact. The Xyris (4000CL) is used to determine any changes in the surface texture and profile of the samples. Furthermore the surface asperities and the average roughness value or surface roughness (R_a) can be determined. EDX is used to observe any changes of the material composition.

4.2 Samples for modified nano-indentation apparatus

4.2.1 Au-Au contact pair (sample 1)

The samples were observed using a Scanning Electron Microscope (SEM) as shown in Figure 4.1. The sample (Au hemispherical probe) can be magnified as shown in Figure 4.2 and 4.3. Figure 4.2 shows the X25 magnification and Figure 4.3 is X20,000 magnification. In the X25 magnification the sample looks smooth, but with the X20000 magnification the grain microstructure of the gold coating is observable. It is apparent that the grain microstructure of sputtered gold varies from 50nm up to 200nm in diameter.

Figure 4.1: Scanning electron microscope (SEM).

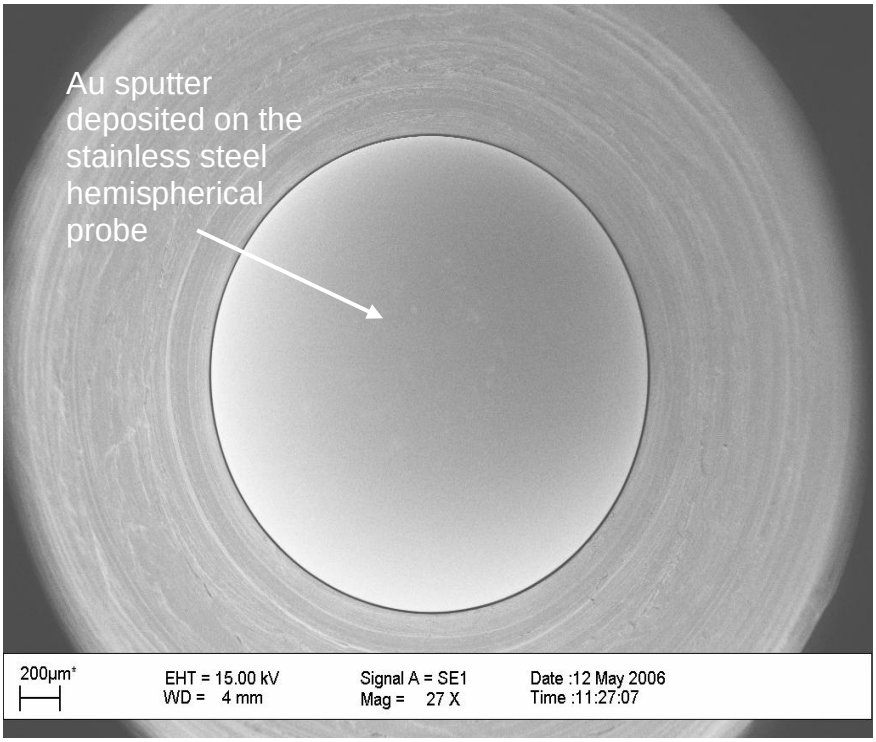

Figure 4.2: SEM image of gold sputter 500nm thickness on the stainless steel hemispherical probe.

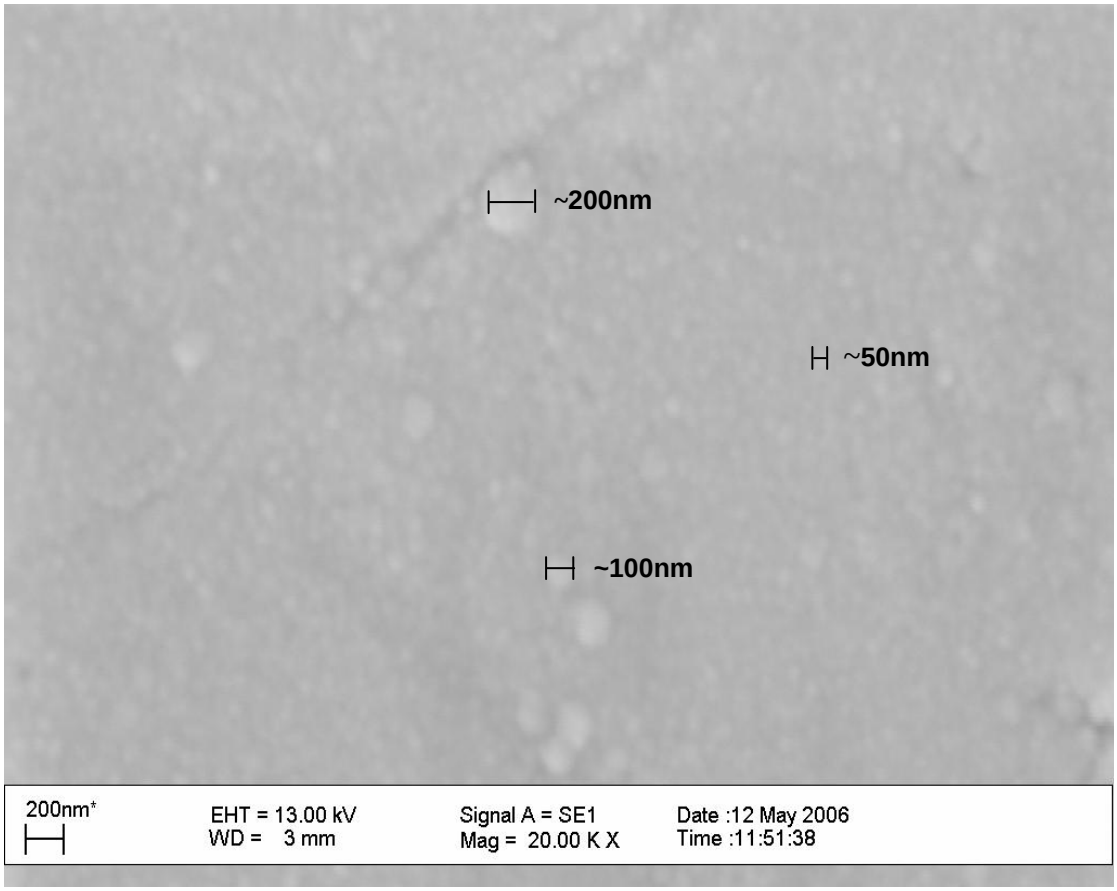

Figure 4.3: 20,000 times magnification of gold sputter deposited on the hemispherical probe, with the grain microstructure ranging from 50 to 200nm.

Another way of viewing the microstructure in detail is by using a laser profiler to generate the 3D image of the microstructure. The measurement of the average roughness and 3D surface of the Au hemispherical probe and substrate can be determined. The topography of the Au hemispherical probe is shown in Figure 4.4. It shows the micro-topography of the Au hemispherical probe (a sputtered thickness of 500nm) with the sphere removed and has average roughness or surface roughness, R_a≈400nm, while the silicon substrate (~5mm by ~5mm, used for the modified nano-indentation apparatus testing), which is sputtered with 500nm thick gold contact layers, has R_a≈30nm.

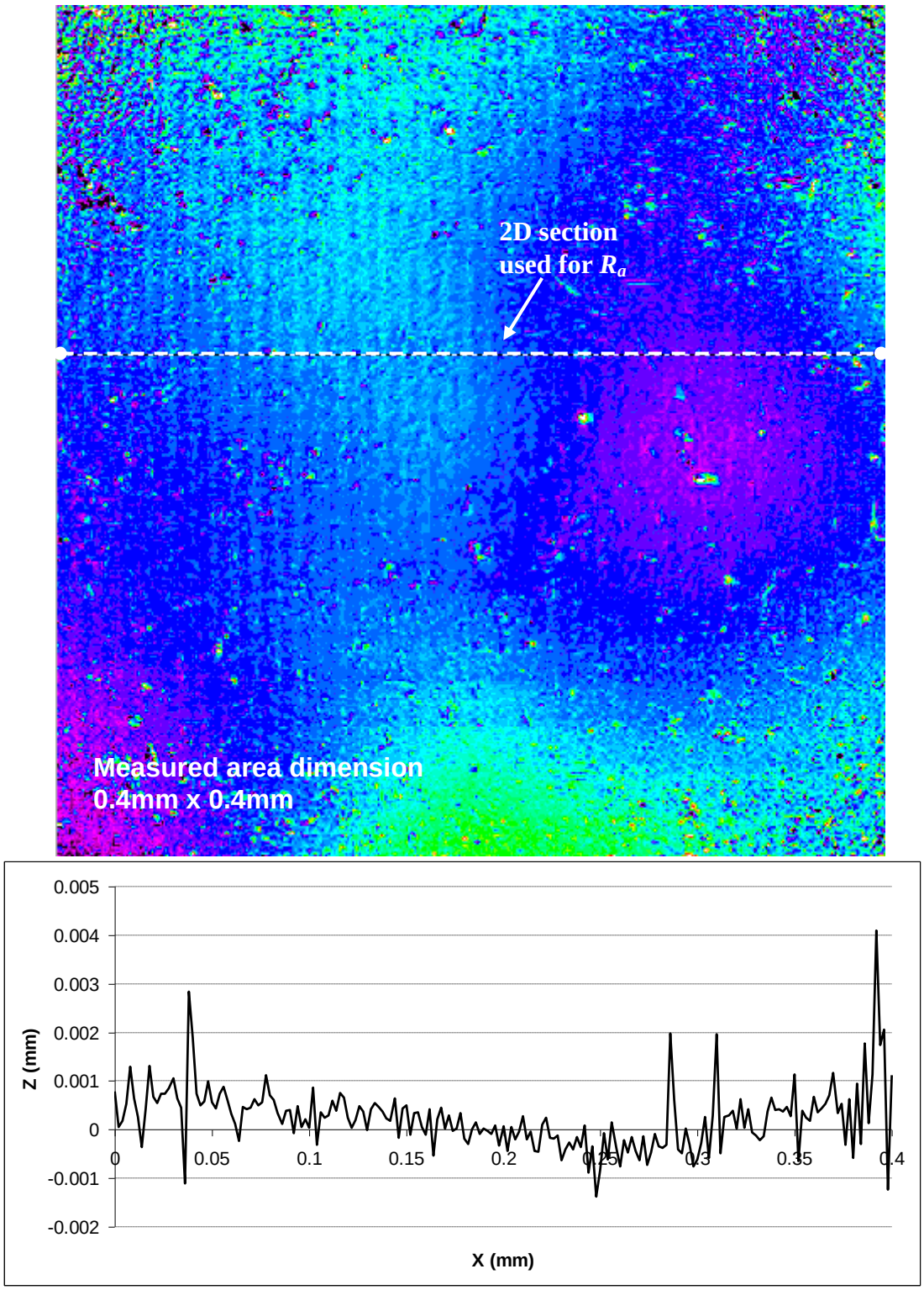

Figure 4.4: 3D image generated by TaiCaan (Xyris 4000CL) for Au-sputtered 500nm thickness with sphere removed, 301x301(400x400μm).

4.2.2 Au-MWCNT contact pair (sample 2)

As explained in the literature review there are several fabrication techniques available for growing CNT; arc-discharge, laser ablation, and CVD. As reported CVD produces single walled carbon nanotubes (SWCNT) and multi walled carbon nanotubes (MWCNT) [121] and arc-discharge and laser ablation produces MWCNT [122] of high quality in terms of electrical transport properties.

To produce pure CNT with a low resistivity one has to find the best fabrication method. CVD is best for growing forests of CNT on the substrate. It provides high purity CNT with equal size, and length. This can be achieved by controlling the thickness of the catalyst, but growing a dense forest of high quality CNT needs more research and experimentation before it can be realised. As stated by Hjortstam et al. (2004), currently the cost of a high quality CNT is too high for commercial use [81].

In this experiment CVD was used because of its potential to produce highly pure, dense and vertically aligned forest of MWCNT. The first forests of CNT were grown on a silicon wafer (5mm by 5mm) as shown in Figure 4.5 (a) and (b) using a thermal CVD furnace. The catalyst used in this experiment is Fe and the gaseous carbon source is ethylene. The growth temperature and time is 875^{o}C and 10 minutes respectively to produce MWCNT of length ~100μm as shown in Figure 4.5 (b). For the study a forest of vertically aligned MWCNT is grown on a 5mm by 5mm silicon wafer (Sample 2). The growth temperature and time is 875^{o}C and ~3 minutes respectively to produce vertically aligned MWCNT of ~50μm in length as shown in Figure 4.6. Figure 4.7 shows the 3D profile of a substrate coated with MWCNT and it shows that the R_a≈1.4μm.

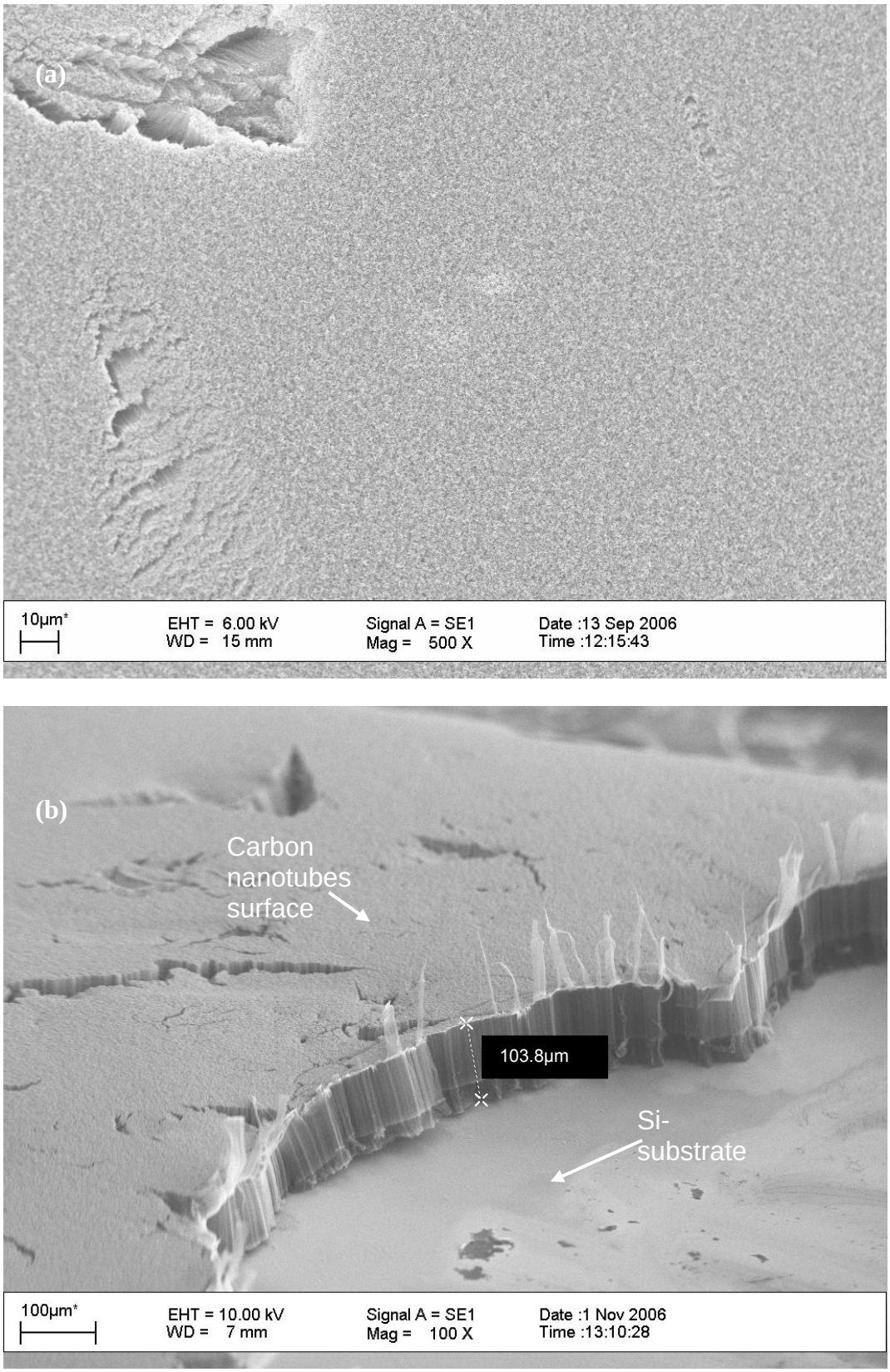

Figure 4.5: (a) Top view and (b) perspective view of SEM image of forest of CNT on Si-substrate.

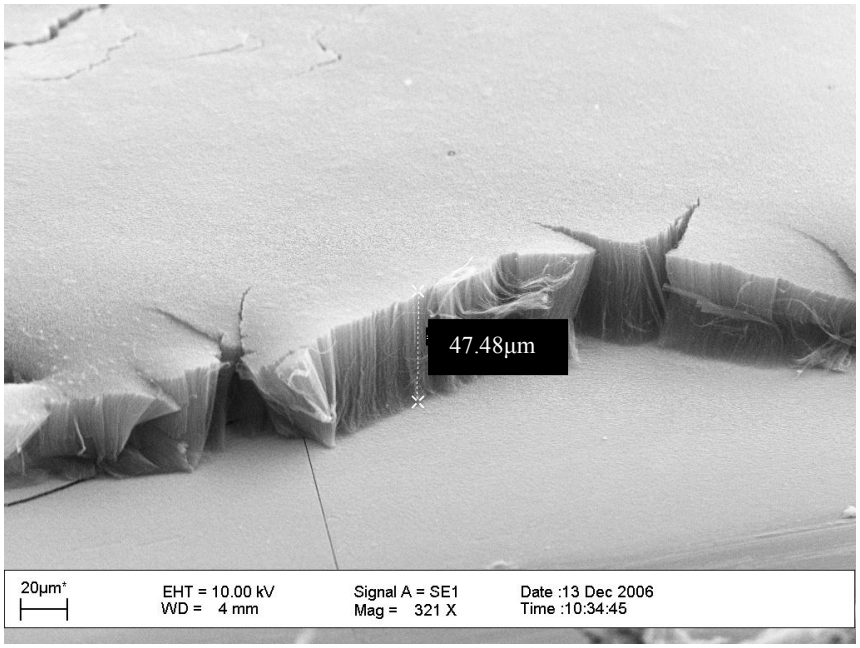

Figure 4.6: SEM image of forest of MWCNT.

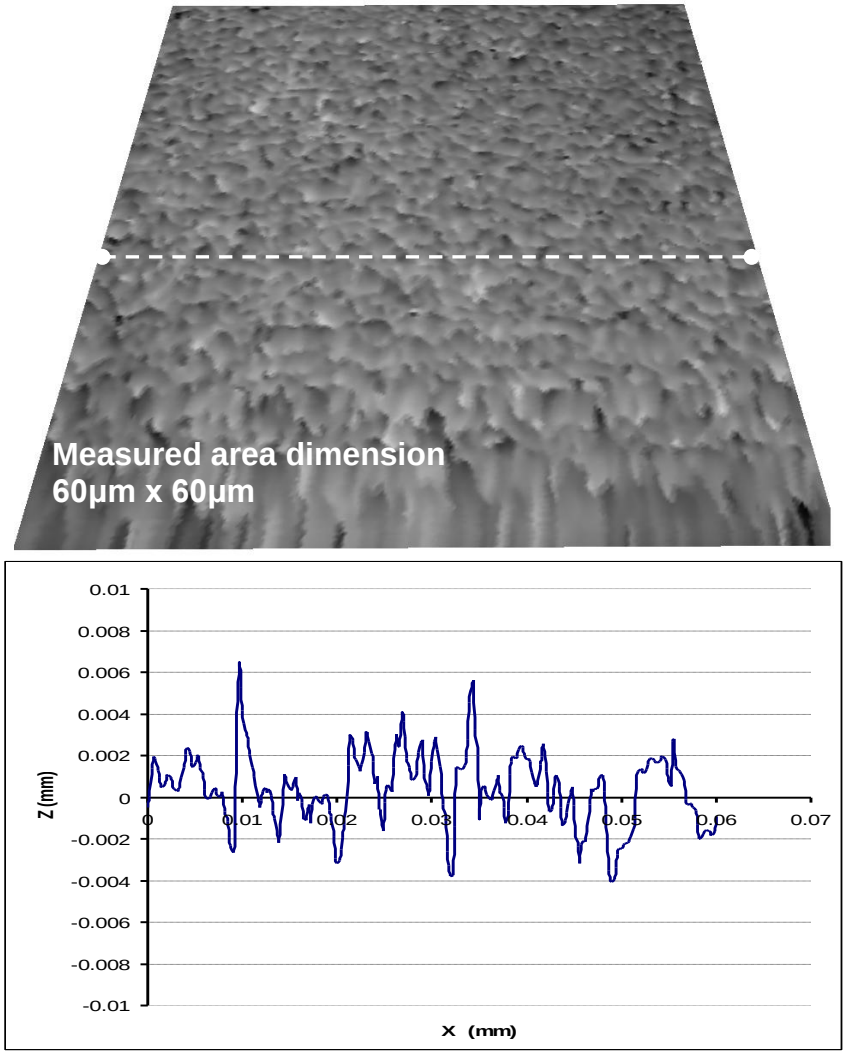

Figure 4.7: Con-focal Laser Scanned image of MWCNT 301x301 (60µm x 60µm) using TaiCaan Technologies (Xyris 4000CL), showing 2D section of data.

Figure 4.8 (a) shows the scanning electron micrograph of an area analysed by electron dispersive X-ray (EDX) spectroscopy. It was clear that the peak originating from CNT and some carbon by-product such as other carbon particles marked ‘C’ was predominantly observed, Figure 4.8 (b). ‘O’ peak indicates that the surface of the CNT could have been oxidised due to exposure of the sample to air. ‘Si’ peak indicates the background of the silicon wafer or silicon dioxide. As explained in chapter 3.2, Fe catalyst and Al_2O_3 were used to grow CNT but the quantity of these substances had a negligible presence. Furthermore the atomic percent of ‘C’ is 95.2%, ‘Si’ was 3.2% and that of ‘O’ was 1.5%.

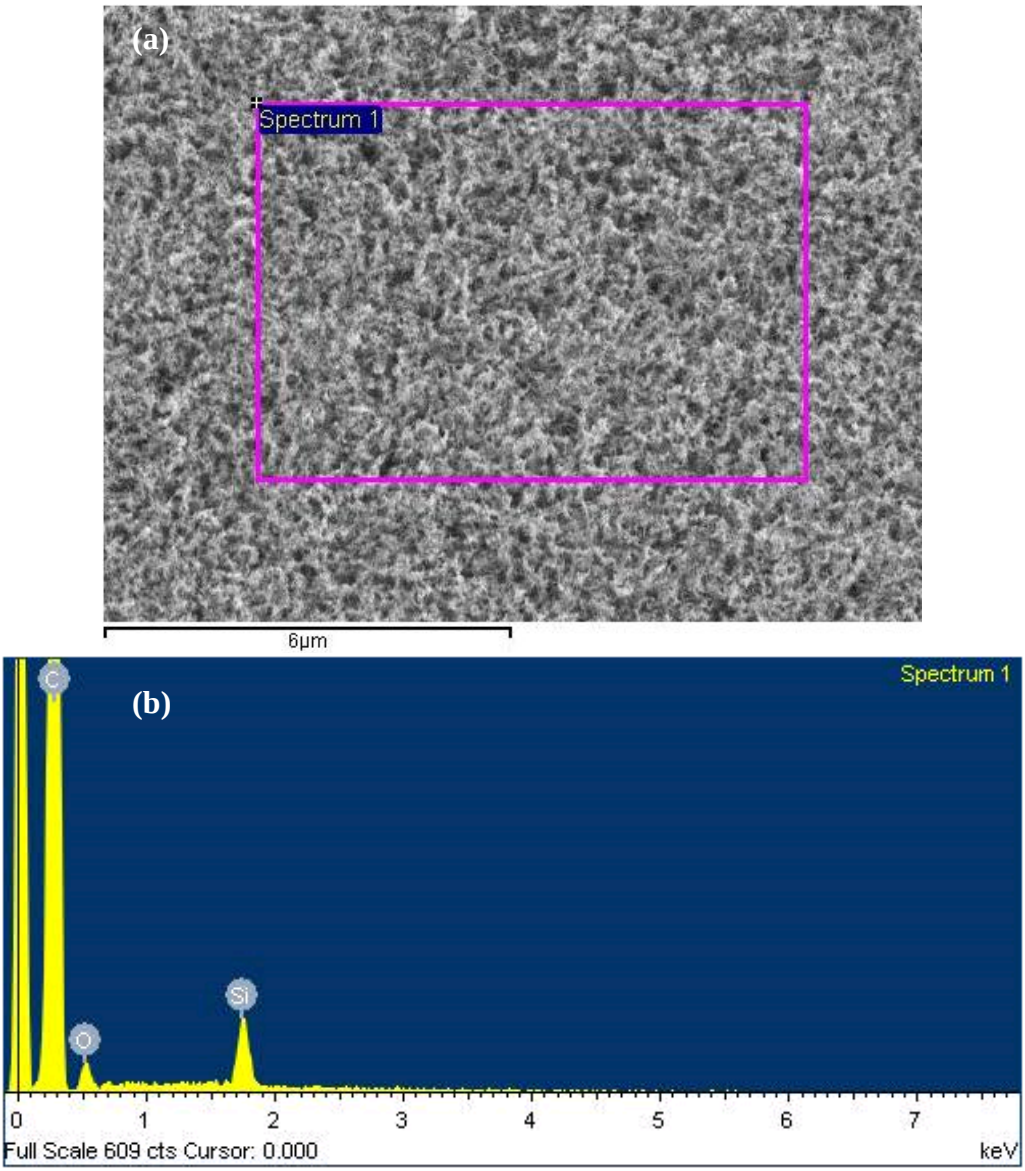

Figure 4.8: (a) Electron image and (b) EDX spectrum of MWCNT surface which shows atomic percent of 95.2% carbon.

4.2.3 Au-Au/MWCNT composite contact pair (sample 3)

A sputterer apparatus has been used to produce the Au/MWCNT composite. The Au coating can be sputtered on to the 50μm CNT length as shown in Figure 4.9 (a) and (b). It is indicated that the sputtered Au can penetrate the MWCNT to around 700nm to 4μm in depth.

(a)

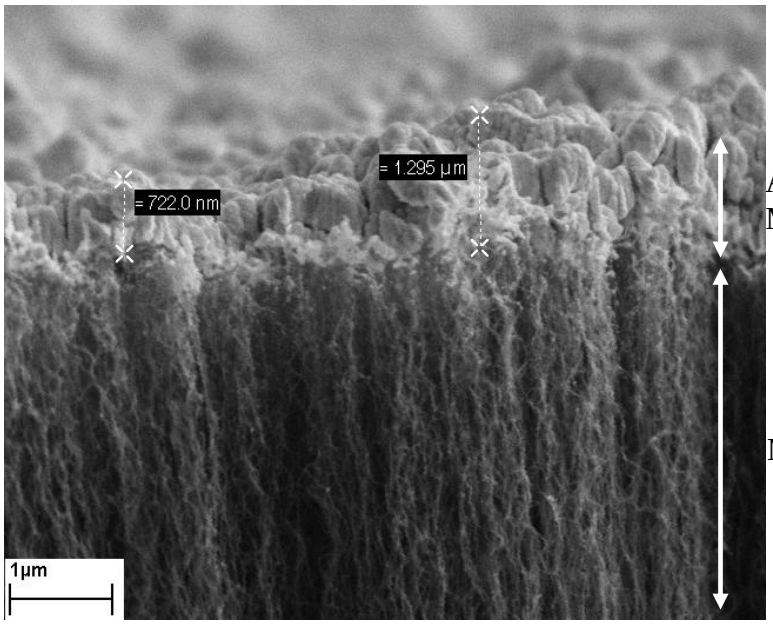

(b)

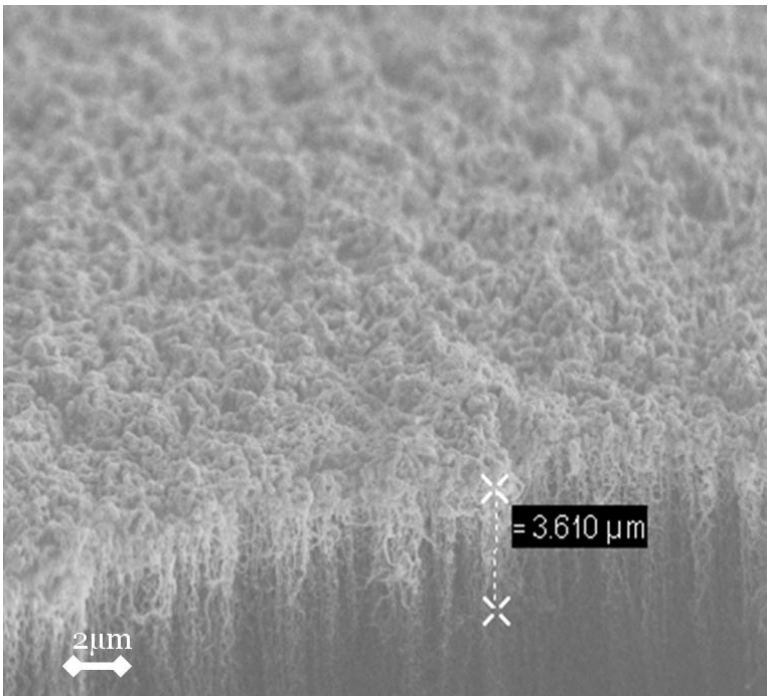

Figure 4.9: (a) Au penetration of ~700nm in depth (b) Au penetration of ~4μm in depth.

The average roughness of this sample is R_a~1.4μm as measured by TaiCaan (Xyris 4000CL) (as shown in Figure 4.7), this is greater than Au coated substrate (R_a~30nm).

(a)

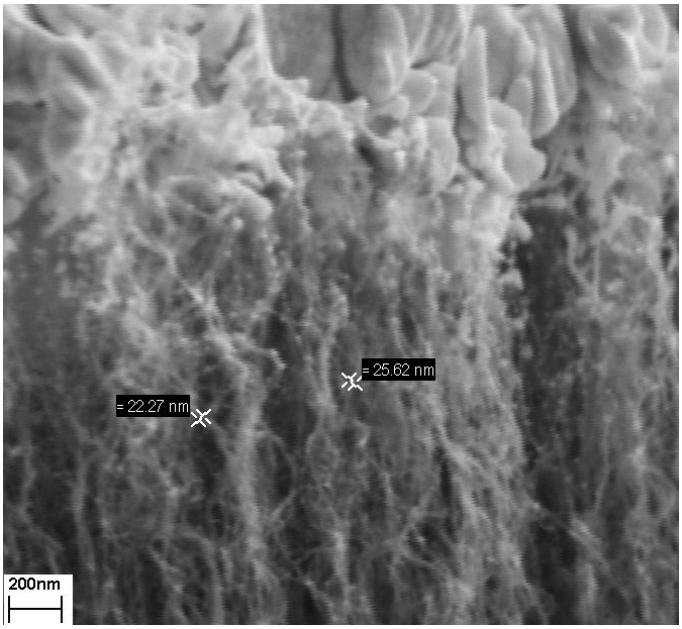

(b)

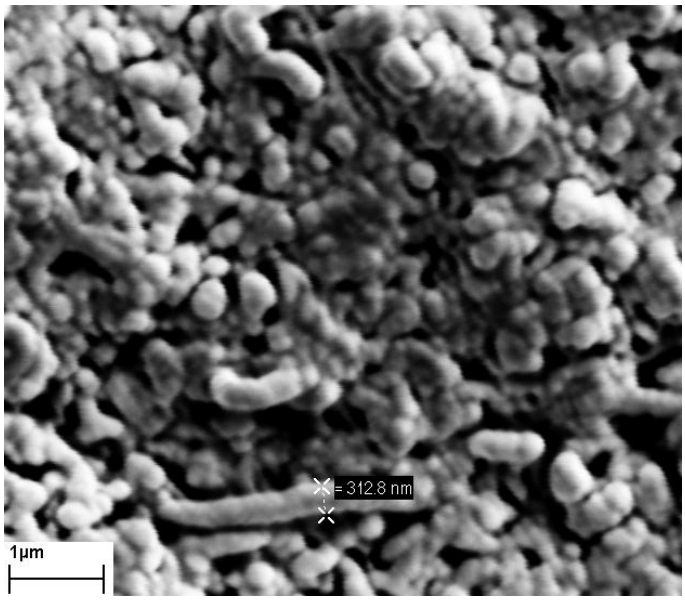

Figure 4.10: (a) Side view SEM image of Au/MWCNT composites and (b) top view SEM image of Au/MWCNT composites.

Figure 4.10 (a) and (b) shows a close up SEM image of the Au/MWCNT composite (side and top view respectively). It was observed (Figure 4.10 (a)) that the MWCNT has an approximate diameter of ~20nm. The sputter coated Au deposited on top of the surface of the forest of vertically aligned MWCNT

(Figure 4.10 (b)) tends to cluster into groups of approximately 300nm in diameter.

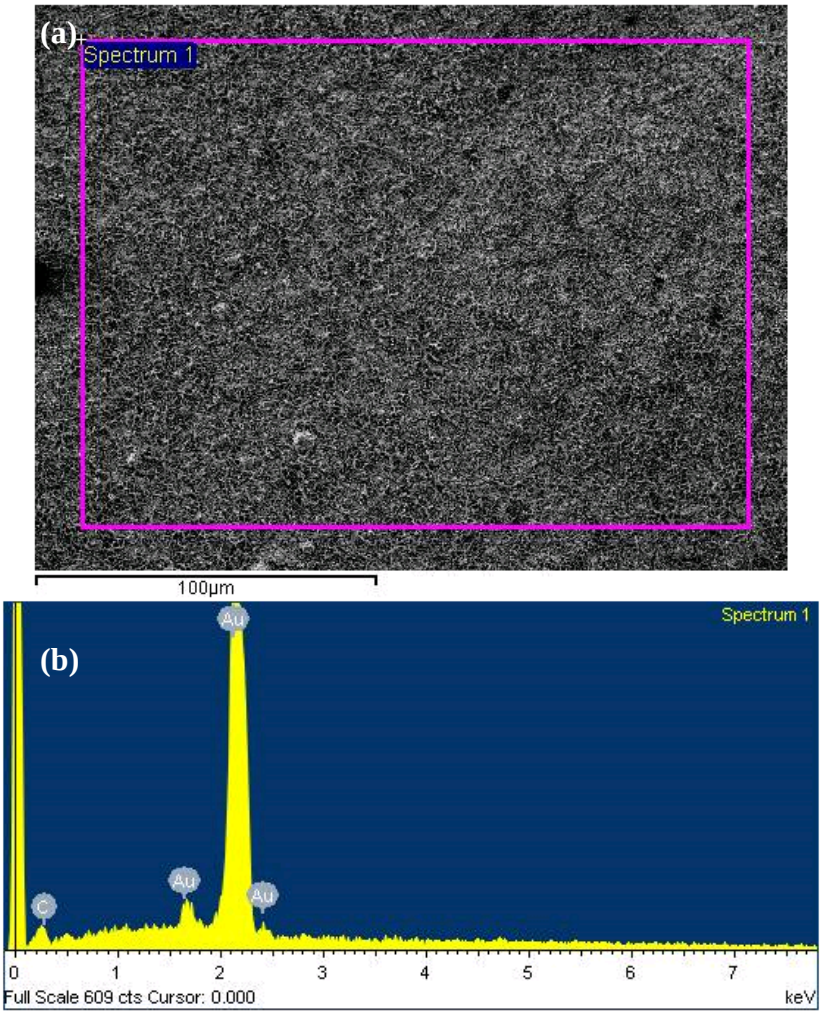

Figure 4.11: (a) Electron image and (b) EDX spectrum of Au/MWCNT surface.

Figure 4.11(a) shows the electron image of an area analysed by X-ray spectroscopy. The 'Au' peak was prominent and the 'C' peak indicates the MWCNT, Figure 4.11 (b). Additionally, the atomic percent of 'Au' was 71.3% and that of 'C' was 28.7%.

4.3 Samples used for test rig apparatus

All the samples for these test were produced using the same method as above, the only difference was the size of the substrate. The size of the substrate was 2mm by 7mm and attached to the end of the PZT actuator as shown in Figure 3.4. The Au hemispherical probe dimensions and method of fabrication was as above (chapter 4.2.1).

4.4 Experiment 1: Modified nano-indentation apparatus (dry-circuit condition)

This section presents the results and discussion of the experiment using a modified nano-indentation apparatus with the dry-circuit condition. The maximum applied load was 1mN and at low frequency response actuation. The experiment used Au-Au, Au-MWCNT and Au-Au/MWCNT contact pairs. This section describes three aspects of the experiment: 1) to observe applied force against the contact resistance characteristics; 2) 10 cycles actuation to see any degradation on the contact materials; and 3) to observe Au-Au, Au-MWCNT and Au-Au/MWCNT contact pairs' mechanical behaviour.

4.4.1 Contact resistance against applied force

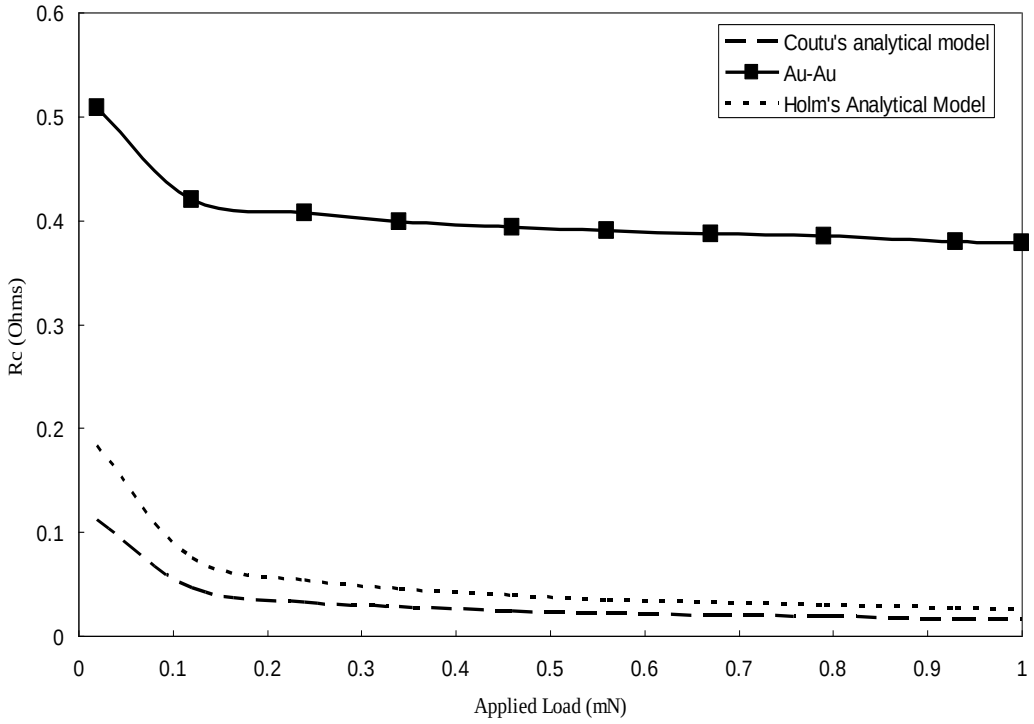

Figure 4.12: Contact resistance between Au-Au contact pair as a function of applied load.

Figure 4.12 shows that the contact resistance vs. applied force characteristic of the Au-Au contact pair is very similar to that calculated using classical contact theory. Assuming that the contact deforms plastically the analytical result is plotted on the same graph using the equation from Holm's analytical model. Figure 4.12 shows that the contact resistance is higher than the analytical model. This is because in the analytical model the contact surfaces are assumed to have no film and are clean. In this experiment, there could be surface films and contaminants thus giving higher contact resistance.

Using the formula from Coutu et al. (2006) from chapter 2.3, which is an updated contact resistance model for low force contact developed using Chang's improvement [34] to Chang, Etsion, and Bogy (CEB) model [35] and [36] Gamma function in Wexler interpolation [14], the calculated contact resistance of Au is shown in Figure 4.12.

Figure 4.12 shows that the contact resistance was lower than the measured Au-Au contact pair resistance. This discrepancy was most likely due to resistive contaminant film layers on the contact surfaces. As Patton et al. (2005) states that Au has the tendency to have a thin layer of carbon on its surface that is a residue from the cleaning process and/or is adsorbed due to exposure to air [40]. It has been reported by Hyman et al. (1999) and Tringe et al. (2001) that there is a 2-4nm thick of adsorbed hydrocarbons on freshly cleaned Au [41,42] and this increases the contact resistance, but nonetheless the trend in the graph is similar to Holm's classical analytical model. Therefore it is concluded that the existing models for contact resistance are not applicable and further consideration should be given for the above effects and the influence of thin film conduction.

The trend of the classical contact theory relation can be seen with the Au-MWCNT contact pair as shown in Figure 4.13. This result is similar to an experiment between metal contacts with a substrate coated with tangled single walled carbon nanotubes by Yaglioglu et al. (2006) [72]. They concluded that a tangled SWCNT film against an Au coated surface works better than two contacting tangled films and the SWCNT conforming to the shape of the Au

contact. The contact resistance of the SWCNT system was lower than in this experiment and this is obvious because of its resistivity. Furthermore the maximum applied force used in their experiment was ~150mN and this affects the contact resistance reading because as the applied force increases the contact area increases.

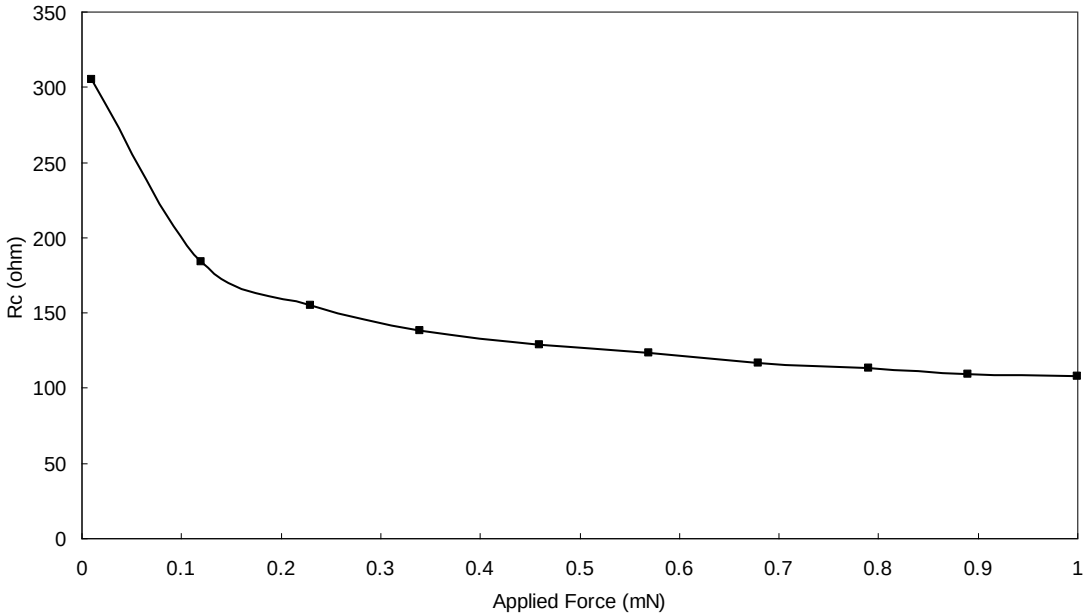

Figure 4.13: Contact resistance between Au-MWCNT contact pair as a function of applied load.

A factor that contributes to contact resistance is the asperities of the contact surfaces. Figure 4.7 shows a scanned image of MWCNT, having average roughness, R_a≈1.4μm much higher than the Au coated substrate. Figure 4.14 shows the SEM image of MWCNT. When two surfaces are in contact the asperities are actually in contact first, thus producing contact spots or “a” spots. As the applied load increases, more contact spots are produced thus increasing the contact radius. By using both the contact resistance formulae from eqn. 2.2.6 and 2.2.8 this can be proved. Both equations present the importance of ρ (resistivity) and contact radius. When ρ is lower and contact radius increases, contact resistance will decrease.

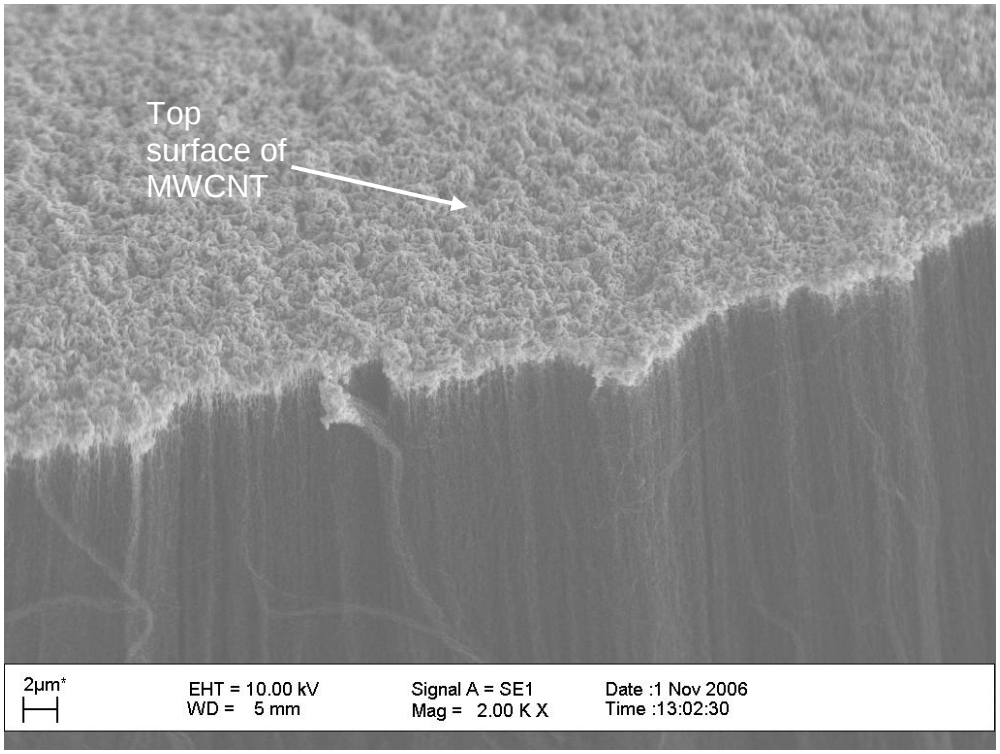

Figure 4.14: SEM image of MWCNT.

Some of the MWCNT's asperities are higher than the rest as shown in Figures 4.7 and 4.14. When the Au hemispherical probe is brought closer to the MWCNT substrate these asperities are in contact, thus producing the contact spots as shown schematically in Figure 4.15. In this experiment, as the applied load is increased more of the MWCNT deflect. As it deflects or buckles or bends more, it reduces the air gaps between the vertically aligned MWCNT thus improves the transfer of electrons through the sidewalls. Due to the deflection of the MWCNT as the load is applied, it will conform more to the shape of the Au hemispherical probe, thus increasing the contact area and lowering the contact resistance, as shown in Figure 4.15 (a) and (b).

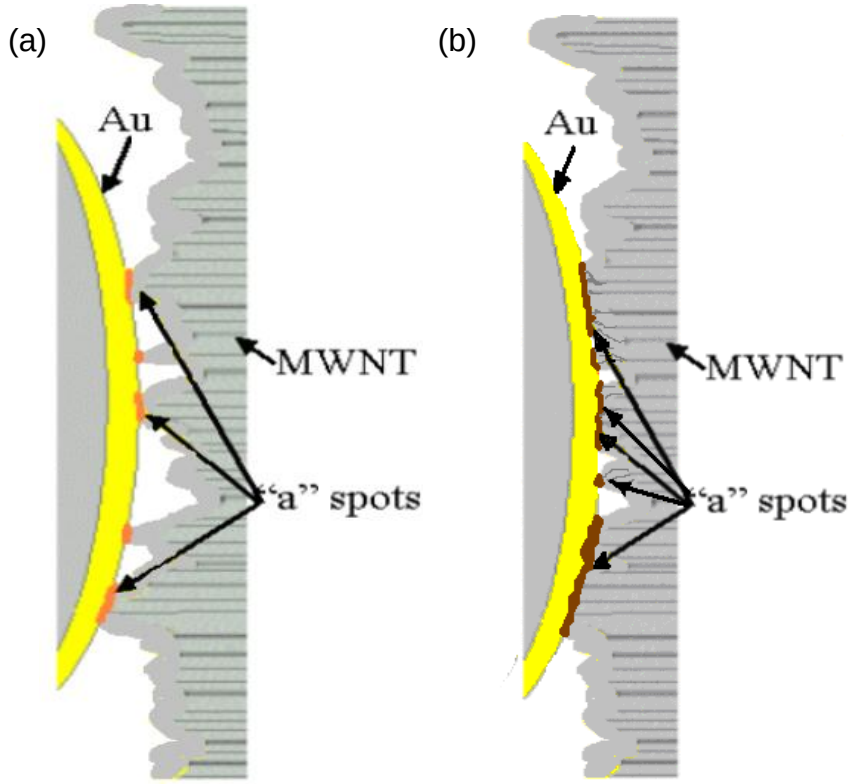

Figure 4.15: Schematic diagram of (a) Au-MWCNT contact pair and (b) increased a-spots.

Another factor that can contribute to reducing the contact resistance is the resistivity. A low resistivity indicates a material that readily allows the movement of electrons. If both the Holm's and modified equations are used, the lower the resistivity the lower the contact resistance. This is why Au has lower contact resistance because its resistivity is less than MWCNT, which has a resistivity of around 2 - $3x10^{-6}\Omega m$ [123].

Figure 4.16 shows that the Au-Au/MWCNT contact pair with increasing applied load from 10μN to 1mN follows a similar pattern to both contact theories. In this case the contact resistance is much lower than Au-MWCNT resistance but slightly higher than for the Au-Au contact pair as shown in Figure 4.16.

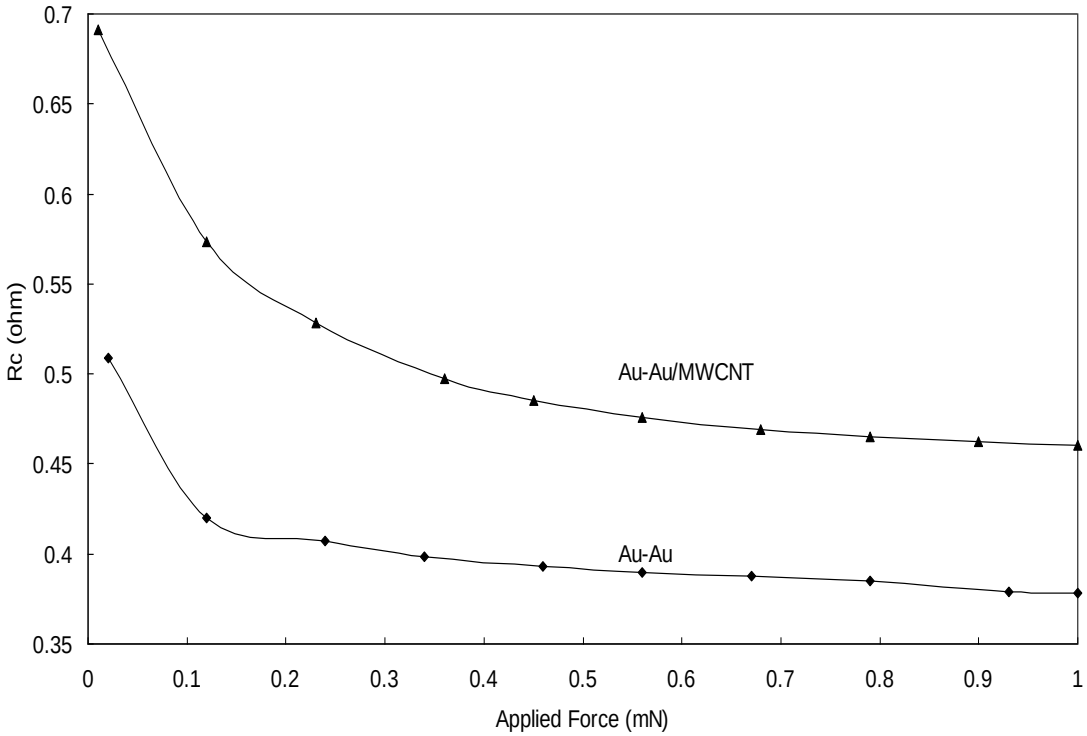

Figure 4.16: Contact resistance between Au-Au and Au-Au/MWCNT coating contact pair as a function of applied load.

In the schematic diagram shown in Figure 4.17 (a) the Au coating on MWCNT is making contact with the Au hemispherical probe, this decreases the contact resistance (when compared with the Au-MWCNT contact pair as shown in Figure 4.13). As the applied force increases, more a-spots were formed thus reducing the contact resistance as shown in Figure 4.16 and this can be seen in Figure 4.17 (b).

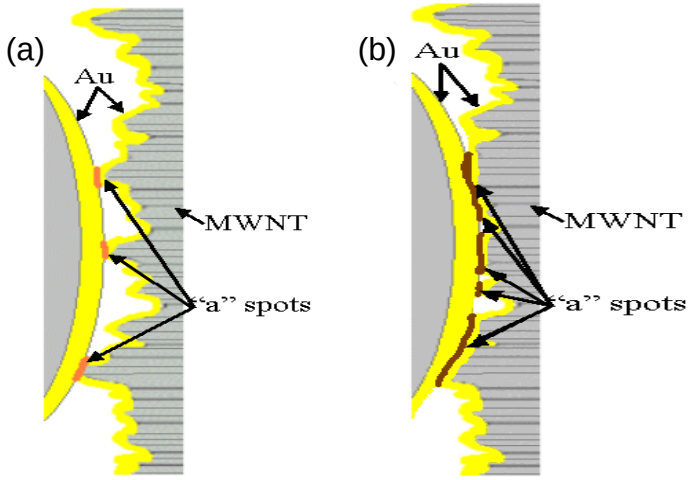

Figure 4.17: Schematic diagram of (a) Au-Au/MWCNT contact pair and (b) increases the a-spots.

Furthermore the Au/MWCNT coated surfaces as shown in Figure 4.18 are rougher (R_a≈1.4μm, as analysed by AFM) than the Au-substrate therefore producing fewer contact spots and thus giving higher contact resistance.

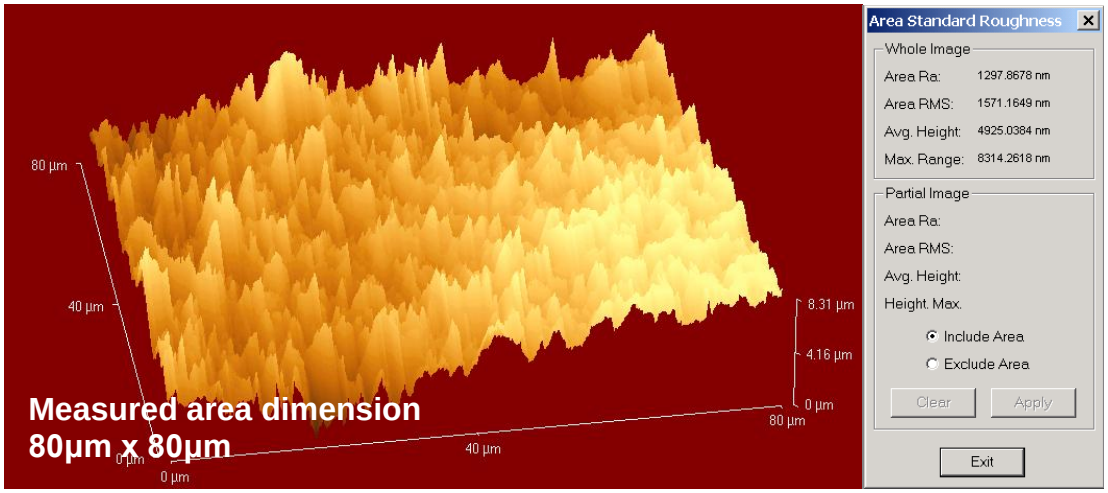

Figure 4.18: AFM image of Au/MWCNT layer.

As stated by Bult et al. (2008) the vertically aligned MWCNT is a compliant surface [73]. This compliant characteristic makes the Au/MWCNT surfaces absorb the applied forces from the Au hemispherical probe. To explain the compliant behaviour of the MWCNT surfaces, the following experiment was performed. A modified nano-indentation apparatus, without wires attached on the Au hemispherical probe, was used. This was to avoid any disturbance from the wires, giving purely the mechanical characteristics of the contact surfaces. Figure 4.19 shows the result from the experiment; an applied force (mN) against displacement (nm) for the Au-Au, Au-MWCNT and Au-Au/MWCNT contact pair.

The indentation force starts from zero until it reaches the maximum applied force of 1mN and after unloading a permanent displacement can be observed on all the samples. Figure 4.19 shows the depth of penetration for MWCNT and Au/MWCNT surfaces. The curve for the Au-Au/MWCNT pair shows that it penetrates ~2500nm (marked ‘A’ on Figure 4.19) and for the Au-MWCNT pair ~3600nm (marked ‘B’ on Figure 4.19). As the applied load was increased, it is possible that more deflection or buckling occurs on the vertically aligned MWNTs. The Au on the vertically aligned MWCNT composites has reinforced the MWCNT, as evident from the different depth penetration between MWCNT

and Au/MWCNT surfaces. In Figure 4.19, once the indentation load was removed permanent displacement can be observed on both Au-MWCNT and Au-Au/MWCNT pair (~1400nm). It has been shown by Bult et al. (2008) that even with deformations in excess of 85%, the nanotube array will maintain its mechanical integrity and return to it's unloaded length with only modest permanent deformation [73]. With this it is believed that the Au/MWCNT surface (for Au-Au/MWCNT contact pair) conforms to the shape of the Au hemispherical probe.

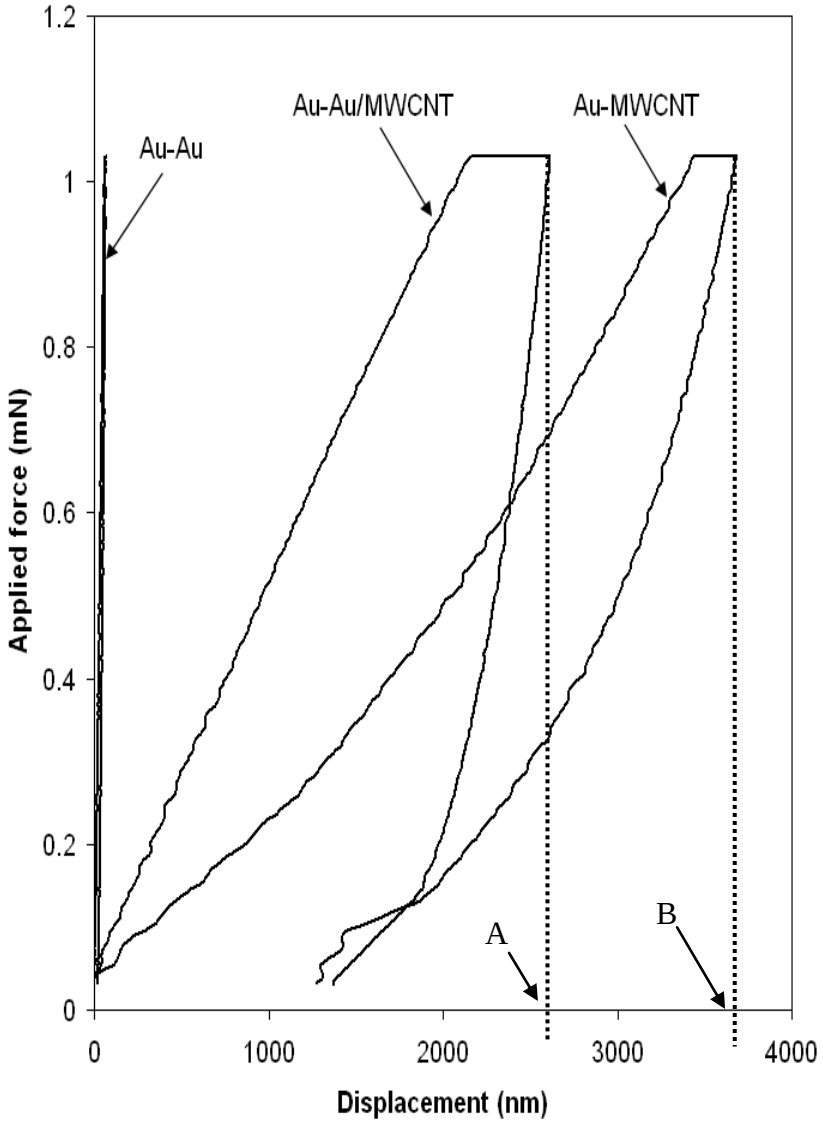

Figure 4.19: Graph of applied force vs. displacement for Au-Au, Au-MWCNT and Au-Au/MWCNT pair with maximum applied load at 1mN.

Figure 4.20 shows the Au-Au pair during the loading with penetration of ~70nm,

and after unloading the permanent displacement of 20nm was observed. This is a typical characteristic of the indentation of Au films on a hard silicon substrate. In an experiment by Cao et al. (2006) a nano-indenter with diamond tip was used (Berkovich, three-sided pyramid tip, 142.3^{o}) to indent a Au film with different thicknesses from 100nm to 2000nm coated on a silicon substrate[124]. It was shown that the hardness of Au decreases with an increasing film thickness. The increase is attributed largely to the effects of the substrate modulus mismatch [124]. Furthermore, in this study a nano-indentation apparatus with a Berkovich indenter was also used on Au, MWCNT, and Au/MWCNT substrates as shown in Appendix 7 at a maximum applied force of 1mN. The calculated elastic modulus for the Au substrate was 191.5GPa, and compared with MWCNT and Au/MWCNT were 67.5MPa and 92.3MPa respectively.

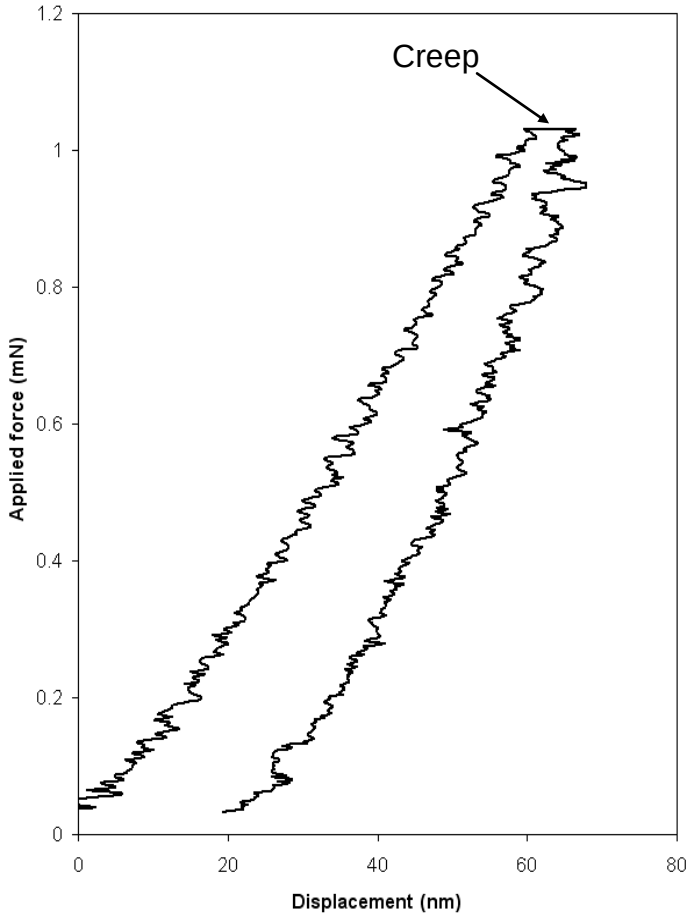

Figure 4.20: Graph of applied force vs. displacement for Au-Au with maximum applied load at 1mN.

4.4.2 Contact resistance vs. number of cycles for 10 cycles

To observe any degradation of the contact pairs, cyclic loading is performed. In this study 10 cycles were performed using the modified nano-indentation apparatus. Figure 4.21 shows the cyclic resistance of the Au-Au contact pair at maximum applied load of 1mN. All the data points include the corresponding standard deviation of the contact resistance data collected during the hold period. Initially the contact resistance starts from ~0.383Ω and increases slightly by about 100mΩ during the cycling.

In a similar experiment by Dickrell et al. (2005) using a modified nano-indentation apparatus it is shown that the Au-Pt contact pair degrades and the contact resistance increases after the 10 cycle [51]. They proposed that this was due to hot-switching arcing affects at the surface. In this experiment no hot-switching loads were used, so the contact does not degrade by “hot-switching”.

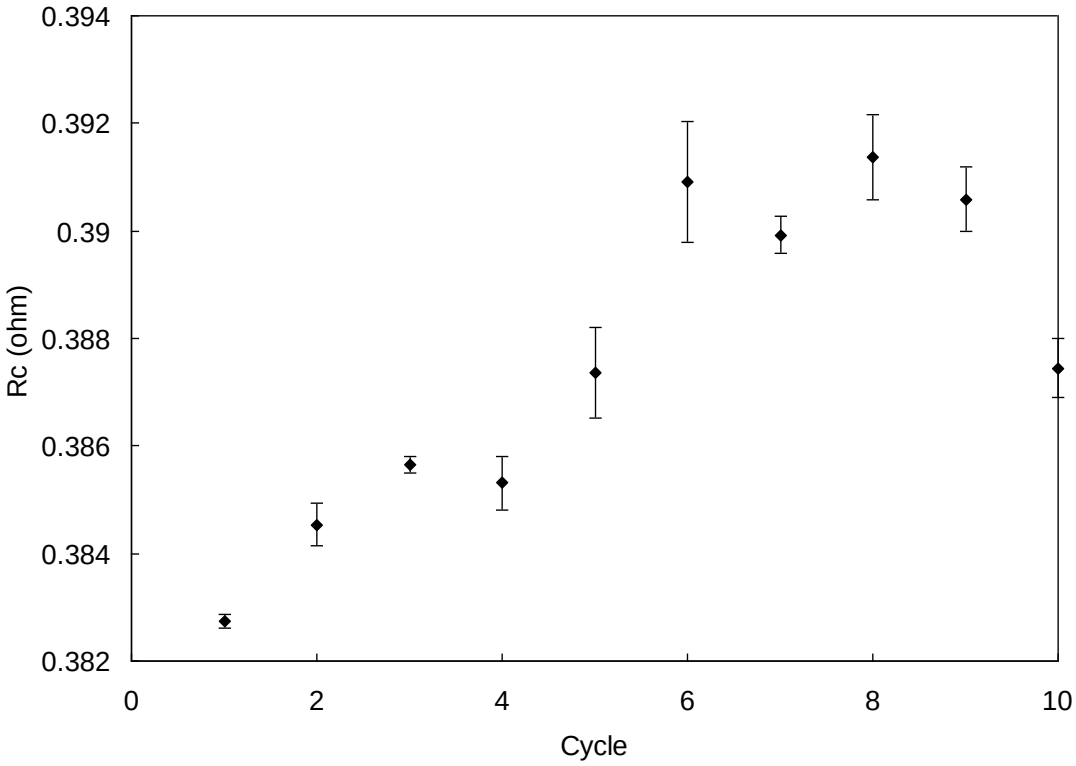

Figure 4.21: Cyclic contact resistance of Au-Au contact pair.

Figure 4.21 shows the results for a low number of cycles for the Au-Au contact pair. The slight increased in the contact resistance is due to the deterioration of

the Au layer on both Au-Au contact surfaces because of the poor mechanical properties of Au (typically a low hardness of 1-2GPa). This has been widely studied and reported in other work. As stated by Coutu et al. (2004), Au is a very soft metal, has a low melting point, adsorbs a carbonaceous layer and is susceptible to erosion and wear [50]. Figure 4.22 shows the contact resistance of the Au-MWCNT contact pair (the points include the corresponding standard deviation of the contact resistance measured during the hold period) to be higher than Au-Au contact pair. The reason was that MWCNT has a higher resistivity and its surface is rougher (shown in Figure 4.7 and 4.14) than Au substrates.

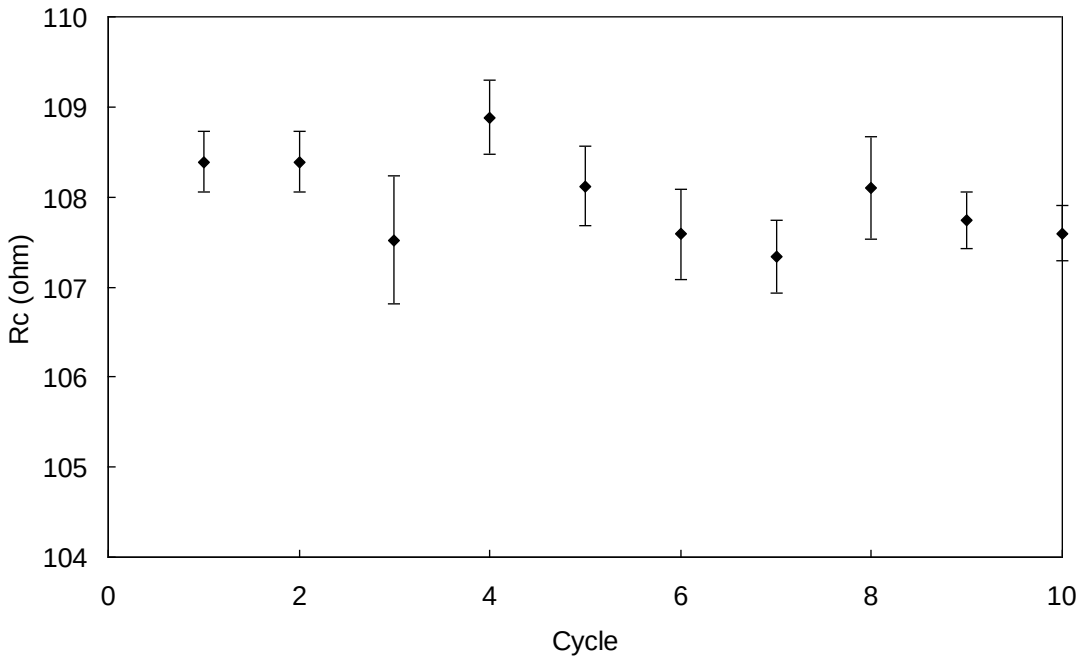

Figure 4.22: Cyclic contact resistance of Au-MWCNT contact pair.

To improve the contact resistance the MWCNT was coated with a conductive material, in this case, Au. Figure 4.23 shows the Au-Au/MWCNT contact pair (it also shows the points including their corresponding standard deviation of the contact resistance measured during the hold period). The contact resistance was much lower (~0.46Ω) than Au-MWCNT contact pair (~108Ω). The probable reason: (1) the Au coating on MWCNT was making contact with the Au on the contact as shown in Figure 4.17; (2) when the contact was pushed against the Au/MWCNT substrate it deflects or buckles and conforms to the shape of the contact thus improving the contact radius as shown in Figure 4.17; and (3) the

slightly higher contact resistance compared with the Au-Au contact pair was most likely due to surface properties such as the lower average roughness than Au/MWCNT surfaces.

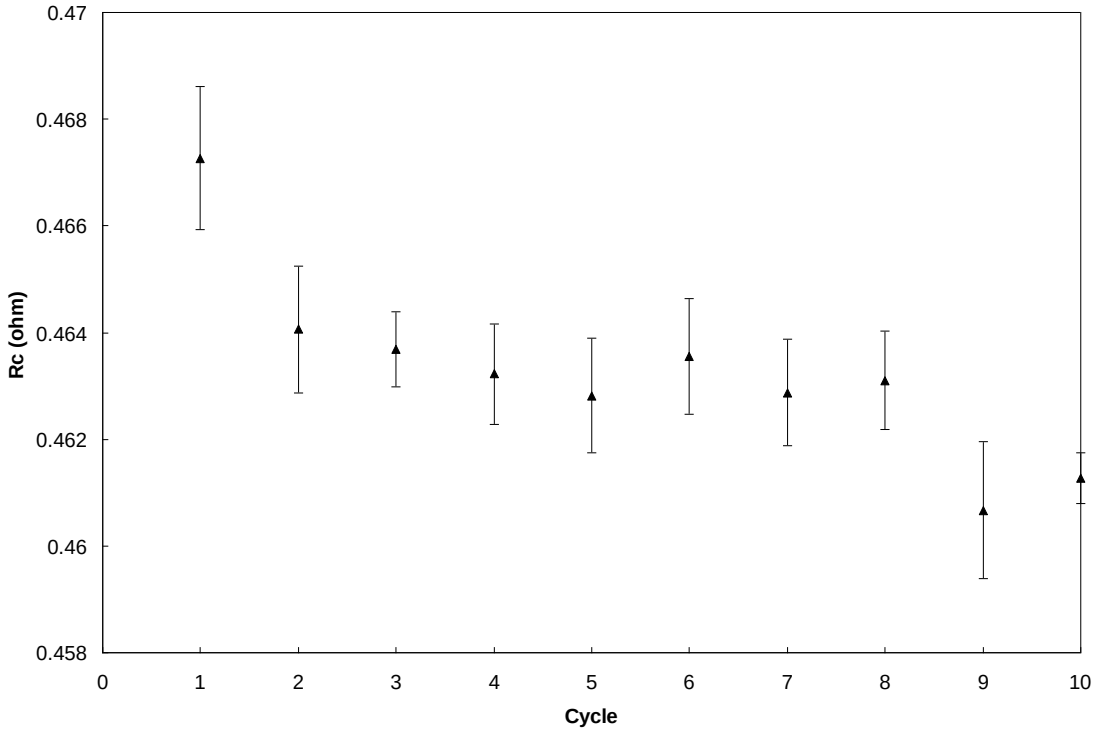

Figure 4.23: Cyclic contact resistance of Au-Au/MWCNT contact pair.

Figure 4.24 shows an SEM image of the Au hemispherical probe contact surface after 10 cycles which has some damage to the Au surfaces where many small impressions on the Au hemispherical probe can be detected. These impressions were due to the asperities on the MWNT surfaces. However, detecting the indentation on the Au contact is not straightforward as for a normal diamond indentation experiment where the indentation is clear and at one defined point on the substrate.

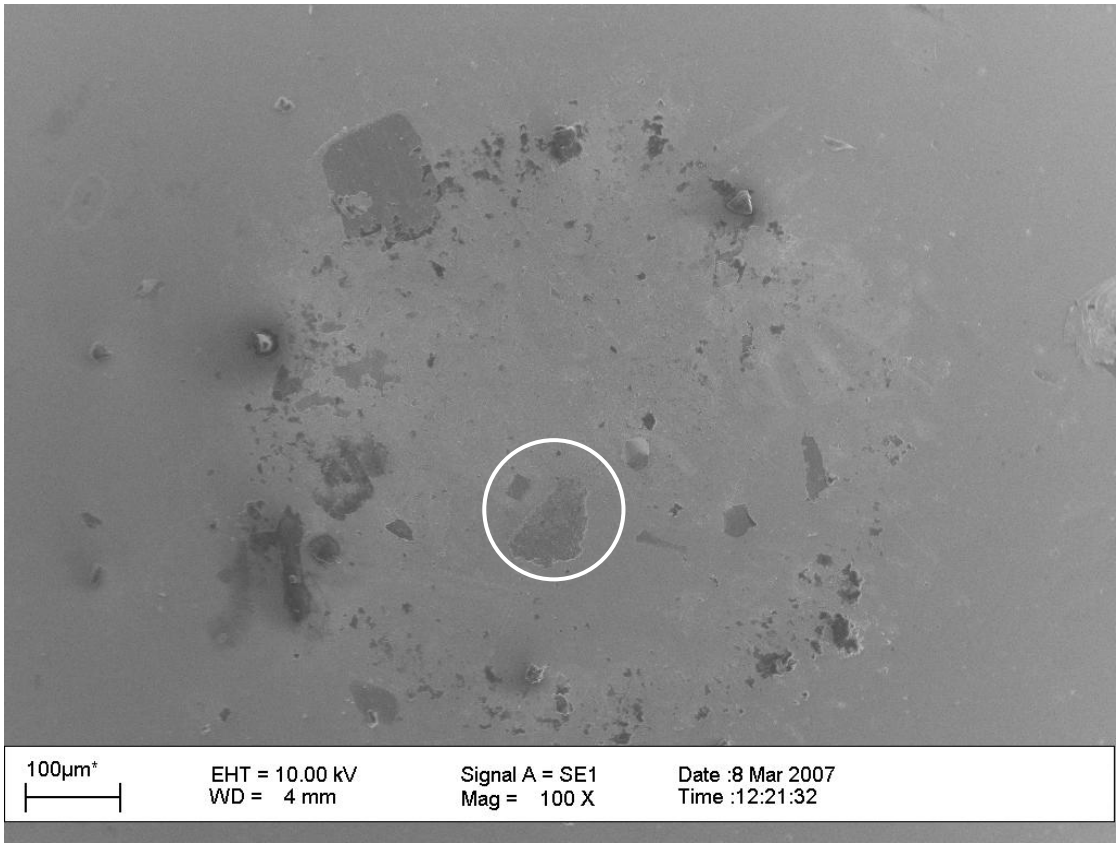

Figure 4.24: Au hemispherical probe after contact with Au/MWCNT substrate.

The scanned images of a fresh and a tested Au (ball) contact were compared as shown in Figure 4.25 (a) and (b) respectively. The area being scanned is as circled in Figure 4.24. It shows damage on the Au contact. Moreover when the surface roughness (R_a) was measured by TaiCaan (Xyris 4000CL) in this region (Figure 4.25 (b)) it had changed from ~400nm to ~1.5µm.

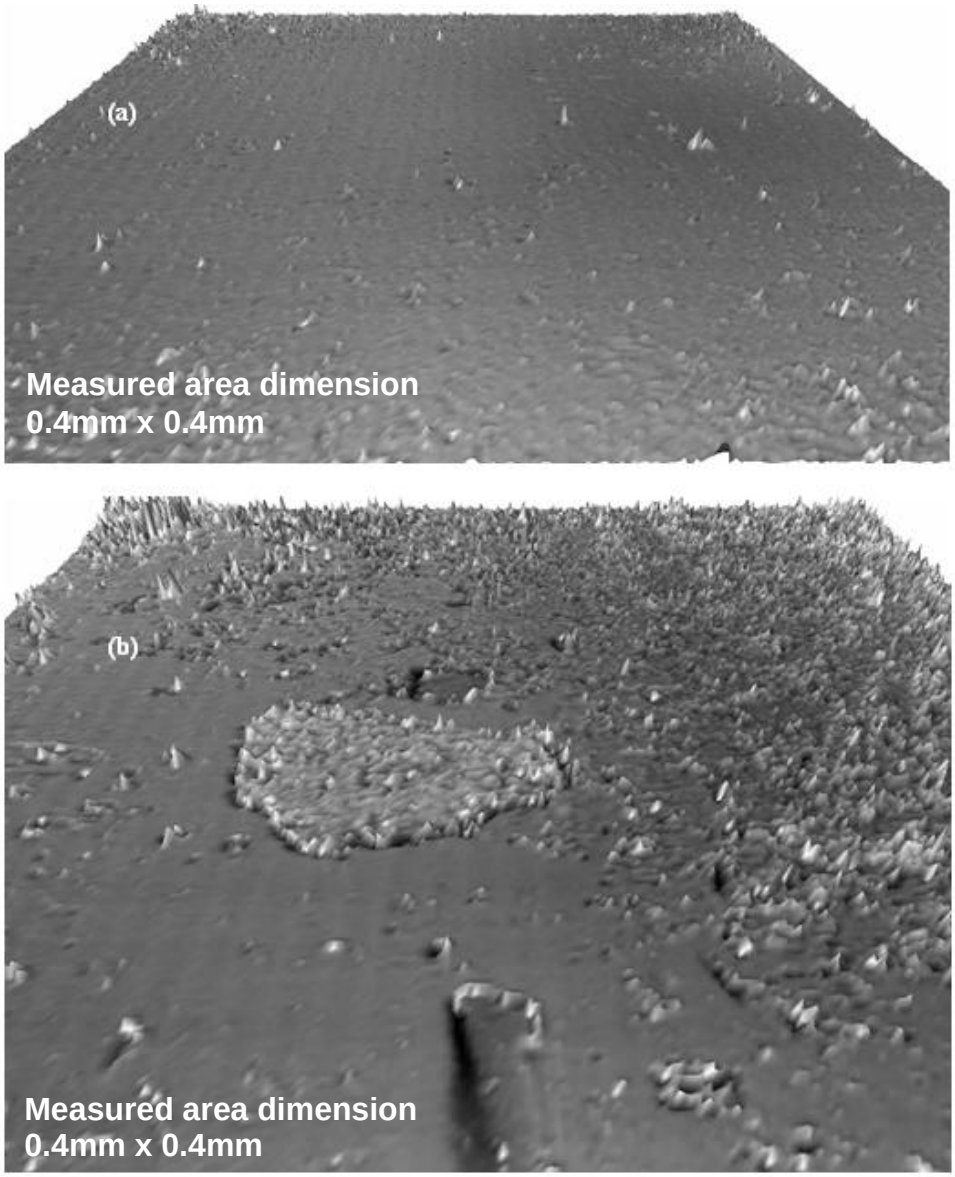

Figure 4.25: (a) Fresh and (b) tested Au (ball) contact with spherical shape removed, 301x301 (400µm x 400µm) using TaiCaan (Xyris 4000CL).

To validate the above experiment an X-ray spectroscopy was performed on the damaged Au hemispherical probe. Figure 4.26(a) shows the electron image of the area analysed by X-ray spectroscopy on the Au contact. The 'Au' peak was predominantly observed, with 'C' and 'O' peaks. This was consistent with the composition of the film, with some additional surface contaminants and water adsorbtion, Figure 4.26(b). The overall atomic percent of 'Au' was 38.6%, 'C' was 55.5% and 'O' 5.9% for the area "Spectrum 1", Figure 4.26(a). 'C' could have come from the MWCNTs surfaces or surface contaminants due to exposure with the environment.

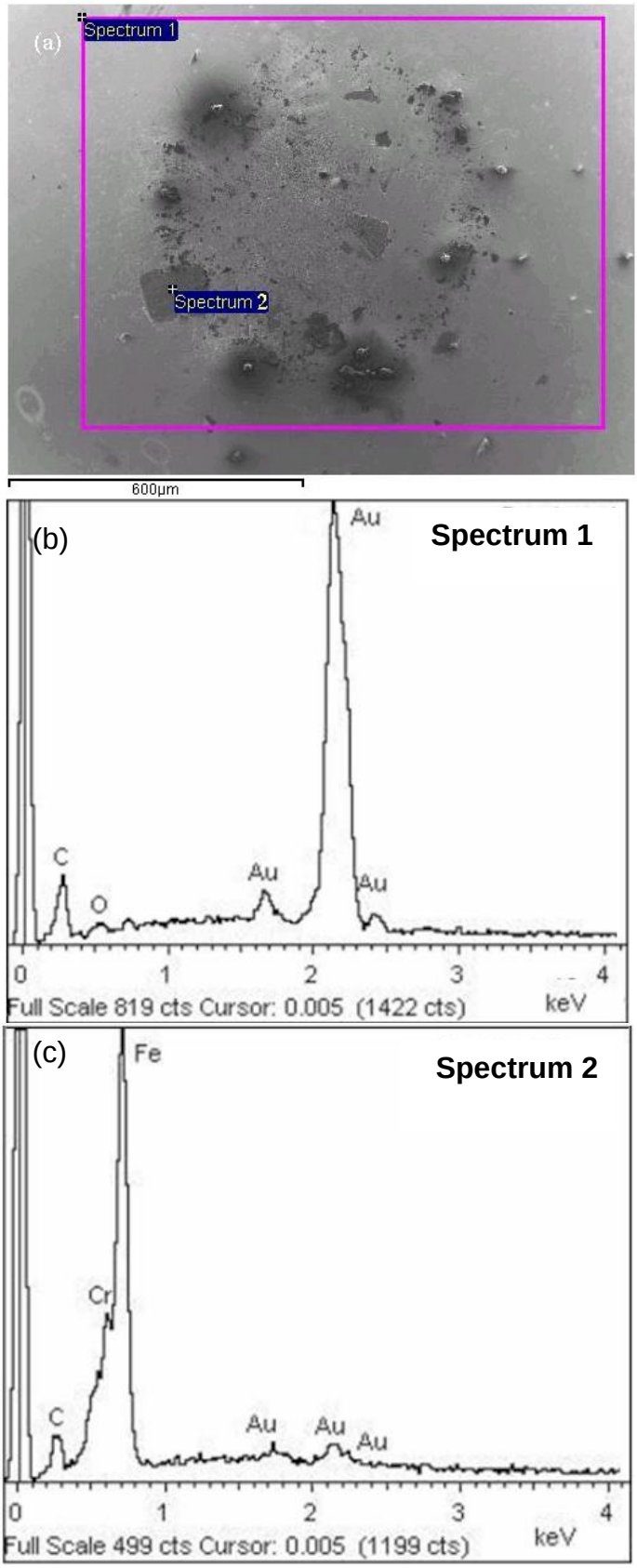

Figure 4.26: (a) Electron image, (b) EDX spectrum 1, and (c) EDX spectrum 2 of Au contact surface.

Au is a soft metal, which makes the Au contact susceptible to wear. Furthermore, only one Au hemispherical probe was used throughout the experiment. This could contribute to the damage of the Au probe. When one point on the exposed hemisphere was analysed, marked ‘Spectrum 2’ as shown in Figure 4.26(a), the ‘Fe’ peak was predominant, but together with a ‘Cr’ peak which suggests that the stainless steel ball is exposed, as seen in Figure 4.26 (c). The atomic percent shows ‘Fe’ was 68.7%, ‘Cr’ was 19.1%, ‘C’ was 11.7% and ‘Au’ was 0.6% thus indicating that wear had occurred on the Au contact exposing the surface of the stainless steel ball. No evidence of damage or change in chemical composition on the Au/MWCNT surface was detected.

Even though the Au-Au/MWCNT contact pair shows a comparable contact resistance with the Au-Au contact pair, further experimentation is needed to avoid adhesion of the contact and substrate, which could degrade the contact resistance during extended cycles. This phenomenon was clearly seen in Figure 3.8 where during unloading there was still contact resistance measured until total separation of the contact pair. Moreover, an indication of creep can be seen in Figure 4.20 and was identified as the mechanism responsible for an increase in stiction [125].

4.4.3 Factors affecting the modified nano-indentation testing

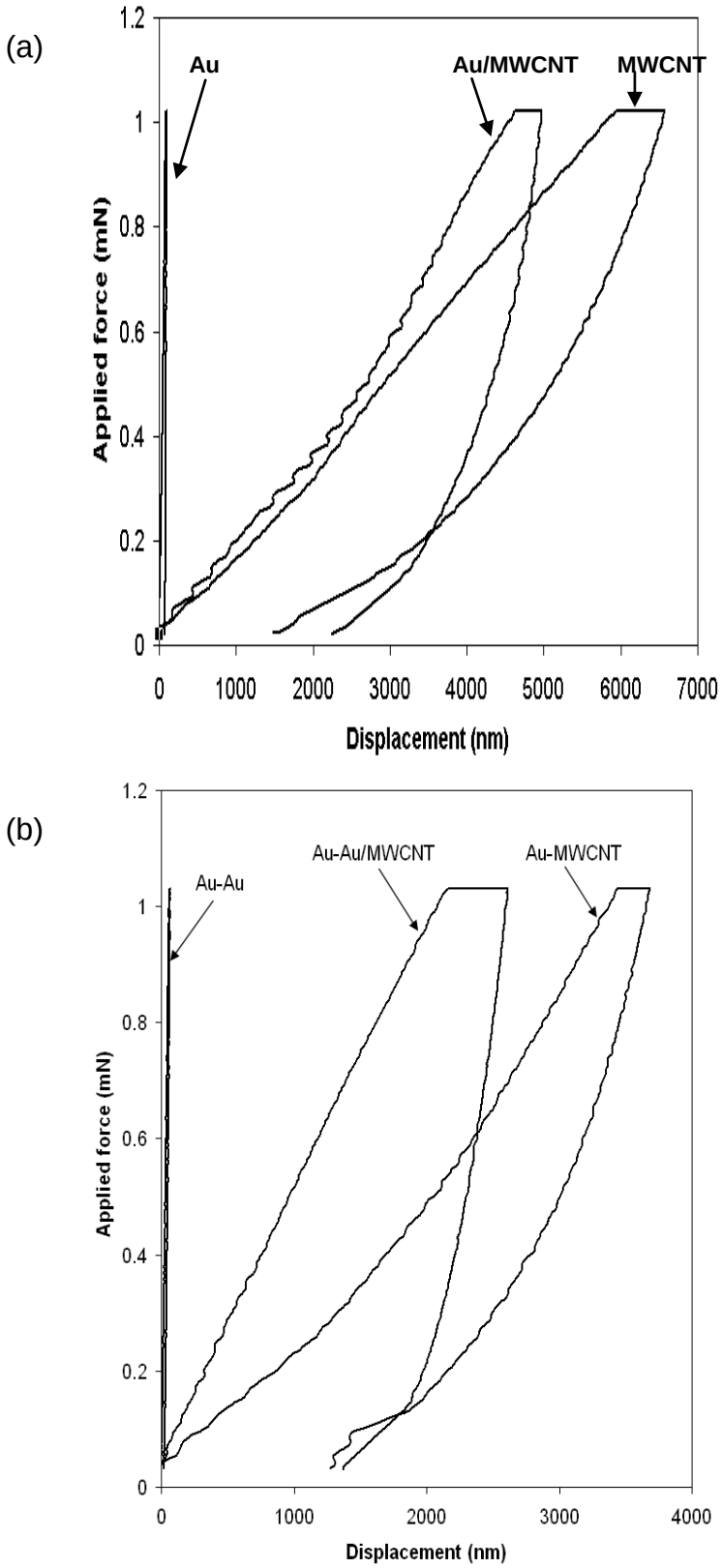

Figure 4.27: Graph of applied force against displacement for (a) Au, MWCNT and Au/MWCNT surface using nano-indentation test with Berkovich indenter (b) for Au-Au, Au-MWCNT and Au-Au/MWCNT contact pair using modified nano-indentation test without wire attached.

In this study the modified nano-indentation apparatus had been used to determine the surface properties. The following test was performed:

(1) nano-indentation test with the Berkovich indenter on Au, MWCNT and Au/MWCNT surfaces,

(2) a modified nano-indentation test for Au-Au, Au-MWCNT and Au-Au/MWCNT contact pairs without 4 wire measurement attached, and

(3) a modified nano-indentation test for Au-Au, Au-MWCNT and Au-Au/MWCNT contact pairs with 4 wire measurement attached.

Figure 4.27 (a) shows the force/displacement graph of Au, MWCNT and Au/MWCNT substrates using nano-indentation testing with the Berkovich indenter. Figure 4.27 (b) shows the force/displacement graph of Au-Au, Au-MWCNT and Au-Au/MWCNT contact pairs using modified nano-indentation apparatus at the maximum applied load of 1mN. Both tests showed similar patterns but the main difference was in the depth of penetration. For example the depth penetration for Au/MWCNT with the Berkovich indenter was ~4500nm and for Au-Au/MWCNT contact pair was ~2400nm. The reason was the Berkovich indenter has a more pointed end (as shown in Figure 4.28 (a)) than the Au hemispherical probe (as shown in Figure 4.28 (b)), thus deeper penetration was obtained.

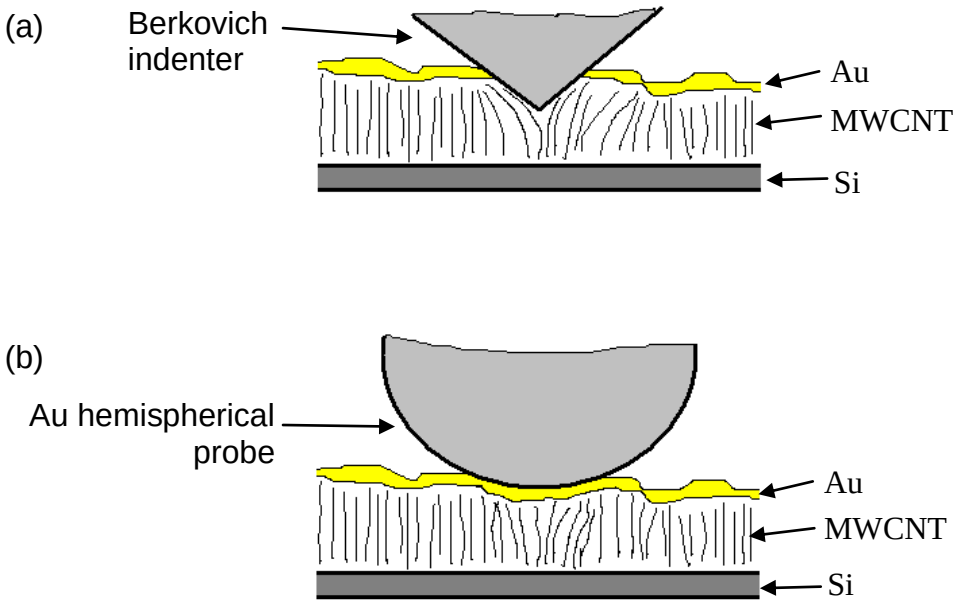

Figure 4.28: (a) Indentation with Berkovich indenter and (b) indentation with Au hemispherical probe on Au/MWCNT surface.

Figure 4.27 (b) shows the normal curve pattern for the Au-Au, Au-MWCNT and Au-Au/MWCNT contact pairs. When the wires (used for the 4-wire measurement) were attached on the Au hemispherical probe as shown in Figure 3.5 (a) the curve pattern was distorted as shown in Figure 4.29. The reason was that the wire has affected the result: (1) the weight of the wire; and (2) the way the wire has been attached on the Au hemispherical probe limited the movement of the probe.

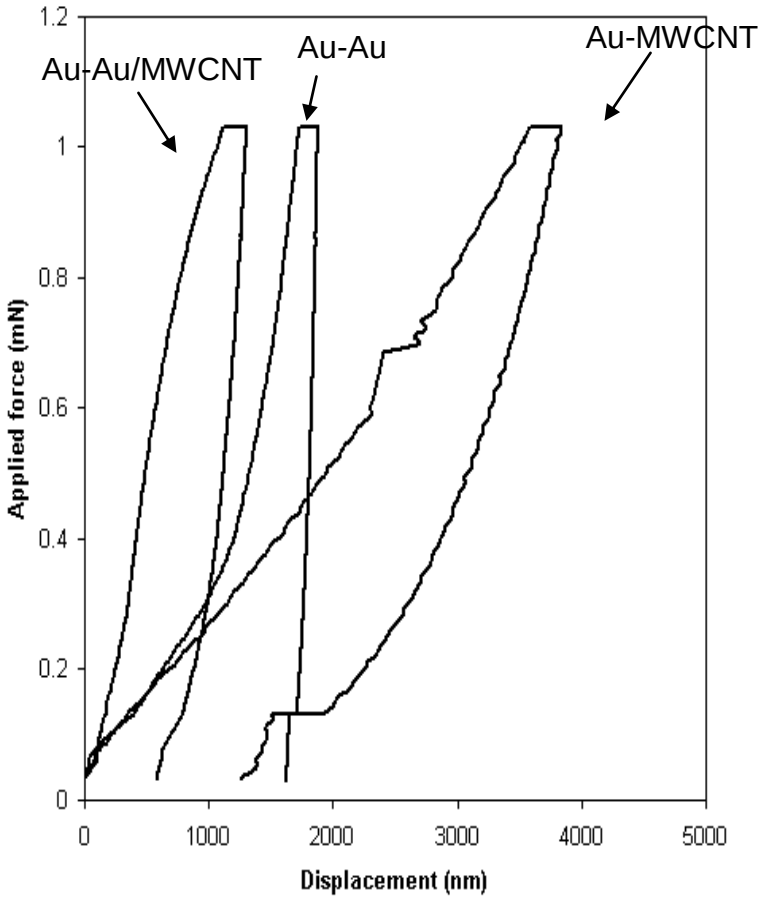

Figure 4.29: Graph of applied force against displacement for Au-Au, Au-MWCNT and Au-Au/MWCNT contact pair using modified nano-indentation test with wire attached.

Moreover, the modified nano-indentation apparatus has a limitation when performing a large number of cycles and due to the factor affecting the movement of the probe, therefore an alternative way to test the contact was needed. Thus, a PZT actuator test rig was designed and fabricated.

4.5 Experiment 2: PZT actuator test rig (dry-circuit condition)

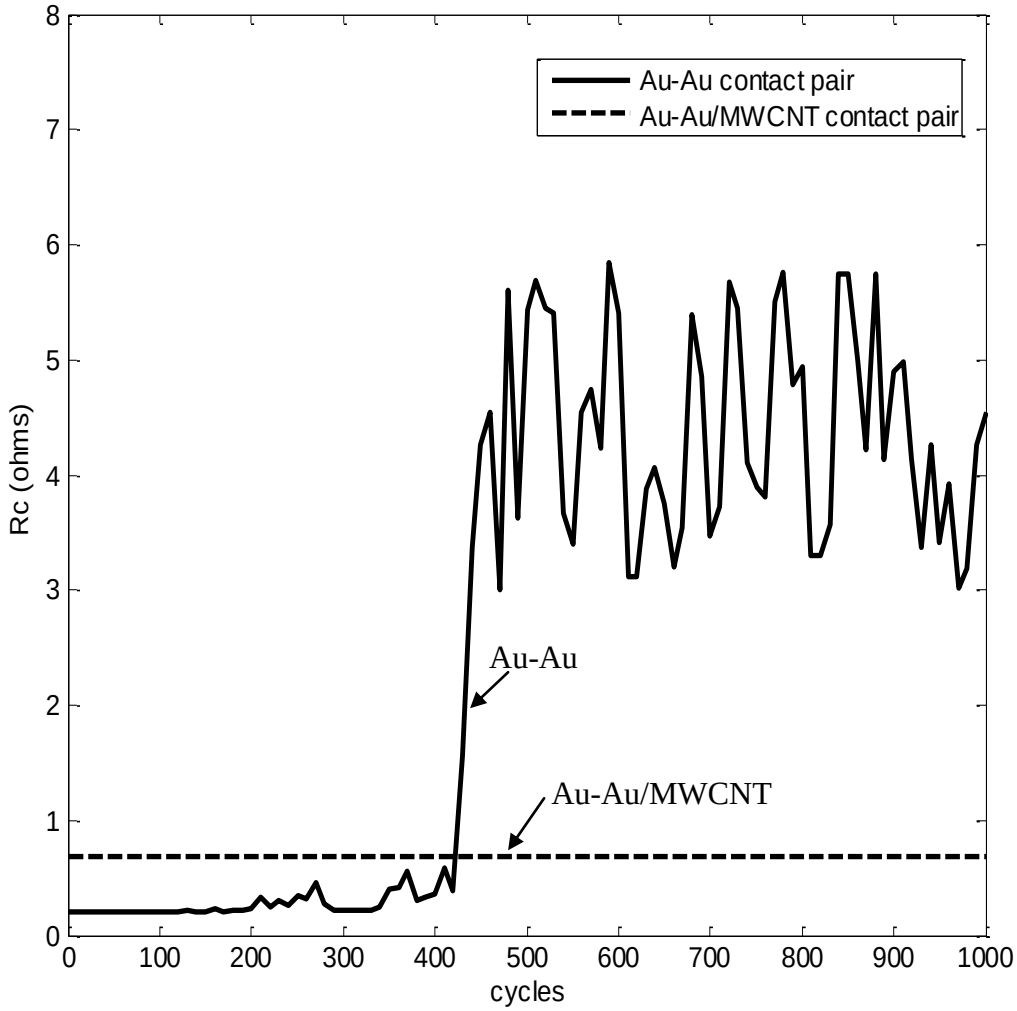

Figure 4.30: Cyclic contact resistance of Au-Au and Au-Au/MWCNT contact pairs.

Figure 4.30 shows the contact resistance of the Au-Au and Au-Au/MWCNT pairs over 1000 cycles at a maximum (quasi static) applied load of 1mN. The contact resistance of the Au-Au pair was initially ~0.2Ω and increased rapidly to 4-6Ω at 430 cycles. Under dry-circuit conditions with 1mA current and a maximum voltage of 20mV (less than melting voltage, 0.43V for Au [31]) the contacts were unlikely to degrade by hot-switching, therefore the increase in contact resistance was solely due to the mechanical deterioration of the Au-Au

contact pair surfaces, reflecting the recognized problems of using soft metals for electrical contacts. The reason for the sharp increase in contact resistance of the Au-Au pair at ~430 cycles was believed to be due to the adhesion [40]. The smoothing is the result of the repeated impacts of the Au. Figure 4.31 shows the damaged Au surface planar from the Au-Au contact pair.

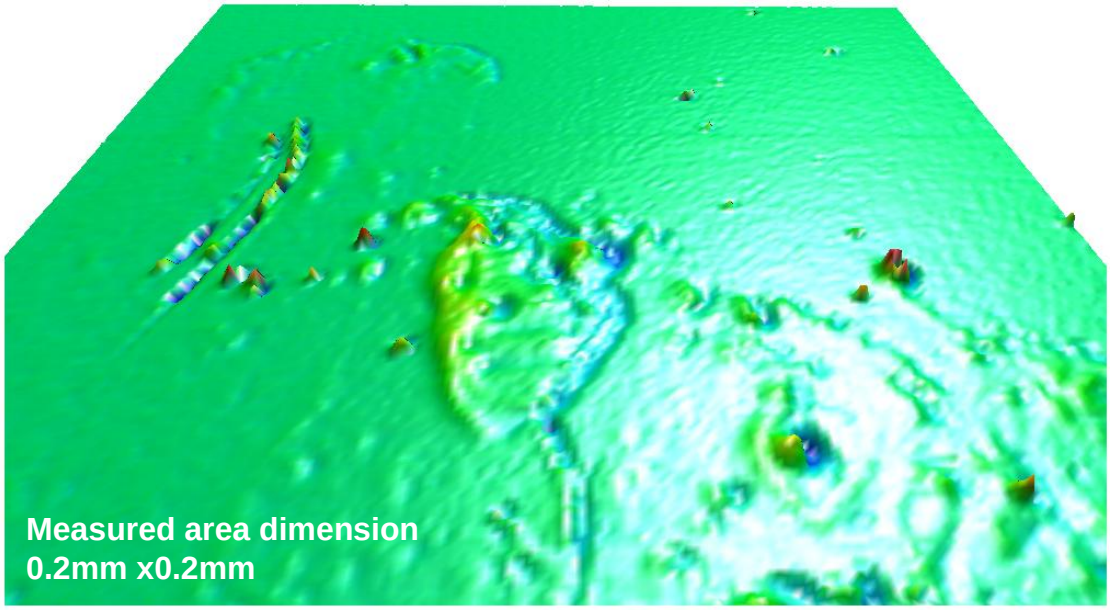

Figure 4.31: Scanned image of Au planar surface 201x201(0.2mmx0.2mm) using TaiCaan (Xyris 4000CL)

The adhesive force increases with the number of cycles and is consistent with creep, being one of the underlying physical mechanisms for the increase in adhesion [125]. The creep of the gold was shown in Figure 4.20 during a single load cycle. Figure 4.20 shows the graph of load against displacement for an Au-Au contact pair. The curve shows there is creep, a deformation that occurs over a period of time when a material is subjected to constant stress, even at room temperature. The force cycle exhibited in Figure 4.20 occurs over a longer time scale than that used in this test procedure, with an impact period of approximately 3 seconds.

Figure 4.30 also shows a contact resistance of the Au-Au/MWCNT contact pair. The initial contact resistance (~0.7Ω) is higher for the Au-Au/MWNT pair when compared with Au-Au contact pair. A possible cause was the difference of

surface roughness between Au and Au/MWCNT coated planar surfaces and the irregularity of the Au film on the MWCNT. It was anticipated that this could be improved in subsequent experiments by better process control. The contact resistance was much more stable than for the Au-Au pair over the 1000 loading cycles. This was believed to be due to the Au/MWCNT surfaces conforming to the shape of the Au hemispherical probe. The dynamic impact on the Au hemispherical probe was absorbed by the Au/MWCNT surfaces thus reducing the wear. The compliant effect on Au-Au/MWCNT helps to reduce the deterioration.

In addition, as the Au/MWCNT surface conforms to the shape of the Au hemispherical probe it increases the contact area. There was a smoothening of the Au asperities and significant indentation marks on the Au covering the surface of the Au hemispherical probe as shown in ‘A’ and ‘B’ respectively on Figure 4.32. No visible damage can be detected on the Au/MWCNT planar composite, further suggesting that the CNT under-layer has improved the mechanical integrity of the gold surface.

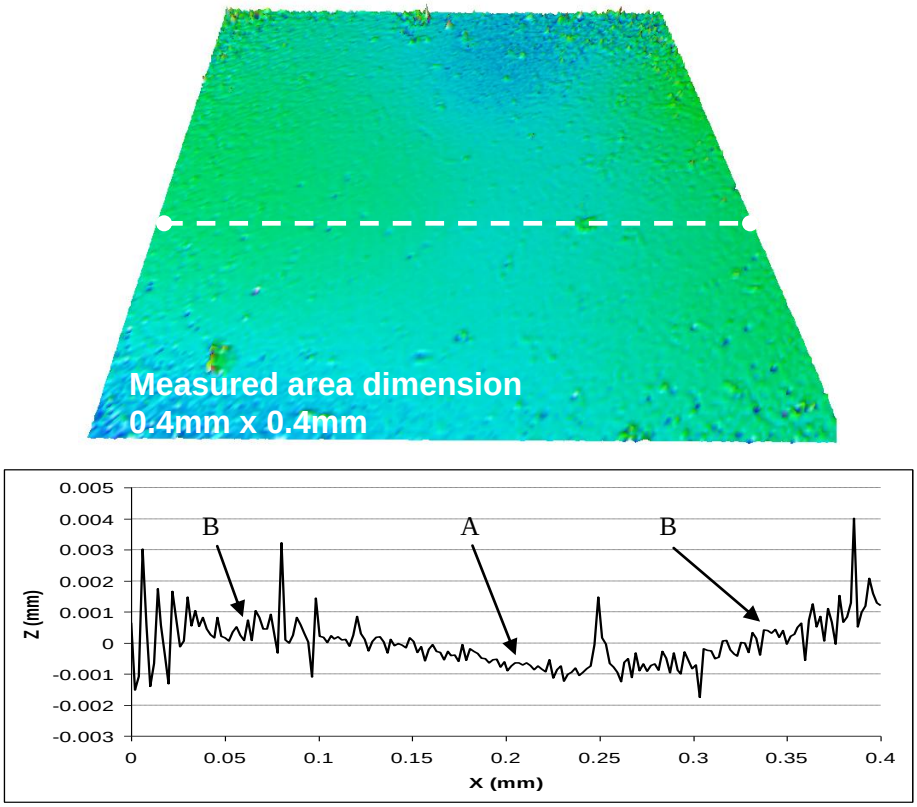

Figure 4.32: Scanned image of Au ball for Au-Au/MWCNT with the sphere removed, contact pair 301x301 (0.4mmx0.4mm) using TaiCaan (Xyris 4000CL).

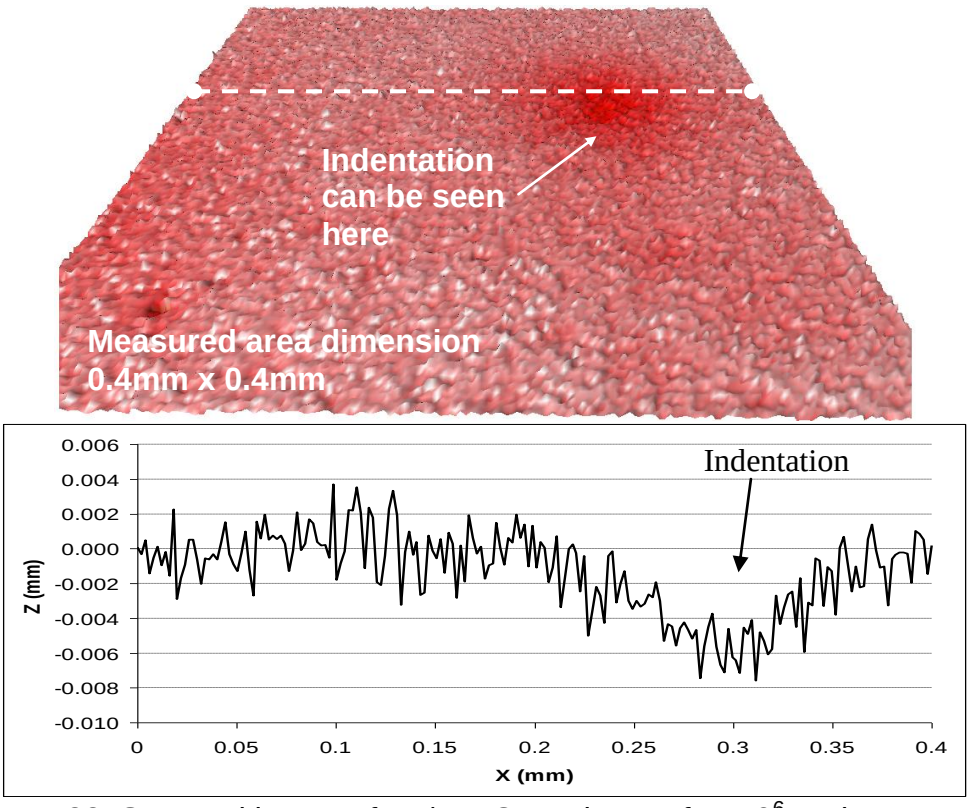

Figure 4.33: Scanned image of Au/MWCNT planar after 10^6 cycles at 1mN of applied load, 201x201 (0.4mmx0.4mm) using TaiCaan (Xyris 4000CL).

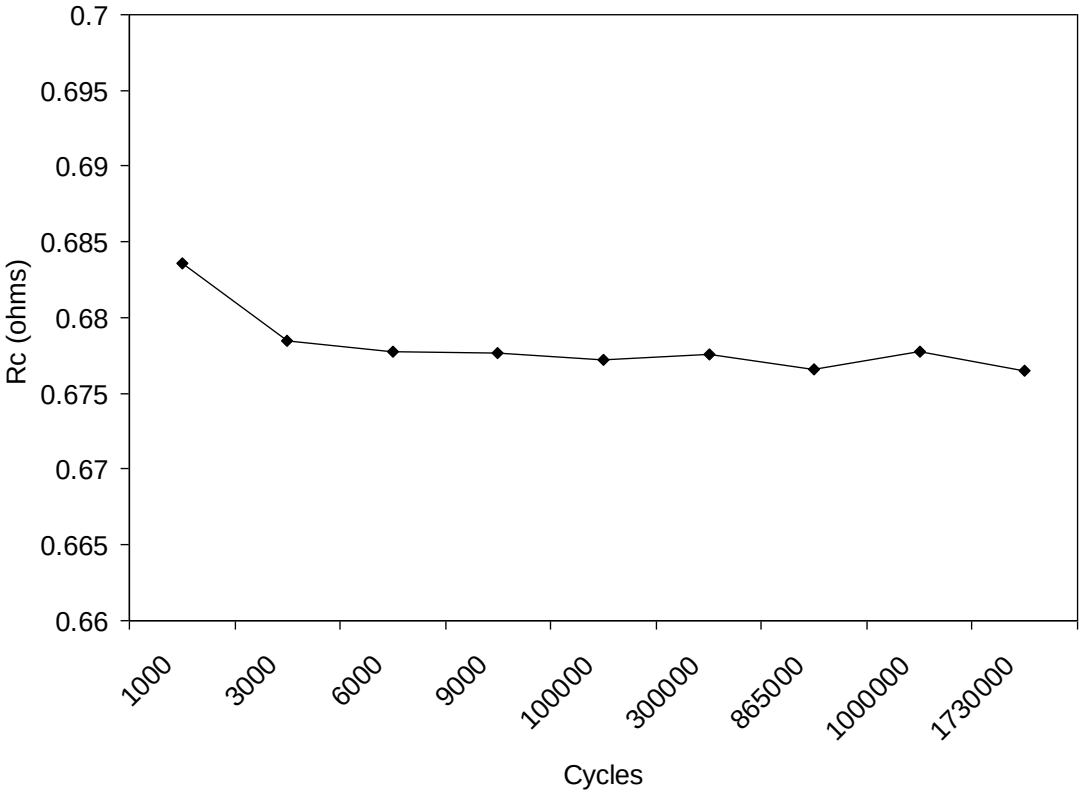

Figure 4.34: Contact resistance after 10^6 cycles at 1mN.

Figure 4.33 shows the indentation by the Au hemispherical probe was visible after more than a million cycles. This experiment was a continuation from the 1000 cycles at 1mN applied load. Figure 4.34 shows the contact resistance for 1000 cycles to greater than 10^6 cycles. After a smaller initial decrease, the contact resistance was constant up to 1.73 million cycles with a value of 0.68Ω. The probable cause of the small changes in the contact resistance was due to the increase in contact radius, that is the Au/MWCNT planar conforms more to the shape of the Au-hemispherical probe. The Au/MWCNT planar has much a higher contact radius than a conventional rigid planar contact surface (in this case Au-planar). After 3000 cycles no observable indentation occurs, thus the contact resistance can be seen to stabilise up to more than a million cycles. It was observed that the Au/MWCNT conforms to the Au hemispherical probe shape as shown in Figure 4.33. This showed how mechanically robust Au/MWCNT surfaces were even after one million cycles, there was only little deformation observed (< 4μm in depth). Further this suggests that the

deformation has occurred on the Au film rather than the MWCNT, thus showing the improvement on the mechanical integrity of the systems.

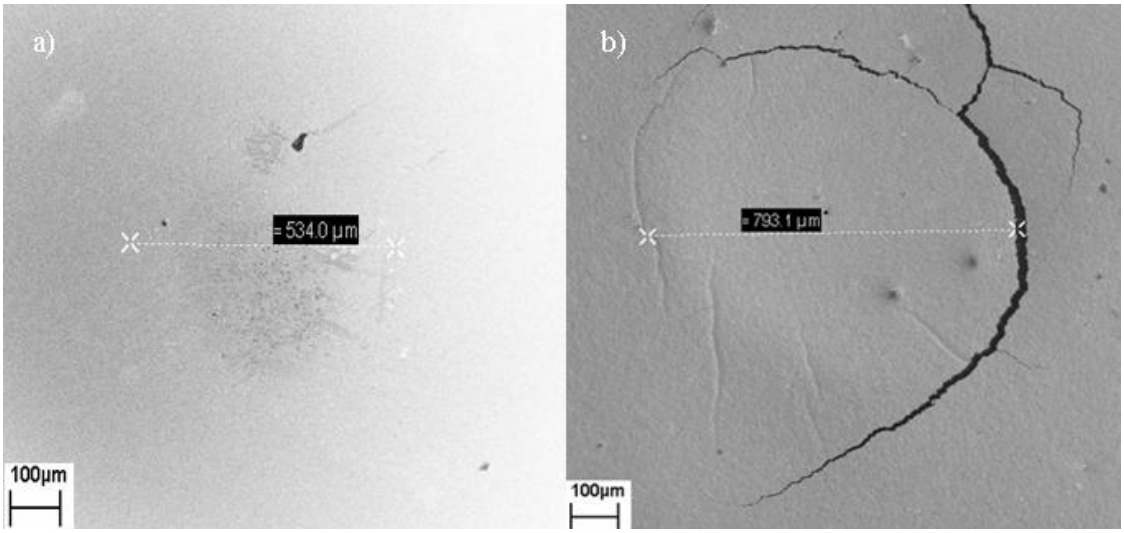

Figure 4.35. SEM images of a) Au hemispherical probe and b) Au/MWCNT surface after 2 million cycles at 3mN.

Figure 4.35 shows an SEM image of the Au hemispherical probe surface and the Au/MWCNT surface after 2 million cycles with a maximum applied force of 3mN. Figure 4.37 also shows the scanned image of the Au/MWCNT composite surface obtained using the TaiCaan (Xyris 4000CL) system. It was observed that there were marks on the Au hemispherical probe of ~530µm (Figure 4.35 (a)) in diameter. Figure 4.35 (b) and 4.36 shows tearing or cracking of the Au/MWCNT and this was consistent with adhesion and/or fatigue of the Au (Figure 4.35 (a)) and Figure 4.36 shows a tear opening of approximately 25µm. This deterioration had not yet resulted in any measurable change in the contact resistance. Another probable reason for the crack was the insufficient infiltration of Au being sputter-coated on some areas of the MWCNT surface to form the composites. The penetration of the Au is between 700nm – 4µm. Due to this it would displace or deflect the MWCNT. Another reason would be poor anchorage or adhesion of the MWCNT to the silicon substrate. It was observed that, where the Au hemispherical probe impacted on the Au/MWCNT surface there was no observable degradation.

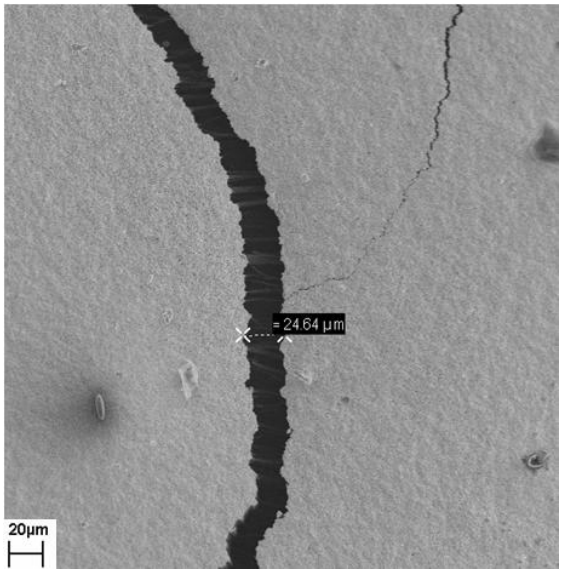

Figure 4.36: Tear or crack surface of Au/MWCNT composite after 2 million cycles at 3mN of applied force.

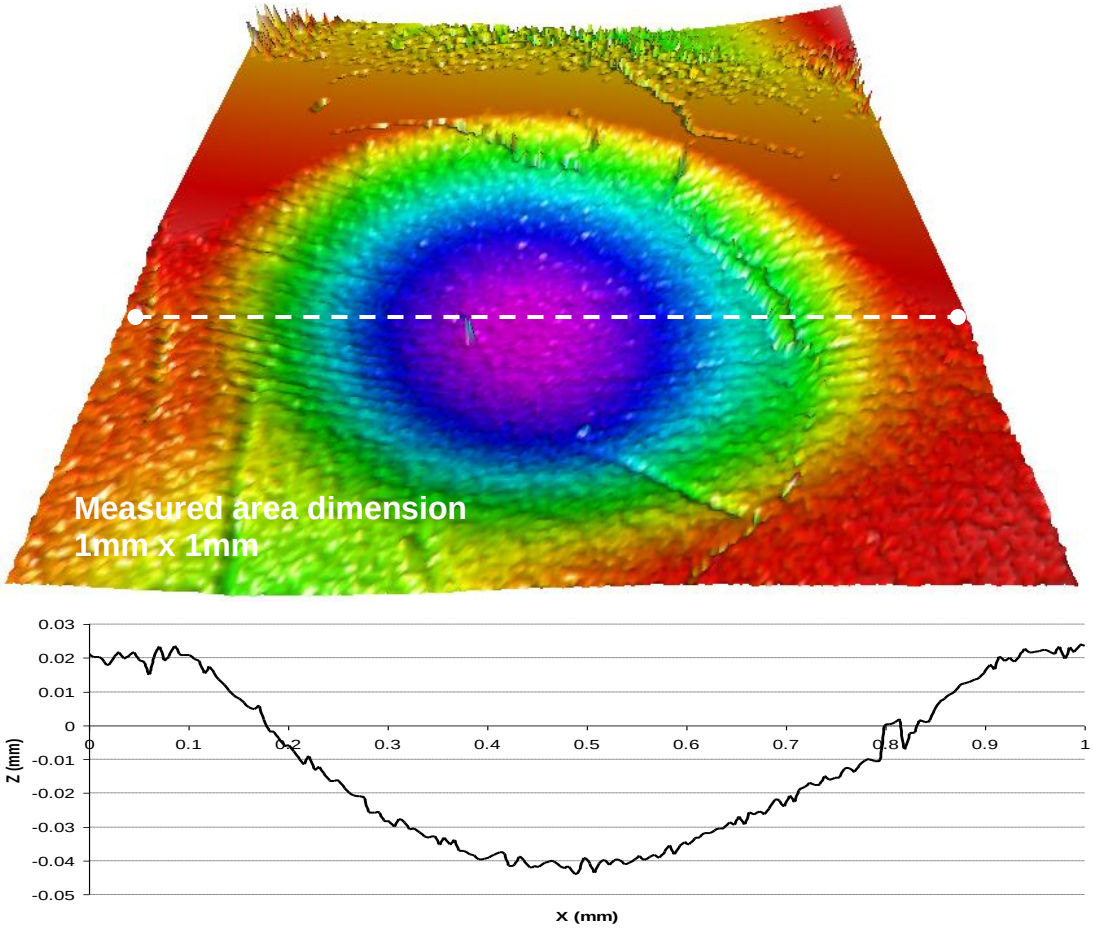

Figure 4.37: Scanned image of Au/MWCNT planar after 2 million cycles at 3mN of applied load, 201x201 (1mmx1mm) using TaiCaan (Xyris 4000CL).

4.6 Experiment 3: PZT actuator test rig (hot-switched condition, 1mA and 10mA)

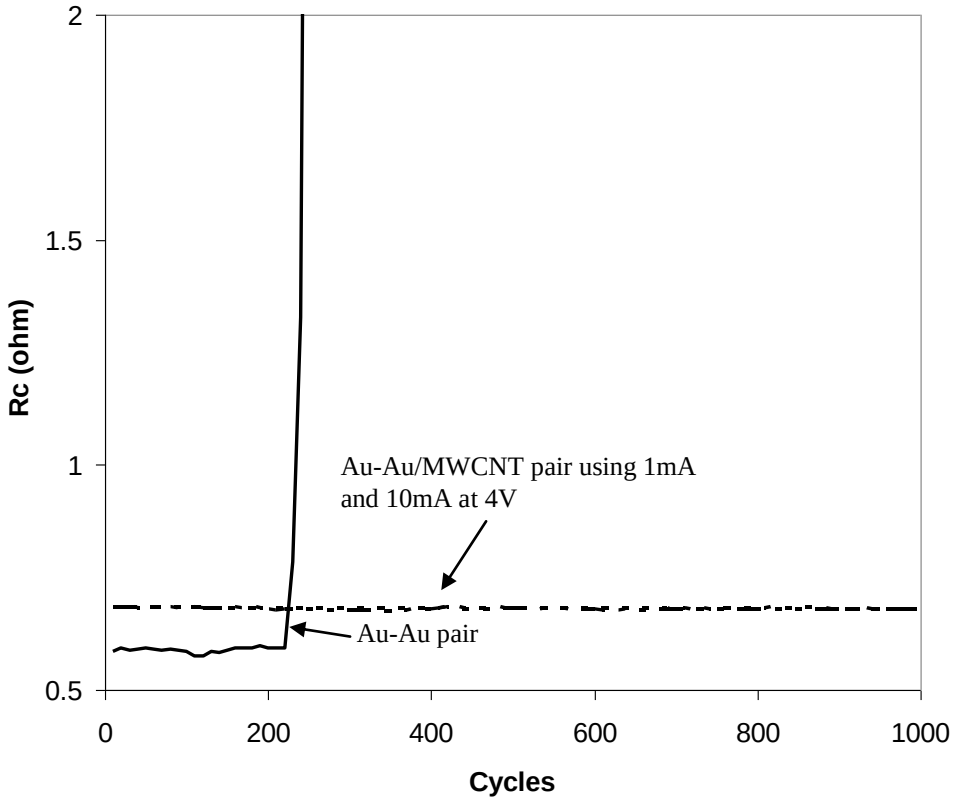

Figure 4.38: Cyclic contact resistance for Au-Au and Au-Au/MWCNT contact pair.

Figure 4.38 shows the contact resistance of the Au-Au pair over 1000 cycles at a maximum applied load of 1mN at quasi static switching cycles. The contact resistance of the Au-Au pair was initially ~0.58Ω and increased rapidly to 4-10Ω at ~220 cycles. The reason for the sharp increase in R_c of the Au-Au pair was due to the softening or melting and smoothening of the Au surfaces which leads to increased adhesion [40,125]. The softening or melting was due the supply voltage (4V) used in this experiment. The theoretical voltage for softening and melting Au contact material is ~0.08V and 0.43V respectively [31]. The smoothing was the result of the repeated impacts and time-dependent deformation of the Au. Figure 4.39 (a) and (b) shows the damage or delamination of the Au hemispherical probe surface which has adhered onto the Au planar for the Au-Au contact pair. Figure 4.39 (c) also shows a scanned

image of the damaged Au hemispherical probe using the TaiCaan (Xyris 4000CL) system. The damage depth measured was ~500nm, thus exposing the under layer.

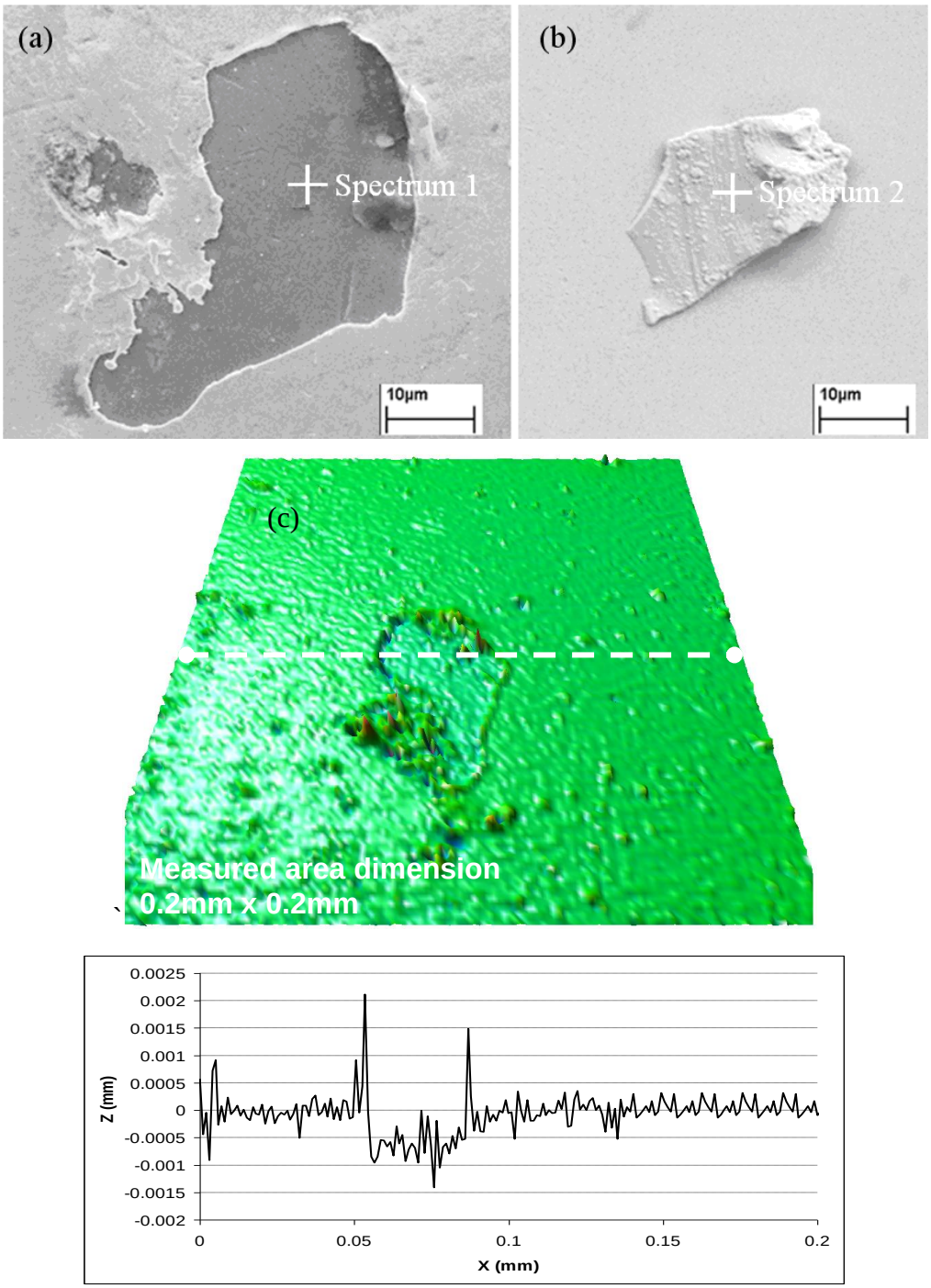

Figure 4.39: (a) SEM image of Au hemispherical probe degradation (b) SEM image of Au planar with Au debris (c) scanned image of damaged Au ball for Au-Au pair (1mA/4V) with the sphere removed, contact pair 201x201 (0.2mmx0.2mm) using the TaiCaan (Xyris 4000CL) system.

This can be confirmed using X-ray spectroscopy. Figure 4.39 (a) shows the point analysed by X-ray spectroscopy on the Au hemispherical probe “Spectrum 1”. Figure 4.40 (a) shows an EDX spectrum for the surface. The ‘Fe’ peak was predominantly observed and the Cr peak indicates both elements come from the stainless steel ball. The atomic percent shows Fe as 73.2% and Cr as 26.3% thus indicating that wear and damage has occurred on the Au hemispherical probe exposing the surface of the ball. Figure 4.39 (b) also shows the point analysed by X-ray spectroscopy of the adhered Au on the Au planar “Spectrum 2”. Figure 4.40 (b) shows an EDX spectrum for the surface. The ‘Au’ peak was predominantly observed with Au atomic percent of 100% thus indicating that Au debris has adhered on the Au planar.

(a)

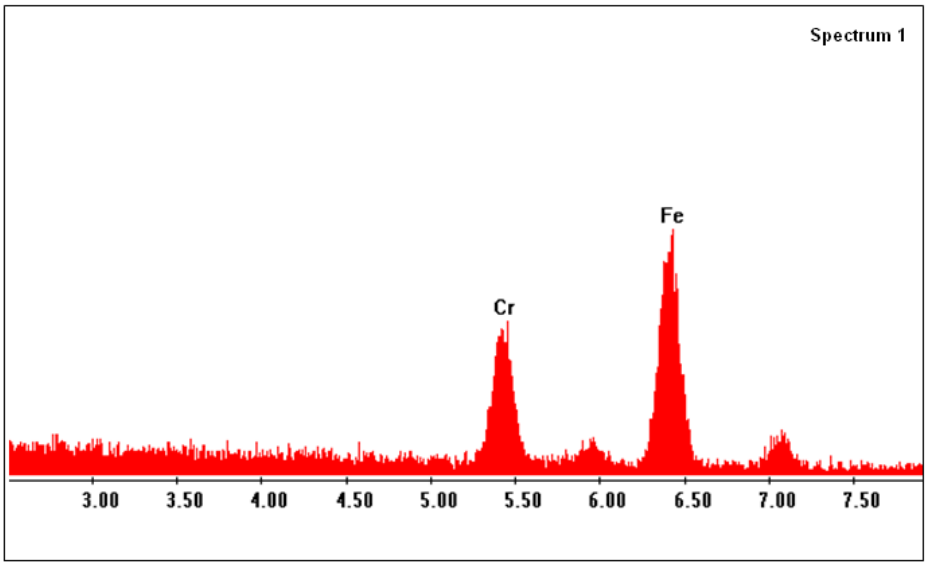

Figure 4.40: (a) EDX spectrum of exposed under layer of Au hemispherical probe surface.

(b)

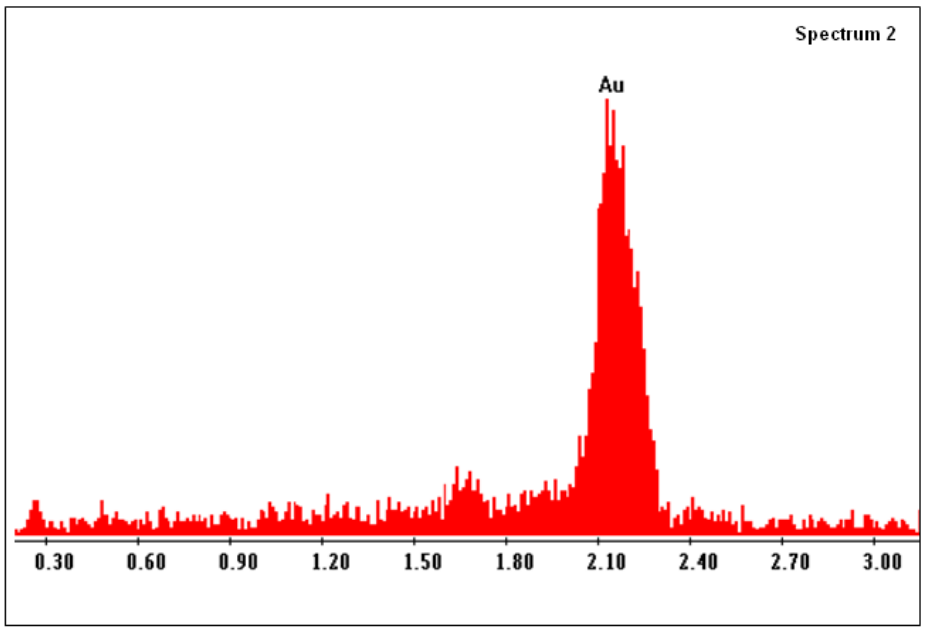

Figure 4.40: (b) EDX spectrum of adhered Au on the Au planar surface.

To explain further, the melting is due to the supply and current load used in this experiment, where the theoretical voltage for softening and melting Au contact material is ~0.08V and 0.43V respectively [31]. Under this condition joule heating occurs within the contact surface. Another reason is that it is more severe in materials that are subjected to heat for a long periods of time because the rate of deformation is a function of the material properties, exposure time, exposure temperature and the applied load.

Figure 4.38 also shows contact resistance of the Au-Au/MWCNT contact pair at different current loads (1mA and 10mA) at 4V. The contact resistance (~0.68Ω) for both current load conditions was slightly higher for the Au-Au/MWCNT pair when compared with the Au-Au pair (~0.58Ω), but the contact resistance was much more stable than for the Au-Au pair over 1000 loading cycles. This again was believed to be due to the Au/MWCNT surfaces conforming to the shape of the Au hemispherical probe. The dynamic impact on the Au hemispherical probe was absorbed by the Au/MWCNT surfaces thus reducing the wear. The compliant or sponge-like effect on Au-Au/MWCNT helps to reduce the wear.

.

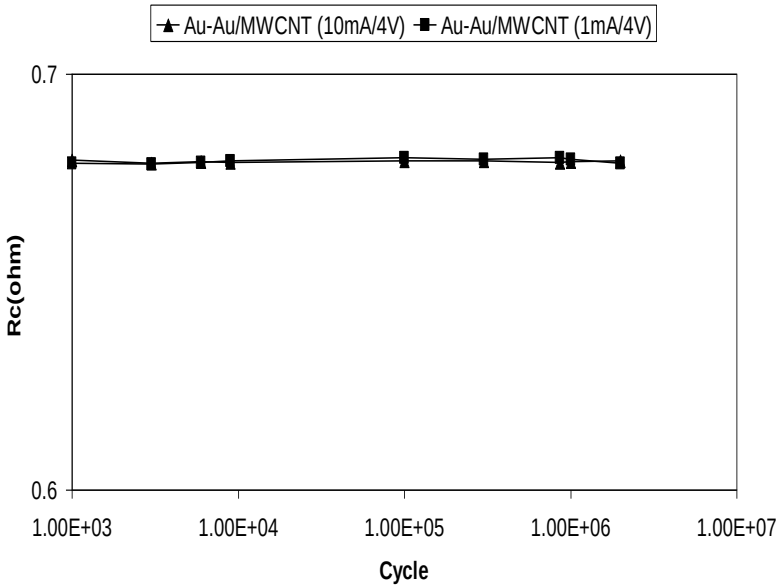

Figure 4.41: Contact resistance up to more than a million cycles for Au-Au/MWCNT contact pair after using current load of 1mA and 10mA, 4V.

Figure 4.41 shows the contact resistance over a million cycles. The contact resistance is stable for both current load (1mA and 10mA) conditions, even though there is some Au adhesion on the Au hemispherical probe (anode) as shown in Figure 4.42 (a) and (b). This Au adhesion is from the coated surface of the Au/MWCNT planar surfaces, which melted and adhered onto the Au hemispherical probe.

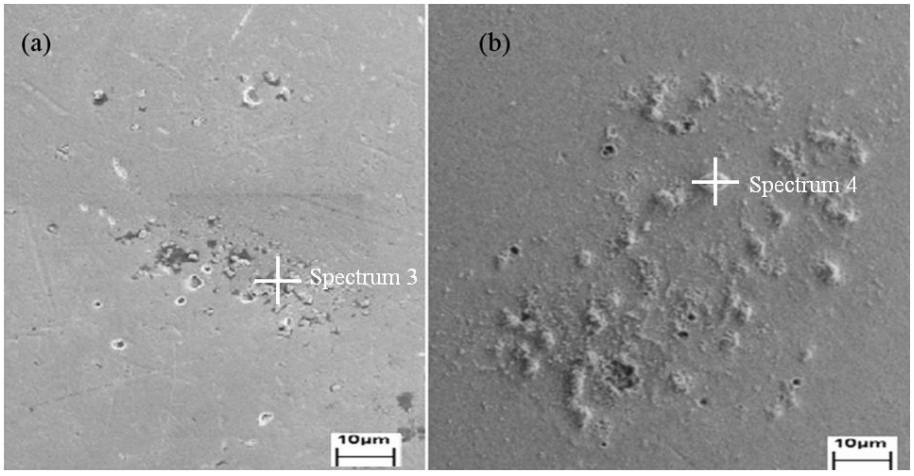

Figure 4.42: SEM image of (a) Au hemispherical probe for Au-Au/MWCNT contact pair at current load 1mA, 4V and (b) Au hemispherical probe for Au-Au/MWCNT contact pair at current load 10mA, 4V after more than a million cycles.

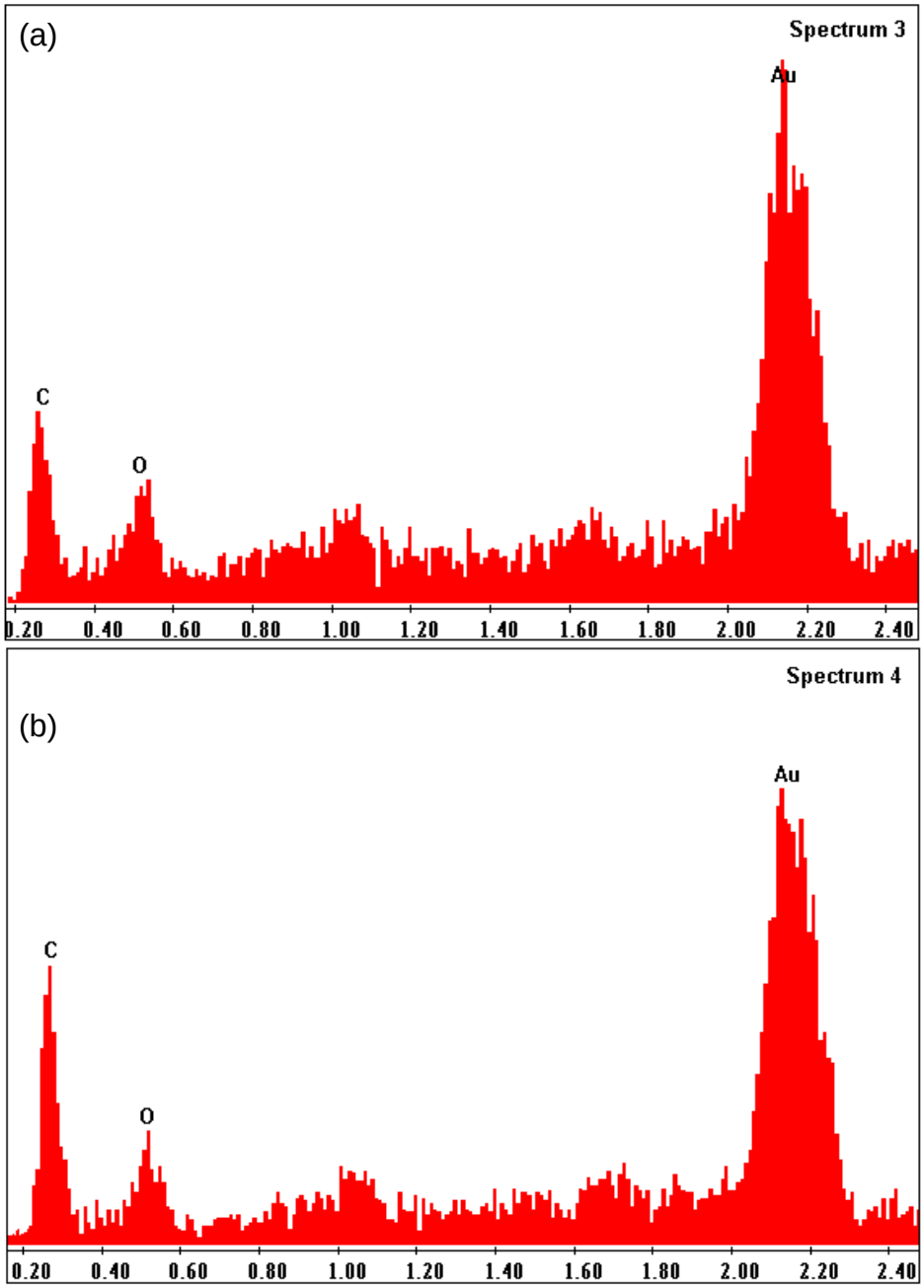

Figure 4.43: (a) EDX spectrum of Au hemispherical probe surface adhered with Au from the coated Au/MWCNT surfaces (1mA) (b) EDX spectrum of Au hemispherical probe surface adhered with Au from the coated Au/MWCNT surfaces (10mA).

This can be confirmed using X-ray spectroscopy. Figure 4.42 (a) and (b) show the points analysed by X-ray spectroscopy on the Au hemispherical probe “Spectrum 3” and “Spectrum 4”. Figure 4.43 (a) and (b) shows an EDX spectrum for the surface. Gold was the predominantly observed element with

carbon and oxygen also observed on both surfaces. This was consistent with the composition of the melted Au, which had adhered on to the Au hemispherical probe surfaces, with some additional surface contamination and water adsorption. The overall atomic percent of Au was 77.2%, C as 16.8% and O as 6.1% for the point “Spectrum 3”, and the overall atomic percent of Au was 71.9%, C as 22.8% and O as 5.4% for the point “Spectrum 4”.

The Au melting and adhesion for the Au-Au/MWCNT contact pair was much less than with the Au-Au pair. The probable reason would be that the MWCNT has improved its heat dissipation generated within the contact surface. The MWCNT have excellent heat-conduction properties [126,127,128,129]. As stated by Hyman et al. (1998) that heat dissipation is the critical design criterion for maintaining a low contact resistance, a high power handling and a minimum surface adhesion wear [67]. Furthermore, with this enhancement of heat flow it could have reduced the temperature between the contact surfaces. Furthermore, the MWCNT acts like a thermal interface material, like an array of fins to increase surface contact with the air which improves heat dissipation, thus leading to a reduction in temperature which in turn reduces degradation due to heat generation and melting of the Au coating. Moreover, the roughness of the Au/MWCNT planar surface could have helped to reduce the tendency of adhesion due to smoothening of the surfaces, which is one of the major causes of MEMS relay failure.

No observable damage, deformation or change in chemical composition on the Au/MWCNT planar composite surfaces can be detected, further suggesting that the CNT under layer has improved the mechanical integrity of the gold surface.

4.7 Experiment 4: PZT actuator test rig (hot-switched condition, 20mA-50mA)

(a)

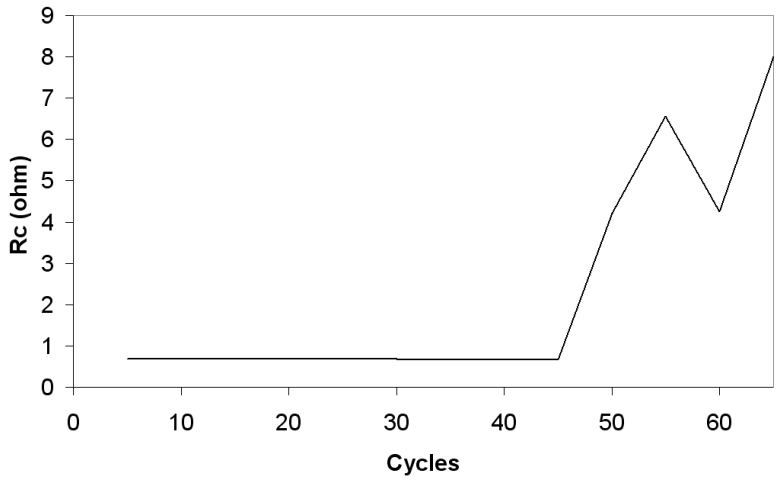

(b)

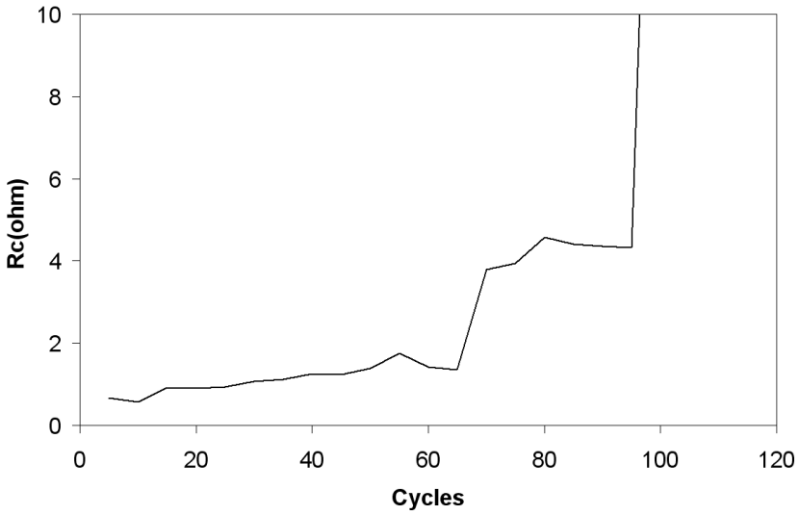

(c)

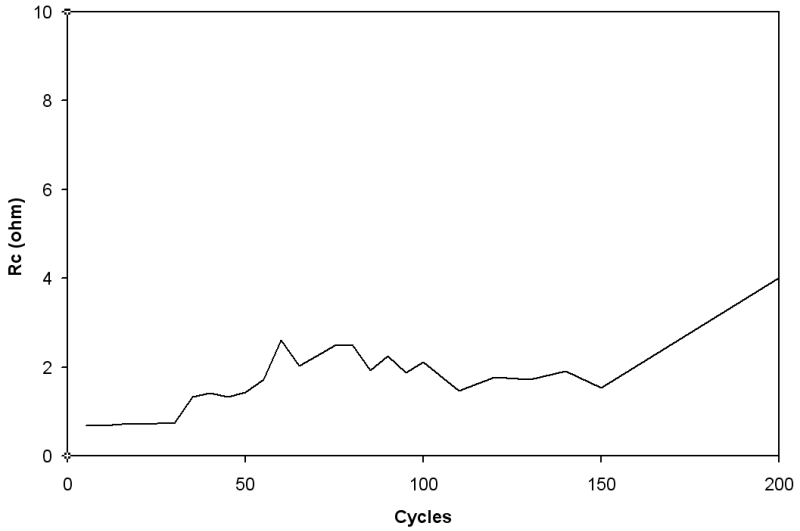

Figure 4.44: Graph of contact resistance against number of cycles for Au-Au/MWCNT contact pair with current load of (a) 50mA, and (b) 40mA and (c) 30mA 4V at applied force of 1mN.

Figure 4.44 (a), (b) and (c) shows the contact resistance against number of cycles for the Au-Au/MWCNT contact pair using a current load between 30mA-50mA and supply of 4V. It was observed that degradation has occurred between 45 to 150 cycles for this range of current loads. The degradation has occurred on the Au surface of the Au hemispherical probe as shown in Figure 4.45. It was observed that delamination on the Au surface accounts for the degradation of the contact resistance. The probable reason would be that enough heat is generated during the contact and between the surfaces to soften or melt the Au layer on the Au hemispherical probe. Two potential factors involved in heat generated and micro welding are Au-Au adhesion and localised current density at the asperity contact peaks [130].

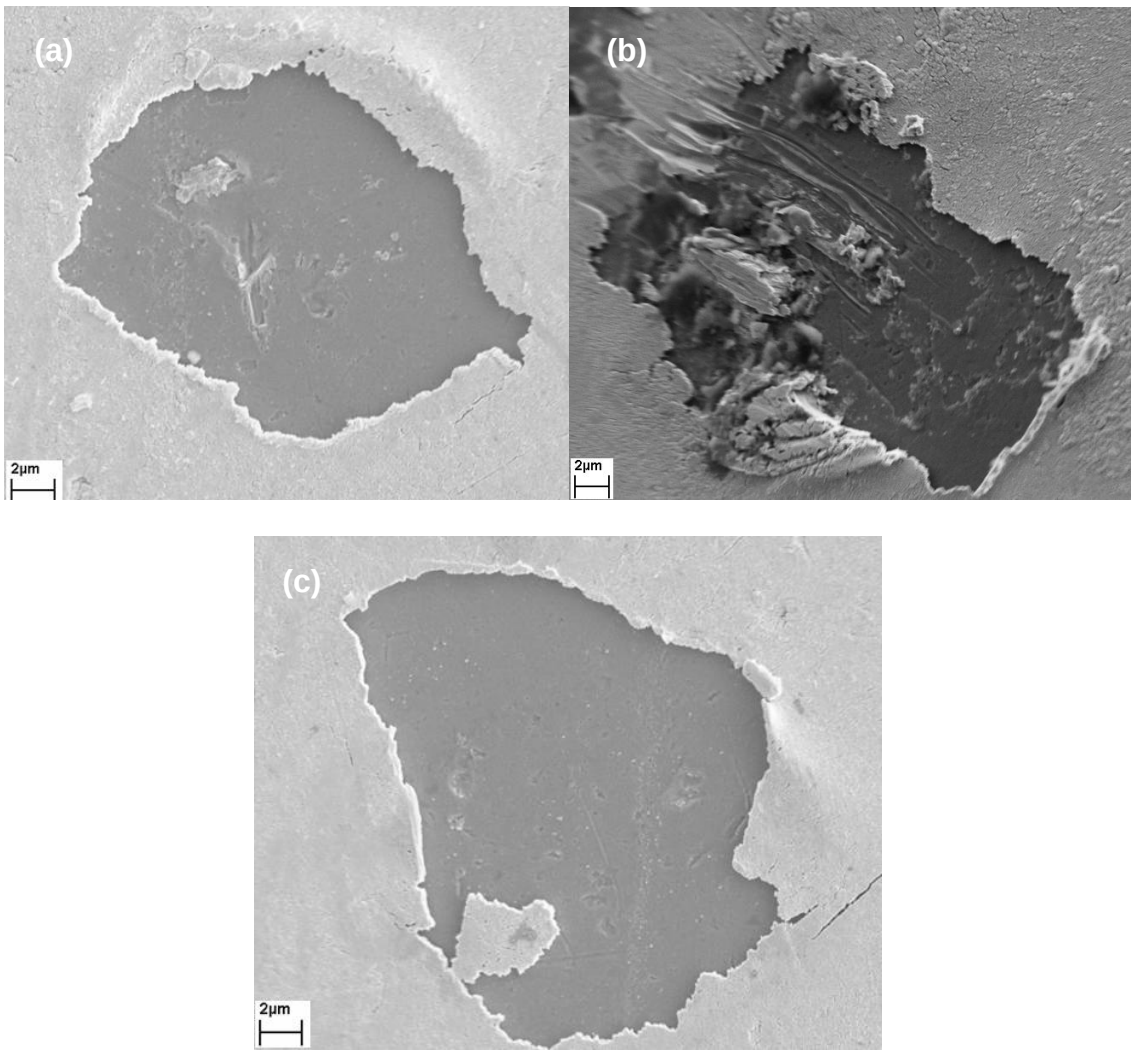

Figure 4.45: Damaged surface of Au hemispherical probe after using current load (a) 50mA (b) 40mA and (c) 30mA, 4V.

Figure 4.46 (a) and (b) shows the Au which has adhered to the Au/MWCNT composite surface (for a current load of 40mA and 50mA, at 4V) after 45 to 65 cycles. This behaviour of degradation was consistent with the 30mA current load, where the damaged Au hemispherical probe and the Au on the Au/MWCNT composite surface can also be seen.

(a)

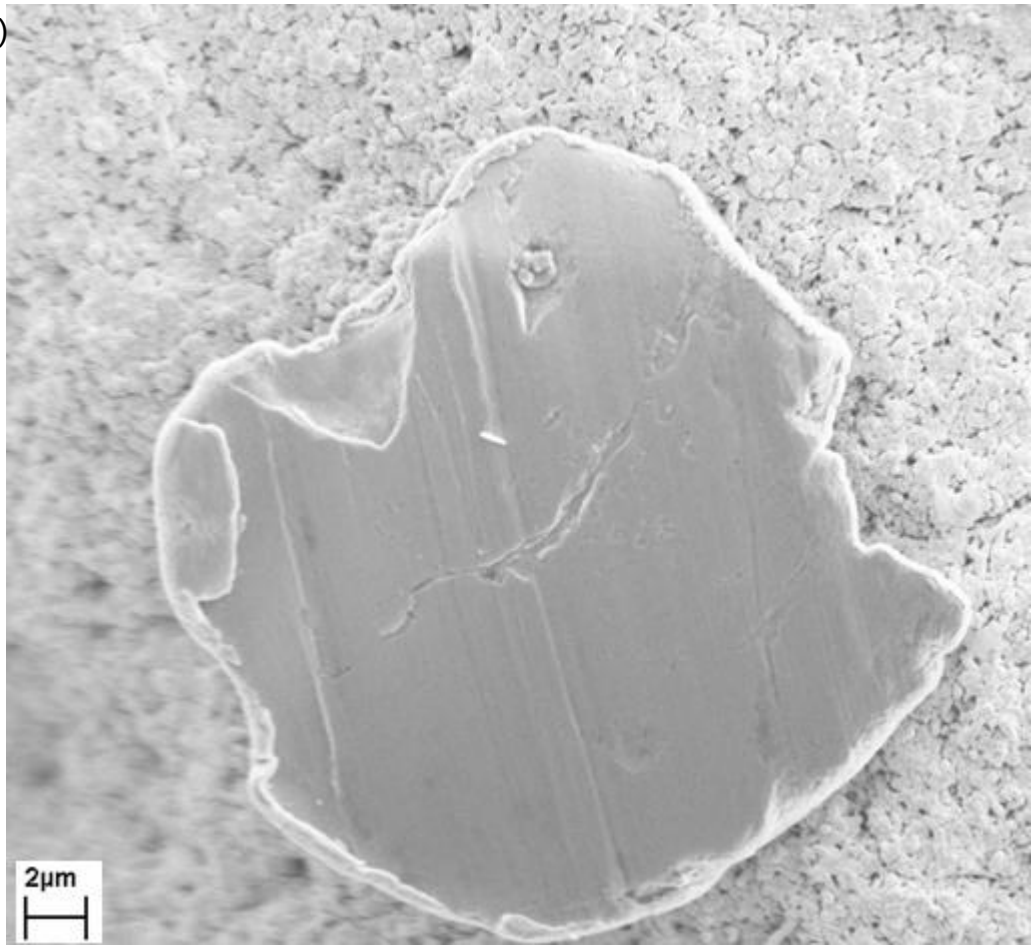

Figure 4.46: Au adhered on the Au/MWCNT composite surface using current load (a) 50mA, 4V.

(b)

Figure 4.46: Au adhered to the Au/MWCNT composite surface using current load (b) 40mA, 4V.

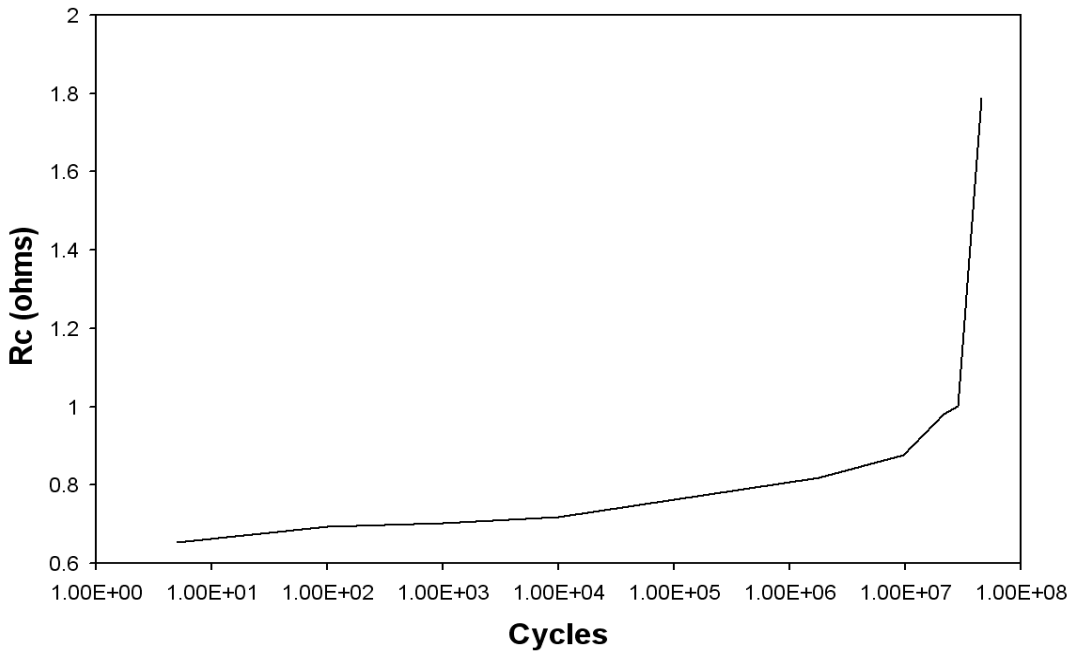

Figure 4.47: Graph of contact resistance against number of cycles for Au-Au/MWCNT contact pair with current load of 20mA, 4V at applied force of 1mN.

Figure 4.47 shows the contact resistance against number of cycles for Au-Au/MWCNT composite with current and supply load of 20mA and 4V

respectively. It was observed that contact resistance increases after ~50 million cycles. This degradation has occurred on both side of the contact surfaces as shown in Figure 4.48 (a) and (b). Au from the top surface of the Au/MWCNT composite surface (cathode) has adhered on the Au hemispherical probe (anode).

(a)

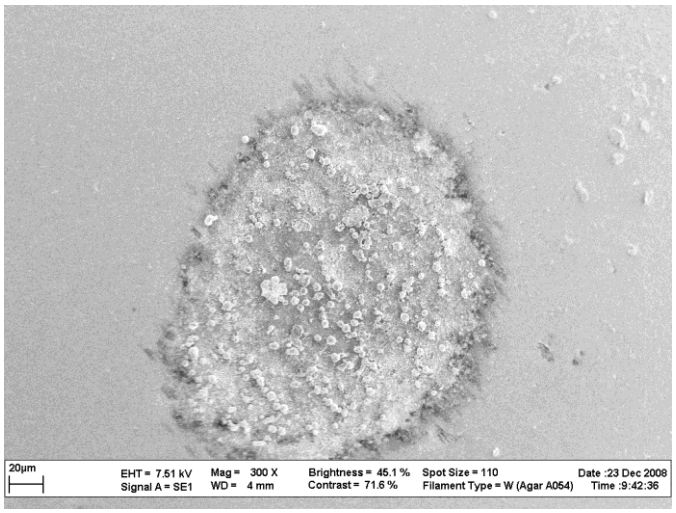

(b)

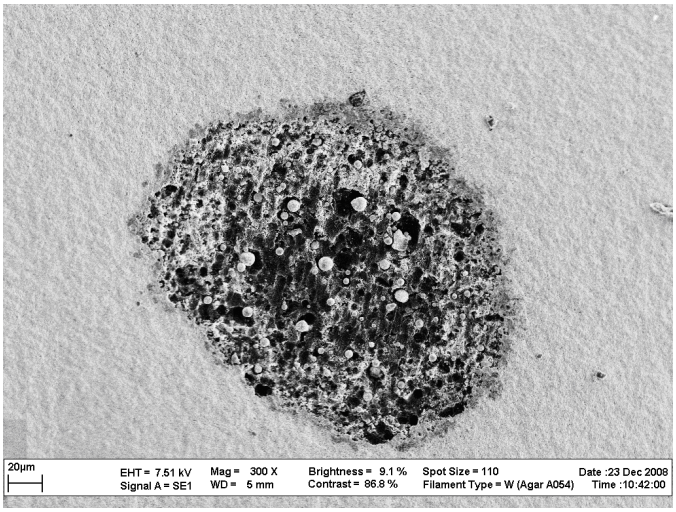

Figure 4.48: (a) Au adhering on the Au hemispherical probe (anode) and (b) damaged image on the Au/MWCNT composite surface (cathode).

The probable reasons for this degradation are as follows: (1) enough heat is generated during the contact between the surfaces to soften or melt the Au layer on the Au/MWCNT surface and adhere on to the Au hemispherical probe; (2) Au fatigue or degradation occurs after a large number of cycles; and 3) material transfer was a result of bridge transfer of a molten metal. As claimed by Slade, this molten metal bridge always forms between the contacts even at low currents and even when the contacts open with a very high acceleration [31].

4.8 Factors affecting the number of cycles in the hot-switched condition

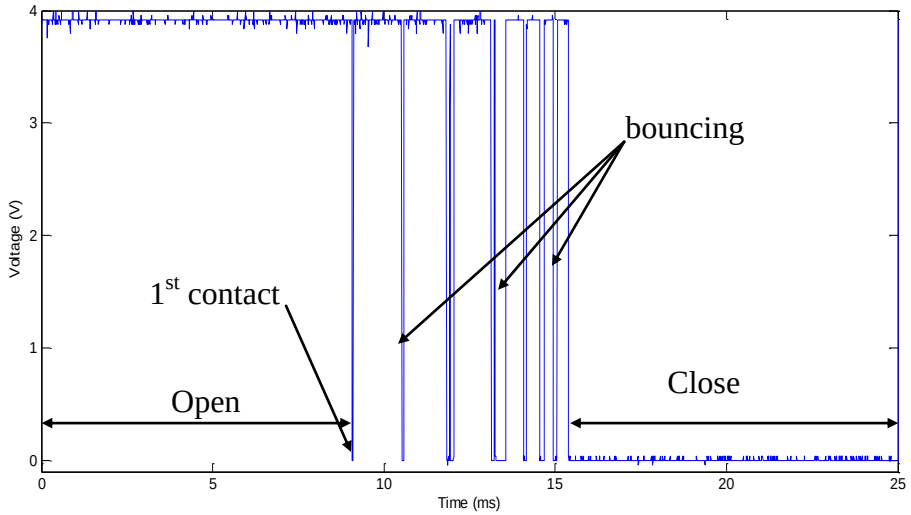

Figure 4.49: Graph of voltage (V) against time (ms) for Au-Au contact pair, during the contact.

Figure 4.49 shows an example of a graph of voltage against time during Au-Au during contact at 0.2Hz and 1mN with current load of 1mA at 4V. It was observed that bouncing during the contact cycle has occurred for the sample attached to the PZT actuator. This is common in MEMS relay devices, contact bounce will occur immediately after the switch closes. This will lead to electrical discontinuity (that is for example it interrupts the power signal continuity through the transmission line on the relay), increase wear, degrades performance, its reliability and durability.

In the experiment, bouncing will be an additional bonus to the number of cycles performed and achieved for testing the new composite material's reliability and durability during hot-switching. As the planar sample hits the Au hemispherical probe it bounces about 10 times before it settles or close completely as shown in Figure 4.49. The number of cycles for the cyclic loading (dry-circuit and hot switched) need to be reconsidered. Assuming the bounce causes a factor of x10 on the number of cycles then, for example the number of cycles presented in Figure 4.30 for the Au-Au contact pair to degrade was truly 4300 cycles and not 430 cycles.

4.9 Discussion

In this study two experimental setups were used: 1) a modified nano-indentation apparatus with dry-circuit condition; and 2) a PZT actuator test rig with dry-circuit and hot-switched conditions. The combination contact pair samples as follows were tested using these equipment: 1) Au-Au; 2) Au-MWCNT; and 3) Au-Au/MWCNT composites contact pairs.

4.9.1 Modified nano-indentation apparatus

A modified nano-indentation apparatus was used to characterise the contact resistance (measured by 4-wire measurement methods) against applied force (with maximum applied force of 1mN) between a Au-Au/MWCNT coated contact pair. This contact pair was compared with Au-Au and Au-MWCNT contact pair. Before continuing with the experiment, the "contact resistance against applied force" pattern of the Au-Au contact pair was compared with Holm's classical theory and the new Wexler contact resistance by Coutu et al. (2006) [14] to observe the similarity. The Au-Au contact pair shows a similar pattern (as shown in Figure 4.12) with these theories. This shows that the modified nano-indentation apparatus could be used to test and replicate the actuation of a MEMS relay.

When the Au-Au pair contact resistance was compared with the calculated model, the contact resistance was higher. The possible reason would be that the model assumes there is no contaminant film and is clean but there could be a contaminant film layer. As Patton et al. (2005) states, Au has the tendency to have a thin layer of carbon on its surface, the residue from the cleaning process and/or is adsorbed due to exposure to air [40]. It has been reported by Hyman et al. (1999) and Tringe et al. (2001) that there is 2-4 nm thick of adsorbed hydrocarbons on freshly cleaned Au [41,42] and this increases the contact resistance.

When a 10 cycles contact resistance characteristic of Au-MWCNT contact pair was compared with that of the Au-Au contact pair (Figures 4.22 and 4.21

respectively), it showed that the contact resistance was higher. The reason was because of the higher resistivity of MWCNT planar surface with the Au planar surfaces. When comparing the Au-Au/MWCNT contact pair with the Au-Au contact pair it was comparable (Figure 4.23 and 4.21 respectively). The reason was the Au hemispherical probe had made direct contact with the Au coating on the MWCNT and the MWCNT acts as a compliant medium, thus reducing the contact resistance. The contact resistance was slightly higher with the Au-Au/MWCNT contact pair. The possible reason would be because of the different surface roughnesses. Nonetheless the Au-Au/MWCNT contact pair works better than the Au-MWCNT contact pair.

It was stated by Bult et al. (2008) that the vertically aligned MWCNT had compliant behaviour [73]. They claimed that because of this behaviour it improved the mechanical and electrical integrity of the contact materials. The "force against displacement" trend was observed for all the samples to measure the compliant behaviour. Figure 4.19 shows that the depth of penetration of the Au-MWCNT (~3600nm) and Au-Au/MWCNT (~2500nm) contact pairs were deeper than for the Au-Au contact pair and when the samples were unloaded modest permanent displacements (~1400nm) were obtained. This shows the MWCNT or Au/MWCNT surfaces' readiness to conform and absorb the Au hemispherical probe when loaded and having the same permanent displacement when unloaded. With this behaviour it was possible that it would reduce the wear between the contacts.

4.9.2 PZT actuator test rig

The modified nano-indentation apparatus has a low frequency response, thus a limitation on tests using a large number of cycles. A reliable MEMS relay contact should perform a large number of cycles preferably 10^{10} – 10^{11} cycles. Furthermore as shown in Figure 4.29, the modified nano-indentation apparatus results were affected by the wire attached on the Au hemispherical probe, thus alternative testing was needed. The applied cyclic load (with maximum applied force of 1mN) and contact resistance between Au-Au/MWCNT contact pair (dry-circuit and hot-switching conditions) were investigated using a PZT actuator test

rig and 4-wire measurement methods. This contact pair combination was compared with an Au-Au contact pair.

Bult et al. (2008) has performed tests using a similar combination of contact materials (Au-Au/MWCNT pair) with a dynamically applied force of ~25mN (hot-switched condition) and up to 3000 cycles [73]. In this study, the number of cycles achieved was beyond 3000 cycles and this was needed to observe a realistic reliable contact materials.

4.9.2.1 Dry-circuit condition

Over 1000 cycles the Au-Au/MWCNT contact pair demonstrated a much more stable contact resistance than the Au-Au contact pair which degrades ~430 cycles as shown in Figure 4.30. The reason was that Au is soft and it wears easily. Increasing the load experiment using 3mN applied force shows a tear and crack as shown in Figure 4.35 (b) and 4.36. The probable reasons for the crack were: 1) the insufficient infiltration of Au being sputter-coated on some areas of the MWCNT surface to form the composites and due to this it has displace or deflect the MWCNT; and 2) the poor anchorage or adhesion of the MWCNT to the silicon substrate. This deterioration has not resulted in any measurable change in the contact resistance. This improvement was believed to be due to the Au/MWCNT surfaces conforming to the shape of the Au hemispherical probe. The dynamic impact on the Au hemispherical probe was absorbed by the Au/MWCNT surfaces thus reducing the wear. The compliant effect on Au-Au/MWCNT helps to reduce the deterioration by reducing the plastic deformation and subsequent adhesion between the Au contact surfaces.

4.9.2.2 Hot-switching condition

An applied cyclic load and contact resistance between Au-Au/MWCNT composite contact pairs was investigated using the test rig at current loads of 1mA and 10mA and supply load of 4V and R_c measurement methods. This contact pair combination was compared with an Au-Au contact pair. The Au-Au contact pair shows degradation over 220 cycles but the Au-Au/MWCNT contact

pair demonstrated a much more stable contact resistance over 1000 cycles (Figure 4.38) and beyond 2 million cycles (Figure 4.41).

These were believed to be due to: 1) the compliant behaviour of the Au/MWCNT surfaces conforming to the shape of the Au hemispherical probe, thus reducing plastic deformation of the contacts; and 2) the MWCNT could have improved the heat dissipation produced by heat generated within the contact surfaces. The MWCNT have excellent heat-conduction properties and this could have reduced the softening or melting temperature between the contact surfaces.

To observe a current load benchmark, the same experimental setting as above was employed but with higher current load (20mA-50mA) and supply voltage of 4V. This is above the high current range for MEMS relays. The sample used was a Au-Au/MWCNT contact pair. It was observed that failure occurred for a current load between 30mA to 50mA after 45 to 150 cycles. This failure was only observed on the Au hemispherical probe where delaminating Au adhered to the Au/MWCNT surface. This was probably due to enough heat generated during the contact to soften or melt the Au on the hemispherical probe. At the current load of 20mA with supply voltage of 4V, failure only occurred after 50 million cycles (Figure 4.47) for the Au-Au/MWCNT contact pair. It was observed (Figure 4.48) that the Au coating from the Au/MWCNT surface had melted and adhered to the Au hemispherical probe. The likely reason: (1) current load has generated enough heat to melt the contact Au coating on the Au/MWCNT surface to adhere on the Au hemispherical probe; and (2) Au fatigue after a large number of cycles.

The above experimental method was the first to test a Au-Au/MWCNT contact pair at large numbers of cycles. It has shown that the MWCNT improves the mechanical integrity and electrical properties of the contact pair. This analysis and these results would be useful for MEMS relay contact development and could serve as a platform for future research and investigation. In this initial study we could observe their behaviour and thus future improvement could be made in terms of their performance.

CHAPTER 5: CONCLUSION

5.1 Findings

This study was the first step towards realising the value and potential of the new material for MEMS relays' application. The contributions are as follows:

1) A new compliant material has been developed; a forest of vertically aligned multi-walled carbon nanotubes and Au/MWCNT composite,
2) A new technique of testing the relationship between electrical contact resistance and contact force using a modified nano-indentation apparatus and a PZT actuator test rig was developed, and
3) The test approach in this study has been used in a parametric study at a low force contact for MEMS relays application, measurement of contact resistance, having different current loads (dry-circuit and hot-switched conditions) and running tests to a large number of cycles for reliability testing.

An increase in the performance of MEMS relays is desired by the MEMS and electronic industries. Currently, the preferred lifetime for a MEMS relay is greater than 10^{10}-10^{11} cycles. It is important at these numbers of cycle failure does not happen with the contact materials. Therefore, a new contact material needs to be developed to withstand such lifetime.

Using CVD, a forest of vertically aligned MWCNT was developed. A composite Au/MWCNT surface was also developed by sputter coating Au. The Au was used to increase the conductivity of the composite. Moreover the vertically aligned MWCNT was used because of Au's infiltration possibility when sputter deposited, to form the composites. This has been observed by Bult et al. (2008), where there is an infiltration of sputtered Au, forming the composites [73]. In this study the Au infiltration was between 700nm to 4µm. These different depths of infiltration are probably because of different compactness of the CNTs surfaces. Moreover, the dimensions of Bult et al. (2008) composite needed to be scaled down [73] for use in MEMS relay with a low force applications. That is why in this study the dimensions of the composites were smaller.

When a new contact material is developed, a method of testing is needed to validate its potential. A modified nano-indentation apparatus was used to test low force response (maximum applied force of ~1mN) of Au-Au/MWCNT contact surfaces. The Au-Au and Au-MWCNT contact pairs were used to observe and benchmark the new material. The study was the first to perform tests on Au/MWCNT contact surfaces at low forces for MEMS relay applications.

Over one load cycle, Au-Au and Au-Au/MWCNT contact pairs have a similar graph patterns as shown in Figure 4.16. During the first 10 cycles of the Au-Au/MWCNT contact pair, the contact resistance was observed to be comparable to the Au-Au contact pair and shows little change. The possible reasons would be because: 1) the contact was between the Au surface on the hemispherical probe and the Au surface of the composites; and 2) the Au/MWCNT surface was compliant thus conforms to the Au hemispherical probe when loaded, increasing the contact area. This was confirmed with the results plotted in this study of "force against displacement" as shown in Figure 4.19. The results showed deeper penetration for Au-Au/MWCNT composites compared to Au-Au contact pair.

Due to the low frequency response of the modified nano-indentation apparatus and the error presented on the results plotted in the graph of "force against displacement" for "with" and "without" wires attached on the Au hemispherical probe; as shown in Figures 4.27(b) and 4.29 respectively, a new method has to be developed. A PZT actuator test rig was designed and fabricated to perform a large number of cycles. Even though Bult et al. (2008) has performed an experiment for Au-plated ball-Au/MWCNT contact pair (hot-switched condition with 5mA and 5V and using a maximum applied load of ~25mN) that had reached up to 3000 cycles with no observable degradation [73], this was not enough to reflect the potential of the new material. MEMS relay lifetime needs to be greater than 10^6 (preferably $>10^{10}$-10^{11}) cycles. In this study the largest number of cycles achieved was 50 million cycles for hot-switched condition at 20mA with 4V supply voltage.

Two experimental set-ups for the test rig were used: dry-circuit and hot-switched conditions. Most significant was the hot-switched results. During hot-switching a current load of 1mA and 10mA (typical high range current load for MEMS relay) and a supply voltage of 4V were used. It was shown that the contact resistance of the Au-Au/MWCNT contact pair was stable up to 2 million cycles compared with Au-Au contact pair which degraded after 220 cycles. The possible reason would be due to the good heat dissipation properties of MWCNT which helps to reduce the heat generated which could soften or melt the contact surfaces.

Furthermore, the current load was increased to 20mA-50mA. This study was the first to test the new material at this high range current load. At 30mA to 50mA the degradation occurred after 45 to 150 cycles respectively. At 20mA the contact resistance was stable, but after 50 million cycles it degraded. The likely causes would be heat generation and Au fatigue due to large number of cycles. Furthermore, bridge transfer has removed the gold from the MWCNT surface. These initial results showed that when using the new material, it has improved the performance of the contacts. Overall the study had shown that MWCNT has improved Au's mechanical and electrical integrity at a low force contact and during hot-switching conditions, and at large number of cycles.

Finally, the above experimental method will be useful for MEMS relay contact analysis and can serve as a platform for future research and investigation. This is mainly applicable to Au/MWCNT-Au/MWCNT and Au/SWCNT-Au/SWCNT contact pairs with different quality, roughness, length of CNT and coating thickness of Au. With this experiment we can observe their effects and improve its performance further. Furthermore, this experimental methodology could fill the gap in terms of using a resilient material (CNTs and its composites) and the data will be useful to MEMS relay's electronic development.

5.2 Future work

This study is the first step to realising the potential of the new material but further experiment is needed to achieve a positive recognition from the MEMS electronic industries. The following explanation is for future work, which can help to motivate the MEMS electronic industries in utilising the new material:

1) It is desirable to grow forests of MWCNT or SWCNT on both the hemispherical probe and the flat substrate contact pairs to observe their mechanical and electrical behaviour. There were difficulties in growing CNT on the hemispherical probe/stainless steel ball as shown in Figure 5.1. No CNTs were detected on the stainless steel ball even though a Fe catalyst and Al_2O_3 were coated on it but when 1µm thick film of SiO_2 was applied followed by the catalyst, agglomerisation and CNT can be detected as shown in Figure 5.2 (a) and (b). This indicates that growing CNT on the stainless steel ball will be impossible unless the ball is coated with very thick Si or SiO_2 to avoid any contamination of the chemical composition on the stainless steel ball which hinders the growth. Furthermore, SiO_2 is needed to stop the Al_2O_3 from cracking. Fe diffuses preferentially into the cracks preventing CNT growth on the ball surface.

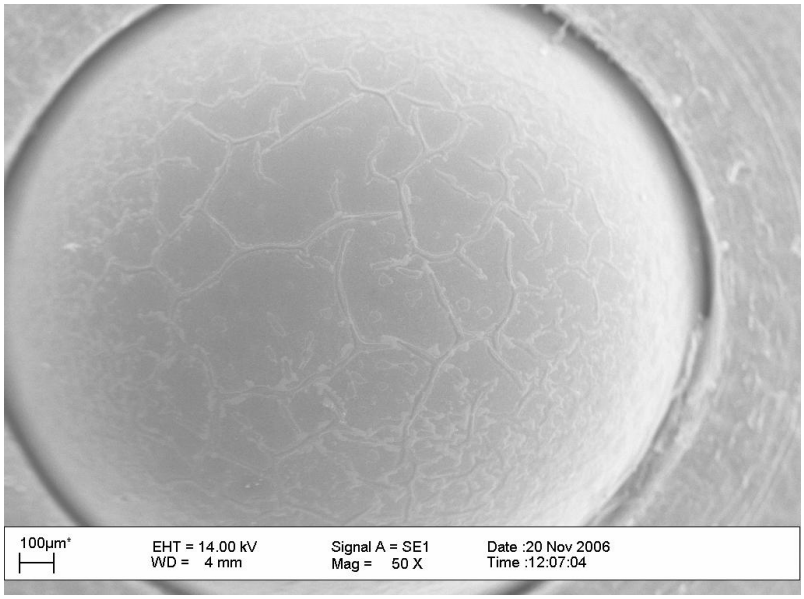

Figure 5.1: Attempts to grow CNT on a stainless steel ball.

(a)

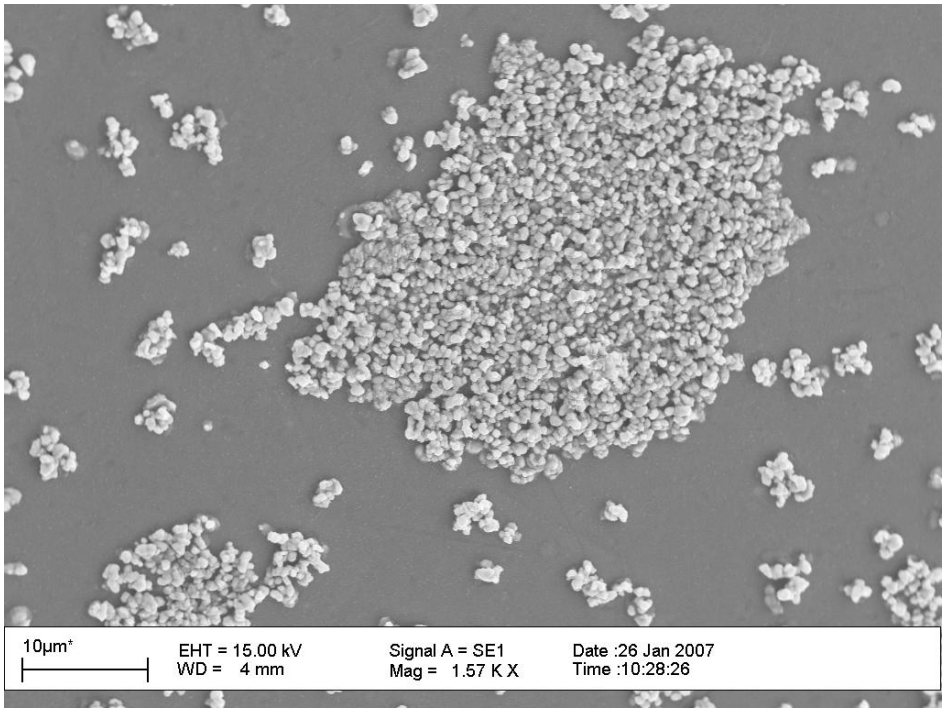

(b)

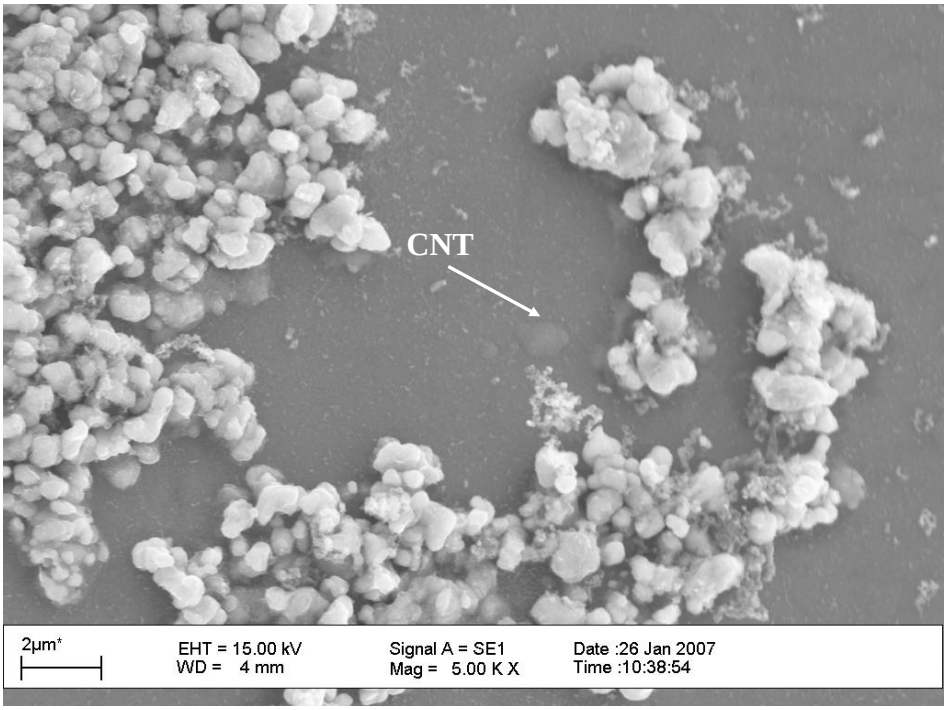

Figure 5.2: (a) Agglomerisation of catalyst, (b) CNT is detected.

2) As claimed by Hjortstam et al. (2004), the single walled CNT offer improved electrical and mechanical properties [81]. To grow an aligned forest of SWCNT, the use of PECVD, experiments on different catalysts and a gaseous carbon source would be necessary. The catalysts that can be utilised include iron, nickel, or cobalt. Moreover, CNT-composite, doping and filling need to be looked at for fabricating the microstructure of a MEMS relay.

3) Reduction of the roughness of CNT and Au/CNT could potentially enhance or improves the conductivity of the material. The average roughness or surface roughness is ~1.3μm compared with the Au-substrate at ~0.03μm. There is a possibility that reduction in roughness will decrease the contact resistance. First suggestion would be to increase the thickness of the Au by sputtering it until the CNTs' trough is levelled and lastly, decreasing the CNT's film thickness. Further experiments and research is needed to make it successful because if the surface is smooth there will be adhesion. MEMS relays need to avoid these situations because it can lead to degradation and failure of the system after longer cycles.

4) The literature review indicates that the experiment does not need an environmental chamber, but to have a contact that can withstand any environmental condition, the use of the environmental chamber would be appropriate for both experimental set ups (modified nano-indentation apparatus, Figure 5.3 (a) and PZT actuator test rig Figure 5.3 (b)). This will make a versatile experimental method. This will mimic the usage of the contact in a MEMS relay in different environments and includes atmospheric pressure, atomic oxygen erosion, a vacuum (contact intended for space applications), organic vapours (emanating from various organic materials e.g. benzene, toluene, and naphthalene which can produce carbon particles), and silicone vapour, to observe if CNT and its composite can withstand such environment. This will be a vital area of the research to see how and why failure may occur in the contact by introducing the contaminants rather than using inert gases.

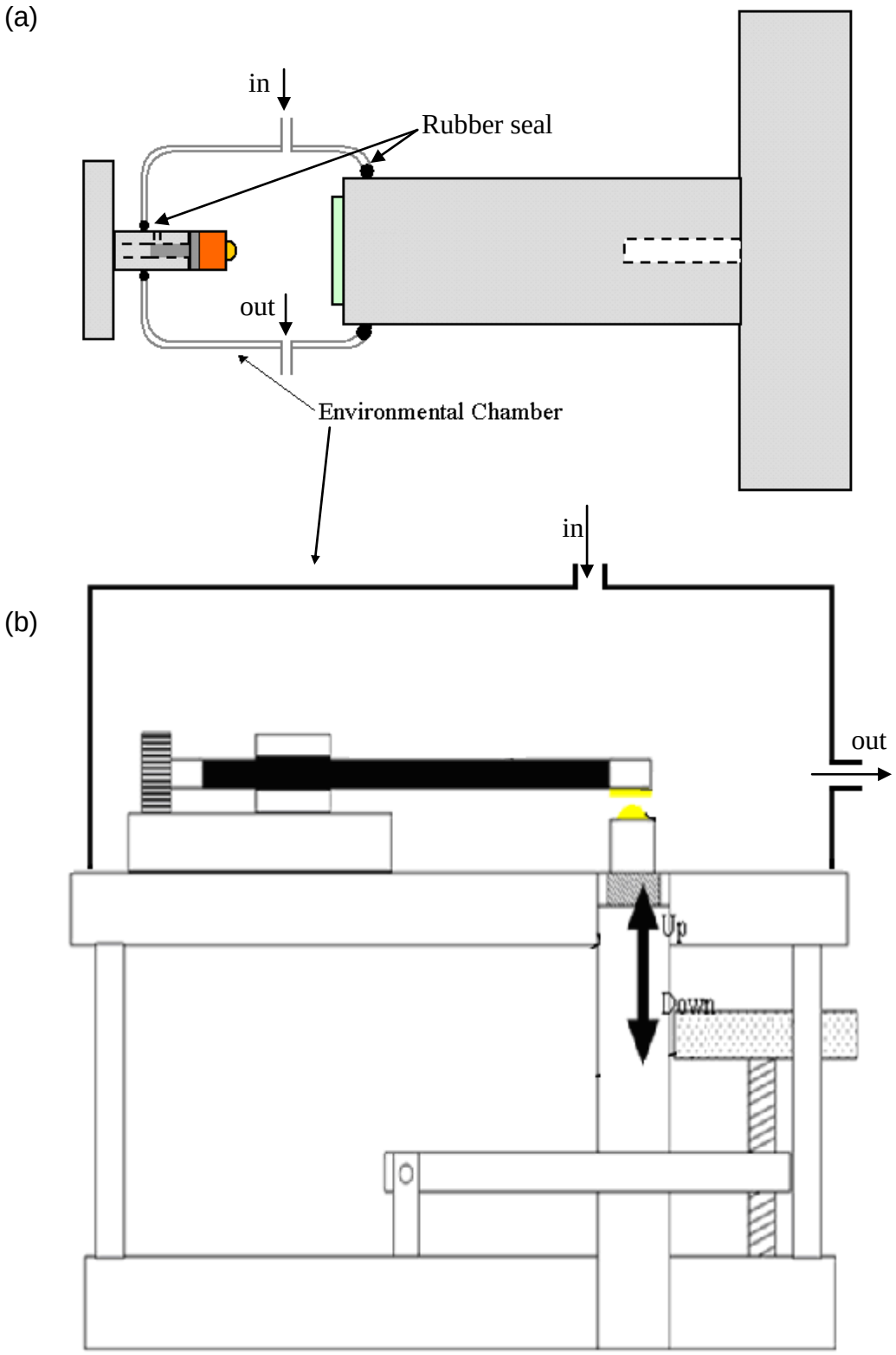

Figure 5.3: (a) Modified nano-indentation apparatus and (b) PZT actuator test rig within an environmental chamber.

5) From the beginning, the goal was to determine the parameters that affect reliability of MEMS relays. It was crucial in the early stage of the design and development phase to subject the contact to operational and environmental extremes. This would help identify and mitigate detrimental issues. Once the above experiment is successful and CNTs are proven to be the best material, it would be appropriate to use finite element analysis to design a MEMS relay using the material. Thus we can test and simulate its performance capability in a simulated safe environment.

6) If the material and the design of the MEMS relay for the contact is found to be reliable then fabricating the actual MEMS relay would be the ultimate test to see its real life performance (the propose fabrication procedure for the MEMS relay is shown on Figure 5.4). The proposed MEMS relay will be fabricated on a Silicon substrate. The following are the proposed fabrication methods (refer to Figure 5.4):
   (a) The Fe Catalyst and Al_2O_3 layers are sputtered on the Si substrate using a very fine patterned metal lift-off technique,
   (b) Growing CNT using chemical vapour deposition,
   (c) Using the lift-off technique, Au is sputtered on top of the CNTs to form the composites,
   (d) Sputtered Au for the anchor and electrode,
   (e) Before fabricating the structural beam, hinge and dimple, a defined photoresist is produced using photolithography techniques,
   (f) A timed reflow in an oven with flowing nitrogen is to be used to reform the hinge and dimple, and
   (g) The upper contact metals are to be sputtered.

   Furthermore with this proposed structure a higher number of cycles can be tested ($>10^{10}$-10^{11}) and studied to see if it can withstand higher frequency actuation up the to MHz range (Figure 5.5 shows Experimental test setup). This would be the ultimate validation of the performance and reliability of the material in use and within a practical MEMS relay design.

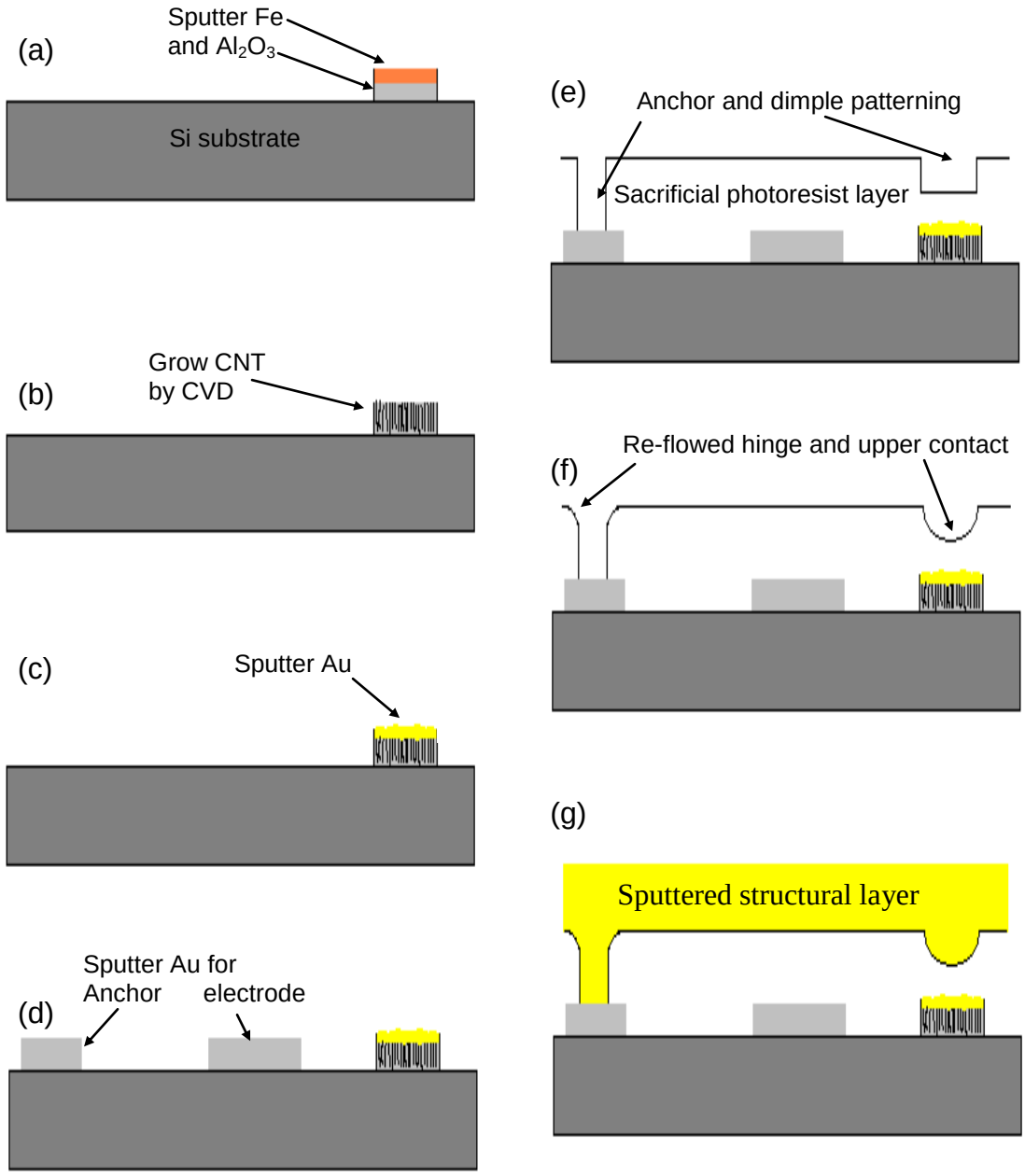

Figure 5.4: Proposed micro-fabrication for the MEMS relay with CNT composites.

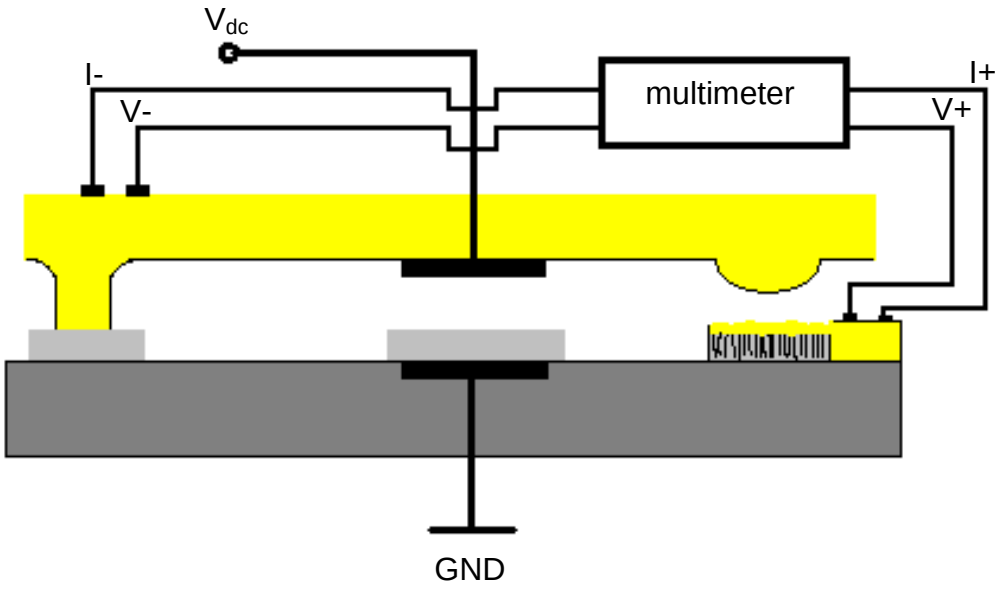

Figure 5.5: Proposed MEMS relay testing actuation and measurement methods.

APPENDIX

Appendix 1: Carbon nanoutubes growth at different growth temperature

This experiment was performed by Dr David Smith. The carbon nanotubes were grown on a Si wafer, which was coated with SiO_2 (1µm). SiO_2 layer is needed to avoid any contamination of the chemical composition of the under-layer which hinders the growth. Furthermore it prevents the Al_2O_3 to crack thus preventing growth of CNT. First the Al_2O_3 is deposited with a thickness of ~7.5nm and followed by Fe with a thickness of ~2nm. Aluminium oxide is a good catalyst support for nanotube growth. The coated sample is then placed in the CVD and once the growth temperature is reached, a gaseous carbon source (ethylene) is then introduced for 10 minutes.

In this experiment, the growth temperature was in the range of 800 ^oC to 875^oC. At growth temperature of 800^oC as shown in Figure 1, a tangled carbon nanotubes was achieved. At the growth temperature of 825^oC and 850^oC, not fully aligned forest of CNT was achieved as shown in Figures 2 and 3, thus not enough CNT supporting each other and making them to crack.

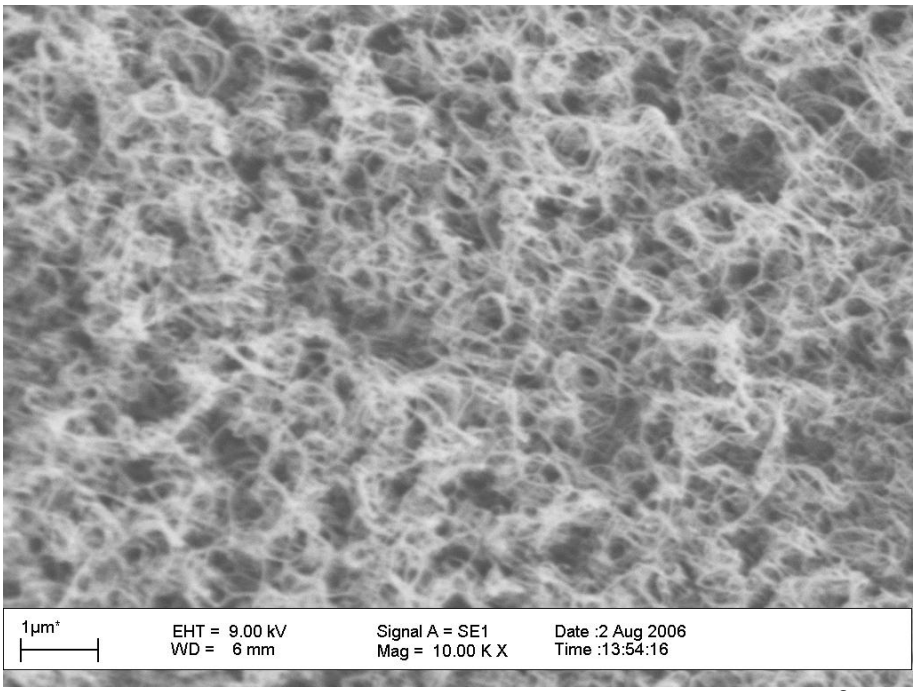

Figure 1: Tangled MWCNT at growth temperature of 800^oC.
(Supplied by Dr. David Smith of the School of Physics and Astronomy, University of Southampton).

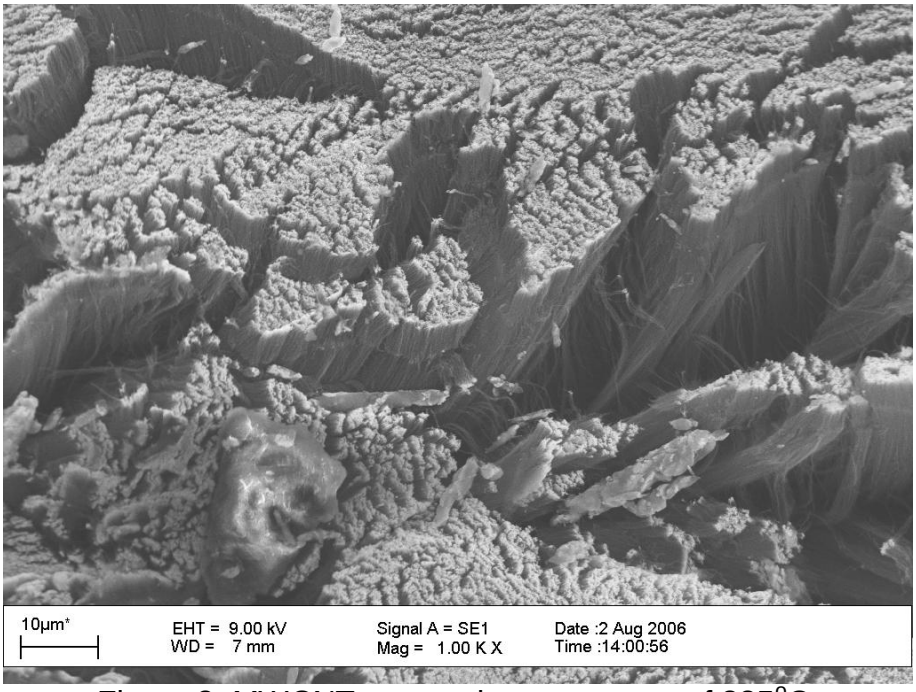

Figure 2: MWCNT at growth temperature of 825^{o}C.
(Supplied by Dr. David Smith).

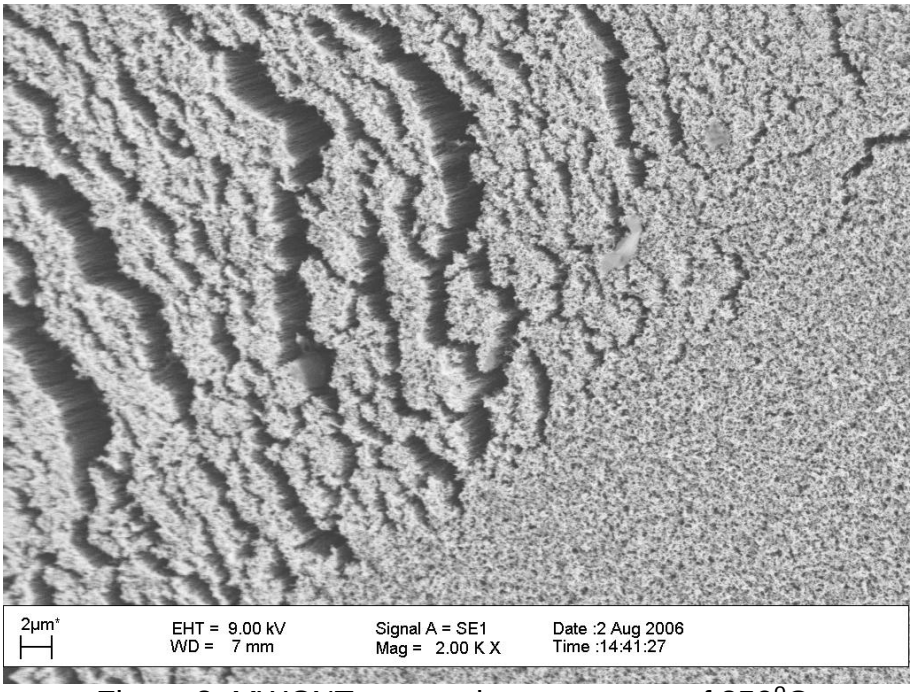

Figure 3: MWCNT at growth temperature of 850^{o}C.
(Supplied by Dr. David Smith).

At growth temperature of 875^{o}C, a dense forest of vertically aligned MWCNT was grown as shown in Figure 4. In this study the temperature of 875^{o}C is therefore used. This is because a dense forest of vertically aligned MWCNT is needed to produce a composite that is compliant and resilient for MEMS relay contact.

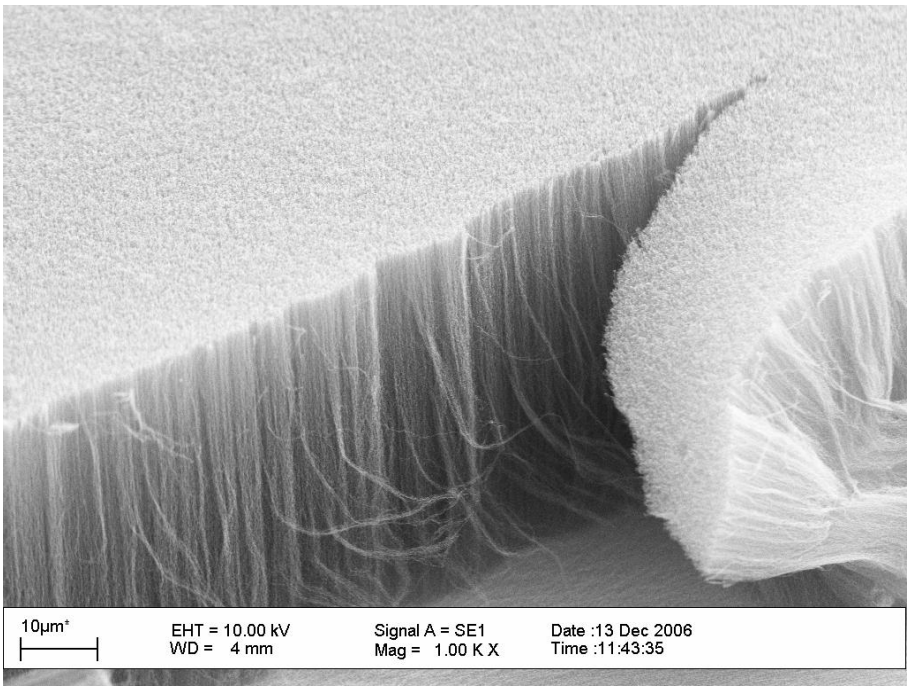

Figure 4: Dense forest of vertically aligned MWCNT after using growth temperature of 875^{o}C.

Appendix 2: Calculation for resistive loss for MEMS relay microstructure

To calculate the electrical or resistive loss of a typical MEMS relay microstructure a system is considered as shown in Figure 1.

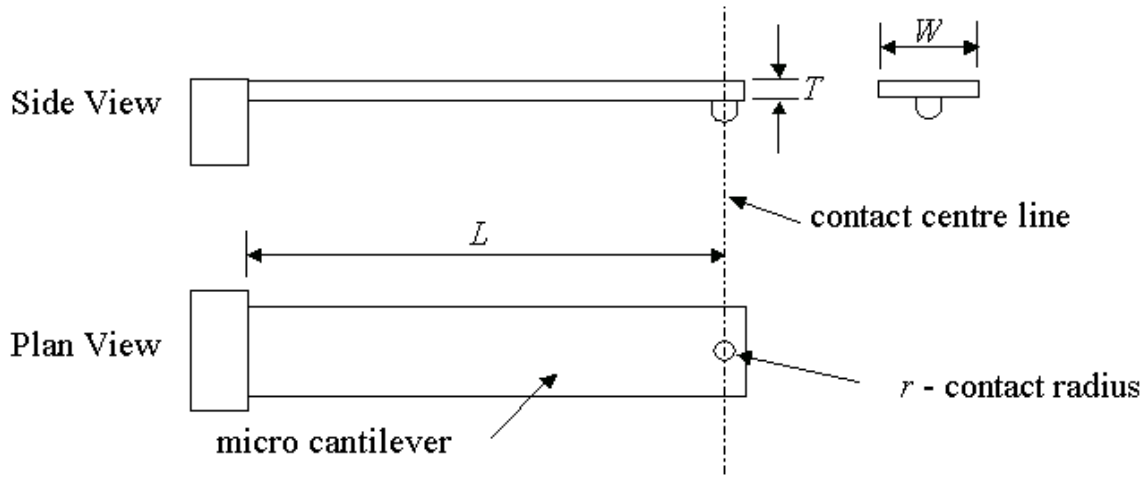

Figure 1: Schematic MEMS relay.

Where,

L – Length of the cantilever from anchor to the contact centre (m)

W- Width of the cantilever (m)

T- Thickness of the cantilever (m)

Then, assuming the current passing through the cantilever and the contact acts as resistor in series as shown in Figure 2.

Figure 2: Schematic resistance in series.

Therefore, $R = R_1 + R_2$ (Equation 2.2.15)

But, $R_1 = \rho L/A$ (Bulk resistance from Equation (2.2.1))

Where;

ρ – resistivity of the material (Ωm)

A- Cross sectional area of the cantilever T x W (m^2)

And assuming the contact area radius r and that no surface films and the surface are smooth are presented the contact resistance R_2 is presented below:

$R_2 = \rho/2\alpha$ (Contact Resistance from Equation 2.2.5)

Where;

α – is the radius of the cluster spot (contact spot) sometimes defined as the Holm radius (m)

Thus substituting equation (2.2.1) and (2.2.5) to (2.2.15)

$R = \rho L/A + \rho/2\alpha$ (Equation 2.2.16)

Now, the electrical or resistive loss = I^2R (Equation 2.2.17)

Where current I (A), which passes through the micro-cantilever and the contact and R is the resistance of the microstructure.

Substituting equation (2.2.16) to (2.2.17) We have:

Electrical or resistive loss (W) = $I^2(\rho L/A + \rho/2\alpha)$ (Equation 2.2.18)

Assuming that the current I is 1mA and the contact radius, α is 10μm, the cross-sectional area of the cantilever A is 2 x $10^{-10}m^2$ (having thickness 2μm and width 100μm) and the length of the cantilever is varied between 900μm to 1.5mm and resistivity of different materials (these materials are used in MEMS relay/devices) as shown in Table 2.

Appendix 3: Contact ball bearing holder.

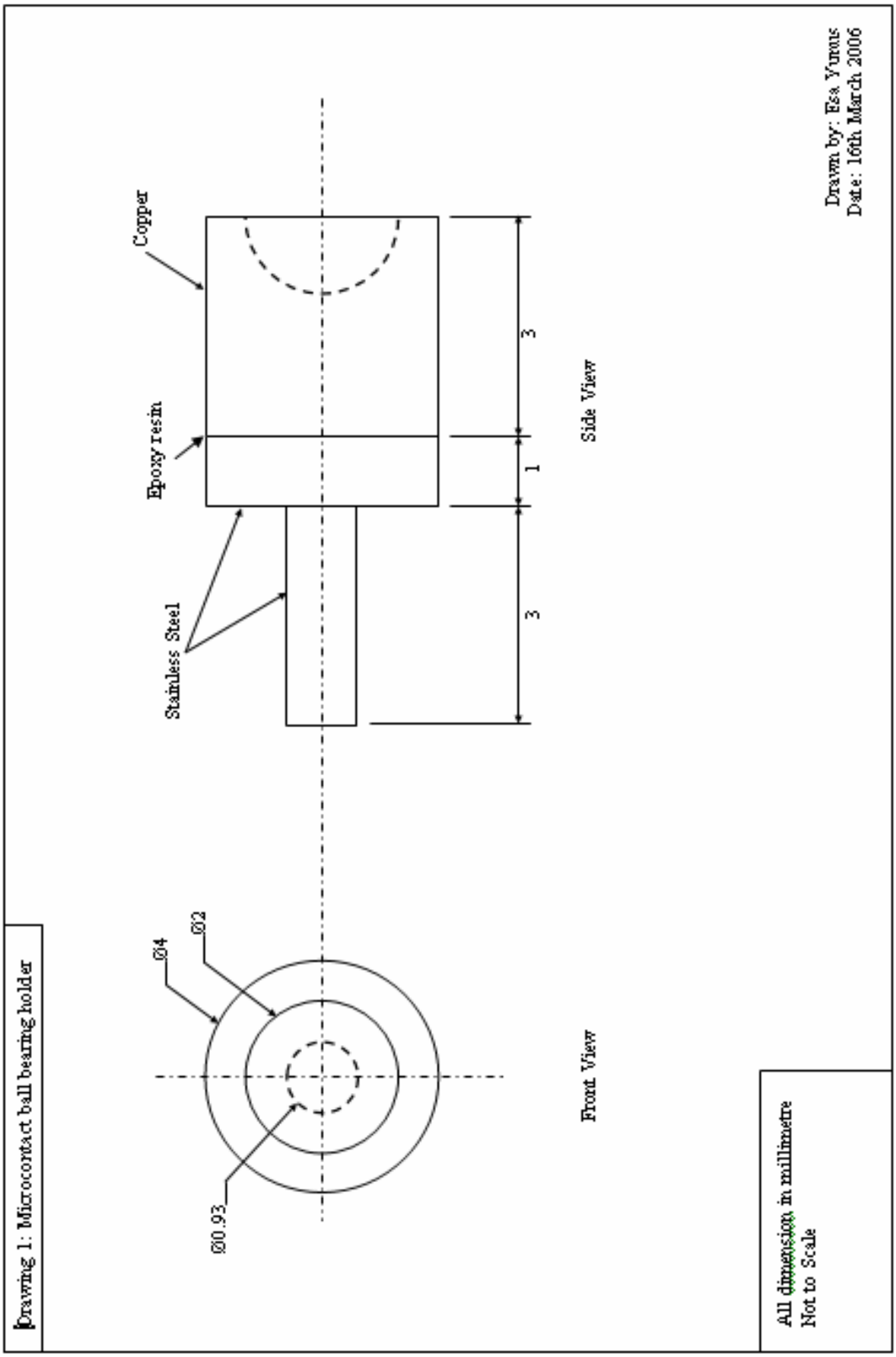

Appendix 4: Contact Substrate holder.

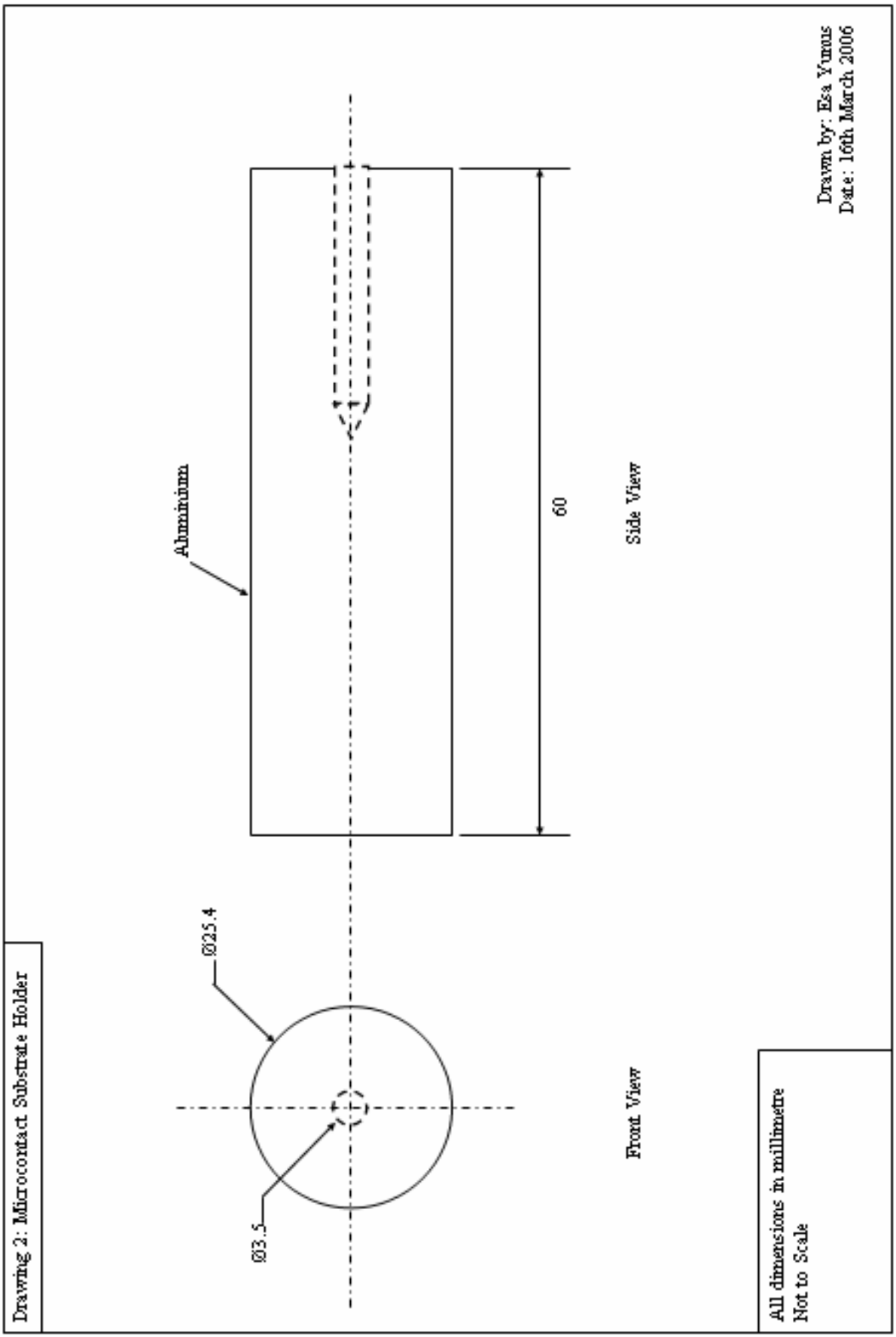

Appendix 5: Test Rig detail designed.

1. Front View.

2. Side View.

3. Plan View.

4. Perspective View.

1. Front View.

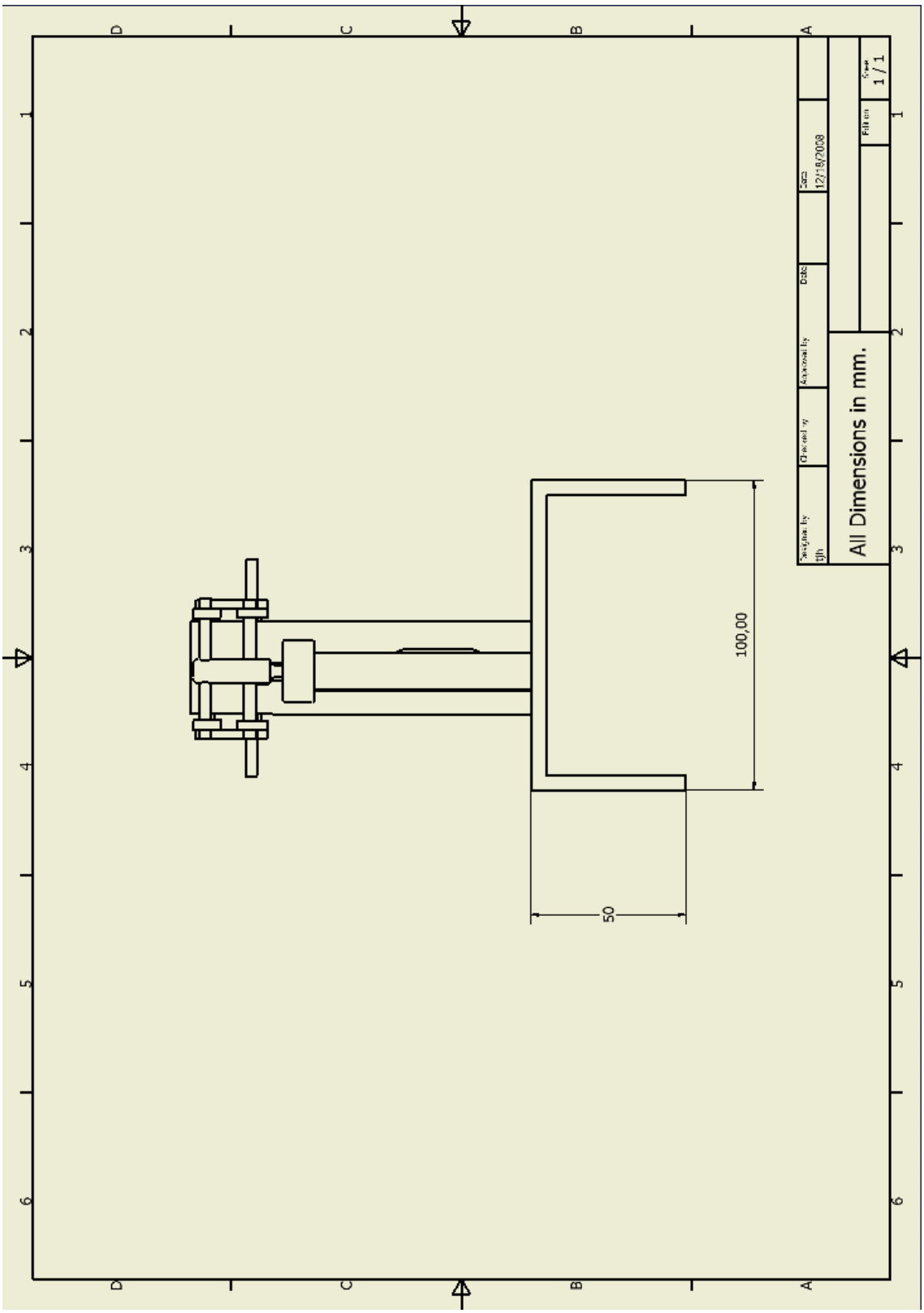

2. Side View.

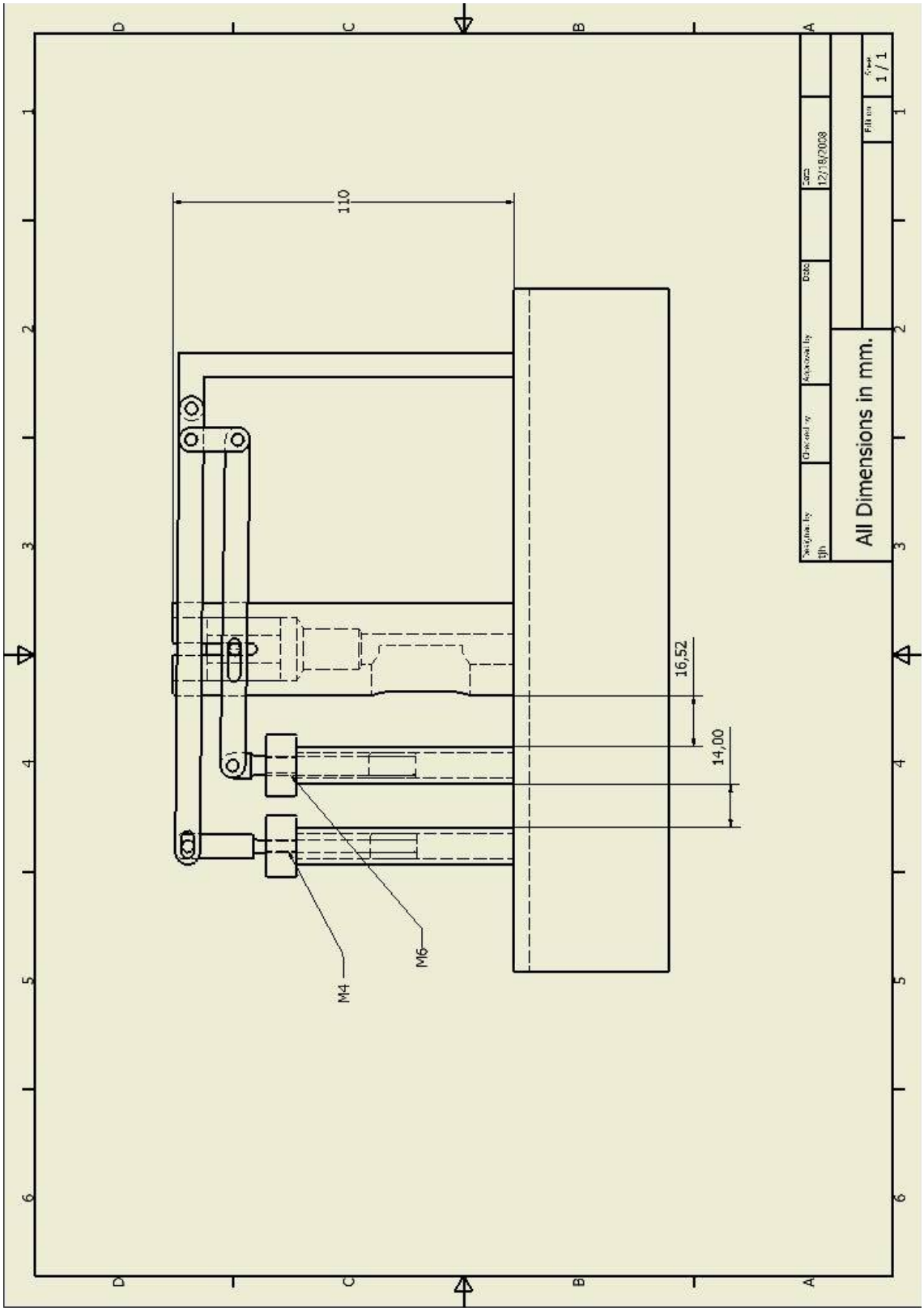

3. Plan View.

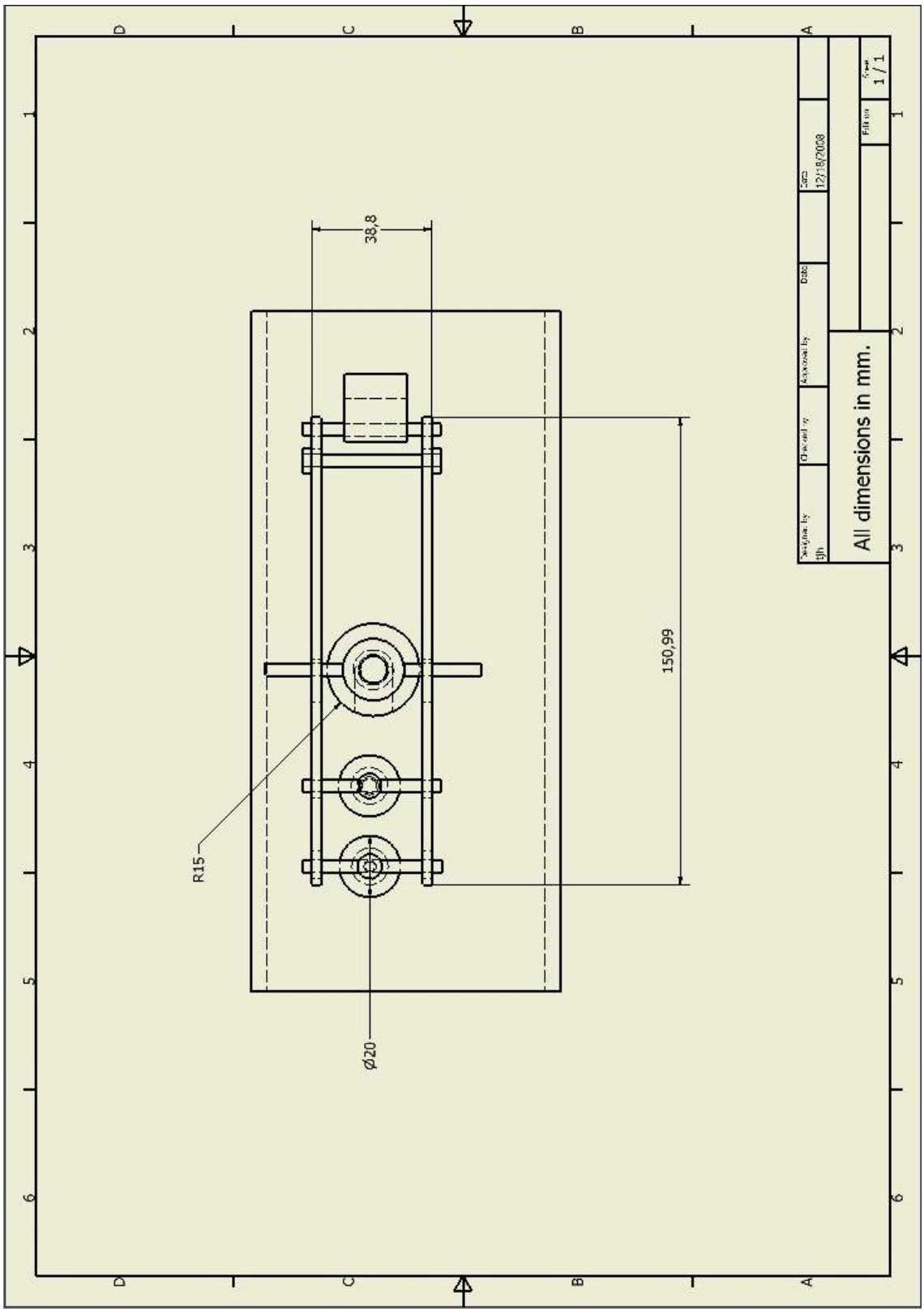

4. Perspective View.

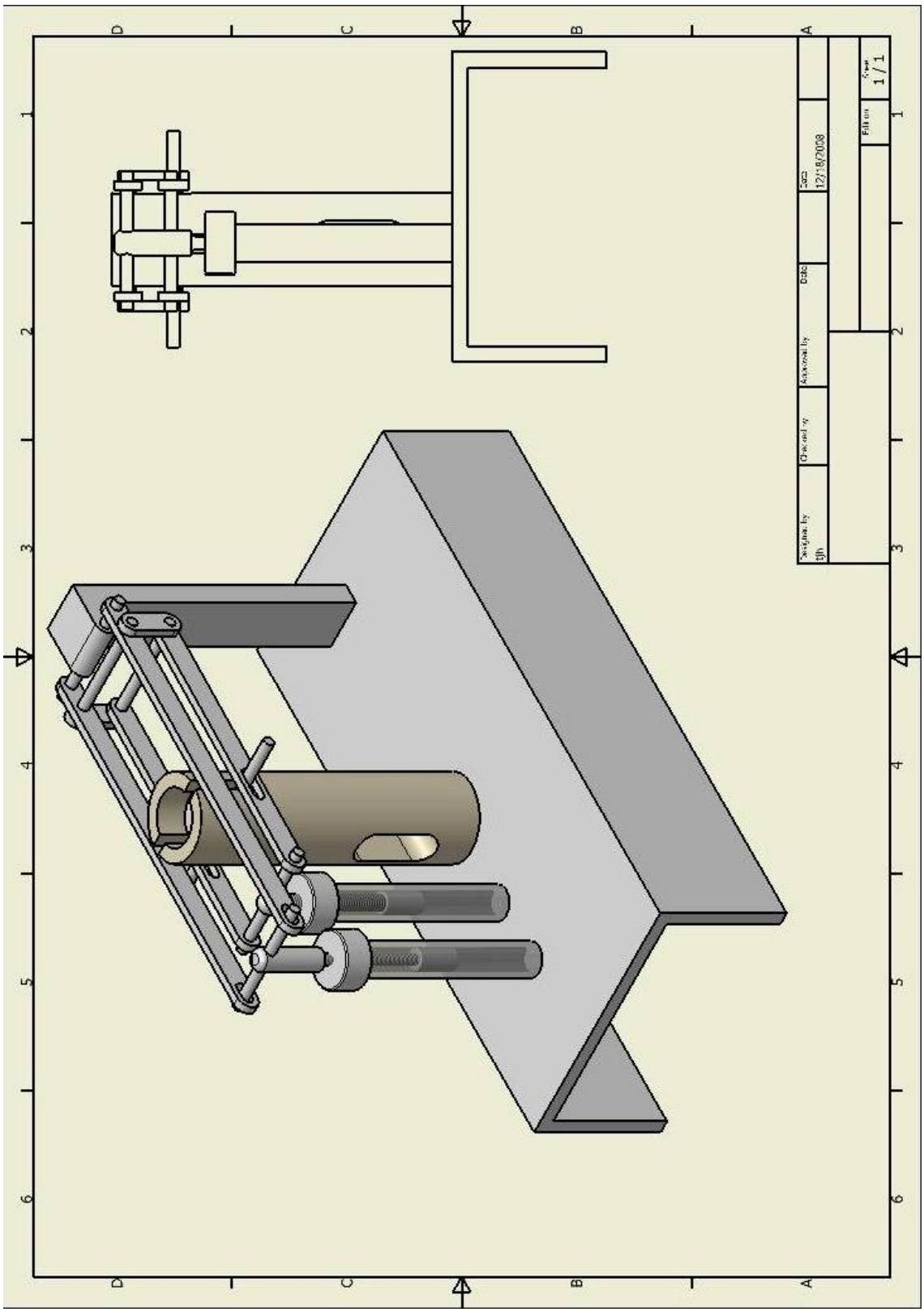

Appendix 6: Natural Frequency of PZT-KOVAR cantilever beam

Before the experiment is performed using the PZT actuator, it is important to identify the natural frequency of the PZT actuator at its 1st harmonic mode. This is the approximate calculation for the natural frequency of the PZT. Figure 1 shows the schematic section of a PZT actuator.

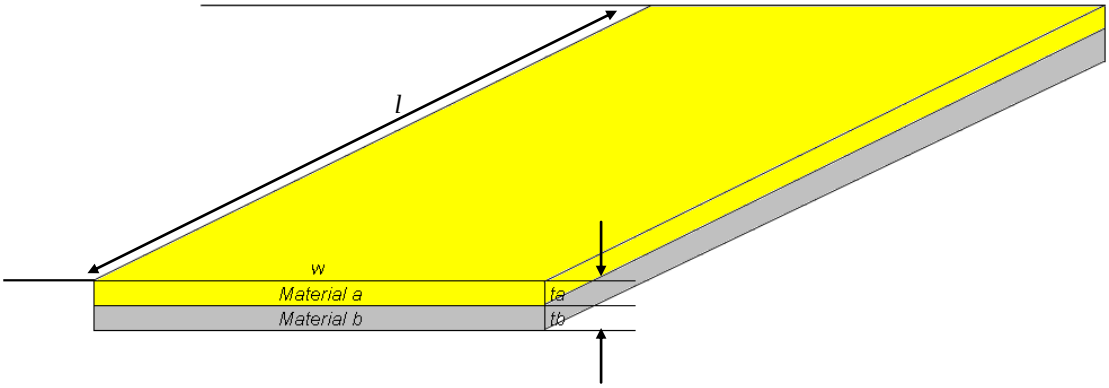

Figure 1: PZT actuator section

The natural frequency is given by [131]:

$$\omega_n = (\beta_n l)^2 \left(\frac{EI}{\rho A l^4} \right)^{1/2} \qquad \text{(Equation 2.2.23)}$$

Where β is a constant depending on the bonding conditions and the mode number, l is the length of the beam (see Figure 1), E is young's modulus, I is area moment of inertia, ρ is mass density, and the area of the cross section.

For "Fixed-Free" end condition of the beam and for the 1st Harmonic, $\beta_1 l$ is 1.875104 [119].

For composite beams:

$$EI = \frac{wt_b^3 t_a E_b E_a}{12\left(t_a E_a + t_b E_b\right)} K_1 \qquad \text{(Equation 2.2.24)}$$

Where K_1 is a constant and defined as below:

$$K_1 = 4 + 6\frac{t_a}{t_b} + 4\left(\frac{t_a}{t_b}\right)^2 + \frac{E_a}{E_b}\left(\frac{t_a}{t_b}\right)^3 + \frac{E_b}{E_a}\frac{t_b}{t_a} \qquad \text{(Equation 2.2.25)}$$

Where w is width, t_a is thickness of material “a”, t_b is thickness of material “b” (see Figure 1), E_a is the Young’s modulus of material “a” (PZT), and E_b is Young’s modulus of material “b” (KOVAR).

Using equation (2.2.25), to calculate K_1,

Where,

t_a = 80μm
t_b = 80μm
E_a = 70GPa [132]
E_b = 137GPa [133]

Thus, K_1 = 16.5

Then using equation (2.2.24), to calculate EI,

Where w = 5 mm

Thus, EI = 0.00014

Therefore using equation (2.2.23), to calculate the natural frequency,

Where mass density for PZT is ρ ~5000kg/m^3 (Equation 2.2.26)

And l= 20mm

Therefore Natural Frequency is

$$\omega_n = (1.875104)^2 \left(\frac{0.00016}{(5000)(t_a + t_b)(w)(l)^4} \right)^{1/2}$$

ω_n ~ 1693Hz

Based on this calculation the PZT actuator's operation should not exceed the determined frequency. Therefore in the case of this experiment there is no worry of the PZT actuator to vibrate beyond the 1st harmonic mode because the frequency used (0.2 to 20Hz) is much less than the natural frequency calculated (~1693Hz).

Appendix 7: To calculate elastic modulus

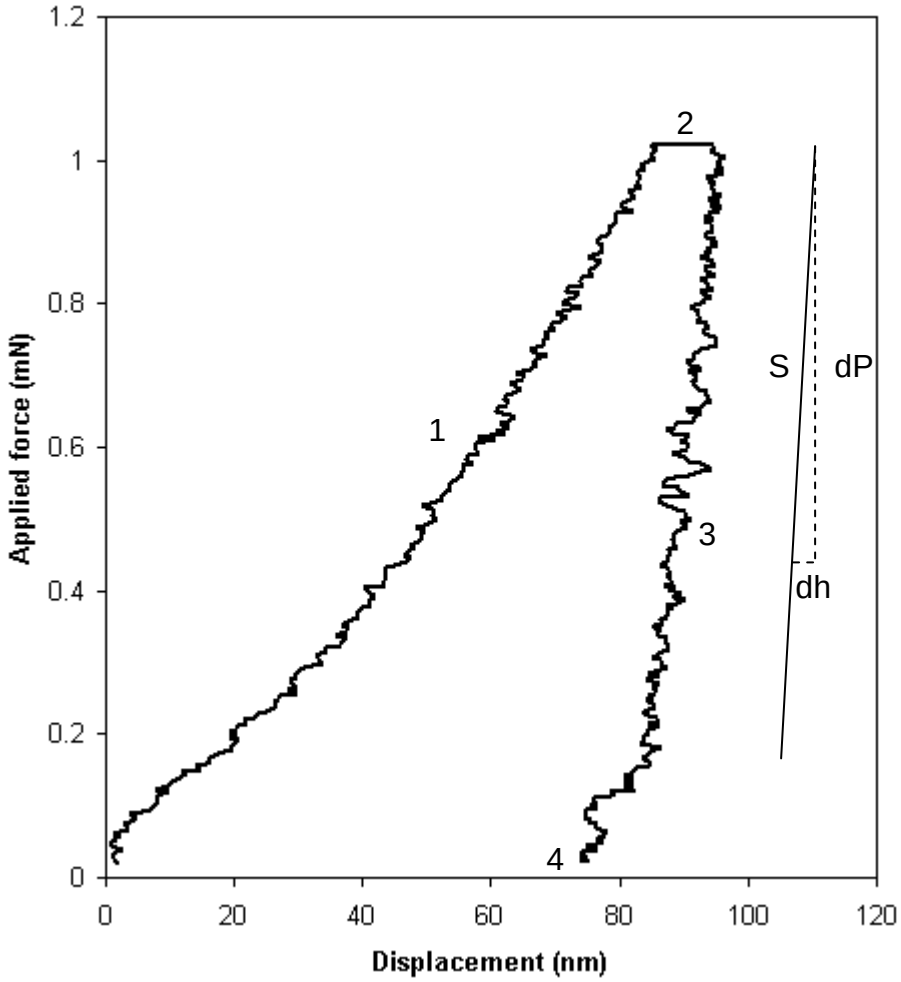

Figure 1: Graph of Applied force against displacement for Au substrate.

Figure 1 shows an example of indentation (Berkovich) on an Au substrate. Region 1 is the loading phase, region 2 is the holding phase (in this case 10 seconds), region 3 is the unloading phase and region 4 is the permanent depth penetration.

To calculate the elastic modulus E_r of the Au substrate is shown as below [134,135]:

$$E_r = \frac{\sqrt{\pi}}{2}\frac{S}{\sqrt{A}} \qquad \text{(Equation 1)}$$

Where S is the initial slope of the unloading phase as shown in Figure 1 and A is the projected contact area.

$$\text{Slope, } S = \left(\frac{dP}{dh}\right) = \frac{y_1 - y_2}{x_1 - x_2} \qquad \text{(Equation 2)}$$

Where y_1 and y_2 are the coordinates from the applied force and x_1 and x_2 are the coordinates from the displacement on the slope.

For a perfect Berkovich indenter, the Projected Area, $A = 24.56\left(h_c^{\,2}\right)$ (Equation 3)

Where h_c is the residual indentation depth.

From the slope (Figure 1, region 3):

y_1 = 1mN and y_2 = 0.81mN

x_1 = 95.44nm and x_2 = 93.08nm

By substituting the values above into equation 2

Slope, S = 80508.47 (Answer 1)

To calculate the projected area:

From Figure 1 (region 4), h_c = 75.2nm, substituting this value into equation 3.

The projected area, A= 1.389 x 10^{-13}m^2 (Answer 2)

By substituting the answer 1 and 2 into equation 1

The elastic modulus E_r for Au substrate ≈191.5GPa. In the calculation a perfect Berkovich indenter was used but in the experiment the diamond indenter could be blunt, thus giving a higher elastic modulus.

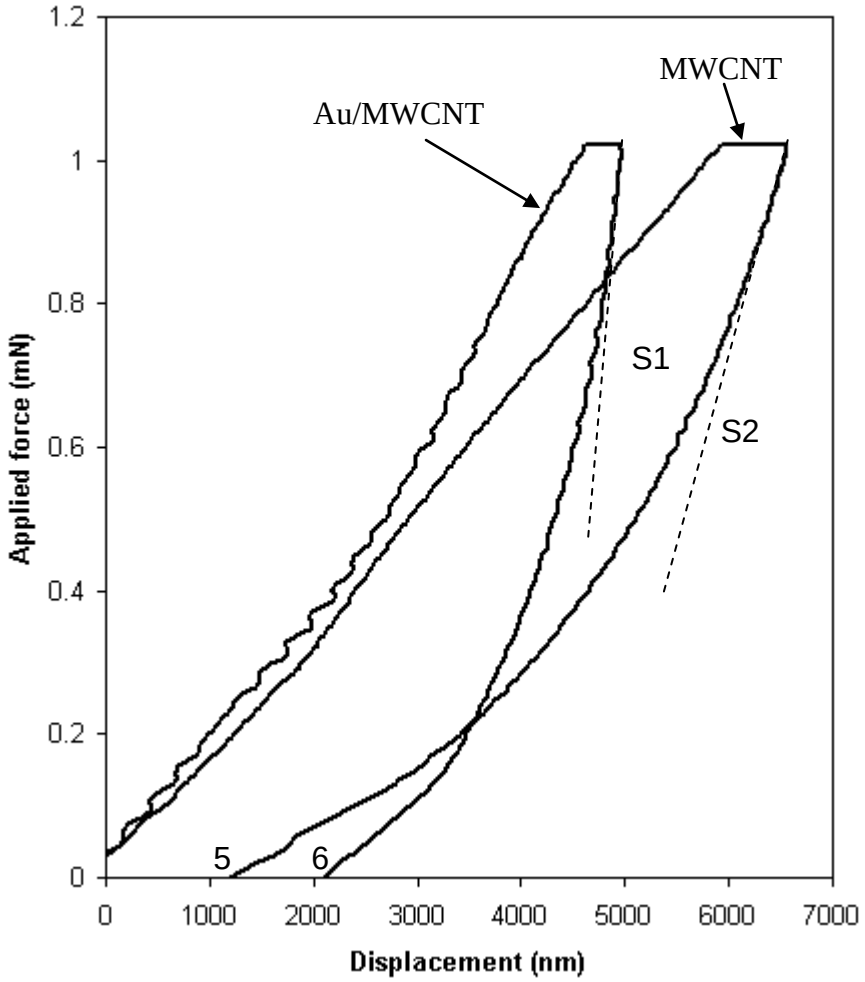

Figure 2: Graph of applied force against displacement for MWCNT and Au/MWCNT surface.

Figure 2 shows the graph of applied force against displacement for MWCNT and Au/MWCNT surfaces. To calculate the elastic modulus of MWCNT and Au/MWCNT surface the data from the slope S1 and S2 and region 5 and 6 are taken from the Figure 2. The same method of calculation as above is used. Thus the effective elastic modulus for Au/MWCNT is 92.3MPa and MWCNT is 67.5MPa.

Appendix 8: Abstracts.

1. 9th Material Engineering Conference, SES, University of Southampton, 2006: **The Relationship between Contact Resistance and Contact Force on Au coated Carbon Nanotube surfaces.**

2. 10th Material Engineering Conference, SES, University of Southampton, 2007: **Improving Microelectromechanical System Relay's Low Force Contact Electrodes Performance And Reliability.**

3. Holm 2007- 53rd IEEE Holm Conference on Electrical Contacts, Pittsburgh, USA, 2007: **The Relationship between Contact Resistance and Contact Force on Au coated Carbon Nanotube surfaces.**

4. The 24th International Conference on Electrical Contacts, St. Malo, France, 2008: **Improving the Contact Resistance at low force using Au coated Carbon Nanotube surfaces.**

5. The International Session on Electro-Mechanical Devices, Sendai, Japan (IS-EMD 2008): **Low force electrical switching using gold sputter coated vertically aligned multi-walled carbon nanotubes surfaces.**

6. The Material Research Society Conference, Boston, USA, Fall 2008: **Investigation of gold sputter coated vertically aligned multi-walled carbon nanotubes for RF MEMS contact surfaces.**

7. Holm 2009- 55rd IEEE Holm Conference on Electrical Contacts, Vancouver, Canada, 2009: **Carbon Nanotube Surfaces for Low Force Contact Application.**

9th Material Engineering Conference, SES, University of Southampton, 2006

The Relationship between Contact Resistance and Contact Force on Au coated Carbon Nanotube surfaces.

E. Yunus, J. W. McBride and S. M. Spearing
Electro-Mechanical/Engineering Materials Research Group, University of Southampton, SO17 1BJ
pgesa@soton.ac.uk, J.W.Mcbride@soton.ac.uk, spearing@soton.ac.uk

Abstract

Carbon-Nanotube (CNT) coated surfaces are investigated to determine the electrical contact performance under low force conditions. The surfaces under investigation are multi-walled CNT formed on a Silicon substrate and coated in with an Au film. These plane surfaces are mated with a hemispherical Au plated probe mounted in a nano-indenter. The contact force used is below 100mN. The contact resistance of these surfaces are investigated as a function of the applied force and also studied under repeated loading cycles. The surfaces are compared with a reference Au-Au study under the same experimental conditions and the results linked to established contact theory. The results show that the multi-walled CNT surface provides a stable contact resistance, but that the performance could be improved further with the application of single-walled CNT coatings. This initial study shows the potential for the application of CNT surfaces as an interface in low force electrical contact applications.

IMPROVING MICROELECTROMECHANICAL SYSTEM RELAY'S LOW FORCE CONTACT ELECTRODES PERFORMANCE AND RELIABILITY.

E. M. Yunus[1]. J.W. McBride[1], S.M. Spearing[2]

1 Electromechanical Engineering Research Group, School of Engineering Sciences, Southampton University, UK.
2 Materials Research Group, School of Engineering Sciences, Southampton University, UK.

Abstract-*Carbon-Nanotube (CNT) coated surfaces are investigated to determine the electrical contact performance under low force conditions. The surfaces under investigation are multi-walled CNTs formed on a Silicon substrate and coated with an Au film. These planar surfaces are mated with a hemispherical Au plated probe mounted in a nano-indentation apparatus. The maximum contact force used is 1mN. The contact resistance of these surfaces is investigated as a function of the applied force and is also studied under repeated loading cycles. The surfaces are compared with a reference Au-Au contact under the same experimental conditions and the results compared to established contact theory. The results show that the multi-walled CNT surface provides a stable contact resistance, but that the performance could be improved further with the application of single-walled CNT coatings. This initial study shows the potential for the application of CNT surfaces as an interface in low force electrical contact applications.*

Holm 2007- 53rd IEEE Holm Conference on Electrical Contacts, Pittsburgh, USA, 2007

The Relationship between Contact Resistance and Contact Force on Au coated Carbon Nanotube surfaces.

E. M. Yunus pgesa@soton.ac.uk
J.W. McBride J.W.Mcbride@soton.ac.uk
S.M Spearing S.M.Spearing@soton.ac.uk
School of Engineering Sciences, University of Southampton SO17 1BJ

Abstract-Carbon-Nanotube (CNT) coated surfaces are investigated to determine the electrical contact performance under low force conditions. The surfaces under investigation are multi-walled CNTs formed on a Silicon substrate and coated with an Au film. These planar surfaces are mated with a hemispherical Au plated probe mounted in a nano-indentation apparatus. The maximum contact force used is 1mN. The contact resistance of these surfaces is investigated as a function of the applied force and is also studied under repeated loading cycles. The surfaces are compared with a reference Au-Au contact under the same experimental conditions and the results compared to established contact theory. The results show that the multi-walled CNT surface provides a stable contact resistance, but that the performance could be improved further with the application of single-walled CNT coatings. This initial study shows the potential for the application of CNT surfaces as an interface in low force electrical contact applications.

The 24th International Conference on Electrical Contacts, St. Malo, France, 2008

Improving the Contact Resistance at low force using Au coated Carbon Nanotube surfaces.

E. M. Yunus pgesa@soton.ac.uk
J.W. McBride J.W.Mcbride@soton.ac.uk
S.M Spearing S.M.Spearing@soton.ac.uk

School of Engineering Sciences, University of Southampton SO17 1BJ

Abstract-*Investigations to determine the electrical contact performance under repeated load cycle at low force conditions for carbon-nanotube (CNT) coated surfaces are performed. The surfaces under investigation are multi-walled CNT synthesized on a silicon substrate and coated with a gold film. These planar surfaces are mounted on the tip of a PZT cantilever and mated with a hemispherical Au plated probe. The maximum dynamic applied force used is 1mN. The contact resistance (R_c) of these surfaces is investigated at the applied force and the repeated loading cycles are performed for reliability testing. The surfaces are compared with a reference Au-Au contact under the same experimental conditions. This initial study shows the potential for the application of CNT surfaces as an interface in low force electrical contact applications.*

The International Session on Electro-Mechanical Devices, Sendai, Japan (IS-EMD 2008)

Low force electrical switching using gold sputter coated vertically aligned multi-walled carbon nanotubes surfaces.

E.M. Yunus pgesa@soton.ac.uk
J.W. McBride J.W.Mcbride@soton.ac.uk
S.M. Spearing Spearing@ soton.ac.uk

School of Engineering Sciences, University of Southampton, SO17 1BJ, UK

Summary
Gold coated vertically aligned carbon-nanotubes (Au/MWCNT) surfaces are investigated to determine the electrical contact performance under low force conditions with repeated load cycling. The multi-walled CNT's are synthesized on silicon planar and sputter coated with a gold film. These planar surfaces are mounted on the tip of a PZT actuator and mated with a coated Au hemispherical probe. The load is typical of MEMs devices, with a 4V supply, 1 and 10mA current, and applied force of 1mN. The contact resistance (R_c) is monitored with the repeated loading cycles (over 1000 and a million cycle) to determine reliability and durability testing. The surfaces are compared with a reference Au-Au contact under the same experimental conditions. This study shows the potential for the application of CNT surfaces as an interface in low force electrical contact applications.

The Material Research Society Conference, Boston, USA, Fall 2008

Investigation of gold sputter coated vertically aligned multi-walled carbon nanotubes for RF MEMS contact surfaces.

E.M. Yunus, S.M. Spearing and J.W. McBride
School of Engineering Sciences, University of Southampton, SO17 1BJ, UK

ABSTRACT

A novel approach has been developed for the long-standing problem of durable contact surfaces for RF MEMS switches. In this work the performance of gold sputter-coated vertically aligned carbon nanotubes are investigated under the low force electrical contact conditions typical of MEMS switches. The carbon nanotubes provide a support for the conducting gold surface layer, minimizing the degradation, and adhesion between the contact surfaces which is the principal source of wear in such contacts. Contact surfaces were prepared by thermal chemical vapour deposition (T-CVD) of a "forest" of multiwalled carbon nanotubes (MWCNTs) on a silicon wafer surface. A thin gold layer is then sputter-deposited on top of the nanotube forest. The counter surface was formed using a gold sputter-coated stainless steel hemispherical probe. Quasi-static and cyclic loading was applied to these contact surfaces. Quasi-static loading using a modified nano-indenter was used to determine the mechanical behaviour of gold coated vertically aligned carbon-nanotubes (Au/MWCNTs) surfaces. The study reveals that the Au/MWCNT conforms to the shape of the Au hemispherical probe during the penetration. The surfaces are compared with a reference Au-Au contact and Au-Au/MWCNT pair under the same experimental conditions. Similar contact resistances were obtained for the Au-Au/MWCNT contact as were achieved for conventional Au-Au contacts. Cyclic loading was conducted using a piezo-driven micro-cantilever (PZT actuator), with load measured using an ultra-high resolution load cell. Electrical contact resistance was monitored throughout. Tests were run out to 1 million cycles. At 1 mN load, the Au-Au contact exhibited a significant increase in contact resistance, and accompanying surface degradation at ~430 cycles. The Au-Au/MWCNT pair contact resistance consistently remained unchanged at this load level out to 1 million cycles and there was significantly less surface degradation. Cyclic loading tests at other load levels and "hot switching" tests were also conducted. This initial study shows the potential for the application of metal-coated CNT surfaces as contact surfaces in RF MEMS electrical switching applications. Combinations of scanning electron microscopy and TaiCaan Technologies XYRIS 4000CL laser scanner were used to characterize the surfaces after quasi-static and cyclic loading.

Holm 2009- 55rd IEEE Holm Conference on Electrical Contacts, Vancouver, Canada, 2009

Carbon Nanotube Surfaces for Low Force Contact Application.

Abstract

An investigation of a gold coated vertically aligned carbon-nanotubes (Au/MWCNT) surfaces are performed to determine the electrical contact performance under low force conditions and hot-switched condition with repeated load cycling. The multi-walled CNT's are synthesized on silicon planar and sputter coated with a gold film. These planar surfaces are mounted on the tip of a PZT actuator and mated with a coated Au hemispherical probe. The load is typical of MEMs devices, with a 4V supply, 1 and 10mA current load, and applied force of 1mN. Moreover the current load is increased to 20mA-50mA to observe and benchmark the performance of these surfaces. The contact resistance (R_c) is monitored with the repeated loading cycles to determine reliability and durability. The surfaces are compared with a reference Au-Au contact under the same experimental conditions. This study shows that Au/MWCNT composite has potential for the application of on MEMS relay contact surfaces due to its durability and mechanical integrity.

Appendix 9: Proceedings.

1. 9th Material Engineering Conference, SES, University of Southampton, 2006: The Relationship between Contact Resistance and Contact Force on Au coated Carbon Nanotube surfaces.

2. 10th Material Engineering Conference, SES, University of Southampton, 2007: Improving Microelectromechanical System Relay's Low Force Contact Electrodes Performance And Reliability.

3. Yunus, E.M., McBride, J.W. and Spearing , S.M., 2007, "The Relationship between Contact Resistance and Contact Force on Au coated Carbon Nanotube surfaces," Proceedings of The 53rd IEEE Holm conference on electrical contact, 6.4, pp. 167-174.

4. Yunus, E.M., McBride, J.W. and Spearing , S.M., 2008, "Improving the contact resistance at low force using gold coated carbon nanotube surfaces," Proceedings of The 24th International conference on electrical contact, pp. 507-513.

5. Yunus, E.M., McBride, J.W. and Spearing , S.M., 2008, "Low Force Electrical Switching Using Gold Sputter Coated Vertically Aligned Multi-Walled Carbon Nanotubes Surfaces," Proceeding of the International Session on Electro-Mechanical Devices, The Institute of Electronics, Information and Communication Engineers, (IS-EMD 2008), pp. 61-64.

6. Yunus, E.M., Spearing, S.M., and McBride, J.W., 2008, "Investigation of gold sputter coated vertically aligned multi-walled carbon nanotubes for RF MEMS contact surfaces," for publication in the Proceedings of the Material Research Society Meeting, Fall Meeting Symposium GG.

Appendix 10: Papers in press for publication.

1) Yunus, E.M., McBride, J.W., and Spearing, S.M., 2009, "*The Relationship between Contact resistance and Contact Force on Au Coated Carbon Nanotube Surfaces Under Low Force Conditions"*, IEEE Transactions on Components and Packaging Technologies.

2) Yunus, E.M., McBride, J.W., and Spearing, S.M., 2009, *"Improving the Contact Resistance at Low Force using Gold Coated Carbon Nanotube Surfaces"*, The European Physical Journal AP section.

The Relationship between Contact Resistance and Contact Force on Au coated Carbon Nanotube surfaces under Low Force Conditions.

E. M. Yunus J.W. McBride S.M Spearing
pgesa@soton.ac.uk J.W.Mcbride@soton.ac.uk Spearing@soton.ac.uk
School of Engineering Sciences, University of Southampton SO17 1BJ

***Abstract*-Carbon-Nanotube (CNT) coated surfaces are investigated to determine the electrical contact performance under low force conditions. The surfaces under investigation are vertically aligned multi-walled CNTs formed on a Silicon substrate and coated with an Au film. These planar surfaces are mated with a hemispherical Au plated probe mounted in a nano-indentation apparatus. The maximum contact force used is 1mN. The contact resistance of these surfaces is investigated as a function of the applied force and is also studied under repeated loading cycles. The surfaces are compared with a reference Au-Au contact under the same experimental conditions and the results compared to established contact theory. The results show that the vertically aligned multi-walled CNT surface provides a stable contact resistance. This study shows the potential for the application of CNT surfaces as an interface in low force electrical contact applications.**

Keywords: nano-indentation apparatus, contact resistance, carbon nanotubes, and Au/multi walled carbon nanotubes.

I. INTRODUCTION.

This paper presents a study of carbon nanotube electrical contact surfaces under low force conditions, typically below 1mN. Such conditions are relevant to micro-contact applications, for example in MEMS relay devices. There are a number of potential contact materials for such applications; gold, palladium or platinum are commonly used [1]. The main disadvantage of these materials is that they are relatively soft and easily wear. Other potential contact materials for the low force applications are silicon carbide and diamond, however both have high elastic moduli, coupled with low electrical conductivity. SiC film doped with NH_3 has a resistivity of to 1 x 10^{-4} Ωm [2] and DLC (Diamond Like Carbon) doped with ruthenium has a resistivity of 1 x 10^{-5} Ωm [3]. Both materials have a much higher resistivity when compared to gold and its alloys (for example Au-6.3% Pt has a resistivity of 7.17 x 10^{-8} Ωm) [1].

Carbon nanotube surfaces (CNT) have shown potential as an electrical contact material for MEMS relay applications. In [4], Au contacts with a substrate coated with tangled single walled carbon nanotubes (SWCNT) were investigated; the resistivity was shown to be between 1 x 10^{-4} and 1.8 x 10^{-4} Ωm. A CNT-CNT pair at a load of 500mN showed an average contact resistance of 0.87Ω. The following mechanical properties have been determined for CNTs; a tensile strength of 63 GPa (compared with 1.2 GPa for high strength steel) [5]. Experiments using atomic force microscopy have been performed to measure the elastic modulus and bending strength of individual structurally isolated multi-wall carbon nanotubes, indicating values of 1.26 TPa and 14.2 GPa respectively [6]. Experiments have been conducted on CNTs using a nano-indentation apparatus; values were obtained for the bending modulus; 1.24 TPa, axial modulus; 1.23 TPa and wall modulus; 5.61 TPa [7]. Another report shows that CNT's have an elastic modulus greater than 1 TPa [8], which is comparable to that of diamond, at 1.2 TPa.

It is estimated that a 4-10 μm long Single Walled Carbon Nanotube (SWNT) with a diameter of 1.2nm has a resistivity of 0.88 x 10^{-8} Ωm [9]. The conduction mechanism is thought to be through ballistic electron transfer process. When a CNT is filled with metal, to form a composite, the resistivity falls to 0.35 x 10^{-8} Ωm [9]. The mechanical and electrical properties are therefore potentially comparable to diamond and gold respectively. No experiments have been reported on CNT materials for micro-contact applications. The study presented here investigates the application of a CNT metal matrix surface as a potential electrical contact material for low force applications.

II. MATERIAL PREPARATION AND EXPERIMENTAL METHODS

In this study three contact pairs have been investigated; sample 1, Au to Au; sample 2, Au to multi walled carbon nano-tubes (MWNT) and sample 3, Au to Au/MWNT composite. The geometry selected is shown in Fig.1 with a 2mm diameter hemisphere contacting a flat surface. In all cases the hemisphere consists of a stainless steel base, sputter coated with Au, 500 nm thick, with surface roughness, $R_a \approx 400$nm.

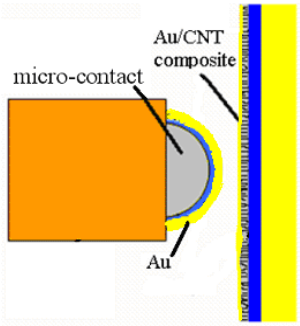

Figure 1: Schematic layout of the Au-Micro-contact and Au/CNT composite Substrate.

In experiment 1, the flat surface is a silicon (Si) substrate (5mm by 5mm), sputter coated with Au 500 nm thick, with a surface roughness, $R_a \approx 30$nm. In experiment 2, a "forest" of MWNT is grown on the Si wafer as shown in Fig. 2 using thermal CVD. The catalyst used is sputter deposited Fe and the gaseous carbon source is ethylene. The growth temperature and time is 875 ^{o}C and 3 minutes respectively to produce vertically aligned MWNT of ~50µm in length. Experiment 3 is the same as experiment 2, but with Au sputtered on the upper surface of the MWNT forest to produce Au/MWNT composite coatings as shown in Fig. 3, where it is also shown that the Au penetrates the MWNT surface to a depth of 2 to 4 µm.

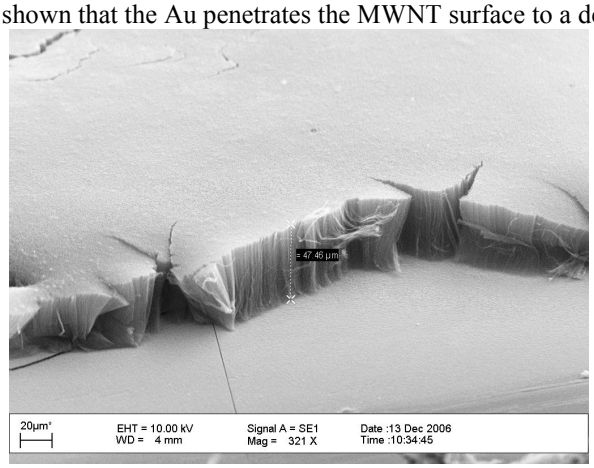

Figure 2: Sample 2, SEM image of a forest of MWNTs on an Si substrate.

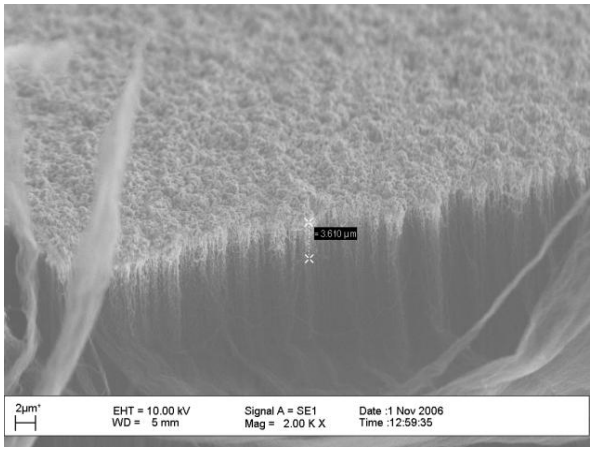

Figure 3: Sample 3, 2 - 4µm of Au coating on MWNT by sputtering.

To achieve a low contact force (<1mN) with a high degree of repeatability; a modified nano-indentation apparatus is used, [10]. The diamond indenter tip is replaced with a hemispherical contact surface shown

in Fig's 4 and 5. The force and electrical contact resistance (CR) is measured simultaneously. The force measurement is intrinsic to the apparatus and the resistance measured using the 4-wire measurement method, as shown Fig 5. The DC current source across the micro-contact and the substrate is set at 1mA, using a micro-ohmmeter. The connections to the surface are made using a conduction epoxy resin. The experimental apparatus is maintained at a constant temperature of 31 ^{o}C, to prevent thermal drift affecting the experiment due to expansion of the apparatus or the specimen. The coated micro-contact and substrate are brought into contact at a controlled loading rate of 0.2 mN/s until the maximum load of 1 mN is reached. The targeted load is held for 10 seconds so that an average peak resistance value can be determined. The contacts are unloaded at the same rate until they are separated.

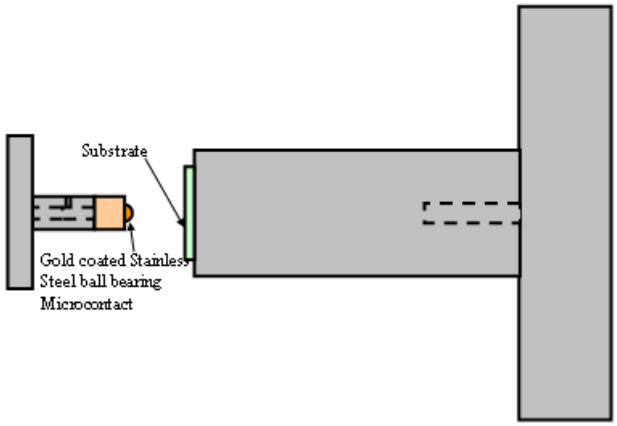

Figure 4: Schematic of modified nanoindenter.

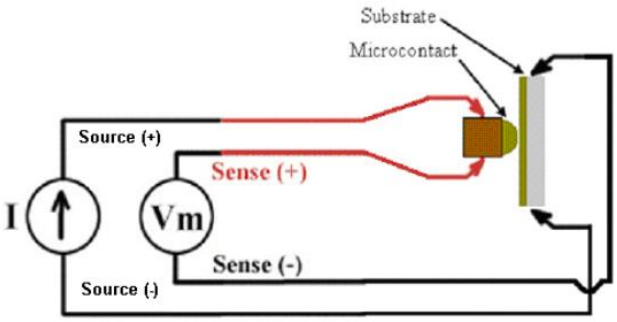

Figure 5: Schematic of contact zone with its electrode and R_c measurement.

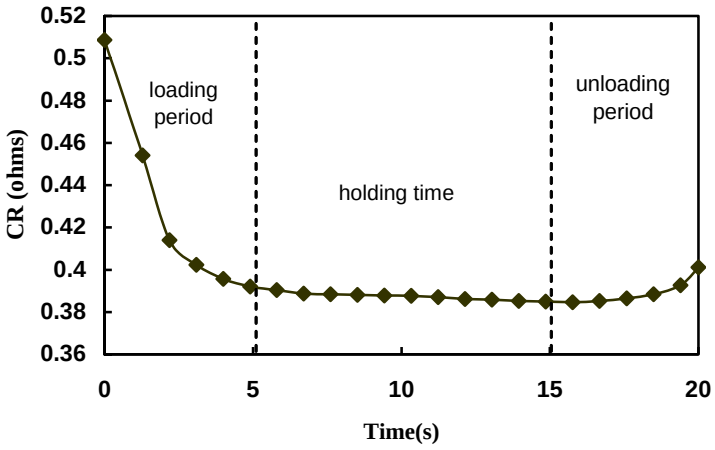

Figure 6: Example of one load cycle for an Au-Au contact pair.

Fig 6 shows an example of the resistance variation over one load cycle. During the first 5 seconds as the force increases the contact resistance falls; the resistance then remains relatively stable during the holding time, and then increases during the unloading period. The result shows that the contacts remain together

after 20 seconds, as a result of the Au contacts "sticking". The procedure is repeated in order to detect any cyclic changes in the electrical contact resistance.

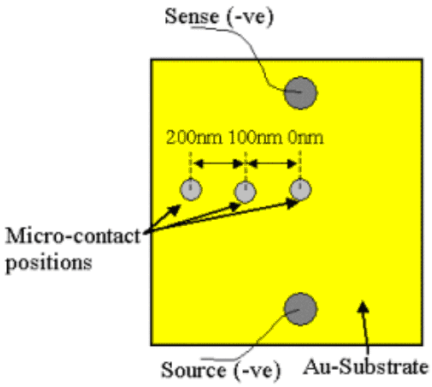

Figure 7: Top view micro-contact positions on the Au-substrate.

Prior to the experiments, two control measures are used. (1); To determine the bulk resistance of the component. By changing the width between the sense (-ve) and source (-ve) point on the substrate, Fig 7. In addition the micro-contact position is moved relative to the current source connections, to positions 100nm and 200nm, shown schematically in Fig 7. Both tests result in the same resistance of 0.38Ω. This confirms that the 4-wire measurement method is a measure of the contact resistance and not the bulk resistance. (2) To determine the nature of the film conduction. In this test the contact resistance across the Au micro-contact with the substrate coated by the catalyst only (i.e. no MWNT) is measured and no conduction is detected. This shows that the electrical conduction mechanism is through the MWNT and Au/MWNT coatings. This observation is expected to have important implications in the evaluation of the contact resistance [11].

III. RESULTS AND DISCUSSION.

A. Contact resistance –force characteristic for experiment 1 (Au-Au)

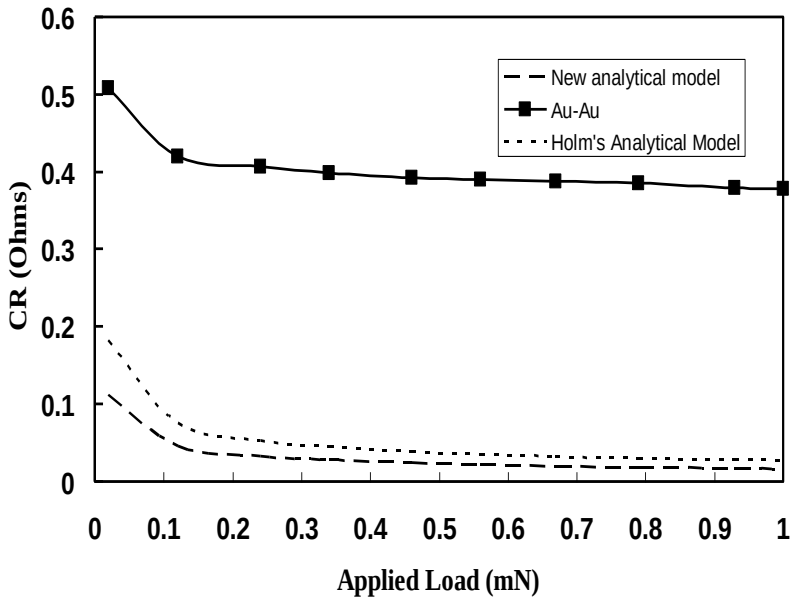

Figure 8: Contact resistance between Au-Au contact pair as a function of the applied load.

Fig 8 shows the experimental contact resistance versus contact force of the Au-Au contact pair up to a maximum load of 1mN. At very low forces below 0.1mN the average contact resistance during the holding period is approximately 0.5Ω, which decreases to 0.4Ω at 1mN. The figure also shows the contact resistance based on theoretical predictions. Assuming that the contact deforms plastically, based on the Holm analytical model, [12], using the following equation:

$$R_c = \left(\frac{\rho^2 \eta \pi H}{4F} \right)^{\frac{1}{2}} \qquad \textit{(eqn. 1)}$$

Where for Au: $\rho = 2.24 \times 10^{-8}\ \Omega m$.

and for sputtered Au. [13]: $H = 1.7 \times 10^{9}\ N/m^{2}$,

The measured contact resistance data are significantly greater than the analytical model using the above formula. There are three possible reasons for this difference:
(i) the contact surfaces are assumed to be clean (thus assume η=1) but in the experiment there are likely to be surface films and contaminants (η >1), thus giving a higher contact resistance.
(ii) the Holm model assumes an electron diffusion dominated conduction model. It has been shown that under low force conditions the model requires modification, to account for ballistic transfer, [13, 22].
(iii) the Holm model assumes an infinitely large conducting body; the model will be compromised by conduction dominated by the thin films.

B. Consideration of Contamination.

Gold is a logical choice as a contact material for MEMS relay applications because it has a low propensity to form alien surface films and is corrosion resistant [13]. However a gold surface has the tendency to have a thin layer of carbon as a residue from cleaning processes and/or adsorbed due to exposure to air [14]. For example, it has been reported that there can be a 2-4 nm layer of adsorbed hydrocarbons on freshly cleaned Au [15,16]. In an investigation of the influence of the position of the resistance sensing probe on the surface, there was no change in the resistance measurement. This suggests that there is negligible contamination as any influence from contamination would be expected to be non-uniform over the surface. It is thus proposed that the contamination is negligible and that the assumption that η=1, is valid.

C. Modification of the Holm model for low contact force.

Consideration is initially given to the breakdown of the classical Holm conduction model. This follows a study by Coutu et.al., where the influence of elastic-plastic material deformation and the associated contact resistance under the low force conditions typical of MEMS relays, where conduction is likely to be dominated by ballistic and diffusive electron transport; were considered [13]. Using the formula from [13];

$$R'_c = R_c(ballistic) + \Gamma(K) R_c(diffusive) \qquad \textit{(eqn. 2)}$$

Where R_c *(ballistic)* is the contact resistance equation based on ballistic electron transport and elastic-plastic material deformation, R_c *(diffusive)* is the contact resistance equation based on diffusive electron transport and elastic-plastic material deformation and $\Gamma(K)$ is the Gamma function. This formulation is an updated micro-contact resistance model for low force contact developed using Chang's [17] improvement to the Chang, Etsion, and Bogy (CEB) model [18] and the Gamma function using a Wexler interpolation [19]. Where;

$$R_c(ballistic) = \frac{4\rho K}{3\pi} \sqrt{\frac{H\pi \left[1.062 + 0.354 \left(\frac{2}{3} K_Y - 3 \left(\frac{\alpha_c}{\alpha} \right) \right) \right]}{F}} \qquad \textit{(eqn. 3)}$$

R_c(ballistic) is the contact resistance equation based on ballistic electron transport and elastic-plastic material deformation, ρ is the resistivity of sputtered Au on the micro-contact, H is the hardness of sputtered Au, F is the applied load (ranging from 10μN to 1mN), K is Knudsen number, K_Y is the yield coefficient, α_c is the critical vertical deformation, α is the asperity vertical deformation.

$$R_c(diffusive) = \frac{\rho}{2}\sqrt{\frac{H\pi\left[1.062+0.354\left(\frac{2}{3}K_Y - 3\left(\frac{\alpha_c}{\alpha}\right)\right)\right]}{F}} \qquad \textit{(eqn. 4)}$$

R_c(diffusive) is the contact resistance equation based on diffusive electron transport and elastic-plastic material deformation. To calculate the Knudsen number [13,20];

$$K = \frac{l_e}{r_{eff}} \qquad \textit{(eqn. 5)}$$

The Knudsen number, *K*, is a dimensionless number describing the flow of the electron particles and is defined as the ratio of the molecular mean free path length to a representative physical length scale; the length scale is the radius of the contact surface. l_e is elastic mean path (for most metals ~50 nm [13,20]) and r_{eff} is the effective contact area radius. In a single asperity model, the individual contact spots are assumed close enough together that their interactions are not independent. In this circumstance [13] assumes that the effective contact area is defined as the sum and not the parallel combination of the individual contact areas.

To understand the implication of the modified contact resistance model consider the 1mN contact force with the values of H and ρ used in eqn. 1, assume η=1; this leads to a predicted contact area of 0.58μm^2 based on A= F/H. This generates a predicted constriction resistance of 26mΩ as shown in Fig.8. The corresponding contact radius is 430nm, based on a single circular contact. The corresponding relationship with force is shown in Fig.8. As reported this shows a significant difference with the measured values. To determine the adjustment to the predicted resistance based on the application of eqn's 2,3 and 4. If we assume the same area of contact then; using eqn. 5, K= 0.000116. Thus for the selected area the contribution to the resistance of the ballistic transmission model is negligible. To determine the contribution to the resistance resulting from the modified diffusive model; the yield coefficient can be calculated using [13];

$$K_Y = 1.1282 + 1.158v \qquad \textit{(eqn. 6)}$$

Where *v* is Poisson's ratio for Au (0.42), thus, K_Y is 1.61456. When the asperities are considered having elastic-plastic deformation, the α (asperity vertical deformation) and α_c (critical vertical deformation) are assumed equal [17,18]. To estimate the *Γ(K)* Gamma function we can use the graph as shown in Fig. 9 [19,21,22]. Since *K* (Knudsen number) is 0.000116, from the graph the Gamma function is ~1. By substituting eqns. 3 and 4 and the above data into eqn. 2 a new analytical model is plotted as shown in Fig 8.

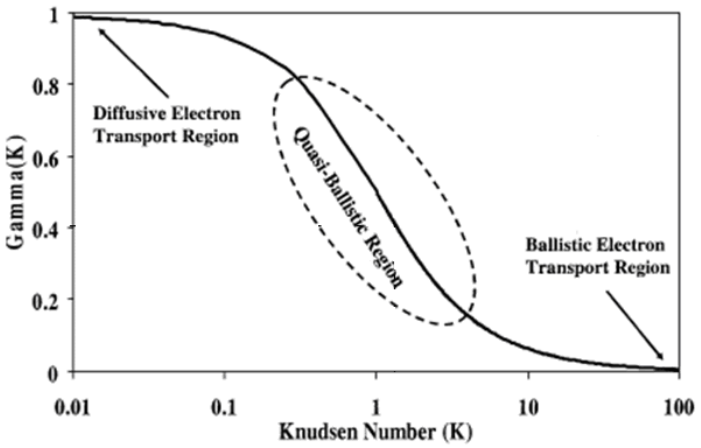

Figure 9: Plot of Mikrajuddin et.al.'s derived gamma function.

The new analytical model defined in (eqn 2) gives a contact resistance slightly lower than Holm's contact resistance model in (eqn 1). In this model; (1) the new micro-contact resistance considers elastic-

plastic material deformation, (2) it uses a single effective contact area rather than multiple a-spots, (3) conduction during the micro-relay's closure is considered to be a mixture of ballistic and diffusive electron transport, and (4) the contact load discontinuity (which exists at the transition from ideal elastic to ideal elastic-plastic behavior) is accounted for. The model falls short of the measured values and it is therefore concluded that the existing models for contact resistance are not applicable and further consideration should be given to the influence of thin film conduction.

D .Modified Contact Resistance for Thin-Films

The theory presented in the previous section is based upon the analysis of bulk materials. There are two additional factors not considered; the conduction in a thin film upon a non-conducting surface, and the local hardness value, which is expected to differ from the bulk value.

When the radius of the contact area is no longer small compared to the film thickness, the contact resistance is no longer dominated by the Holm constriction resistance, [22]. In this case a spreading resistance is required from the contact area to the thin metallic film. In this study the radius of the contact area was estimated to be 430nm, which is comparable with the film thickness of 500nm. In [11] an FEM model was used to show an increase in the constriction resistance from 1mΩ using a modified version of the Holm equation, to 12mΩ using the FEM model, for a 1µm film, with a 5µm contact radius. In this study an FEA model was created with a 500nm Au film, shown in Fig. 10, modelled on the 1mN contact force with the same values of H and ρ used in Eqn. 1. The model is a simple 2D axi-symmetric system, which models a 3D system with the current fed through a cylindrical electrode. This generates a predicted constriction resistance of 62mΩ, compared to the 26mΩ in Fig.8. The result from the FEM study identifies the importance of thin film conduction mechanisms, as being the most likely contribution to the increase in the measured values of resistance over the predicted values.

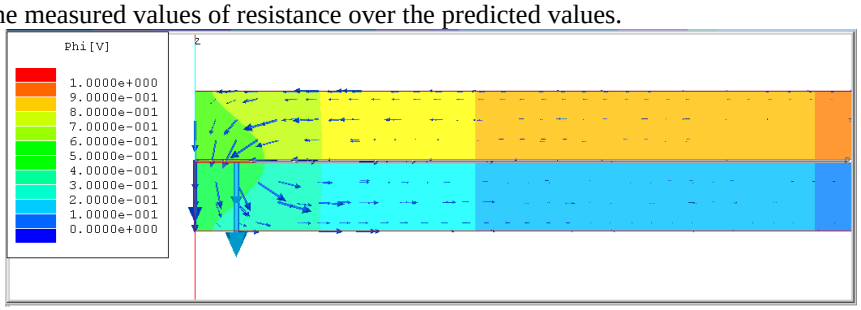

Figure 10: FEA model of thin film with current flow through a 500nm Au film with a contact area of $0.58\mu m^2$.

E. Contact Resistance - Force Characteristic for Experiments 2(Au-MWNT) and 3(Au-Au/MWNT)

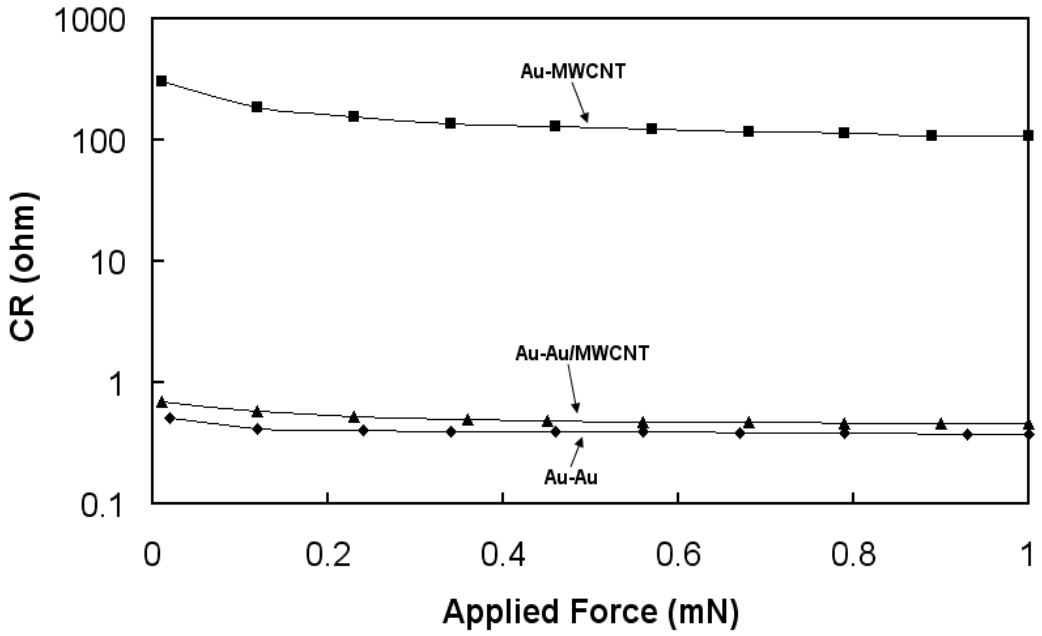

Figure 11: Contact resistance between Au-MWCNT, Au-Au/MWCNT and Au-Au coating contact pair as a function of applied load.

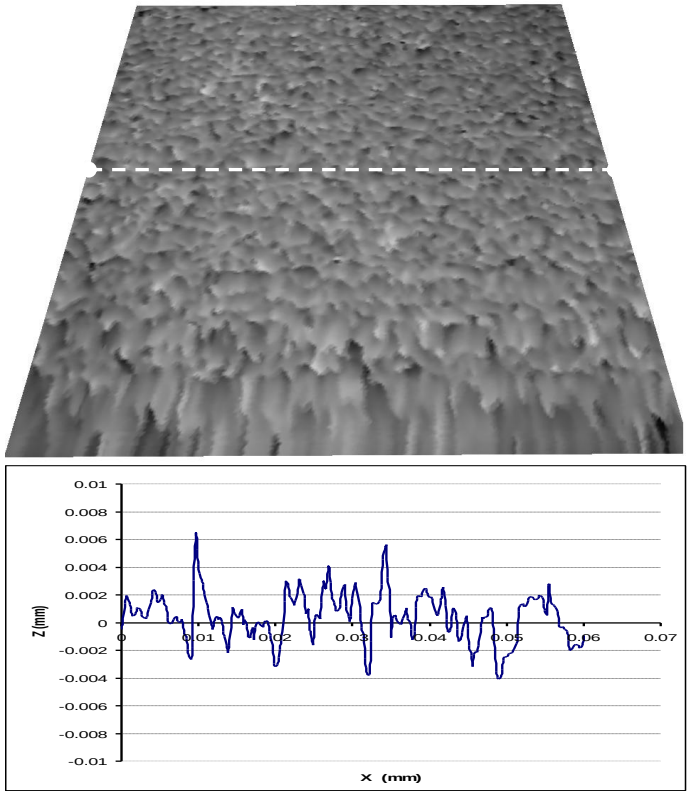

Figure 12: Con-focal Laser Scanned image of MWNT 301x301 (60µm x 60µm) using TaiCaan Technologies (Xyris 4000CL), showing 2D section of data.

Experiment 2. Fig 11 shows the contact resistance against an applied load for the Au-MWNT contact pair. The surface roughness was shown to be $R_a \approx 1.3\mu m$. Fig 12 shows a corresponding SEM image of the top surface of a MWNT coated surface. In this experiment, the dominant factor is expected to be the elastic deflection of the MWNTs rather than plastic indentation. As the applied load is increased, more deflection occurs of the MWNTs closing the air gaps between the vertically aligned MWNTs, thus improving the transfer of electrons. Furthermore the MWNTs will conform to the form of the Au micro-contact, increasing the contact area.

Experiment 3. In this case the contact resistance is lower than the Au-MWNT contact pair and higher than Au-Au contact pair as shown in Fig. 11. The Au coating on MWNT makes contact with the Au coated ball thus leading to a decrease in the contact resistance when compared to the un-coated surface.

G. Cyclic loading

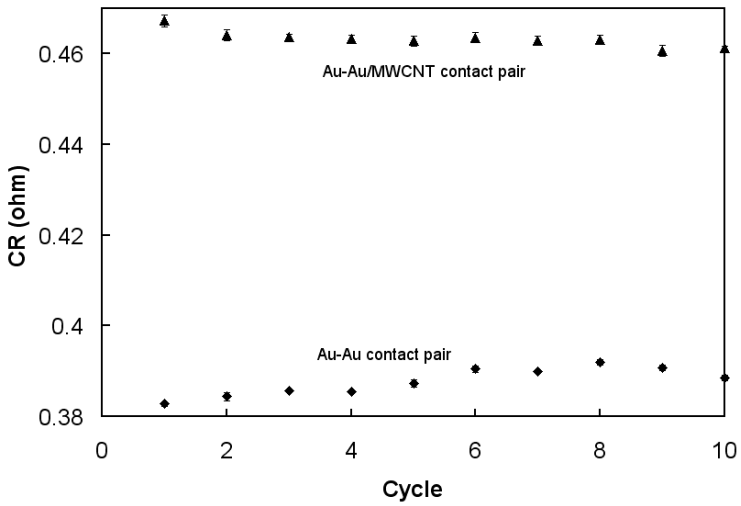

Figure 13: Cyclic contact resistance of Au-Au and Au-Au/MWCNT contact pair.

To determine the performance of these materials under cyclic loading conditions, an initial study is presented using the nano-indenter apparatus to cycle for 10 repeated operations. Fig 13 shows the contact resistance of an Au-Au pair over 10 load cycles at a maximum applied load of 1mN. The points include the corresponding standard deviation of the contact resistance measured during the hold period. A recent experiment using a modified nano-indenter with a Au-Pt surface showed that the contact resistance increased after the 10^{th} cycle, [10]. It was proposed that this was due to the "hot-switched" contact resulting in arcing. In this experiment the contact are under the "dry circuit" condition with negligible current loading, therefore changes in contact resistance are only due to the mechanical deterioration of the Au-Au contact surfaces. Au is a soft metal with low hardness 1-2GPa [13], it has a low melting point, and is susceptible to wear.

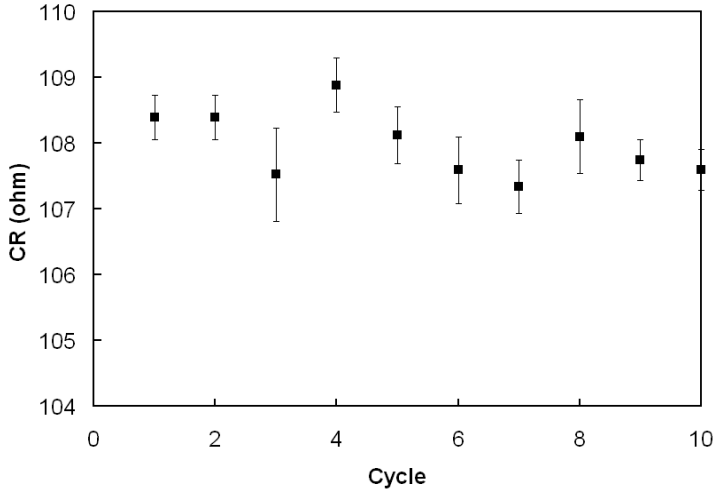

Figure 14: Cyclic contact resistance of an Au-MWCNT contact pair.

Fig 14 shows the contact resistance of an Au-MWNT contact pair during cyclic load. The contact resistance of the Au-MWNT contact pair during cyclic load is much higher (~108 Ω) than the Au-Au contact pair (~0.39 Ω). Fig 13 also shows the contact resistance of an Au-Au/MWNT contact pair. The contact resistance of the Au-Au/MWNT pair shows a small decrease over the first 10 loading cycles, but with a reduced resistance (~0.46Ω) when compared to the Au-MWNT contact pair (~108 Ω).

H. Load-Displacement Characteristic of the surfaces

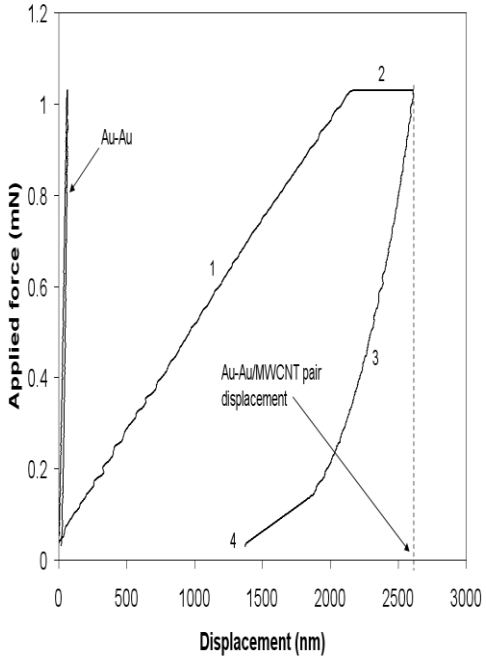

Figure 15: Graph of applied indentation load vs. displacement.

Fig 15 shows a graph of indentation load versus displacement, for the hemispherical contact on the plane surface, as shown in Fig.1, (with data extracted from the nano-indentation apparatus). We first describe the general features of the load-displacement responses we have observed from the experiment. The curve in region 1 shows the loading and the curve in region 3 shows the unloading of the contact. Region 2 shows there is creep, a deformation that occurs over a period of time when a material is subjected to constant stress, which may also be temperature-dependent. Region 4 is the permanent depth deformation after the contact pair separates. From Fig 15 it is observed that the displacement of the Au-Au/MWNT contact pair is greater than for the Au-Au contact pair, 70nm compared to 2800nm; this will provide a larger conducting surface area. The results suggest that the Au-Au/MWNT sample exhibits a residual plastic deformation of approximately 1300nm depth. This is a result of the Au film deforming on the surface of the CNT surface.

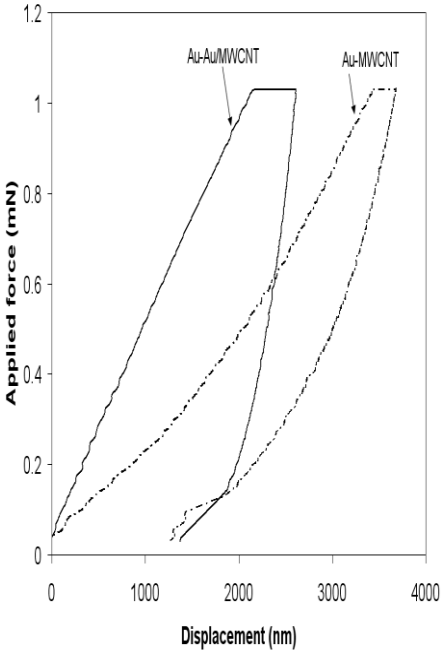

Figure 16: Graph of indentation load vs. displacement (depth) for Au-MWCNT.

The characteristic for the Au-Au/MWNT sample is also shown in Fig 16 for comparison to the Au-MWNT contact pair. For the Au-MWNT sample the deformation of the surface is further increased over the Au-Au/MWNT sample, to 3800nm compared to the 2800nm, however the residual deformation is similar for both samples. This indicates that the plastic deformation process is dominated by the CNT surface.

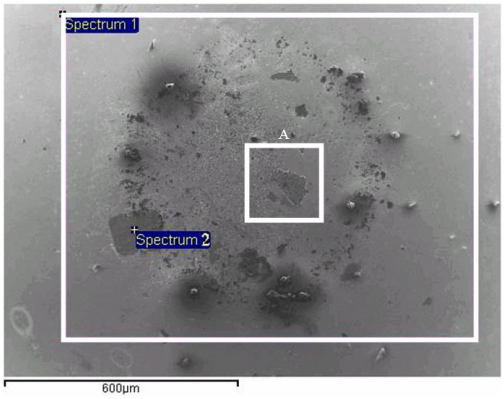

Figure 17: Au micro-contact after contact with Au/MWNT substrate.

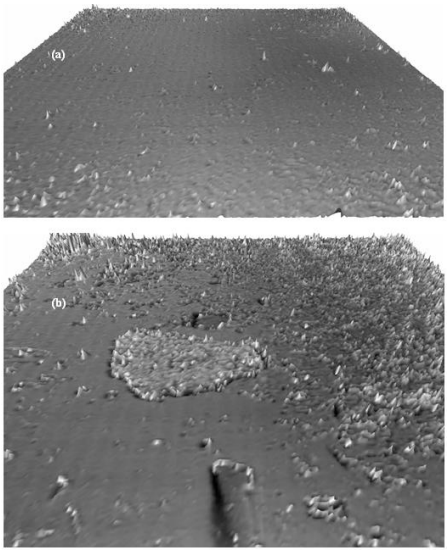

Figure 18: (a) Fresh and (b) tested Au (ball) micro-contact with spherical shape removed, 301x301 (400μm x 400μm) using TaiCaan (Xyris 4000CL).

Fig 17 shows an SEM image of the Au (ball) contact surface after the load cycles for the Au-MWNT surface, showing areas of damage. When the area marked 'A' was scanned using a non-contact 3D laser profiler (TaiCaan Xyris 4000CL) many small impressions on the Au micro-contact are detected as shown in a 3D scanned surface in Fig 18 (b), which can be compared to a new surface in Fig 18 (a). These impressions are due to the asperities on the MWNT surfaces. Moreover the surface roughness, R_a in this region has increased from ~400 nm in (a) to ~1.5μm (b). X-ray spectroscopy of the Au (ball) micro-contact at the position named "Spectrum 1", in Fig 17, has shown gold to be the predominant element with carbon and oxygen also observed. This is consistent with the composition of the film, with some additional surface contamination and water adsorbtion. The overall atomic percent of Au is 38.60%, C is 55.49% and O 5.91%. When a point on the exposed hemisphere (Au ball contact) was analysed, marked 'Spectrum 2', in Fig 17. The 'Fe' peak was predominantly observed and Cr peak indicates both elements come from the stainless steel ball. The atomic percent shows Fe is 68.69%, Cr is 19.08%, C is 11.67% and Au is 0.57% thus indicating that wear has occurred on the Au micro-contact exposing the surface of the ball. No evidence of deformation or change in chemical composition on Au/MWNT surfaces has been detected. The creep shown in Fig's 15 and 16 is identified as the mechanism responsible for the increase in stiction [23]. A fundamental understanding of the relationships between contact force, adhesion, and contact resistance is needed for MEMS relay design [24].

IV. CONCLUSION.

The contact force and contact resistance between Au-Au/MWNT composite contact pairs was investigated using a modified nano-indentation apparatus and 4-wire measurement methods. The contact pair combination was compared to a Au-MWNT pair, and showed a decrease in the measured contact resistance. The contact resistance characteristic of the Au-Au/MWNT composite surface was shown to be comparable to a Au-Au contact pair studied as a benchmark for the new material. Furthermore during ten load cycles, the Au-Au/MWNT contact pair showed a stable contact resistance.

A study of contact resistance modeling based on existing analytical models shows that there is a discrepancy with the benchmark Au-Au surface. This leads to the conclusion that the mechanics of such surfaces at low force must fall outside the current understanding. An initial study suggests that the main reason for the difference is due to the conduction mechanisms associated with thin film surfaces. FEA analysis shows that conduction through the thin film conductor leads to an increase in the predicted resistance.

Acknowledgements
The authors would like to thank Dr. S.Abu-Sharkh of the School of Engineering Sciences for his contribution to the FEA study, and to Dr D.C. Smith of the School of Physics and Astronomy, for providing the facilities for depositing the MWNT and Au.

References

[1] Coutu, R. A., Kladitis, P. E., Leedy, K. D. and Crane, R. L., 2004, "*Selecting Metal Alloy Electric Contact Materials for MEMS Switches*," Journal of Micromechanics and Microengineering, (14) pp. 1157-1164.

[2] Gao, D., Wijesundara, M. B. J., Carraro, C., Low, C. W., Howe, R. T. and Maboudian, R., 2003, "*High Modulus Polycrystalline 3C-SiC Technology for RF MEMS*," The 12th International Conference on Solid State Sensors, Actuators and Mircosystems, 3D3.4, pp. 1160-1163.

[3] Lian, G. D., Dickey, E. C., Ueno, M. and Sunkara, M. K., 2002, "*Ru-doped Nanostructured Carbon Films*," Diamond and Related Materials, 11, pp. 1890-1896.

[4] Yaglioglu, O., Hart, A. J., Martens, R. and Slocum, A. H., 2006, *"Method of characterizing electrical contact properties of carbon nanotube coated surfaces,"* Review of Scientific Instruments, 77, pp 095105/1-3.

[5] Yu, M. F., Lourie, O., Dyer, M. J., Moloni, K., Kelly, T. F. and Ruoff, R.S., 2000, "*Strength and Breaking Mechanism of Multiwalled Carbon Nanotubes Under Tensile Load*," Science, 287(5453), pp. 637 – 640.

[6] Wong EW, Sheehan PE, Lieber CM, 1997 "*Nanobeam Mechanics: Elasticity, Strength, and Toughness of Nanorods and Nanotubes*," Science, 277, pp. 1971-5.

[7] Qi, H.J., Teo, K.B.K., Lau, K.K.S., Boyce, M.C., Milne, W.I., Robertson, J. and Gleason, K.K., 2003, "*Determination of Mechanical Properties of Carbon Nanotubes and Vertically Aligned Carbon Nanotube forests using Nanoindentation*," Journal of Mechanics and Physics of Solids, 51, pp. 2213-2237.

[8] Thostenson, E. T., Ren, Z. and Chou, T.W., 2001, "*Advances in the Science and Technology of Carbon Nanotubes and their Composites: A review*," Composites Science and Technology, 61, pp. 1899-1912.

[9] Hjortstam, O., Isberg, P., Söderholm, S. and Dai, H., 2004, *"Can we achieve ultra-low resistivity in carbon nanotube-based metal composites?"* Journal of Applied Physics A, Materials Science & Processing, 78, pp. 1175-1179.

[10] Dickrell III, D. J. and Dugger, M. T., 2005, "*The effects of surface contamination on resistance degradation of hot-switched low-force MEMS electrical contacts*," Electrical Contacts, Proceedings of the Annual Holm Conference on Electrical Contacts, v 2005, Electrical Contacts 2005 - Proceedings of the Fifty-First IEEE Holm Conference on Electrical Contacts, pp. 255-258. [11] Norberg, G., Dejanovic, S., and Hesselbom, H., 2006, *"Contact Resistance of Thin Metal Film Contacts,"* IEEE Transactions on Component and Packaging Technologies, v.29, n.2, pp. 371-378.

[12] McBride, J. W. 2006, *"The Loaded Surface Profile: A new technique for the investigation of contact surfaces,"* International Conference on Electrical Contacts 2006, pp. 150-156.

[13] Coutu, R.A., Jr., Reid, J.R., Cortez, R., Strawser, R.E., and Kladitis, P.E., 2006, "*Microswitches with sputtered Au, AuPd,Au-on-AuPt, and AuPtCu alloy electric contacts*," IEEE Transactions on Components and Packaging Technologies, v 29, n 2, pp. 341-9.

[14] Patton, S.T., Zabinski, J.S., 2005, *"Fundamental studies of Au contacts in MEMS RF switches,"* Tribology Letters, v18, n 2, pp. 215-230.

[15] Hyman, D. and Mehregany, M., 1999, *"Contact physics of gold microcontacts for MEMS switches,"* IEEE Transactions on Components and Packaging Technologies, v 22, pp.357-64.

[16] Tringe, J., Wilson, W.G., and Houston, J.E., 2001, *"Conduction properties of microscopic gold contact surfaces Source,"* Proceedings of the SPIE - The International Society for Optical Engineering, v 4558, pp. 151-8.

[17] Chang. W., 1997, "*An elastic-plastic model for a rough surface with an ion-plated metallic coating*," Journal of Wear, v.212, pp. 229-237.

[18] Chang, W.R., Etsion, I. and Bogy, D.B., 1987, "*An elastic-plastic model for the contact of rough surfaces*," Transactions of the ASME. Journal of Tribology, v 109, n 2, pp. 257-63.

[19] Mikrajuddin, A., Shi, F.G., Kim, H.K. and Okuyama, K., 1999, "*Size-dependent electrical constriction resistance for contacts of arbitrary size: from Sharvin to Holm limits*," Materials Science in Semiconductor Processing, v 2, n 4, pp. 321-7.

[20] Agrait, N., Yeyati, A.L., and van Ruitenbeek, J.M., 2003, *"Quantum properties of atomic-sized conductors,"* Physics Reports, v 377, n 2-3, pp. 81-279.

[21] Wexler, G., 1966, "*The size effect and the nonlocal Boltzmann transport equation in orifice and disk geometry*," in Proceedings of the Physical Society, v 89, pp. 927-941.

[22] Timsit, R.S., 2006, *"Electrical Conduction Through Small Contact Spots*," IEEE Transactions on Components and Packaging Technologies, v.29, n 4, pp. 727-734

[23] Gregori, G. and Clarke, D. R., 2006, "*The interrelation between adhesion, contact creep, and roughness on the life of gold contacts in radio-frequency microswitches*," Journal of Applied Physics, 100, pp.094904-1/10.

[24] Schimkat, J., 1999, *"Contact measurements providing basic design data for microrelay actuators*," Sensors and Actuators A (Physical), v A73, n 1-2, pp. 138-43.

Improving the contact resistance at low force using gold coated carbon nanotube surfaces.

E. M. Yunus, J.W. McBride, and S.M Spearing

School of Engineering Sciences, University of Southampton SO17 1BJ, UK

Abstract. Investigations to determine the electrical contact performance under repeated cycles at low force conditions for carbon-nanotube (CNT) coated surfaces were performed. The surfaces under investigation consisted of multi-walled CNT synthesized on a silicon substrate and coated with a gold film. These planar surfaces were mounted on the tip of a PZT actuator and contacted with a plated Au hemispherical probe. The dynamic applied force used was 1mN. The contact resistance (R_c) of these surfaces was investigated with the applied force and with repeated loading cycles performed for stability testing. The surfaces were compared with a reference Au-Au contact under the same experimental conditions. This initial study shows the potential for the application of gold coated CNT surfaces as an interface in low force electrical contact applications.

PACS. Contact force, contact resistance, carbon nanotubes, and Au/multi walled carbon nanotubes.

1 Introduction

This paper presents a study of electrical contact between surfaces under low dynamic force conditions, typically 1mN. Such conditions are relevant to a number of micro-contact applications, for example MEMS relay devices. There are a number of potential materials commonly used for this application including gold, palladium and platinum [1]. The weakness of such materials is that they are relatively soft and wear easily. Other materials which are of interest on MEMS relay's micro-contact include silicon carbide and diamond films. Both have high moduli but low electrical conductivity. The latter makes them unsuitable for electrical contact applications. There have been attempts to increase the conductivity. When doping SiC film with NH3 the resistivity drops to 1×10^{-4} Ωm [2] and doping DLC with ruthenium the resistivity drops to 1×10^{-5} Ωm [3], however, both materials still have a high resistivity compared to gold and even gold alloys (for example Au-6.3% Pt has a resistivity of 7.17×10^{-8} Ωm) [1].

A carbon nanotube (CNT) coated surface has potential as a material for MEMS relay applications specifically as a contact material because of its excellent mechanical and electrical properties. An experiment has been performed [4] to measure the contact resistance, R_c between CNT coated electrodes in ambient air and in a vacuum. The author concluded that the contact resistance, R_c was found to be much lower in ambient air (~160 Ω) than in vacuum (>4kΩ). In a more recent experiment [5], Au contacts with a substrate coated with tangled single walled carbon nanotubes were investigated. The authors concluded that a tangled Single Walled Carbon Nanotube (SWCNT) film against an Au coated surface has a better performance than two contacting tangled films.

The following mechanical properties have been determined; CNTs tensile strength of up to 63 GPa has been measured [6]. Experiments using an atomic force microscope were performed to measure the elastic modulus and bending strength of individual, structurally isolated, multi-wall carbon nanotubes and indicated values of 1.26 TPa and 14.2 GPa [7] respectively. Experiments were also conducted on CNTs using a nano-indentation apparatus and values were obtained for the bending modulus; 1.24 TPa, axial modulus; 1.23 TPa and wall modulus; 5.61 TPa [8]. Another report shows that CNT's have an elastic modulus greater than 1 TPa [9] compared to diamond, which has a modulus of 1.2 TPa.

In terms of its electrical properties, it is calculated that a 4-10 μm long SWCNT with a diameter of 1.2nm has a resistivity of 0.88×10^{-8} Ωm and is thought to exhibit ballistic electrical conduction. The calculation is performed using the theory of ballistic conductors and it is assumed that the CNT is defect-free. In addition, if a CNT were to be filled with metal, to form a composite its resistivity would fall to 0.35×10^{-8} Ωm [10]. The mechanical and electrical properties are therefore potentially comparable to diamond and gold respectively, however, as yet no experiments have been reported on CNT metal composites for

micro-contact applications. In the present work a novel approach is used in which a CNT "forest" is over coated with gold, in order to provide a high conductivity surface layer with a compliant under layer.

This paper presents a continuation of previous experimental work. In this previous work a modified nano-indentation apparatus [11] was used to determine the contact resistance, R_c, as a function of contact force and load cycling up to ten load cycles. These initial results showed that the performance and contact resistance of Au-Au/MWCNT contact pairs is comparable to Au-Au contact pairs and during ten load cycles of Au-Au/MWNT contact pair shows stable and constant contact resistance.

2 Material preparation

In the present study two contact pairs have been investigated; Au to Au and Au to Au/multi walled carbon nano-tubes (MWCNTs) composite. The geometry selected is a 2mm diameter hemisphere contacting a flat surface. In all cases the hemisphere consists of a stainless steel base, sputter coated with Au, ~500 nm thick, with surface roughness Ra≈400nm. In the Au to Au case (Sample 1), the flat surface is a silicon (Si) substrate (~2mm by 7mm), sputter coated with Au ~500 nm, with a surface roughness Ra≈30nm.

For the Au to Au/MWCNT case (Sample 2), a "forest" of MWCNTs is grown on the Si wafer using thermal CVD. The catalyst used is sputter deposited Fe and the gaseous carbon source is ethylene. The growth temperature and time is 875^{o}C and 3 minutes respectively to produce a dense forest of vertically aligned MWCNT of an average length of ~50μm as shown in Fig 1. Au is then sputtered on the upper surface of the MWCNT forest to produce Au/MWCNT composite coatings as shown in Fig 2. It is shown in Fig 3, that the Au penetrates the MWCNT surface to a depth of ~4 μm.

3 Experimental

In order to determine the performance of the surfaces under repeated switching actions, an apparatus has been designed, in which a PZT actuator is used to support the planar coated surfaces as shown in Fig 4. This surface makes electrical contact with the hemispherical Au-coated probe to mimic the actuation of a MEMS relay micro-contact. The apparatus has been designed to allow control of the gap and to allow the performance of the contact materials to be investigated ultimately over large numbers of switching cycles (>10^6).

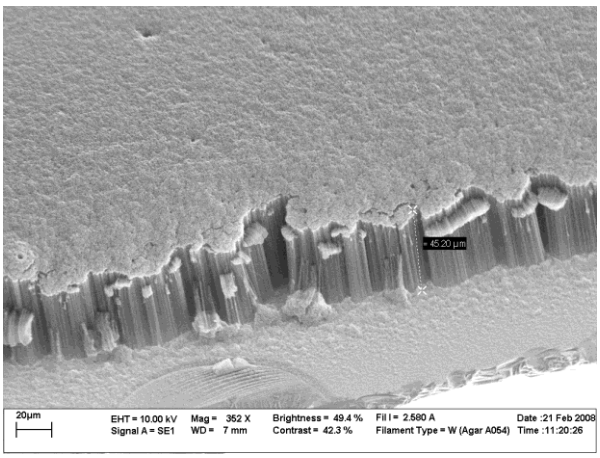

Fig. 1. Dense forest of MWCNT with average length ~50μm.

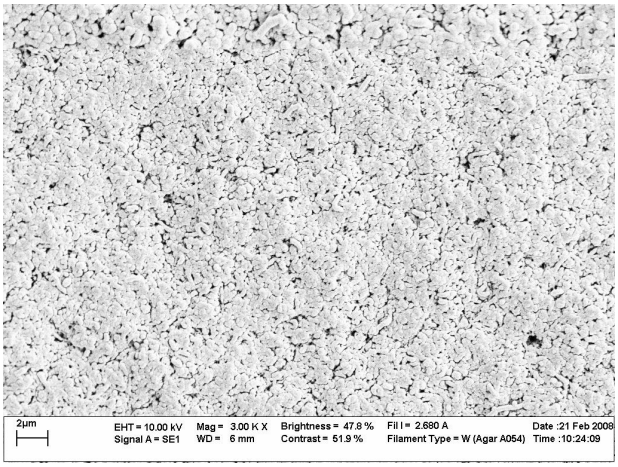

Fig. 2. Sample 2, Au/MWCNT composite contact surface.

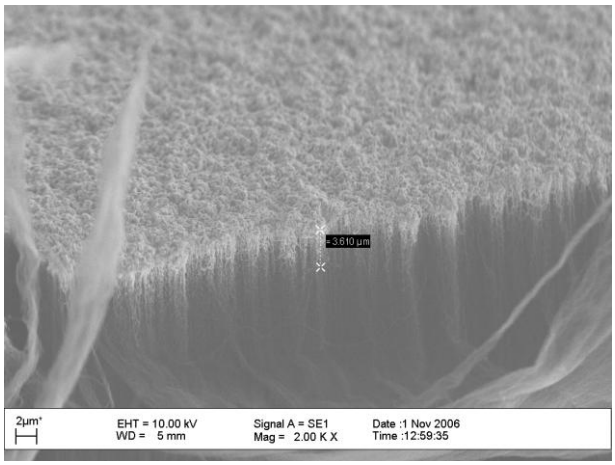

Fig. 3. Au penetration on MWCNT by sputtering.

.

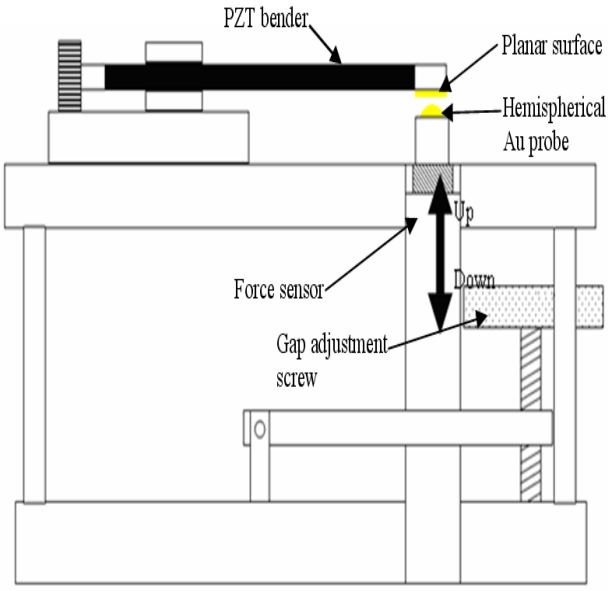

Fig. 4. Schematic side view of the test rig.

A signal generator with voltage amplification is used to actuate the PZT actuator as shown in Fig 5. The PZT actuator's layers consist of Nickel (1st layer), PZT material (Lead Zirconate Titanate) (2nd layer), Nickel (3rd layer) and Kovar (Nickel-Cobalt ferrous alloy, final layer). The resonance frequency of the PZT actuator is ~900Hz (1st harmonic). In this experiment the PZT actuator is actuated at low frequency 0.2Hz to allow a quasi-static study of the contact surfaces. The dynamic force is measured using a piezoelectric force sensor [12-15] situated as shown in Figs 4 and 5. The force sensor is amplified using a charge amplifier and the dynamic force monitored.

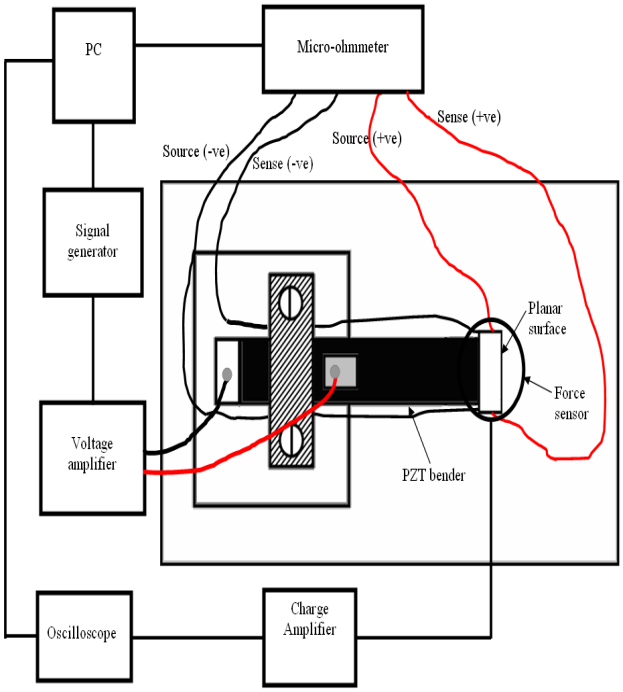

Fig. 5. Schematic top view of the test system.

There are several methods to control the applied force as follows; 1) By controlling the gap [16]. This can be achieved by turning the adjustment screw as shown in Fig 4 and the contact gap is monitored using a triangular laser, 2) By controlling the length of the actuator [14], and 3) By controlling the amplitude of the supply voltage to the actuator. In the experiment presented here all other parameters are held constant, with the contact gap used to set the contact force at 1mN.

The contact resistance, R_c is measured using the 4 wire-measurement methods as shown in Fig 5 and 6. The DC current source across the planar coated surfaces and micro-contact is set at 1mA using a Keithley 580 micro-ohmmeter. The number of cycles and contact resistance can be controlled and extracted by using the control and data acquisition program. The apparatus is enclosed and held at ambient air and room temperature.

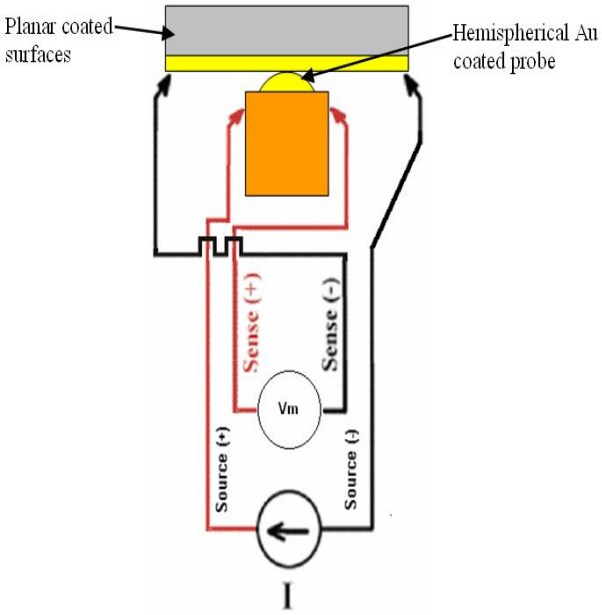

Fig. 6. Schematic of contact zone with its electrode and R_c measurement.

In this experiment, the PZT actuator is actuated up to 1000 cycles at 0.2 Hz under dry circuit conditions (maximum supply of 20mV at 1mA) with the contact resistance R_c measured simultaneously. The aim of this initial study is to determine the stability of the contact surfaces, prior to longer duration testing at higher frequencies.

In order to replicate the conditions of a MEMS relay, a dynamic applied force of 1mN is used. The coated planar surface and Au ball are brought into contact at 0.2Hz using an applied square wave form, and the gap and amplitude adjusted so that a maximum load of 1 mN is reached. The targeted load is applied for ~3 seconds so that a representative average contact resistance value can be determined.

Fig 7 shows an example of the load history over a period of time. Fig 8 shows the variation in R_c over a period of time at a frequency of 0.2Hz. This procedure is repeated in order to detect any cyclic changes in the electrical contact resistance.

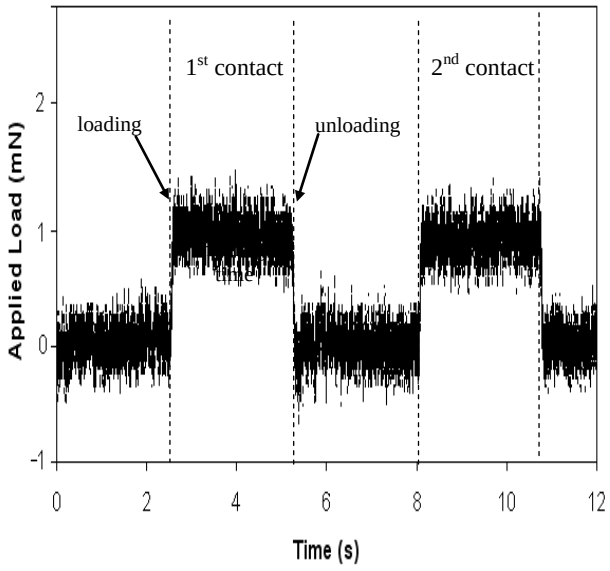

Fig. 7. Example of load cycles (0.2 Hz) for an Au-Au contact pair at 1mN.

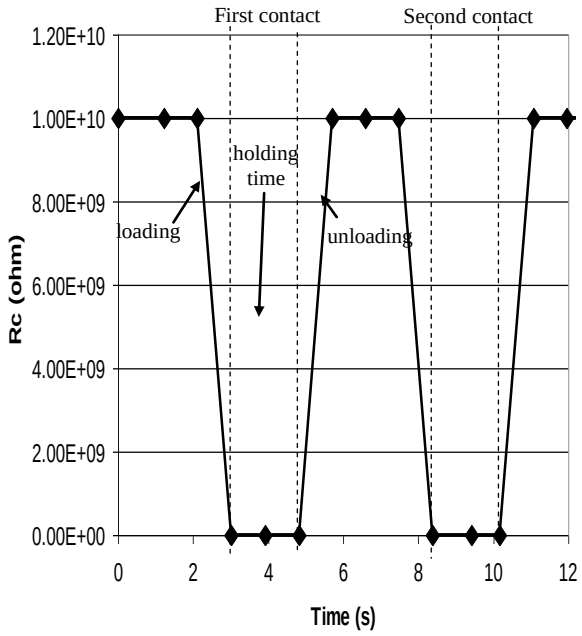

Fig. 8. Example of contact resistance during load cycling for Au-Au contact pair.

The performance of the Au-Au/MWCNT surfaces is compared to a reference Au-Au contact pair under the same experimental conditions in order to assess their mechanical and electrical stability. A TaiCaan Technologies XYRIS 4000CL laser scanner is used to confirm any changes on the contact surfaces samples such as degradation and wear.

4 Results and discussion

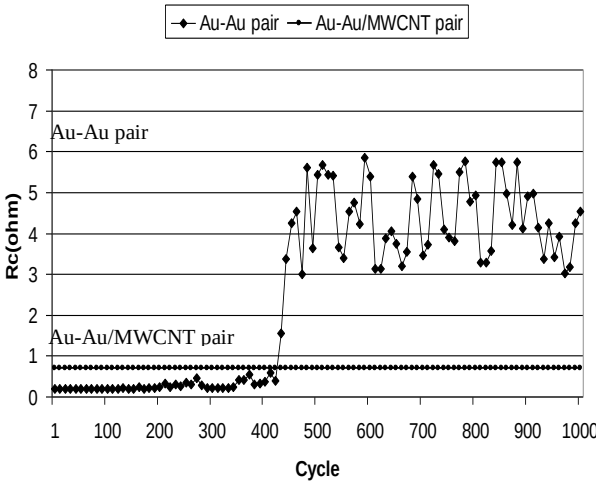

Fig. 9. Cyclic contact resistance of Au-Au and Au-Au/MWNT contact pairs.

Fig 9 shows the contact resistance of Au-Au and Au-Au/MWCNT pairs over 1000 load cycles at a maximum (quasi static) applied load of 1mN. The contact resistance of the Au-Au pair is initially ~0.2Ω and increases rapidly to 4-6Ω at 450 cycles. Under dry circuit conditions the contacts are unlikely to degrade by "hot-switching", therefore the increase in contact resistance is solely due to the mechanical deterioration of the Au-Au contact pair surfaces, reflecting the recognized problems of using soft metals for electrical contacts on a hard substrate. The reason for the sharp increase in R_c of Au-Au pair at ~430 cycles is believed to be due to the initial smoothing of the Au surfaces which leads to increased adhesion

[17]. The smoothing is the result of the repeated impacts and time-dependent deformation of the Au. Fig 10 which shows the damaged Au surface planar for the Au-Au contact pair.

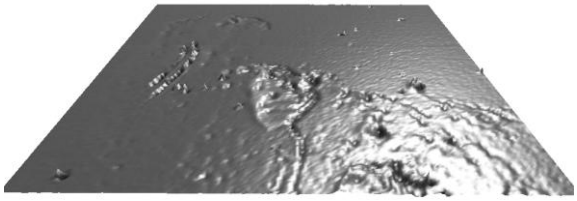

Fig. 10. Scanned image of Au planar surface 201x201(0.2mmx0.2mm) using TaiCaan (Xyris 4000CL).

The adhesive force increases with the number of cycles and is consistent with creep being one of the underlying physical mechanisms for the increase in adhesion [18]. The creep of the gold was shown in [11] during a single load cycle, as shown in Fig 11. Fig 11 shows the graph of load against displacement for an Au-Au contact pair. The experiment was carried out by replacing the diamond tip indenter with the Au hemispherical probe of a nano-indentation apparatus. The curve shows there is creep, a deformation that occurs over a period of time when a material is subjected to constant stress, even at room temperature. The force cycle exhibited in Fig 11 occurs over a longer holding time scale than that used in the test procedure.

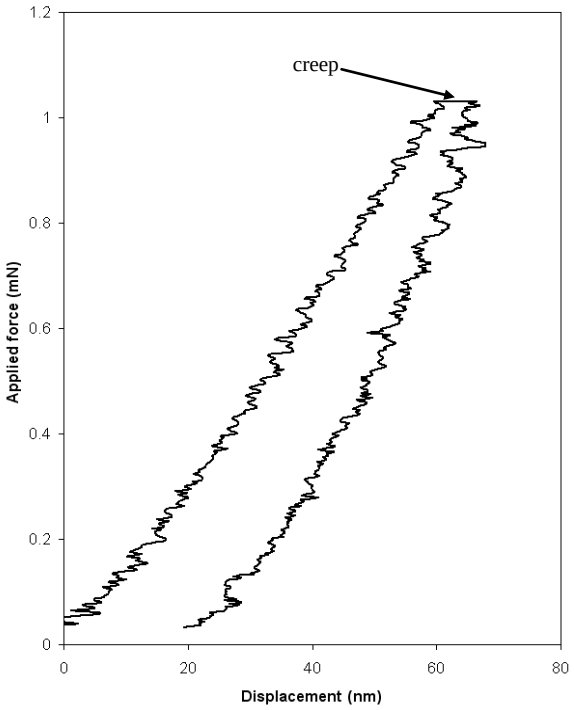

Fig. 11. Graph of load against displacement for Au-Au contact pair.

Fig 9 also shows contact resistance of Au-Au/MWCNT contact pair. The initial contact resistance (~0.7Ω) is higher for the Au-Au/MWNT pair. The likely cause is the difference of surface roughness between Au and Au/MWCNT coated planar surface and the irregularity of the Au film on the MWCNT. It is anticipated that this can be improved in subsequent experiments by better process control. The contact resistance is much more stable than for the Au-Au pair over the 1000 loading cycles. This is believed to be due to the Au/MWCNT surfaces conforming to the shape of the Au hemispherical probe. The dynamic impact on the Au hemispherical probe is absorbed by the Au/MWCNT surfaces thus reducing the wear. The sponge-like effect on Au-Au/MWCNT helps to reduce the deterioration. Furthermore, as the applied load is increased, more deflection occurs of the MWNTs closing the air gaps between the vertically aligned MWNTs thus improving the transfer of electrons [11].
Fig 12 shows a graph of load against displacement using a modified nano-indentation apparatus with Au-Au, and Au-Au/MWCNT contact pair. It shows the depth of penetration during the impact. The curve for

Au-Au/MWCNT pair shows that there is much depth penetration compared with Au-Au pair (~70 nm and ~2500nm respectively). Once the indentation load is removed permanent displacement can be observed (~1400 nm). In [[11] the results show an SEM image of the Au hemispherical probe contact surface after the load cycles having some damage to the Au surfaces where many small impressions on the Au hemispherical probe are detected. These impressions are due to the asperities on the MWNT surfaces. Moreover when the surface roughness (R_a) is measured in this region it has changed from ~400 nm to ~1.5µm.

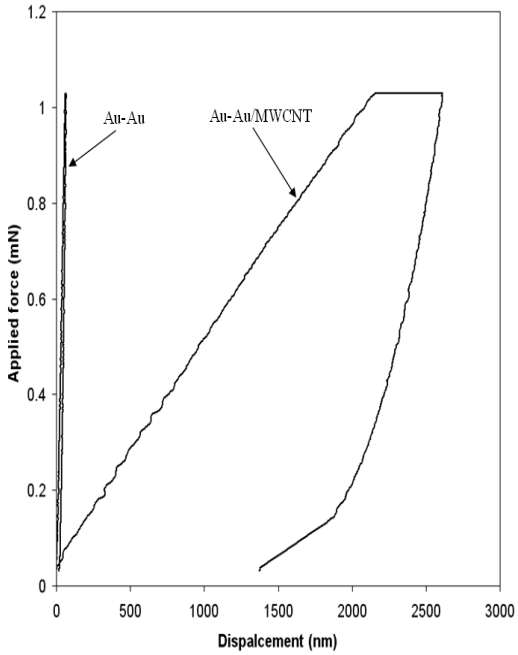

Fig. 12. Graph of load against displacement for an Au-Au, Au-MWCNT and Au-Au/MWCNT contact pair.

In addition, as the Au/MWNTs surface conform to the shape of the Au hemispherical probe it increases the contact area. There is a smoothening of the Au asperity and a significant indentation marks on the Au covering the surface of the Au hemispherical probe as shown in 'A' and 'B' respectively on Fig 13. No visible damage can be detected on the Au/MWCNT planar composite, further suggesting that the CNT under layer has improved the mechanical integrity of the gold surface.

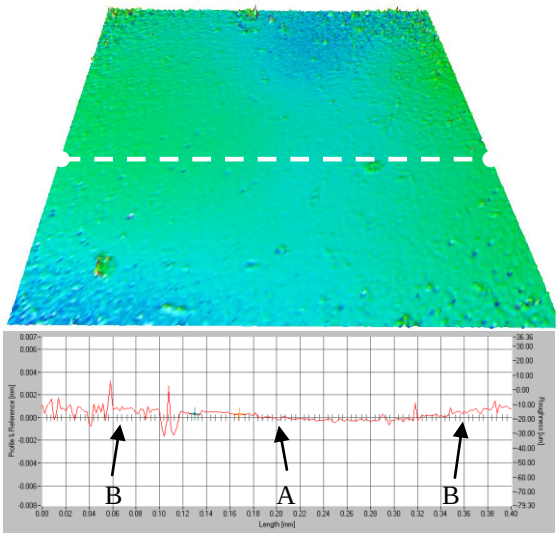

Fig. 13. Scanned image of Au ball for Au-Au/MWCNT with the sphere removed, contact pair 301x301 (0.4mmx0.4mm) using TaiCaan (Xyris 4000CL).

5 Conclusion

The applied cyclic load and contact resistance between Au-Au/MWCNT composite contact pairs was investigated using a PZT actuator apparatus and R_c measurement methods. This contact pair combination was compared with an Au-Au contact pair. Over 1000 load cycles the Au-Au/MWCNT contact pair demonstrated a much more stable contact resistance than Au-Au contact pair. This improvement is believed to be due to Au/MWCNT surface conforming readily with the dynamic impact of the Au hemispherical probe thus decreasing the tendency of smoothing and adhesion that damages the surfaces.

Acknowledgments

The authors thank Dr. David Smith of the School of Physics and Astronomy, for providing the facilities for developing the MWCNT deposition, and to Mr. Tim Hartley for his dedication in designing and fabricating the test apparatus.

References

[1] Coutu, R. A., Kladitis, P. E., Leedy, K. D. and Crane, R. L., 2004, "*Selecting Metal Alloy Electric Contact Materials for MEMS Switches*," Journal of Micromechanics and Microengineering, (14) pp. 1157-1164.

[2] Gao, D., Wijesundara, M. B. J., Carraro, C., Low, C. W., Howe, R. T. and Maboudian, R., 2003, "*High Modulus Polycrystalline 3C-SiC Technology for RF MEMS*," The 2th International Conference on Solid State Sensors, Actuators and Mircosystems, 3D3.4, pp. 1160-1163.

[3] Lian, G. D., Dickey, E. C., Ueno, M. and Sunkara, M. K., 2002, "*Ru-doped Nanostructured Carbon Films*," Diamond and Related Materials, 11, pp. 1890-1896.

[4] Tzeng, Y., Chen, Y. and Liu, C., 2003, *"Electrical contacts between carbon-nanotube coated electrodes,"* Diamond and Related Materials, 12, pp. 774-779.

[5] Yaglioglu, O., Hart, A. J., Martens, R. and Slocum, A. H., 2006, *"Method of characterizing electrical contact properties of carbon nanotube coated surfaces,"* Review of Scientific Instruments, 77, pp 095105/1-3.

[6] Yu, M. F., Lourie, O., Dyer, M. J., Moloni, K., Kelly, T. F. and Ruoff, R.S., 2000, "*Strength and Breaking Mechanism of Multiwalled Carbon Nanotubes Under Tensile Load*," Science, 287(5453), pp. 637 – 640.

[7] Wong EW, Sheehan PE, Lieber CM, 1997 *"Nanobeam Mechanics: Elasticity, Strength, and Toughness of Nanorods and Nanotubes,"* Science, 277, pp. 1971-5.

[8] Qi, H.J., Teo, K.B.K., Lau, K.K.S., Boyce, M.C., Milne, W.I., Robertson, J. and Gleason, K.K., 2003, *"Determination of Mechanical Properties of Carbon Nanotubes and Vertically Aligned Carbon Nanotube forests using Nanoindentation,"* Journal of Mechanics and Physics of Solids, 51, pp. 2213-2237.

[9] Thostenson, E. T., Ren, Z. and Chou, T.W., 2001, "*Advances in the Science and Technology of Carbon Nanotubes and their Composites: A review*," Composites Science and Technology, 61, pp. 1899-1912.

[10] Hjortstam, O., Isberg, P., Söderholm, S. and Dai, H., 2004, *"Can we achieve ultra-low resistivity in carbon nanotube-based metal composites?"* Journal of Applied Physics A, Materials Science & Processing, 78, pp. 1175-1179.

[11] Yunus, E.M., McBride, J.W., and Spearing, S.M., 2007, *"The Relationship between Contact Resistance and Contact Force on Au coated Carbon Nanotubes surfaces,"* Electrical Contact, Proceedings of The 53rd IEEE Holm Conference on Electrical Contacts, Vol.6.4, pp.167-174.

[12] Beckwith, T.G., Marangoni, R.D. and Lienhard V, J.H., 5th Ed, 1993, *"Mechanical Measurements,"* Addison-Wesley Publishing Company.

[13] Usher, M.J., 1985, *"Sensors and Transducers,"* Macmillan.

[14] Duval, F.F.C., Wilson, S.A., Ensell, G., Evanno, N.M.P., Cain, M.G., and Whatmore, R.W., 2007, *"Characterisation of PZT thin film micro-actuators using a silicon micro-force sensor,"* Sensors and Actuators A 133, pp. 35-44.

[15] Dong, W., Lu, X., Cui, Y., Wang, J. and Liu, M. 2007, *"Fabrication and Characterization of microcantilever integrated with PZT thin film sensor and actuator,"* Thin Solid Films, 515, pp. 8544-8548.

[16] Young, C. W. 1989, *"Roark's: Formulas for Stress & Strain,"* McGRAW-HILL International Edition, General Engineering Series.

[17] Patton, S.T. and Zabinski, J. S., 2005, *"Fundamental studies of Au contacts in MEMS RF switches,"* Tribology Letters, Vol 18, No.2, pp. 215-230.

[18] Gregori, G. and Clarke, D.R., 2006, *"The interrelation between adhesion, contact creep, and roughness on the life of gold contacts in radio-frequency microswitches,"* Journal of Applied Physics, 100, pp. 09494-1-10.

Appendix A (Keitley 580 Micro Ohmeter)

Appendix B (KISTLER Dynamic Force Sensor)

REFERENCE

(1) Lucyszyn, S., 2004, "*Review of radio frequency microelectromechanical systems technology*," (IEE) Instituition of Electrical Engineers, Proceedings: Science, Measurement and Technology, v 151, n 2, MEMS and Microsystems Engineering, pp. 93-103.

(2) Zong, Z., Cao, Y., Rahbar N. and Soboyejo, W., 2006, "*Nano- and microscale adhesion energy measurement for Au-Au contacts in microswitch structures*," Journal of Applied Physics, v 100, n 10, pp. 104313-1-10.

(3) Sattler R., Voigt P., Pradel H. and Wachutka G., 2001, "*Innovative design and modelling of a micromechanical relay with electrostatic actuation*," Journal of Micromechanics and Microengineering, 11,pp. 428–433.

(4) Lee, K. K. and Kim, B.C., 2003, "*RF MEMS switch for wireless LAN applications*," Proceedings International Conference on MEMS, NANO and Smart Systems, pp. 100-2.

(5) Gretillat, M A, Gretillat, F and Rooij, N F, 1999, "*Micromechanical relay with electrostatic actuation and metallic contacts*," Journal of Micromechincal and Microengineering, 9, pp 324–331.

(6) Tilmans, H.A.C., De Raedt, W., and Beyne, E., 2003, "*MEMS for wireless communications*," Journal of Micromechanics and Microengineering, v 13, n 4, pp. S139-63.

(7) Tomonari, S., Yoshida, H., Kamakura, M., Yoshida, K., Kawahito, K., Saitoh, M., Kawada, H., Juodkazis, S., and Misawa, H., 2003, "*Miniaturization of a thermally driven Ni/Si bimorph*," Japanese Journal of Applied Physics, Part 1 (Regular Papers, Short Notes & Review Papers), v 42, n 7A, pp. 4464-8.

(8) De, S.K., and Aluru, N.R., 2006, "*A hybrid full-Lagrangian technique for the static and dynamic analysis of magnetostatic MEMS*," Journal of Micromechanics and Microengineering, v 16, n 12, pp. 2646-58.

(9) Yao, J.J., 2000, *"Topical review: RF MEMS from a device perspective,"* Journal of Micromechanical & Microengineering, 10, R9-R38.

(10) http://en.wikipedia.org/wiki/Image:Reedrelay.jpg.

(11) Milosavljevic, Z. D., 2004, "*RF MEMS switches*," Microwave Review, pp. 2-8.

(12) Gupta, R.; Zaghloul, A.; Fassal, F.; Mahle, C., 1995, "*The impact of miniaturized RF technologies on payload architectures of future digital communications satellites,"* Tenth International Conference on Digital Satellite Communications, vol.2, pp. 637 -645.

(13) Rebeiz, G., 2003, "*RF MEMS theory, design, and technology,*" John Wiley and Sons Publications, Hoboken, New Jersey.

(14) Coutu, R.A., Jr., Reid, J.R., Cortez, R., Strawser, R.E., and Kladitis, P.E., 2006, *"Microswitches with sputtered Au, AuPd,Au-on-AuPt, and AuPtCu alloy electric contacts,"* (IEEE) Institute of Electrical and Electronics Engineers, Transactions on Components and Packaging Technologies, v 29, n 2, pp. 341-9.

(15) Bell, D.J., Lu, T.J., Fleck, N.A. and Spearing, S.M., 2005, "*MEMS actuators and sensors: observations on their performance and selection for purpose,*" Journal of Micromechanics and Microengineering, 15, S153-S164.

(16) Wood, R., Mahadevan, R., Dhuler, V., Dudley, B., Cowen, A., Hill, E., and Markus, K., 1998, "*MEMS microrelays*," Mechatronics, 8, pp. 535-547.

(17) Mehregany, M., and Hyman, D., 1999, "*Microelectromechanical systems:application to switches*," Dept. EECS, Case Western Reserve University, Cleveland, Ohio 44106, pp. 1-54.

(18) Yao, J. J., 2000, "*RF MEMS from a device perspective: topical review*," Journal of Micromechanical & Microengineering, (10) R9-R38.

(19) Geneva, 2003, "*Dual action RF-MEMS switch suits system-on-chip integration: innovative RF switching technology reduces power consumption in mobile phones and terminals*," STMicroelectronics (NYSE: STM), http://www.st.com/stonline/press/news/year2003/t1310h.htm#top.

(20) Wellman, J., 2003, "*RF MEMS switches-description of technology*," NASA Electronic Parts & Packaging Program:Technology for Future NASA Mission, http://nepp.nasa.gov/index_nasa.cfm/813/.

(21) Rebeiz, G.M., 2004, "*MEMS for reconfigurable wireless communications*," Dept. ECE, Jacobs College of Engineering, University of California, San Diego, pp. 1-16.

(22) Jeon, Y.B., Sood, R., Jeong, J.-H. and Kim, S.G., 2004, "*MEMS power generator with transverse mode thin film PZT*," Sensors & Actuators A Physical, pp. 1-7.

(23) Milosavljevic, Z. D., 2004, "*RF MEMS switches*," Microwave Review, pp. 2-8.

(24) Trew, R. J., 2005, "*High-frequency solid-state electronic devices*," (IEEE) Institute of Electrical and Electronics Engineers, Transactions on Electron Devices, 52 (5), pp. 638-649.

(25) (a) MEMS Relay, *ME-X Relays:Ultra-Small Devices PIMITES*, (b) Matsushita (Panasonic-Ideas for Life), (c) Miniature Relay:*2 Poles-1 to 2 A (For*

Signal Switching) A Series, Fujitsu-The Possibilities are Infinite, (d) Power Relay:*2 Poles-5 A Low Profile Type, FTR-F1 Series*, Fujitsu-The Possibilities are Infinite, (e) Miniature Relay:*1 Poles (High Frequence Signal Switching) UM1 Series*, Fujitsu-The Possibilities are Infinite, (f) Low Profile *2 Form C Relay*, TQ Relays, Matsushita (Panasonic-Ideas for Life).

(26) Electrical Engineering Division Code 560, NASA GSFC Greenbelt, Maryland, 2005 "*Parts, packaging, and assembly technologies office,"* Code 562, http://eed.gsfc.nasa.gov/562/mems_accelerometer.htm.

(27) McKillop, J. S., 2007, "*RF MEMS: ready for prime time,"* Microwave Journal, pp. 24-38.

(28) McKillop J. S., and Goins, D. A., 2007, *"High performance K-band MEMS switches,"* Proceedings of the 2nd European Microwave Integrated Circuits Conference, pp. 435-438.

(29) Bouchaud, J. and Wicht, H., 2005, *"RF MEMS: status of the industry and roadmaps,"* Proceedings of (SPIE) the International Society for Optical Engineering, Vol. 5717, pp. 50.

(30) Pruitt, B.L.and Kenny, T.W., 2003, "*Piezoresistive cantilevers and measurement system for characterizing low force electrical contacts*," Sensors and Actuators A (Physical), v A104, n 1, pp. 68-77.

(31) Slade, P. G., 1999, *"Electrical contacts: principles and application,"* Marcel Dekker, Inc.

(32) Greenwood J.A, 1966, "*Constriction resistance and the real area of contact,*" Journal of Applied Physics, 12, pp. 1621.

(33) White C.T., and Todorov T.N., 1998, *"Carbon nanotubes as long ballistic conductors,"* Nature, 393, pp. 240-242.

(34) Chang. W., 1997, "*An elastic-plastic model for a rough surface with an ion-plated metallic coating*," Journal of Wear, Vol.212, pp. 229-237.

(35) Chang, W.R., Etsion, I. and Bogy, D.B., 1987, "*An elastic-plastic model for the contact of rough surfaces*," Transactions of the American Society of Mechanical Engineers, Journal of Tribology, v 109, n 2, pp. 257-63.

(36) Mikrajuddin, A., Shi, F.G., Kim, H.K. and Okuyama, K., 1999, "*Size-dependent electrical constriction resistance for contacts of arbitrary size: from Sharvin to Holm limits*," Materials Science in Semiconductor Processing, v 2, n 4, pp. 321-7.

(37) Agrait, N., Yeyati, A.L. and van Ruitenbeek, J.M., 2003, *"Quantum properties of atomic-sized conductors,"* Physics Reports, v 377, n 2-3, pp. 81-279.

(38) Wexler, G., 1966, *"The size effect and the nonlocal Boltzmann transport equation in orifice and disk geometry,"* Proceedings of the Physical Society, v 89, pp. 927-941.

(39) Timsit, R.S., 2006, *"Electrical conduction through small contact spots*," (IEEE) Institute of Electrical and Electronics Engineers, Transactions on Components and Packaging Technologies, v.29, n 4, pp. 727-734.

(40) Patton, S.T. and Zabinski, J. S., 2005, *"Fundamental studies of Au contacts in MEMS RF switches,"* Tribology Letters, Vol 18, No.2, pp. 215-230.

(41) Hyman, D. and Mehregany, M. 1999, *"Contact physics of gold microcontacts for MEMS switches,"* (IEEE) Institute of Electrical and Electronics Engineers, Transactions on Components, Packaging, and Manufacturing Technology, Vol.22, pp. 357-364.

(42) Tringe, J., Wilson, W.G. and Houston, J.E., 2001 *"Conduction properties of microscopic gold contact surfaces,"* Proceedings of the SPIE - The International Society for Optical Engineering, Vol. 4558, pp. 151-8.

(43) McBride, J.W. 2006, *"The loaded surface profile: a new technique for the investigation of contact surfaces,"* Proceedings of the International Conference on Electrical Contacts, pp. 150-156.

(44) Holm, R., 2000, "*Electric contacts, theory and applications,"* Heidelberg, Germany, Springer-Verlag.

(45) Auciello, O., Birrell, J., Carlisle, J. A., Gerbi, J. E., Xiao, X., Peng, B. and Espinosa, H. D., 2004, "*Materials science and fabrication processes for a new MEMS technology based on ultrananocrystalline diamond thin films*," Journal of Physics:Condensed Matter, (16) R539-R552.

(46) Ruitenbeek, J. V., 2005, "*Silver nanoswitch*," Nature; International Weekly Journal of Science, pp. 21-22.

(47) Gray, E.W., 1976, "*The particles of contact activation*," (IEEE) Institute of Electrical and Electronics Engineers, Transactions on Parts, Hybrids, and Packaging, 12(1), pp. 11-15.

(48) Neufeld, C.N. and Rieder, W. F., 1995, "*Electrical characteristics of various contact contaminations*," (IEEE) Institute of Electrical and Electronics Engineers, Transactions on Components, Packaging, and Manufacturing Technology-Part A, 18(2), pp. 369-374.

(49) Tringe, J.W. and Uhlman, T.A., 2003, "*A single asperity study of Au/Au electrical contacts,*" Journal of Applied Physics, 93(8), pp. 4661-4669.

(50) Coutu, R. A., Kladitis, P.E., Leedy, K.D. and Crane, R.L., 2004, "*Selecting metal alloy electric contact materials for MEMS switches*," Journal of Micromechanics and Microengineering, (14) pp. 1157-1164.

(51) Dickrell III, D. J. and Dugger, M. T., 2005, "*The effects of surface contamination on resistance degradation of hot-switched low-force MEMS electrical contacts*," Electrical Contacts, Proceedings of the Annual Holm Conference on Electrical Contacts, v 2005, Electrical Contacts 2005 - Proceedings of the Fifty-First *(IEEE)* Institute of Electrical and Electronics Engineers, Holm Conference on Electrical Contacts, pp. 255-258.

(52) Maluf N. and Williams, K., 2nd Ed, 2004 "*Microelectromechanical systems series: an introduction to microelectromechanical systems engineering*," Artech House, Inc.

(53) Mehregany M., Zorman C. A., Rajan N. and Wo, C.H., 1998 "*Silicon carbide MEMS for harsh environments*," Proceedings of the Institute of Electrical and Electronics Engineers, Vol. 86, No. 8, pp. 1594-1610.

(54) Gao, D., Wijesundara, M. B. J., Carraro, C., Low, C.W., Howe, R. T. and Maboudian, R., 2003, "*High modulus polycrystalline 3C-SiC technology for RF MEMS*," The 12th International Conference on Solid State Sensors, Actuators and Mircosystems, 3D3.4, pp. 1160-1163.

(55) Ertl, S., Adamschik, M., Schmid, P., Gluche, P., FlÖter, A. and Kohn, E., 2000, "*Surface micromachined diamond microswitch*," Diamond and Related Materials, 9, pp. 970-974.

(56) Beerschwinger, U., Mathieson, D., Reuben, R.L. and Yang, S.J., 1994, "*A study of wear on MEMS contact morphologies*," Journal of Micromechanical and Microengineering, (4) pp. 95-105.

(57) Yamada, T., Kojima, A., Sawabe, A. and Suzuki, K., 2004 "*Passivation of hydrogen terminated diamond surface conductive layer using hydrogenated amorphous carbon*," Journal of Diamond and Related Materials, 13, pp. 776-779.

(58) Yoon, E.. Singh, R. A., Oh, Y. J. and Kong, H., 2005 "*The effect of contact area on nano/micro-scale friction*," Journal of Wear, 259, pp. 1424-1431.

(59) Adamschik M., Kusterer J., Schmida P., Schad K.B., Grobe D., Floter A., and Kohn E., 2002, "*Diamond microwave micro relay*," Diamond and Related Materials, 11, pp. 672–676.

(60) Yan X. B., Xu T., Chen G., Wang X. B., Liu H. W. and Yang S. R., 2005 "*Preparation and characterization of amorphous hydrogenated carbon films containing Au nanoparticles from heat-treatment of polymer precursors*," Applied Physics A, Materials Science & Processing, 81, pp. 197-203.

(61) Ekimov E. A., Sidorov V. A., Bauer E. D., Mel'nik N. N., Curro N. J., Thompson J. D., and Stishov S. M., 2004, "*Superconductivity in diamond*," International Weekly Journal of Science, Vol 428, pp. 542-545.

(62) Lian G. D., Dickey E. C., Ueno M., and Sunkara M. K., 2002, "*Ru-doped nanostructured carbon films*," Diamond and Related Materials, 11, pp. 1890-1896.

(63) Charlier, J. C. and Iijima, S., 2001, "*Growth mechanisms of carbon nanotubes*," Springer Berlin/Heidelberg.

(64) Meyyappan M., 2005, "*Carbon nanotubes: science and applications,*" CRC Press.

(65) Wang, B.J., Saka, N. and Rabinowicz, E., 1992, "*The failure mechanism of low-voltage electrical relays*," Electrical Contact, Proceeding of the Thirty-Eighth IEEE Holm Conference on Electrical Contacts, pp. 191-202.

(66) Schiele I, Huber J, Evers C, Hillerich B, Kozlowski F, 1997, "*Micromechanical relay with electrostatic actuation,*" International Conference on Solid-State Sensors and Actuators, pp.1165-1168.

(67) Hyman, D. and Mehregany M., 1998, "*Contact physics of gold microcontacts for MEMS switches,*" Electrical Contacts, Proceedings of the Annual Holm Conference on Electrical Contacts, pp. 133-140.

(68) Schimkat, J., 1998, "*Contact materials for microrelays,*" Proceedings MEMS 98. IEEE. 11th Annual International Workshop on Micro Electro Mechanical Systems. An Investigation of Micro Structures, Sensors, Actuators, Machines and Systems, pp. 190-194.

(69) Tamai, T., 2000, "*Effect of Mg doping on increase in the life with low contact resistance of Ag-Pd alloy switching contact in silicone vapor environments,*" Institute of Electrical and Electronics Engineers (IEEE) Transactions on Components and Packaging Technologies, 23(2), pp.234-239.

(70) Tzeng, Y., Chen, Y. and Liu, C., 2003, *"Electrical contacts between carbon-nanotube coated electrodes,"* Diamond and Related Materials, 12, pp. 774-779.

(71) Wang, M., Liechti, K.M., White, J.M., Winter, R.M., 2004 "*Nano-indentation of polymeric thin film with an interfacial force microscope,*" Journal of the Mechanics and Physics of Solids, 52, pp. 2339-2354.

(72) Yaglioglu, O., Hart, A. J., Martens, R. and Slocum, A. H., 2006, *"Method of characterizing electrical contact properties of carbon nanotube coated surfaces,"* Review of Scientific Instruments, 77, pp 095105/1-3.

(73) Bult, J., Sawyer, W. G., Voevodin, A., Muratore, C., Dickrell, P., Pal, S., Ajayan, P. and Schadler, L., 2008, *"Electrical switching using complaint metal infiltration multi-walled nanotube arrays,"* Proceedings of Material Research Society, Vol. 1085E.

(74) Rebeiz, G., 2003, "*RF MEMS theory, design, and technology,"* John Wiley and Sons Publications, Hoboken, New Jersey.

(75) Yu M.F., Lourie O., Dyer M.J., Moloni K., Kelly T.F., and Ruoff R.S., 2000, "*Strength and breaking mechanism of multiwalled carbon nanotubes under tensile load*," Science, 287(5453), pp. 637 – 640.

(76) Wong EW, Sheehan PE, Lieber CM, 1997 "*Nanobeam mechanics: elasticity, strength, and toughness of nanorods and nanotubes*," Science, 277, pp. 1971-5.

(77) Qi H.J., Teo K.B.K., Lau K.K.S., Boyce M.C., Milne W.I., Robertson J. and Gleason K.K., 2003, "*Determination of mechanical properties of carbon nanotubes and vertically aligned carbon nanotube forests using nano-indentation,*" Journal of Mechanics and Physics of Solids, 51, pp. 2213-2237.

(78) Thostenson E.T., Ren Z., and Chou T.W., 2001, "*Advances in the science and technology of carbon nanotubes and their composites: a review,*" Composites Science and Technology, 61, pp. 1899-1912.

(79) Kim, K. T., Cha, S. I., and Hong, S. H., 2007, "*Hardness and wear resistance of carbon nanotube reinforced Cu matrix nanocomposites*," Materials Science and Engineering A, v 448-451, pp. 46-50.

(80) Collins PG, Avouris P, 2000, "*Nanotubes for electronics,*" Scientific American, 283 (6), pp. 62-9.

(81) Hjortstam O., Isberg P., Söderholm S., and Dai H., 2004, *"Can we achieve ultra-low resistivity in carbon nanotube-based metal composites?"* Journal of Applied Physics A, Materials Science & Processing, 78, pp. 1175-1179.

(82) Dequesnes M., Tang, Z. and Aluru N.R., 2004, "*Static and dynamic analysis of carbon nanotube-based switches,*" Transaction of the American Society of Mechanical Engineers, 126, pp. 230-237.

(83) Fagan S. B., Filho A.G. S., J. Filho M., Corio P., and Dresselhaus M.S., 2005, "*Eletronic properties of Ag- and Cro3-filled single-wall carbon nanotubes,*" Chemical Physics Letters, 406, pp. 54-59.

(84) Hwang H.J., and Kang J. W., 2005, "*Carbon-nanotube-based nanoelectromechanical switch*," Physica E: Low-dimensional Systems and Nanostructures, Vol. 27, Issues 1-2, pp. 163-175.

(85) Cha S.N., Jang J.E., Choi Y., Amaratunga G.A.J. Kang D.J., Hasko D.G., Jung J.E. and Kim J.M., 2005, "*Fabrication of nanoelectromechanical switch using a suspended carbon nanotube,*" Applied Physics Letters, 86, 083105-1-3.

(86) Dujardin E., Derycke V., Goffman M.F., Lefèvre R. and Bourgoin J.P., 2005, "*Self-assembled switches based on electroactuated multiwalled nanotubes,*" Applied Physics Letters, 87, 193107-1-3.

(87) Lee S.-B., Robinson L. A. W., Teo K. B. K., Chhowalla M., Amaratunga G. A. J., Milne C. W. I., Hasko D. G., and Ahmed H., 2003, "*Suspended multiwalled carbon nanotubes as self-aligned evaporation masks,*" Journal Of Nanoscience And Nanotechnology, 3, pp. 325-328.

(88) Cao, A., Dickrell, P. L., Sawyer, G.,Nejhad, M.N.G., and Ajayan, P.M., 2005, *"Super-compressible foamlike carbon nanotube films,"* Science, Vol. 310, pp. 1307-1310.

(89) Iijima S., 1991, *"Helical microtubules of graphitic carbon,"* Nature, 354, pp. 56-58.

(90) Saito Y, Nishikubo K, Kawabata K, and Matsumoto T, 1996, "*Carbon nanocapsules and single-layered nanotubes produced with platinum-group metals (Ru, Rh, Pd, Os, Ir, Pt) by arc discharge,*" Journal of Applied Physics, 80(5), pp. 3062-7.

(91) Collins PG and Avouris P, 2000, "*Nanotubes for electronics,*" Scientific American, 283 (6), pp. 62-9.

(92) Thostenson E.T., Ren Z., and Chou T.W., 2001, "*Advances in the science and technology of carbon nanotubes and their composites: a review,*" Journal of Composites Science and Technology, 61, pp. 1899-1912.

(93) http://ipn2.epfl.ch/CHBU/images/cvd.gif

(94) Ren Z F, Huang ZP, Xu JW, Wang JH, Bush P, and Siegal MP, 1998, "*Synthesis of large arrays of well-aligned carbon nanotubes on glass,*" Science, 282, pp. 1105-7.

(95) Nikolaev P, Bronikowski MJ, Bradley RK, Fohmund F, Colbert DT, and Smith KA, 1999, "*Gas-phase catalytic growth of single-walled carbon nanotubes from carbon monoxide,*" Chemical Physics Letters, 313(1-2), pp. 91-7.

(96) Bower C, Zhu W, Jin S, and Zhou O, 2000, "*Plasma-induced alignment of carbon nanotubes*" Applied Physics Letters, 77(6), pp. 830-2.

(97) Wei B., Spolenak R., Redlich P.K., Ruhle M. and Arzt E., 1999, "*Electrical transport in pure and boron-doped carbon nanotubes*," Applied Physics Letters, Vol 74, No. 21, pp. 3149-3151.

(98) Pantano, A., Boyce, M.C., and Parks, D.M., 2004, "*Mechanics of axial compression of single and multi-wall carbon nanotubes*," Journal of Engineering Materials and Technology, Vol.126, pp. 279-284.

(99) Hsu S. M. and Ying Z.C., 2004, "*Nanotribology, critical assessment and research needs*," Journal of Tribology International, (37) pp. 677-678.

(100) Kassner M.E., Nasser S.N., Suo Z., Bao G., Barbour J.C., Brinson L.C., Espinosa H., Gao H., Granick S., Gumbsch P., Kim K.S., Knauss W., Kubis L., Langer J., Larson B.C., Mahadevan L., Majumdar A., Torquato S.and Swol F.V., 2005, "*New directions in mechanics*," Journal of Mechanics of Materials, (37) pp. 231-259.

(101) Wang, Y., Li, Z. McCormick, D. T., and Tien, N.C., 2004, *"A low-voltage lateral MEMS switch with high RF performance,"* Journal of Microelectromechanical Systems, Vol 13, No.6, pp. 902-911.

(102) Lafontan, X., Pressecq, F., Perez, G., Dufaza, C., and Karam, J.-M., 2001 *"Physical and reliability issues in MEMS microrelays with gold contacts,"* Proceedings of the SPIE - The International Society for Optical Engineering, Vol. 4558, pp. 11-21.

(103) Wang, Y. Li, Z., McCormick, D.T. and Tien, N.C. 2002, *"Low-voltage lateral-contact microrelays for RF application,"* Proceedings of the IEEE Micro Electro Mechanical Systems (MEMS), pp. 645-648.

(104) Moisala, A. Nasibulin, A. G. and Kauppinen, E. I., 2003, *"The role of metal nanoparticles in the catalytic production of single-walled carbon nanotubes-a review,"* Journal of Phusics: Condensed Matter, 15, pp. S3011-S3035.

(105) Noda, S., Hasegawa, K., Sugime, H. Kakehi, K. Zhang, Z., Maruyama, S. and Yamaguchi, Y. 2007, *"Millimeter-thick single-walled carbon nanotube forests: hidden role of catalyst support,"* Japanese Journal of Applied Physics, Part 2: Letters, v 46, n 17-19,pp. L399-L401.

(106) Hongo, H., Nihey, F. Ichihashi, T. Ochiai, Y. Yudasaka, M. and Iijima, J., 2003, *"Support materials based on converted aluminum films for chemical vapor deposition growth of single-wall carbon nanotubes,"* Chemical Physics Letters, v 380, n 1-2, pp. 158-164.

(107) Arcos, T. de los, Wu, Z.M. and Oelhafen, P., 2003, *"Is aluminium a suitable buffer layer for carbon nanotubes growth?"* Chemical Physics Letters, 380, pp. 419-423.

(108) Hart, A. J., 2006, *"Chemical, mechanical and thermal control of substrate-bound carbon nanotube growth,"* Extended Abstract of Doctoral Thesis.

(109) Lee, H.C. Alegaonkar, P.S., Kim, D.Y., Lee, J.H. and Yoo,J.B., 2007, "*Growth of carbon nanotubes: effect of Fe diffusion and oxidation,"* Philosophical Magazine Letters, Vol. 87, No. 10, pp. 767-780.

(110) http://www.micromaterials.co.uk/word%20and%20pdf%20files/useremailjuly2005_final_draft.pdf.

(111) Huber, J.E., Fleck, N.A. and Ashby, M.F. 1997, *"The selection of mechanical actuators based on performance indices*," Proceedings of the Royal Society of London, Series A (Mathematical, Physical and Engineering Sciences), Vol.453, n. 1965, pp.2185-2205.

(112) Rodgers, M.S., Kota, S., Hetrick, J., Li, Z., Jensen, B.D., Krygowski, T.W., Miller, S.L., Barnes, S.M. and Burg, M.S. 2000, *"A new class of high force, low-voltage, compliant actuation systems,"* Technical Digest. Solid-State Sensor and Actuator Workshop (TRF Cat. No.00TRF-0001), 2000, pp. 210-13.

(113) Grade, J.D., Jerman, H. and Kenny, T.W. 2003, *"Design of large deflection electrostatic actuators,"* Journal of Microelectromechanical Systems, Vol. 12, n. 3, pp. 335-343.

(114) Senturia S. D., 2001, *"Microsystem design,"* Kluwer Academic Publishers.

(115) Beckwith, T.G., Marangoni, R.D. and Lienhard V, J.H., 5th Ed, 1993, *"Mechanical measurements,"* Addison-Wesley Publishing Company.

(116) Usher, M.J., 1985, *"Sensors and transducers,"* Macmillan.

(117) Duval, F.F.C., Wilson, S.A., Ensell, G., Evanno, N.M.P., Cain, M.G., and Whatmore, R.W., 2007, *"Characterisation of PZT thin film micro-actuators using a silicon micro-force sensor,"* Sensors and Actuators A 133, pp. 35-44.

(118) Dong, W., Lu, X., Cui, Y., Wang, J. and Liu, M. 2007, *"Fabrication and characterization of microcantilever integrated with PZT thin film sensor and actuator,"* Thin Solid Films, 515, pp. 8544-8548.

(119) Young, C. W. 1989, *"Roark's: formulas for stress & strain,"* McGRAW-HILL International Edition, General Engineering Series.

(120) Dickrell III, D.J. and Dugger, M. T., 2007, *"Silicone oil contamination and electrical contact resistance degradation of low-force gold contacts,"* Journal of Microelectromechanical Systems, Vol. 16, No. 1, pp. 24-28.

(121) Kong J., Yenilmez E., Tombler T. W., Kim W., Dai H., Laughlin R., Liu L., Jayanthi C.S., and Wu S. Y., 2001, *"Quantum interference and ballistic transmission in nanotube electron waveguides,"* Physical Review Letters, v. 87, n. 10, pp. 106801/1-91/4.

(122) Frank S., Poncharal P., Wang Z. L., and Herr W.A. D., 1998, *"Carbon nanotube quantum resistors," Science*, v 280, n 5370, pp. 1744-6.

(123) Ma R.Z., Xu C.L., Wei B.Q., Liang J., Wu D.H. and Li D.J., 1999, *"Electrical conductivity and field emission characteristics of hot-pressed sintered carbon nanotubes,"* Materials Research Bulletin, v. 34, n. 5, pp. 741-747.

(124) Cao, Y., Allameh, S., Nankivil, D., Sethiaraj, S., Otti, T., and Soboyejo, W., 2006, *"Nano-indentation measurements of the mechanical properties of polycrystalline Au and Ag thin films on silicon substrates: effects of grain size and film thickness,"* Material Science and Engineering A 427, pp. 232-240.

(125) Gregori, G. and Clarke, D. R., 2006, *"The interrelation between adhesion, contact creep, and roughness on the life of gold contacts in radio-frequency microswitches,"* Journal of Applied Physics, 100, pp. 094904-1/10.

(126) Zhong, H. A., Rubinsztajn, S., Gowda, A., Esler, D. Gibson, D. Buckley, D., Osaheni, J., and Tonapi, S., 2005, *"Utilization of carbon fibers in thermal management of microelectronics,"* Proceedings of the International Symposium and Exhibition on Advanced Packaging Materials Processes, Properties and Interfaces, pp. 259-265.

(127) Lisa, E., Zhimin, M., Yan, Z., and Johan, L., 2005, *"Modelling of carbon nanotubes as heat sink fins in microchannels for Microelectronics cooling,"* Polytronic 2005: Proceeding of the 5th International Conference on Polymers and Adhesives in Microeletronics and Photonics, pp. 185-187.

(128) Xu, J., and Fisher, T.S., 2006, "*Enhancement of thermal interface materials with carbon nanotube arrays,"* International Journal of Heat and Mass Transfer, 49, pp. 1658-1666.

(129) Zhang, K., and Yuen, M.M.F., 2006, *"Heat spreader with aligned CNTs designed for thermal management of HB-LED packaging and microelectronic packaging,"* 7th International Conference on Electronic Packaging Technology, pp. 1-4.

(130) Almeida, L., Ramadoss, R., Jackson, R., Ishikawa, K., and Yu, Q., 2006, *"Study of the electrical contact resistance of multi-contact MEMS relays fabricated using the MetalMUMPs process,"* Journal of Micromechanics and Microengineering, v 16, n 7, pp. 1189-94.

(131) Rao, S.S., 1986, *"Mechanical vibrations,"* Addison Wesley, pp.381-390.

(132) Hoffmann, M., Kuppers, H., Schneller, T., Bottger, U., Schnakenberg, U., Mokwa, W., and Waser, R., 2003, *"Theoritical calculations and performance results of a PZT thin film actuator,"* IEEE Transaction on Ultrasonics, Ferroelectrics, and Frequency Control, Vol. 50, No. 10, pp. 1240-1246.

(133) Cheng, W.H., Wang, W.H., Yang, D., and Kuang, J.H., 1997,*"Effects of Au coating on thermal stresses in stainless-to-Kovar packages,"* Optical and Quantum Electronics, 29, pp. 939-951.

(134) Doerner, M.F. and Nix, W.D., 1986, *"A method for interpreting the data from depth-sensing indentation instruments,"* Journal of Materials Research, v. 1, n. 4,pp. 601-9.

(135) Oliver W.C., and Pharr G.M., 1992, *"Improved technique for determining hardness and elastic modulus using load and displacement sensing indentation experiments,"* Journal of Materials Research, v. 7, n. 6, Jun, 1992, pp. 1564-1580.